



The  
University  
Of  
Sheffield.

# **Development of a Radiopaque Liquid Embolic for Therapeutic Embolisation**

**Jasmine Lord**

A thesis submitted in partial fulfilment of the requirements for the  
degree of Doctor of Philosophy

The University of Sheffield

Faculty of Science

Department of Chemistry

In Collaboration with Biocompatibles UK Ltd.

August 2019

---

## **Author's Declaration**

The work described in this thesis was carried out at the University of Sheffield and Biocompatibles UK Ltd. laboratories between October 2015 and August 2019 and has not been submitted, either wholly or in part, for this or any other degree. All work is the original work of the author, except where acknowledged by references.

Signature: \_\_\_\_\_

Jasmine Lord

August 2019

---

## Abstract

Therapeutic embolisation is a commonly used medical procedure in the treatment of conditions such as arteriovenous malformations, aneurysms, haemorrhaging and hypervascularised tumours. The procedure involves the deliberate blocking of blood vessels by the insertion of an embolic material. The wide variety of commercially available embolic agents allows the interventional radiologist performing the procedure to tailor the selection of embolic materials to the blood vessels being treated and the desired clinical outcome. Liquid embolic materials provide an ideal route to embolisation in that the liquid agents can be easily delivered by the minimally invasive placement of a microcatheter. On exiting the microcatheter the liquid embolic agents gel within the blood vessels to form a solid cast of the vasculature blocking blood flow. This thesis outlines the development of inherently radiopaque *in situ* gelling materials in an attempt to address some of the issues faced with the clinically used liquid embolics of cyanoacrylate glues and Onyx<sup>®</sup>. The inherent radiopacity imparted to the materials allows them to be visualised by X-ray imaging methods both during and after the procedure if they were to be used in an embolisation procedure.

An inherently radiopaque *in situ* gelling system was developed based on a precipitation mechanism. The radiopaque polymer was formulated using dimethyl sulfoxide (DMSO) as a carrier solvent and precipitated from solution on contact with aqueous environments due to the hydrophobicity imparted by the radiopaque group 2,3,5-triiodobenzaldehyde (TIBA) used to modify poly(vinyl alcohol) (PVA). The precipitating system was tested using a range of specifically developed characterisation and imaging test methods designed to evaluate the performance of the materials as liquid embolic agents. Suitable liquid embolic properties were demonstrated in these tests and it was found that the liquid embolic properties could be tailored by varying the amount of radiopaque 2,3,5-triiodobenzaldehyde group, polymer molecular weight and concentration of the radiopaque polymer in the carrier solvent.

The liquid embolic properties of the precipitating system were further modified by the synthesis of radiopaque polymers using a combination of radiopaque groups. The radiopaque group TIBA used to initially develop the system was used in combination with the more hydrophilic sulfonated radiopaque group S-TIBA and the less hydrophobic mono-iodinated radiopaque group IBA. It was found that use of TIBA in combination with a 25% portion of the alternative radiopaque groups was optimal for tailoring the liquid embolic properties. When the alternative radiopaque groups were used at portions of 50% or higher in combination with TIBA, this resulted in poor liquid embolic properties when tested using the developed characterisation test methods.

A suitable inherently radiopaque *in situ* gelling system was developed using the DMSO based precipitating system. However, the ideal liquid embolic agent should be aqueous based as this removes the associated complications that come with the injection of organic solvent into the body. Two methods were trialled in the development of an aqueous based radiopaque *in situ* gelling material. The first approach utilised a PVA macromonomer modified with the radiopaque group TIBA which polymerised under redox conditions at 37 °C. The addition of the radiopaque group to the PVA macromonomer system was found to have a detrimental impact on the water solubility of the macromonomer resulting in the inability to achieve the solution concentrations required to form distinct gels. Attempts were made to improve the water solubility of the materials, however insufficient improvements were made to be able to form radiopaque gels. Instead a second approach was trialled using PVA modified with S-TIBA which had the dual function of imparting radiopacity and inducing precipitation of the polymer in the presence of Ca<sup>2+</sup> ions. Precipitation of the system was successfully induced by the addition of calcium chloride. However, the quantities of Ca<sup>2+</sup> ions required to induce precipitation would likely be toxic if injected into the body. Hence, this system was deemed unsuitable as a liquid embolic material.

---

## Acknowledgements

I am immensely grateful to so many people who have supported me throughout this PhD project. Foremost, I would like to thank my supervisors' Dr Seb Spain, Prof Steve Armes and Prof Andy Lewis for giving me the opportunity to undertake this research and for their continued input and guidance throughout the process of this PhD. Seb, your ideas and advice have been invaluable in the progress of the project. This research would also not have been possible without funding from the EPSRC, Biocompatibles UK Ltd. and the University of Sheffield.

To the talented scientists at Biocompatibles UK Ltd., it has been a privilege to collaborate with you on this research. Thank you for welcoming me back to your labs with open arms and your continued support and friendship over the years. In particular, I would like to thank Prof Andy Lewis, Dr Yiqing Tang and Dr Koorosh Ashrafi for their input of ideas and enthusiasm for driving the liquid embolics project within the Innovation Group. Also, thank you to the Liquid Embolics team for making me think critically about the attributes required to develop a successful liquid embolic. Invaluable to the generation of ideas for developing characterisation test methods of the novel materials were Jade Nind, Yiqing Tang and Quentin Boffi. Special mentions are also due to Dr Hugh Britton and Dr Francesco Cuda for their excellent chemistry discussions and advice.

It has been a pleasure to work alongside the talented chemists of the Spain and Armes group past and present. The regular smell of fresh bakes featuring so frequently in the office and the friendly faces have made it a wonderful place to work for the last 4 years. I would also like to thank Fiona Revell, an MChem project student I supervised in her final year, for her work on the phase transitioning project. Also, to the friends I have made along the way with the other members of the polymer centre CDT, it has been really interesting to hear about the fantastic research carried out across the university.

I am grateful to numerous members of staff within the chemistry department, particularly Elaine Frary for all of the iodine analysis I have needed during this project. I would also like to thank Caroline Fry at Skelet.AL Lab for the training and support she provided with microCT imaging.

To all my family and friends who have put up with me throughout this PhD process; you have listened to many of my PhD moans and provided sound advice. To Sophie, Alice and Gemma thank you for your continued friendship from our undergraduate days and giving me the much needed break from my project with our regular weekends away and holidays. To my husband, Ian, you have been monumental in supporting me through all my endeavours. I would not have got through this PhD without you and the motivation you have given me when I was lacking it. I am excited to see what the next chapter of our lives hold following this PhD. I am also hugely grateful to my parents for instilling in me the drive to follow the work that I enjoy and for feigning a vague understanding of the work I have been doing. Your love and support throughout my studies has never wavered. Dad, I hope you have a blast reading this thesis, a promise is a promise, good luck for not falling asleep before the first chapter!

---

## **Publications & Patents**

Lord, J., Lewis, A., Radiopaque Polymers, Patent application filed by Biocompatibles UK Ltd., 29/06/2018, GB201810784.

Lord, J., Lewis, A., Spain, S., A radiopaque *in situ* precipitating gel for use in therapeutic embolisation, Poster at Biomaterials Conference 2018, Bradford UK.

Lord, J., Lewis, A., Spain, S., Development of an inherently radiopaque polymer capable of gelling *in situ*. Presentation at Biomaterials Conference 2019, Liverpool UK.

---

## Table of Contents

Author’s Declaration.....	i
Abstract.....	ii
Acknowledgements.....	iii
Publications & Patents.....	iv
List of Figures.....	xii
List of Tables.....	xx
List of Schemes.....	xxvii
List of Equations.....	xxvii
List of Abbreviations.....	xxviii
<b>1. Introduction.....</b>	<b>1</b>
1.1. Therapeutic Embolisation.....	2
1.1.1. Mechanical Devices.....	4
1.1.1.1. Coils.....	5
1.1.1.2. Balloons.....	6
1.1.2. Particulates & Spheres.....	7
1.1.2.1. Particles.....	8
1.1.2.2. Microspheres.....	10
1.1.3. Sclerosing Agents.....	17
1.2. Embolisation using Liquid Embolic Agents.....	18
1.2.1. Current Liquid Embolic Agents.....	21
1.2.1.1. Cyanoacrylate glues.....	22
1.2.1.2. Onyx®.....	25

---

1.2.1.3.	Lipiodol® .....	28
1.2.2.	Emerging Liquid Embolic Technologies .....	29
1.2.2.1.	Squid™ .....	29
1.2.2.2.	PHIL® .....	30
1.2.2.3.	Easyx™ .....	31
1.2.2.4.	GPX.....	32
1.2.2.5.	Instylla Hydrogel Embolic System .....	33
1.2.2.6.	Silk Elastin Protein Polymer (SELP) .....	33
1.2.2.7.	Shear Thinning Biomaterials .....	34
1.3.	Research Aims .....	35
1.3.1.	Important Properties of a Radiopaque Liquid Embolic .....	37
1.3.1.1.	Delivery.....	37
1.3.1.2.	Function .....	39
1.3.1.3.	Visibility .....	40
<b>2.</b>	<b>Development of Characterisation Test Methods.....</b>	<b>43</b>
2.1.	Introduction.....	44
2.2.	Experimental.....	46
2.2.1.	Statistics .....	46
2.2.2.	Nuclear Magnetic Resonance Spectroscopy .....	47
2.2.3.	Mass Spectrometry.....	47
2.2.4.	Infrared Spectroscopy .....	47
2.2.5.	Melting Point Analysis.....	47
2.2.6.	Elemental Analysis .....	48

---

---

2.2.7.	Size Exclusion Chromatography.....	48
2.2.8.	Precipitation Under Flow Conditions.....	49
2.2.9.	Rate of Solidification .....	50
2.2.10.	Rheometry .....	51
2.2.11.	Precipitate Fill Volume .....	52
2.2.12.	Fragmentation and Particulate Generation.....	52
2.2.13.	Scanning Electron Microscopy .....	54
2.2.14.	Solid Content Study .....	54
2.3.	Results and Discussion .....	55
2.3.1.	Preparation Time.....	55
2.3.2.	Deliverability Under Flow Conditions.....	55
2.3.3.	Rate of Solidification .....	58
2.3.4.	Rheology of Solidification Process.....	61
2.3.5.	Fill Volume After Solidification .....	64
2.3.6.	Fragmentation and Particulate Generation.....	66
2.3.7.	Porosity of Internal Structure.....	70
2.3.8.	Stability of Precipitate.....	72
2.3.9.	Biocompatibility.....	72
2.4.	Conclusions.....	73
<b>3.</b>	<b>MicroCT Method Development for Sample Imaging .....</b>	<b>75</b>
3.1.	Introduction.....	76
3.2.	Experimental .....	76
3.2.1.	Sample Preparation – Free-Formed Structures .....	76

---



---

3.2.2.	Sample Preparation – Tubing Constraints.....	76
3.2.3.	Sample MicroCT Scan Method.....	77
3.2.4.	Reconstruction Parameters of Scan Data .....	77
3.2.5.	Radiopacity Calculations .....	77
3.2.6.	Porosity Calculations .....	78
3.3.	Results and Discussion .....	78
3.3.1.	Development of MicroCT Scan Method.....	78
3.3.2.	Calibration with Hydroxyapatite Standards .....	80
3.3.3.	Scans of Free-Formed Samples.....	82
3.3.4.	Standardising Sample Preparation with Tubing.....	83
3.3.5.	Standardising Scan Analysis .....	86
3.3.6.	Impact of Sample Delivery on Radiopacity Measurements.....	92
3.3.7.	Scans Across Whole Precipitate Lengths.....	101
3.4.	Conclusions.....	107
<b>4.</b>	<b>Synthesis and Characterisation of a Precipitating Liquid Embolic .....</b>	<b>109</b>
4.1.	Introduction.....	110
4.2.	Experimental.....	112
4.2.1.	Synthesis of 2,3,5-Triiodobenzaldehyde (TIBA).....	113
4.2.2.	Synthesis of Iodinated PVA (I-PVA).....	114
4.2.3.	Water Solubility Test .....	115
4.2.4.	Preparation of I-PVA Liquid Embolic Prototypes .....	116
4.3.	Results and Discussion .....	116
4.3.1.	Preparation of a Radiopaque Substituent .....	116

---

4.3.2.	Preparation of Iodinated PVA.....	118
4.3.3.	Feasibility Testing.....	119
4.3.3.1.	Solubility in Water.....	119
4.3.3.2.	Precipitation under Aqueous Conditions .....	120
4.3.3.3.	Precipitation under Flow Conditions .....	122
4.3.4.	Preparation Time.....	126
4.3.5.	Deliverability Under Flow Conditions.....	127
4.3.6.	Rate of Solidification .....	135
4.3.7.	Rheology of Precipitation Process .....	141
4.3.8.	Fill Volume After Solidification .....	149
4.3.9.	Fragmentation and Particulate Generation.....	154
4.3.10.	Stability of Precipitate.....	159
4.3.11.	Biocompatibility.....	162
4.3.12.	Radiopacity .....	164
4.3.13.	Porosity .....	169
4.4.	Conclusions.....	172
<b>5.</b>	<b>Synthesis and Characterisation of a Precipitating Liquid Embolic with Alternative Radiopaque Groups.....</b>	<b>174</b>
5.1.	Introduction.....	175
5.2.	Experimental .....	176
5.2.1.	Synthesis of S-TIBA .....	177
5.2.2.	Modification of PVA with S-TIBA and TIBA .....	178
5.2.3.	Modification of PVA with IBA and TIBA .....	179

---

5.2.4.	Formulation as Solutions in DMSO .....	180
5.3.	Results and Discussion .....	180
5.3.1.	Iodinated PVA in Combination S-TIBA.....	180
5.3.2.	Iodinated PVA in Combination with IBA.....	182
5.3.3.	Preparation Time.....	183
5.3.4.	Deliverability Under Flow Conditions.....	184
5.3.5.	Rate of Solidification .....	187
5.3.6.	Rheology of Precipitation Process .....	192
5.3.7.	Fill Volume after Solidification .....	196
5.3.8.	Fragmentation and Particulate Generation.....	199
5.3.9.	Biocompatibility.....	201
5.3.10.	Radiopacity .....	203
5.3.11.	Porosity .....	206
5.4.	Conclusions.....	208
<b>6.</b>	<b>Synthesis and Characterisation of Aqueous-Based Liquid Embolics .....</b>	<b>209</b>
6.1.	Introduction.....	210
6.2.	Experimental.....	212
6.2.1.	N-Acryloyl aminoacetaldehyde dimethyl acetal (NAAADA).....	213
6.2.2.	PVA Macromonomer.....	214
6.2.3.	I-PVA Macromonomer .....	215
6.2.4.	PVA Macromonomer with Pendent Groups .....	216
6.2.5.	Water Solubility Test .....	217
6.2.6.	Gelation Test using an Azo Initiator .....	217

---

6.2.7.	Gelation Test using Redox Initiators.....	217
6.2.8.	PVA Modified with S-TIBA.....	218
6.2.9.	Precipitation Test with Ca <sup>2+</sup> .....	218
6.3.	Results and Discussion .....	219
6.3.1.	Approach 1: In Situ Polymerising Embolic .....	219
6.3.1.1.	Preparation of PVA macromonomer.....	221
6.3.1.2.	Gelation Tests .....	222
6.3.1.2.1.	Azo Initiator.....	222
6.3.1.2.2.	REDOX System.....	223
6.3.1.3.	Modification of PVA Macromonomer with Radiopaque Substituent.....	225
6.3.1.3.1.	Gelation Testing of I-PVA Macromonomer .....	227
6.3.1.3.2.	Water Solubility Study of I-PVA Macromonomer .....	229
6.3.1.4.	Modification of PVA Macromonomer with Hydrophilic Groups.....	234
6.3.1.4.1.	Water Solubility Testing of Modified PVA Macromonomers.....	236
6.3.2.	Approach 2: Precipitating Embolic.....	239
6.3.3.	Modification of PVA with a Water Soluble Radiopaque Substituent.....	239
6.3.4.	Precipitation Test with Calcium Chloride.....	240
6.4.	Conclusions.....	241
<b>7.</b>	<b>Conclusions &amp; Outlook.....</b>	<b>242</b>
7.1.	Conclusions & Outlook.....	243
7.2.	References.....	249
<b>8.</b>	<b>Appendix.....</b>	<b>261</b>
8.1.	Cross-Sectional Videos of Reconstructed MicroCT Scans.....	262

---

---

## List of Figures

Figure 1.1 - Diagram of femoral and radial access points for catheterisation. ....	3
Figure 1.2 - Diagram representing areas of proximal embolisation, distal embolisation and embolic reflux relative to the placement of the microcatheter within a blood vessel. ....	4
Figure 1.3 - Embolic coils marketed by Cook Medical Llc.; (A) Nester <sup>®</sup> , (B) Torando <sup>®</sup> , (C) MReye <sup>®</sup> , (D) Hilal Straight <sup>™</sup> . ....	6
Figure 1.4 - Diagram of an inflated balloon delivered into the vasculature via a microcatheter. ....	7
Figure 1.5 - Preparation of Gelfoam <sup>®</sup> particles; (A) Material supplied as a foam sheet, (B) Manually cutting of sheet into irregular shaped particles, (C) Mixing of particles with contrast agent to create slurry, (D) Thick slurry ready for injection (images from Angiofellow educational resources). ....	9
Figure 1.6 - Transarterial embolisation process of a hypervascularised tumour; (A) Insertion of microcatheter into the femoral artery, (B) Placement of microcatheter tip in blood vessels supplying the tumour, (C) Embolisation of the tumour by delivery of microspheres with distal penetration, (D) Reduced tumour size as a result of microsphere occlusion within the feeding blood vessels (images courtesy of Biocompatibles UK Ltd.). ....	11
Figure 1.7 - Diagram of an inflated balloon microcatheter to reduced blood flow during the delivery of the embolic material. ....	21
Figure 1.8 - In situ polymerisation of N-butyl-2-cyanoacrylate (nBCA). ....	22
Figure 1.9 - In situ polymerisation of isostearyl-2-cyanoacrylate. ....	24
Figure 1.10 - In situ polymerisation of 2-hexyl cyanoacrylate. ....	24
Figure 1.11 - Poly(vinyl alcohol-co-ethylene). ....	25
Figure 1.12 - Beam hardening and streak artefact (indicated by white arrow) observed with Onyx <sup>®</sup> in the right hepatic artery by contrast enhanced axial CT (image from Clin. Radiol., 2015, <b>70</b> , 326–32). ....	28

---

Figure 1.13 - X-ray images showing the longer tantalum suspension time (as indicated by the white arrow) of Squid™ 18 (A) in comparison to Onyx® 18 (B) 15 minutes after agitation (image from Emboflu promotional brochure for Squid™). .....	30
Figure 1.14 - Schematic of the complexation of a polyelectrolyte from polyanions and polycations on reduction of the solution ionic strength. ....	32
Figure 1.15 - Amino acid composition of a silk elastin protein polymer (SELP-47K)(image adapted from Biomaterials, 2015, 57, 142-52). ....	34
Figure 1.16 - Diagram of shear thinning behaviour of a nanocomposite hydrogel containing gelatin and silicate nanoplatelets (image adapted from Sci. Transl. Med., 2016, 8, 365-77) 34	
Figure 2.1 - Desirable properties of a radiopaque liquid embolic at preparation, delivery and implantation stages.....	45
Figure 2.2 - Vascular flow model system set-up; (A) PBS reservoir (B) Peristaltic pump (C) Elevated PBS Reservoir (D) Vascular model (E) Microcatheter inlet.....	49
Figure 2.3 - Rheometer experimental set-up with flow of saline through cell.....	51
Figure 2.4 - Volume measurement device set-up. ....	52
Figure 2.5 - Vascular flow model. ....	56
Figure 2.6 - Liquid embolic injection into tubing under PBS flow. ....	57
Figure 2.7 - Solidification profile of a liquid embolic prototype (n=3). ....	60
Figure 2.8 - Solidification of a liquid embolic sample on surface of PBS close to the UV outlet. ....	61
Figure 2.9 - Solidification profile of a rapidly solidifying liquid embolic prototype (n=1)...	61
Figure 2.10 - Viscosity of a liquid embolic prototype in DMSO at 37 °C (n=1).....	62
Figure 2.11 - Viscosity profile of the solidification process of a liquid embolic prototype at 37 °C (n=1). ....	63
Figure 2.12 - Liquid embolic sample following rheology solidification testing.....	63
Figure 2.13 - Volume measurement device calibration graph (n=3). ....	65

---

---

Figure 2.14 - Process of fill volume test; (A) Precipitation of liquid embolic sample. (B) Solidified sample test tube for height measurement in volume measurement device. ....	65
Figure 2.15 - SEM cross-sectional image of a precipitated liquid embolic prototype (500 $\mu\text{m}$ scale). ....	71
Figure 2.16 - SEM cross-sectional image of a precipitated liquid embolic prototype (50 $\mu\text{m}$ scale). ....	71
Figure 3.1 – Liquid embolic sample precipitate by the free-form solidification method. ....	79
Figure 3.2 - Reconstructed scan images with increasing beam hardening correction applied; (A) 0% (B) 10% (C) 20%. ....	80
Figure 3.3 - Reconstructed 2D cross-section of HA phantom with selected 200 and 1200 mg HA $\text{cm}^{-3}$ rods highlighted. ....	81
Figure 3.4 - HA phantom radiopacity calibration plot (imaging cross-sections, n=198). ....	82
Figure 3.5 - Reconstructed 2D cross-sections of free-form solidified liquid embolic prototypes of varying radiopaque (RO) group concentrations; (A) 0.1 eq RO, (B) 0.15 eq RO, (C) 0.2 eq RO, (D) 0.25 eq RO. ....	83
Figure 3.6 – (A) Reconstructed 2D cross-section image (B) Same cross-section image after binarization. ....	87
Figure 3.7 – (A) Binarized image with low thresholding (B) Binarized image with optimal thresholding (C) Binarized image with high thresholding. ....	87
Figure 3.8 - Histogram of background and object pixels with a visual representation of the point of curve intersection used to determine position of automatic threshold. ....	88
Figure 3.9 – (A) Reconstructed 2D cross-section image (B) Binarized cross-section image with global thresholding (C) Binarized cross-section image with adaptive thresholding. ....	88
Figure 3.10 - Measured radiopacity of manual injection replicates 1-3 prepared under flow of PBS with thresholding methods of manual, automatic and adaptive (imaging cross-sections, n=198). ....	90

---

---

Figure 3.11 - Measured radiopacity of manual injection replicates 1-3 prepared under no flow of PBS with thresholding methods of manual, automatic and adaptive (imaging cross-sections, n=198).....	90
Figure 3.12 - Reconstructed 2D cross sections of liquid embolic sample delivered by continuous syringe pump method under PBS flow (A) hollow remaining after removal of microcatheter (B) bright region immediately proximal to the catheter hollow.....	101
Figure 4.1 - Proposed structure of a precipitating radiopaque embolic liquid.....	111
Figure 4.2 - 2,3,5-triiodobenzaldehyde (TIBA).....	113
Figure 4.3 - Iodinated PVA (I-PVA). ....	114
Figure 4.4 - Water solubility results of I-PVA samples (n=3 for I-PVA samples and n=15 for PVA control).....	120
Figure 4.5 - Photo of I-PVA precipitation test.....	122
Figure 4.6 - Photo of precipitation test of I-PVA synthesised at 0.25 equivalents of TIBA under varying flow rates of PBS.....	123
Figure 4.7 - Areas of reflux and proximal flow of the liquid embolic with respect to the injection point during deliverability test.....	128
Figure 4.8 - Percentage of proximal flow of solidified liquid embolic prototypes over a range of equivalents of TIBA and concentrations in DMSO (n=1).....	132
Figure 4.9 - Percentage of proximal flow of solidified liquid embolic prototypes over a range of polymer molecular weights (n=1).....	133
Figure 4.10 - Solidification results of liquid embolic prototypes over a range of TIBA equivalents and concentrations in DMSO (n=1).....	136
Figure 4.11 - Solidification profiles of liquid embolic prototypes over a range of TIBA equivalents at 20 w/w% solutions in DMSO (n=1). ....	137
Figure 4.12 - Solidification profiles of liquid embolic prototypes over a range of concentrations in DMSO at 0.1 equivalents of TIBA (n=1). ....	138

---



---

Figure 4.13 - Solidification results of liquid embolic prototypes over a range of polymer molecular weights at 0.1 and 0.25 equivalents of TIBA (n=1).....	138
Figure 4.14 - Solidification profiles of liquid embolic prototypes over a range of molecular weights at 0.1 equivalents of TIBA (n=1).....	139
Figure 4.15 - Solidification profiles of liquid embolic prototypes over a range of molecular weights at 0.25 equivalents of TIBA (n=1).....	140
Figure 4.16 - Complex viscosity profile of precipitation process for liquid embolic prototype 1.9 of 0.2 equivalents of TIBA for 67 kDa PVA at 20 w/w% in DMSO (onset of precipitation at 3.5 mins) (n=1).....	142
Figure 4.17 - Storage and loss modulus profiles of precipitation process for liquid embolic prototype 1.9 of 0.2 equivalents of TIBA for 67 kDa PVA at 20 w/w% in DMSO (onset of precipitation at 3.5 mins) (n=1). ....	142
Figure 4.18 - Complex viscosity results of liquid embolic prototypes for low and high molecular weights at 0.1 and 0.25 equivalents of TIBA in liquid and precipitate states (n=1). ....	145
Figure 4.19 - Storage modulus results of liquid embolic prototypes for low and high molecular weights at 0.1 and 0.25 equivalents of TIBA in liquid and precipitate states (n=1). ....	146
Figure 4.20 - Loss modulus results of liquid embolic prototypes for low and high molecular weights at 0.1 and 0.25 equivalents of TIBA in liquid and precipitate states (n=1). ....	146
Figure 4.21 - Complex viscosity results of liquid embolic prototypes at 0.2 equivalents of TIBA over a range of concentrations in DMSO in liquid and precipitate states (n=1).....	147
Figure 4.22 - Storage modulus results of liquid embolic prototypes at 0.2 equivalents of TIBA over a range of concentrations in DMSO in liquid and precipitate states (n=1). ....	147
Figure 4.23 - Loss modulus results of liquid embolic prototypes at 0.2 equivalents of TIBA over a range of concentrations in DMSO in liquid and precipitate states (n=1). ....	148
Figure 4.24 - Fill volume results of liquid embolic prototypes over a range of TIBA equivalents and concentrations in DMSO (n=3).....	152

---

---

Figure 4.25 - Fill volume results of liquid embolic prototypes over a range of polymer molecular weights at 0.1 and 0.25 equivalents of TIBA (n=3).....	153
Figure 4.26 - Fragmentation ratings of liquid embolic prototypes of a range of DMSO concentrations and TIBA equivalents (n=3).....	156
Figure 4.27 - Particulate ratings of liquid embolic prototypes of a range of DMSO concentrations and TIBA equivalents (n=3).....	157
Figure 4.28 - Fragmentation ratings of liquid embolic prototypes of a range of polymer molecular weights at 0.1 and 0.25 equivalents of TIBA (n=3).....	157
Figure 4.29 - Particulate ratings of liquid embolic prototypes of a range of polymer molecular weights at 0.1 and 0.25 equivalents of TIBA (n=3).....	158
Figure 4.30 - Solid content results for liquid embolic prototypes of different TIBA equivalents (n=3).....	161
Figure 4.31 - Solid content results over time of liquid embolic prototypes over a range of TIBA equivalents (n=3). .....	162
Figure 4.32 - MicroCT results for I-PVA samples over a range of TIBA equivalents and DMSO concentrations synthesised using 67 kDa PVA (imaging cross-sections, n=198)...	166
Figure 4.33 - MicroCT results for I-PVA samples over a range of polymer molecular weights at 0.1 and 0.25 equivalents of TIBA (imaging cross-sections, n=198).....	166
Figure 4.34 - Measured radiopacity of Histodenz controls (imaging cross-sections, n=198). .....	167
Figure 4.35 - Reconstructed 2D cross section of Onyx <sup>®</sup> sample. ....	169
Figure 4.36 - Porosity results for I-PVA samples over a range of TIBA equivalents and DMSO concentrations synthesised using 67 kDa PVA (imaging cross-sections, n=198). .....	171
Figure 4.37 - Porosity results for I-PVA samples over a range of polymer molecular weights at 0.1 and 0.25 equivalents of TIBA (imaging cross-sections, n=198).....	171
Figure 5.1 - Hydrophobicity difference of S-TIBA, IBA and TIBA. ....	176
Figure 5.2 - 3-(2,4,6-triido-5-formylphenoxy)-1-propanesulfonic acid (S-TIBA). .....	177

---

---

Figure 5.3 - PVA modified with S-TIBA and TIBA. ....	178
Figure 5.4 - PVA modified with IBA and TIBA. ....	179
Figure 5.5 - Percentage of proximal flow of solidified liquid embolic prototypes prepared using combinations of S-TIBA, IBA and TIBA (n=1). ....	187
Figure 5.6 - Solidification results of liquid embolic prototypes prepared using combinations of S-TIBA, IBA and TIBA (n=1).....	190
Figure 5.7 - Images of liquid embolic prototypes during solidification test; (A) 25% S-TIBA (B) 50% IBA (C) 50% S-TIBA.....	191
Figure 5.8 - Solidification profiles of liquid embolic prototypes prepared using combinations of S-TIBA, IBA and TIBA (n=1).....	192
Figure 5.9 - Complex viscosity results of liquid embolic prototypes prepared using combinations of S-TIBA, IBA and TIBA in their liquid and precipitate states (n=1).....	194
Figure 5.10 - Storage modulus results of liquid embolic prototypes prepared using combinations of S-TIBA, IBA and TIBA in their liquid and precipitate states (n=1).....	195
Figure 5.11 - Loss modulus results of liquid embolic prototypes prepared using combinations of S-TIBA, IBA and TIBA in their liquid and precipitate states (n=1). ....	196
Figure 5.12 - Fill volume results of liquid embolic prototypes prepared using combinations of S-TIBA, IBA and TIBA (n=3).....	199
Figure 5.13 - Fragmentation ratings of liquid embolic prototypes prepared using combinations of S-TIBA, IBA and TIBA (n=3).....	201
Figure 5.14 - Particulate ratings of liquid embolic prototypes prepared using combinations of S-TIBA, IBA and TIBA (n=3).....	201
Figure 5.15 - MicroCT results for liquid embolic samples prepared using combinations of S-TIBA, IBA and TIBA (imaging cross-sections, n=198).....	205
Figure 5.16 - Porosity results for liquid embolic samples prepared using combinations of S-TIBA, IBA and TIBA (imaging cross-sections, n=198).....	207
Figure 6.1 - N-Acryloyl aminoacetaldehyde dimethyl acetal (NAAADA). ....	213

---

---

Figure 6.2 - PVA macromonomer.....	214
Figure 6.3 - I-PVA macromonomer.....	215
Figure 6.4 - PVA macromonomer modified with pendent groups.....	216
Figure 6.5 - PVA macromonomer modified with S-TIBA. ....	218
Figure 6.6 - Delivery of LiquiGel™ using a dual-lumen microcatheter. ....	220
Figure 6.7 - I-PVA macromonomer.....	220
Figure 6.8 - Comparison of water solubility results for PVA macromonomer samples prepared using 31 & 67 kDa PVA (n=3). ....	231
Figure 6.9 - Comparison of water solubility results for I-PVA macromonomer samples synthesised at 0, 0.01 & 0.1 eq of TIBA for 31 kDa PVA (n=3).....	232
Figure 6.10 - Comparison of water solubility results for I-PVA macromonomer samples synthesised at 0, 0.01 & 0.1 eq of TIBA for 67 kDa PVA (n=3).....	233
Figure 6.11 - Comparison of water solubility results during the preparation of I-PVA macromonomer synthesised using 31 kDa PVA over 7-63 double bond equivalents (n=3). ....	234
Figure 6.12 - Comparison of water solubility results for PVA macromonomer and PVA macromonomers modified with hydrophilic groups (n=3). ....	237
Figure 6.13 - Comparison of PBS solubility results for PVA macromonomer and PVA macromonomers modified with hydrophilic groups. ....	238
Figure 6.14 - Image of precipitate formed after excess addition of CaCl <sub>2</sub> to Ringer's solution. ....	240

---

## List of Tables

Table 1.1 - Characteristics of commercially available microspheres (data obtained from manufacturers data sheets).....	13
Table 2.1 - Fragmentation rating criteria. ....	53
Table 2.2 - Particulate rating criteria. ....	54
Table 2.3 - Delivery results for the tubing method under flow of PBS (n=3). ....	58
Table 2.4 - Solidification data a liquid embolic prototype (n=3).....	59
Table 2.5 - Rheology data of a liquid embolic prototype in DMSO at 37 °C (n=216).....	62
Table 2.6 - Rheology data of the solidification process of the liquid embolic prototype at 37 °C (n=1). ....	63
Table 2.7 - Volume measurement device calibration data (n=3). ....	64
Table 2.8 - Fill volume data for a liquid embolic prototype (n=3). ....	66
Table 2.9 - Fragmentation data for liquid embolic prototypes (500 µm scale).....	68
Table 2.10 - Particulate generation data for liquid embolic prototypes (200 µm scale). ....	69
Table 2.11 - Solid content measurements over time for a liquid embolic prototype (n=3). ..	72
Table 3.1 - HA phantom microCT data (imaging cross-sections, n=198). ....	81
Table 3.2 - Data for sample delivery of a liquid embolic prototype performed under flow and no flow of PBS (n=3).....	85
Table 3.3 - Images of a liquid embolic prototype delivered under flow and no flow of PBS (n=3).....	86
Table 3.4 - Radiopacity data for manual injections performed under flow and no flow of PBS with thresholding methods; manual, automatic, adaptive (imaging cross-sections, n=198)..	89
Table 3.5 - Radiopacity data for manual injections performed under flow and no flow of PBS analysed over short and long VOIs (imaging cross-sections; n=198 and 792, respectively).	91
Table 3.6 - Porosity data for manual injections performed under flow and no flow of PBS analysed over short and long VOIs (imaging cross-sections; n=198 and 792, respectively).	91
Table 3.7 - Radiopacity data of HA phantoms used for calibration (n=396).....	92

---

Table 3.8 - Precipitate length data for samples delivered by continuous syringe pump injection method under flow and no flow of PBS (n=1).....	93
Table 3.9 - Precipitate length data for samples delivered by pulsed syringe pump injection method under flow and no flow of PBS (syringe pump injection rate of 0.1 mL min <sup>-1</sup> )(n=1). .....	94
Table 3.10 - Radiopacity and porosity data for continuous syringe pump injections performed under PBS flow and no flow (imaging cross-sections, n=198).....	95
Table 3.11 - X-ray shadowgraphs and reconstructed 2D cross-sectional images of continuous syringe pump injected liquid embolic sample prepared under flow of PBS.....	96
Table 3.12 - X-ray shadowgraphs and reconstructed 2D cross-sectional images of continuous syringe pump injected liquid embolic sample prepared under no flow of PBS.....	97
Table 3.13 - Radiopacity and porosity data for pulsed syringe pump injections performed under PBS flow and no flow (imaging cross-sections, n=198).....	98
Table 3.14 - X-ray shadowgraphs and reconstructed 2D cross-sectional images of pulsed syringe pump injected liquid embolic sample prepared under PBS flow (0.1 mL min <sup>-1</sup> injection rates).....	99
Table 3.15 - X-ray shadowgraphs and reconstructed 2D cross-sectional images of pulsed syringe pump injected liquid embolic sample prepared under no flow of PBS (0.1 mL min <sup>-1</sup> injection rates).....	100
Table 3.16 - Radiopacity and porosity data across length of liquid embolic sample prepared by continuous syringe pump injection (0.1 mL min <sup>-1</sup> ) under PBS flow (imaging cross-sections, n=198).....	102
Table 3.17 - X-ray shadowgraphs and reconstructed 2D cross-sectional images across length of liquid embolic sample prepared by continuous syringe pump injection (0.1 mL min <sup>-1</sup> ) under PBS flow.....	103

---

Table 3.18 - Radiopacity and porosity data across length of liquid embolic sample prepared by pulsed syringe pump injection ( $0.1 \text{ mL min}^{-1}$ ) with 30 sec intervals under PBS flow and no flow (imaging cross-sections, n=198).....	104
Table 3.19 - X-ray shadowgraphs and reconstructed 2D cross-sectional images across length of liquid embolic sample prepared by pulsed syringe pump injection ( $0.1 \text{ mL min}^{-1}$ ) with 30 sec intervals under PBS flow. ....	105
Table 3.20 - X-ray shadowgraphs and reconstructed 2D cross-sectional images across length of liquid embolic sample prepared by pulsed syringe pump injection ( $0.1 \text{ mL min}^{-1}$ ) with 30 sec intervals without PBS flow. ....	106
Table 4.1 - Reaction quantities used in the synthesis of iodinated PVA samples.....	115
Table 4.2 – Formulations of liquid embolic prototypes.....	116
Table 4.3 - I-PVA theoretical and determined iodine contents by elemental analysis (n=2). .....	118
Table 4.4 - Water solubility data of I-PVA samples (n=3 for I-PVA samples and n=15 for PVA control).....	119
Table 4.5 - Data of I-PVA precipitation test in PBS at $37 \text{ }^\circ\text{C}$ (n=1).....	121
Table 4.6 - Results of precipitation test of I-PVA synthesised at 0.25 equivalents of TIBA under varying flow rates of PBS (n=1). ....	123
Table 4.7 - Results of precipitation in vascular flow model using varying injection techniques (n=1).....	124
Table 4.8 - Results of precipitation in vascular flow model at different delivery sites (n=1). .....	125
Table 4.9 - Results of long-term solution stability of liquid embolic prototypes 1 year after formulation in DMSO (n=1). ....	127
Table 4.10 - Delivery results of liquid embolic prototypes over a range of TIBA equivalents and DMSO concentrations (n=1). ....	130

---

---

Table 4.11 - Delivery results of liquid embolic prototypes over a range of polymer molecular weights at 0.1 and 0.25 equivalents of TIBA (n=1).....	131
Table 4.12 - Delivery results of Onyx <sup>®</sup> 18 (n=1).....	135
Table 4.13 - Solidification data of liquid embolic prototypes over a range of TIBA equivalents and concentrations in DMSO (n=1).....	135
Table 4.14 - Solidification data of liquid embolic prototypes over a range of polymer molecular weights at 0.1 and 0.25 equivalents of TIBA (n=1).....	136
Table 4.15 - Solidification data of Onyx <sup>®</sup> 18 (n=1).....	141
Table 4.16 - Rheology data of liquid embolic prototypes in liquid states for a range of TIBA equivalents, polymer molecular weights and concentrations in DMSO (n=1). ....	144
Table 4.17 - Rheology data of liquid embolic prototypes in precipitate states for a range of TIBA equivalents, polymer molecular weights and concentrations in DMSO (n=1). ....	144
Table 4.18 - Fill volume data of liquid embolic prototypes over a range of TIBA equivalents and concentrations in DMSO (n=3).....	150
Table 4.19 - Fill volume data of liquid embolic prototypes over a range of polymer molecular weights at 0.1 and 0.25 equivalents of TIBA (n=3).....	151
Table 4.20 - Fill volume data of Onyx <sup>®</sup> 18 (n=1).....	153
Table 4.21 - Fragmentation data of liquid embolic prototypes over a range of TIBA equivalents and concentrations in DMSO (n=3).....	154
Table 4.22 - Particulate generation data of liquid embolic prototypes over a range of TIBA equivalents and concentrations in DMSO (n=3).....	155
Table 4.23 - Fragmentation data for liquid embolic prototypes over a range of polymer molecular weights at 0.1 and 0.25 equivalents of TIBA (n=3).....	155
Table 4.24 - Particulate generation data for liquid embolic prototypes over a range of polymer molecular weights at 0.1 and 0.25 equivalents of TIBA (n=3).....	155
Table 4.25 - Fragmentation data for Onyx <sup>®</sup> 18 (n=3).....	159
Table 4.26 - Particulate generation data for Onyx <sup>®</sup> 18 (n=3). ....	159

---



---

Table 4.27 - Solid content data for liquid embolic prototypes of different TIBA equivalents (n=3).....	160
Table 4.28 - Residual reactant traces as determined from <sup>1</sup> H NMR spectra of liquid embolic prototypes (n=1).....	163
Table 4.29 - Results of molecular weights determined by SEC for liquid embolic prototypes (n=1).....	164
Table 4.30 - MicroCT data for I-PVA samples over a range of TIBA equivalents and DMSO concentrations synthesised using 67 kDa PVA (imaging cross-sections, n=198). ....	165
Table 4.31 - MicroCT data for I-PVA samples over a range of polymer molecular weights at 0.1 and 0.25 equivalents of TIBA (imaging cross-sections, n=198).....	165
Table 4.32 - Comparison of radiopacity values of liquid embolic prototypes against Omnipaque™ 180 (imaging cross-sections, n=198). ....	168
Table 4.33 - Radiopacity data of solidified Onyx® (imaging cross-sections, n=198).....	169
Table 4.34 - Porosity data for I-PVA samples over a range of TIBA equivalents and DMSO concentrations synthesised using 67 kDa PVA (imaging cross-sections, n=198). ....	170
Table 4.35 - Porosity data for I-PVA samples over a range of polymer molecular weights at 0.1 and 0.25 equivalents of TIBA (imaging cross-sections, n=198).....	170
Table 4.36 - Porosity data of Onyx® 18 and Onyx® 34 (imaging cross-sections, n=198). ..	172
Table 5.1 - Reaction quantities used in the modification of PVA with S-TIBA and TIBA.	178
Table 5.2 - Reaction quantities used in the modification of PVA with IBA and TIBA.....	179
Table 5.3 - Formulations of liquid embolic prototypes modified with combinations of S-TIBA, IBA and TIBA.....	180
Table 5.4 - Liquid embolic samples synthesised using S-TIBA and TIBA theoretical and determined iodine contents by elemental analysis (n=2). ....	182
Table 5.5 - Liquid embolic samples synthesised using IBA and TIBA theoretical and determined iodine contents by elemental analysis (n=2). ....	183

---

---

Table 5.6 - Results of long-term solution stability of liquid embolic prototypes 6-12 months after formulation in DMSO (n=1).....	184
Table 5.7 - Delivery results of liquid embolic prototypes prepared using combinations of S-TIBA and TIBA (n=1). .....	185
Table 5.8 - Delivery results of liquid embolic prototypes prepared using combinations of IBA and TIBA (n=1).....	185
Table 5.9 - Solidification data of liquid embolic prototypes prepared using combinations of S-TIBA, IBA and TIBA (n=1). .....	189
Table 5.10 - Rheology data of precipitation process for liquid embolic prototypes prepared combinations of S-TIBA, IBA and TIBA (n=1). .....	193
Table 5.11 - Fill volume data of liquid embolic prototypes prepared using combinations of S-TIBA and TIBA (n=3). .....	197
Table 5.12 - Fill volume data of liquid embolic prototypes prepared using combinations of IBA and TIBA (n=3).....	198
Table 5.13 - Fragmentation and particulate generation of liquid embolic prototypes prepared using combinations of S-TIBA and TIBA (n=3). .....	200
Table 5.14 - Fragmentation and particulate generation of liquid embolic prototypes prepared using combinations of IBA and TIBA (n=3). .....	200
Table 5.15 - Residual reactant traces as determined from <sup>1</sup> H NMR spectra of liquid embolic prototypes (n=1).....	202
Table 5.16 - Results of molecular weights determined by SEC for liquid embolic prototypes (n=1).....	203
Table 5.17 - MicroCT data for liquid embolic samples prepared using combinations of S-TIBA, IBA and TIBA (imaging cross-sections, n=198).....	204
Table 5.18 - Comparison of radiopacity values of liquid embolic prototypes against Omnipaque™ 180 (imaging cross-sections, n=198). .....	206

---

---

Table 5.19 - Porosity data for liquid embolic prototypes prepared using combinations of S-TIBA, IBA and TIBA (imaging cross-sections, n=198).....	207
Table 6.1 - Experimental details of PVA macromonomer synthesis.....	214
Table 6.2 - Experimental details of I-PVA macromonomer synthesis.....	215
Table 6.3 - Reaction quantities used in the modification of PVA macromonomer with hydrophilic pendent groups.....	216
Table 6.4 - Results of PVA macromonomer gelation test using REDOX initiator at room temperature (n=1).....	224
Table 6.5 - Results of PVA macromonomer gelation test using REDOX initiator at 37 °C (n=1).....	225
Table 6.6 - Formulation of PVA macromonomer prototypes.....	227
Table 6.7 - Gelation results of PVA macromonomers synthesised using 0.01 equivalents of TIBA at 37 °C.....	228
Table 6.8 - Gelation results of PVA macromonomers synthesised using 0.1 equivalents of TIBA at 37 °C.....	228
Table 6.9 - Water solubility results of PVA macromonomers (n=3).....	230
Table 6.10 - Water solubility results of I-PVA macromonomers synthesised using 0.01 equivalents of TIBA (n=3).....	230
Table 6.11 - Water solubility results of I-PVA macromonomers synthesised using 0.1 equivalents of TIBA (n=3).....	231
Table 6.12 - Hydrophilic groups used in the modification of PVA macromonomers.....	235
Table 6.13 - Water solubility results of modified PVA macromonomers (n=3).....	236
Table 6.14 - Solubility results of modified PVA macromonomers in PBS (n=3 where sufficient sample).....	237
Table 6.15 - Solubility results of modified PVA macromonomers in DMSO (n=1).....	238

---

## List of Schemes

Scheme 4.1 - Synthesis of 2,3,5-triodobenzaldehyde (TIBA) using T3P.....	117
Scheme 4.2 - Synthesis of 2,3,5-triodobenzaldehyde (TIBA) using oxalyl chloride. ....	117
Scheme 4.3 - Synthesis of iodinated PVA (I-PVA).....	118
Scheme 5.1 - Synthesis of 3-(2,4,6-triiodo-5-formylphenoxy)-1-propanesulfonic acid (S-TIBA).....	180
Scheme 5.2 - Modification of PVA with varying ratios of S-TIBA and TIBA. ....	181
Scheme 5.3 - Modification of PVA with varying ratios of IBA and TIBA. ....	182
Scheme 6.1 - Gelation of radiopaque PVA macromonomer.....	211
Scheme 6.2 - Gelation of radiopaque PVA on contact with Ca <sup>2+</sup> ions.....	212
Scheme 6.3 - Synthesis of N-acryloyl aminoacetaldehyde dimethyl acetal (NAAADA)....	221
Scheme 6.4 - Synthesis of PVA macromonomer.....	221
Scheme 6.5 - Synthesis of PVA gel using azo initiator. ....	222
Scheme 6.6 - Synthesis of PVA gel using redox system. ....	223
Scheme 6.7 - Initial synthetic route for the preparation of I-PVA macromonomer.....	226
Scheme 6.8 - Preferred synthetic route for the preparation of PVA macromonomer.....	226
Scheme 6.9 - Incorporation of hydrophilic groups onto PVA macromonomer. ....	236
Scheme 6.10 - Modification of PVA with S-TIBA. ....	239

## List of Equations

Equation 2.1 - Standard deviation equation for samples where n>3.....	46
Equation 2.2 - Standard error of the mean equation for samples where n≤3.....	46
Equation 6.1 - Radical formation in redox driven superoxide Fenton reaction. ....	219

---

## List of Abbreviations

BPH	Benign prostatic hyperplasia
CT	Computed tomography
DMF	Dimethylformamide
DMSO	Dimethyl sulfoxide
GPC	Gel Permeation Chromatography
h	Hours
HCC	Hepatocellular carcinoma
HU	Hounsfield units
IBA	3-iodobenzaldehyde
mCRC	Malignant colorectal cancer metastasised to the liver
NMR	Nuclear Magnetic Resonance
PBS	Phosphate buffered saline
PTFE	Polytetrafluoroethylene
PVA	Poly(vinyl alcohol)
RI	Refractive Index
s	Seconds
SEC	Size Exclusion Chromatography
SEM	Scanning Electron Microscopy
S-TIBA	3-(2,4,6-triiodo-5-formylphenoxy)-1-propanesulfonic acid
TAE	Transarterial embolization
THF	Tetrahydrofuran
TIBA	2,3,5-triiodobenzaldehyde
VOI	Volume of Interest
w/w%	Weight/weight percent

---



# Chapter One

## 1. Introduction

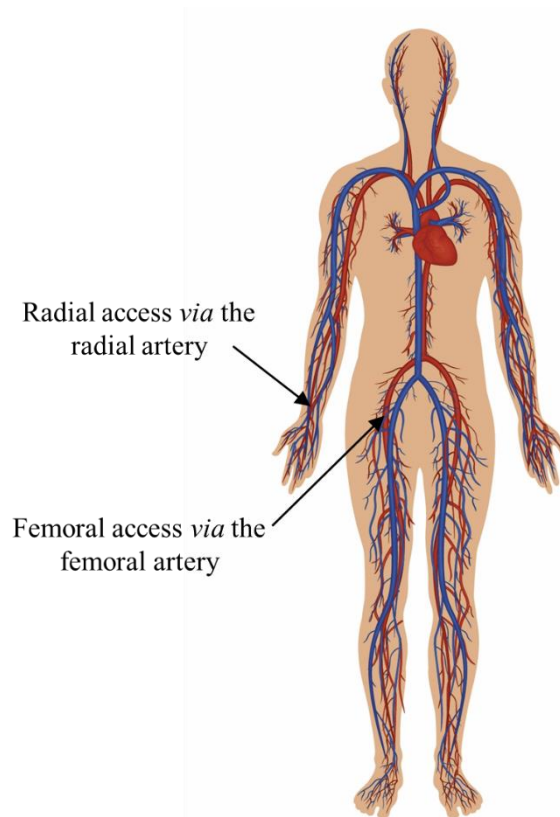


## **1.1. Therapeutic Embolisation**

Therapeutic embolisation is a minimally invasive medical procedure involving the insertion of an embolic material to selectively occlude blood vessels. The occlusion process involves mechanically blocking the blood flow through the vessel. Following delivery of the embolic material, the initiation of thrombus formation around the delivered embolic material further hinders the blood flow for more efficient occlusion of the blood vessel.<sup>1</sup>

The selective occlusion of blood vessels is used in the treatment of a range of vascular diseases including arteriovenous malformations (AVMs, an abnormal entanglement of poorly formed blood vessels with a higher bleed rate than normal blood vessels),<sup>2</sup> aneurysms (localised swelling of the wall of a blood vessel which poses the risk of rupture) and haemorrhaging (loss of blood from a ruptured blood vessel).<sup>3</sup> In oncological diseases, embolisation is commonly used in the treatment of tumours, particularly in late stage cancers in which the disease is too far progressed for surgical resection<sup>4</sup> or in cases of highly vascularised tumours in which embolisation may aid surgical removal.<sup>5</sup>

The procedure is predominately carried out using a microcatheter which is fed into the vasculature either at the groin for femoral access or at the wrist for radial access (Figure 1.1). The microcatheter is guided through the vasculature until positioned at the target site of embolic material delivery. The location of the microcatheter tip is often easily locatable on X-ray angiograms performed during the placement due to the presence of distinctive radiopaque markers embedded at the microcatheter tip which are opaque to X-rays enabling their location to be visualised. An injection of contrast agent is also used to confirm the microcatheter placement and provides a roadmap of the vasculature to be treated during the procedure. Accessing the targeted blood vessels by microcatheter insertion circumvents the need for open surgery thereby reducing recovery time and patient discomfort. There is also the additional advantage of being able to access vasculature which might otherwise be difficult to treat using surgical methods, such as brain aneurysms.<sup>6</sup>



*Figure 1.1 - Diagram of femoral and radial access points for catheterisation.*

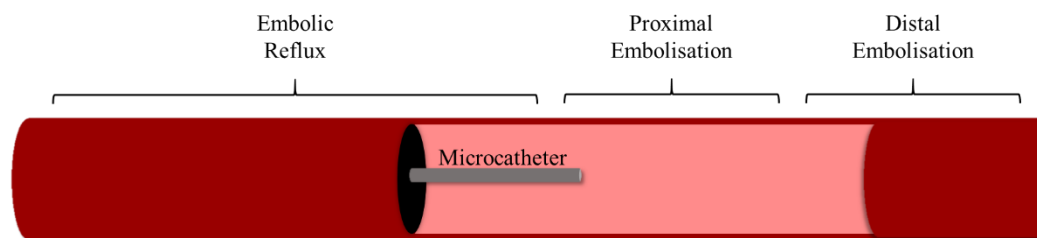
There are a variety of commercially available embolic devices which fall into three main treatment categories. The first, mechanical devices, are commonly used to treat medium-large sized blood vessels whereas particulates, the second category, are used for the much smaller terminal arterioles. Finally, liquid agents, including sclerosing agents, are able to penetrate much further to reach the capillary vascular bed and ultimately result in tissue infarction as a result of a lack of oxygen supplying the tissue due to the interruption of the blood supply.

The desired clinical outcome will dictate which embolic material is ideal for use in the procedure. A choice needs to be made as to whether permanent or temporary occlusion of the vessel is required. Hence, the interventional radiologists and neuroradiologists performing the procedures must have a detailed understanding of the different embolic classes along with the subtle differences between materials of the same class in order to tailor the procedure to particular treatments and individual cases. The choice of embolic agent can be further complicated as many embolic devices can be teamed with therapeutic drugs, such as

chemotherapeutic agents to provide local drug delivery to tumour sites and hence reduce the overall systemic toxicity. Therefore, if the embolic agent is to be used with a therapeutic drug then consideration must be given to select a suitable combination. The wide range of treatment options available highlights the need to choose the appropriate treatment on a case-by-case basis as the optimal choice will be ultimately dependent on the condition being treated, location and desired clinical outcome.

### ***1.1.1. Mechanical Devices***

Mechanical devices are permanent embolic materials ideal for treating high flow and large diameter blood vessels, such as arteries. The mechanical devices typically used include coils and balloons which are marketed in a range of shapes and sizes to tailor treatment to the blood vessels being targeted. The size of the targeted blood vessels needs to be taken into account so that the appropriately sized mechanical device can be selected. Consideration must also be given as to whether the vessel is tapering or of similar diameter for the length being occluded. If the device is too small for the vessel, then this will lead to unintended distal embolisation downstream of the target site. Whereas devices which are too large will result in proximal embolisation upstream of the targeted embolisation site and may prevent the device from reaching its final shape further reducing the occlusion efficiency (Figure 1.2).



*Figure 1.2 - Diagram representing areas of proximal embolisation, distal embolisation and embolic reflux relative to the placement of the microcatheter within a blood vessel.*

### *1.1.1.1. Coils*

Coils are mechanical devices consisting of metallic wires which are tightly coiled into a variety of shapes. The large variety of different shapes and sizes of coil devices available on the market means that a suitable device can be selected based on the type and location of blood vessels to be treated (Figure 1.3). During the embolisation procedure, the device is misshapen by delivery through a microcatheter and returns to its original shape on entering the vasculature. Coils can be deployed from the microcatheter by pushable, detachable or injectable mechanisms to give precise positioning of the material. Dacron<sup>®</sup> fibres are often embedded into the steel coil to promote blood clotting throughout the coil to provide effective embolisation of the blood vessel.<sup>7</sup> Also, due to the metallic composition of the coils, the devices possess inherent radiopacity meaning the coil devices can be easily visualised by X-ray imaging methods allowing detection both during and after the embolisation procedure.

Hydrogel-coated coils are also available, HydroSoft<sup>®</sup> and HydroFrame<sup>®</sup> embolic systems marketed by MicroVention rely less on thrombus formation to achieve occlusion due to the ability of the hydrogel to swell on contact with the fluid in the blood vessel. The systems are based on platinum coils of helical and coiled shapes coated with a crosslinked polymeric material which have a high capacity for absorbing water. This allows the gel to fill any voids between the embolic coils and the walls of the blood vessel providing a more effective occlusion. The higher packing density achieved using the hydrogel coated coil systems reduces the reliance on thrombosis formation to form blood clots to complete the occlusion which often recanalises if unstable thrombosis which results in the restoration of the previously interrupted blood supply. Hence, the use of hydrogel coated coil systems reduces the rate of recanalisation particularly in the treatment of aneurysms.<sup>8</sup>

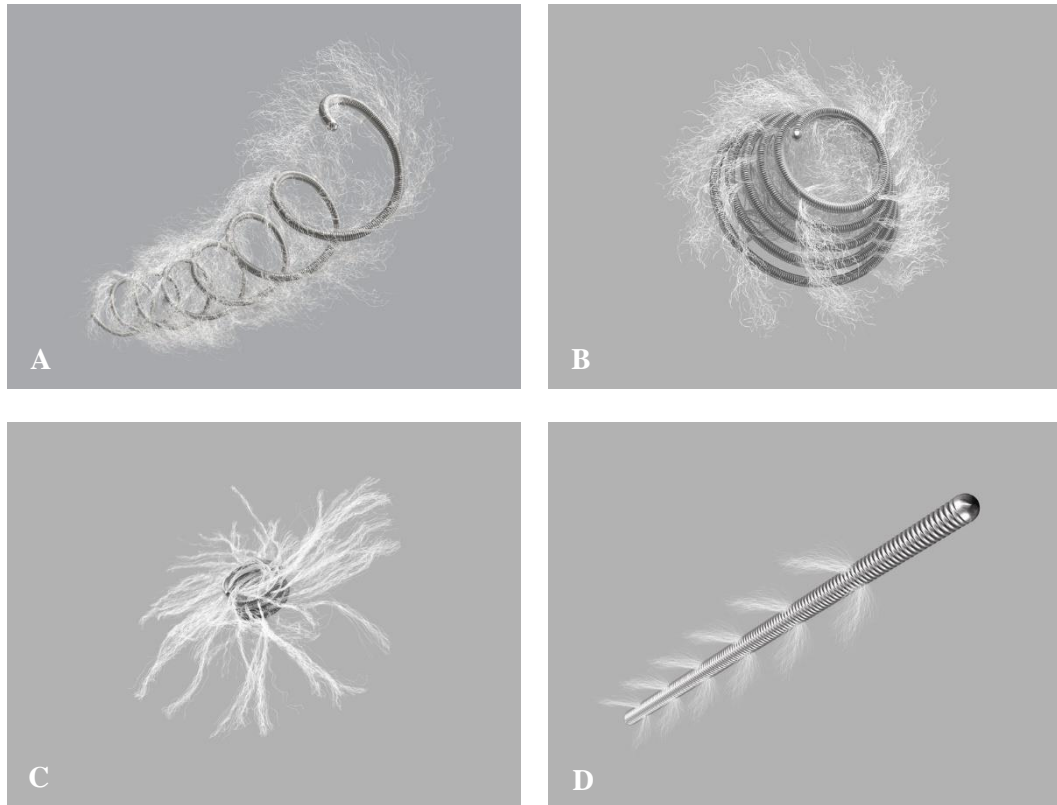


Figure 1.3 - Embolic coils marketed by Cook Medical LLC.; (A) Nester<sup>®</sup>, (B) Torando<sup>®</sup>, (C) MReye<sup>®</sup>, (D) Hilal Straight<sup>™</sup>.

### 1.1.1.2. **Balloons**

Detachable balloons are another commonly used mechanical device, primarily used to treat neurological diseases.<sup>9</sup> These devices provide an advantage over coils in the treatment of particular blood vessels as they can expand when inflated with contrast agent to rapidly occlude vessels of much larger diameter than the microcatheter being used to deliver the device (Figure 1.4). This makes them ideal for the treatment of arteries with high flow rates. Also, detachable balloons have the advantage that they can be repeatedly repositioned to enable their optimal placement. Furthermore, they can be floated out to distal locations allowing the occlusion of otherwise difficult to reach blood vessels, such as tortuous vessels with many twists and bends which would otherwise prevent the passage of a microcatheter.<sup>10</sup> One limitation of detachable balloons is that the balloon materials typically used are composed either of silicone or latex and hence do not possess inherent radiopacity. Therefore, the devices

must be used along with a contrast agent to enable visualisation during the procedure. However, if a compatible contrast agent is not used then the devices pose the risk of deflation or rupture during the delivery procedure.<sup>11</sup> Early deflation can also be a problem due to damage of the balloon during the detachment process.<sup>12</sup>



*Figure 1.4 - Diagram of an inflated balloon delivered into the vasculature via a microcatheter.*

### ***1.1.2. Particulates & Spheres***

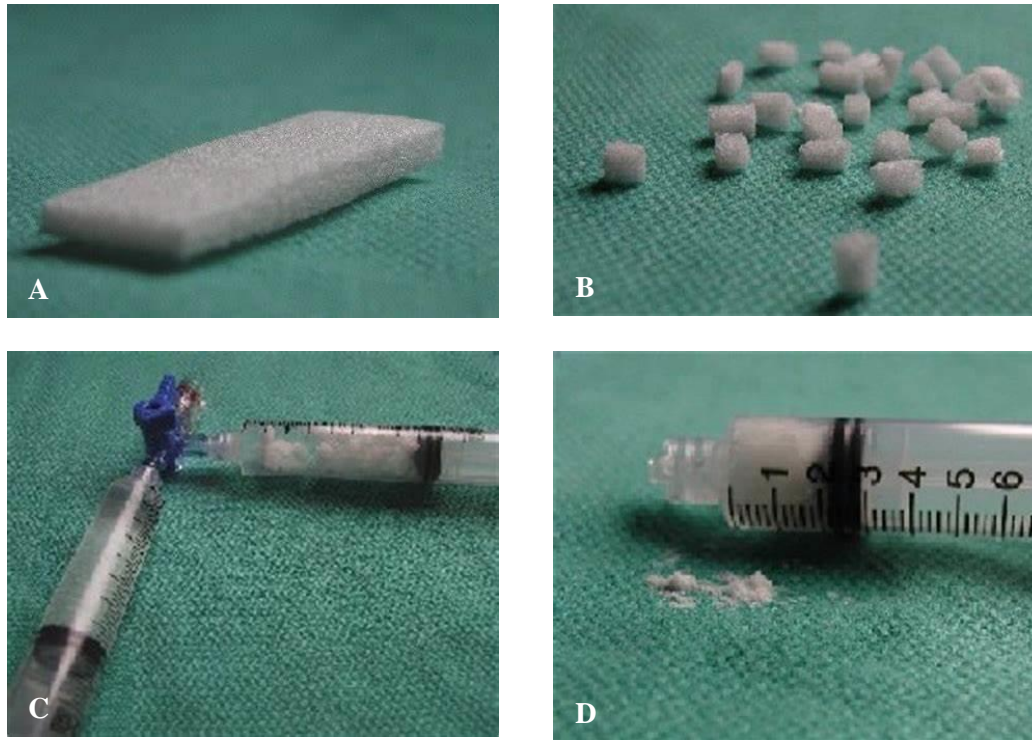
Embolic materials used for treating smaller blood vessels than those treated by coils and balloons include the class of particulates consisting of irregular shaped particles or microspheres over a range of sizes. These embolic agents are commonly used to treat haemorrhaging and aneurysms.<sup>13</sup> The materials are delivered *via* the same method as mechanical devices using a microcatheter fed through the vasculature to the intended treatment site. The size of particulates used must be carefully selected in order to occlude the desired blood vessel diameter to be treated. This minimises the risk of proximal or distal embolisation.

Due to the small particle sizes used for this class of embolic materials, there is a higher risk of distal embolisation. Hence, particulates are not suitable for the embolisation of large arteriovenous vessels and high flow rate arteries. The consequence of distal embolisation could lead to fatal complications if the materials embolise within important organs, such as the lungs, leading to organ ischemia by the interruption of the arterial blood supply which if left untreated may result in tissue death.<sup>14,15</sup> Therefore, precautions must be taken during the administration of these materials in order to prevent distal embolisation outside of the target area being treated.

### ***1.1.2.1. Particles***

Commonly used materials in embolisation with particles include PVA and gelatin. Contour™ PVA Embolisation Particles, marketed by Boston Scientific, provide a tool for permanent embolisation commonly used in the treatment of AVMs.<sup>16</sup> Whereas, Gelfoam®, marketed by Pfizer, offers an off-label tool for temporary embolisation which is particularly useful in cases of vascular trauma.<sup>17</sup> In these cases the temporary embolic material is used to control the bleeding with the potential for recanalisation of the blood vessel following bio-absorption of gelatin to restore blood flow through the vessel following treatment of the trauma with larger diameter blood vessels undergoing higher rates of recanalisation in comparison to small blood vessels.<sup>18</sup>

These materials are often provided as sheets which can be manually broken up prior to the procedure to give irregular shaped particles or supplied as ready to use particles which have often been sieved within a known size range (Figure 1.5). The particles are administered with contrast agent during the procedure to aid the visualisation of the delivery using real-time fluoroscopy.<sup>19</sup> Once injected into blood vessels, the particles aggregate and swell on hydration with blood allowing the material to form a cast of the surrounding vessel structure to provide effective occlusion of the blood vessels being treated. The end-point of the embolisation process is inferred when the flow of the particle suspension becomes sluggish indicating suitable penetration of the vasculature. Complete occlusion is achieved once thrombus formation occurs as the irregular shapes of the particles blood flow is not completely blocked by the embolic agent alone. Thrombus formation is therefore required to fill the voids between the particles to occlude the flow through the vessel.



*Figure 1.5 - Preparation of Gelfoam® particles; (A) Material supplied as a foam sheet, (B) Manually cutting of sheet into irregular shaped particles, (C) Mixing of particles with contrast agent to create slurry, (D) Thick slurry ready for injection (images from Angiofellow educational resources).*

The irregularity of particle shapes and sizes can however cause problems with microcatheter clogging during delivery.<sup>20</sup> The occurrence of microcatheter blockage requires a new microcatheter to be placed which can result in damage to vessel walls from the mechanical action of removal and insertion of several microcatheters. Hence, the occurrence of microcatheter clogging leads to an increase in procedural time, patient risk and cost. The tendency of particles to aggregate, along with their irregular shapes and sizes, can also lead to more proximal embolisation than intended.<sup>21</sup> Also the variability of the particles shapes and sizes, with large variation seen between operators,<sup>22</sup> often gives unreliable levels of occlusion.<sup>23,24</sup> The process of preparing the embolic prior to the procedure is also much more time consuming than the preparation of other embolic materials. The problem of aggregation can be alleviated by optimal suspension of the particles in contrast agent, lower concentrations and slower injection of the suspension mixture. However, the expertise of delivery will be highly dependent on the experience of the physician performing the procedure.



### ***1.1.2.2. Microspheres***

Microspheres are commonly used in the treatment of hypervascularised tumours in a process known as transarterial embolisation (TAE). The procedure is an effective treatment for kidney tumours,<sup>25</sup> liver tumours<sup>26,27</sup> and uterine fibroids which present as benign growths of muscle within the uterus.<sup>28</sup> The procedure involves guiding the microcatheter through the common femoral artery and placement within the blood vessels feeding the tumour. Once the microcatheter is in place, the microspheres are injected often in a suspension of contrast agent to provide a surrogate marker for the position of the microspheres as visualised by real-time fluoroscopy during the procedure (Figure 1.6). Depending on the type of microspheres used, the microspheres injected cover a range of sizes which requires a steady injection to prevent segmentation of sizes. A fast injection of microspheres can result in the occurrence of a false endpoint in which the microspheres temporarily occlude the vessel until they are dislodged by the blood flow leading to less control over the final end-point of the microspheres. A targeted delivery of microspheres interrupts the blood supply and starves the tumour of nutrients limiting tumour growth, potentially reducing the tumour size. Hence, TAE provides a useful tool to limit tumour progression.

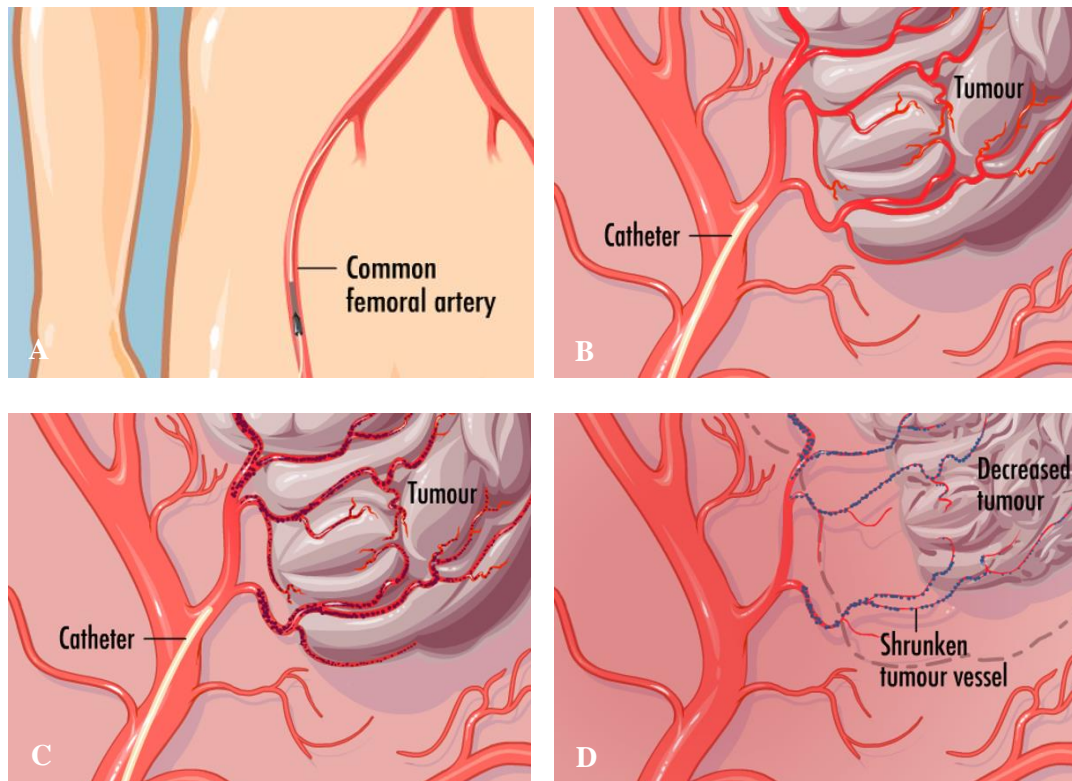


Figure 1.6 - Transarterial embolisation process of a hypervascularised tumour; (A) Insertion of microcatheter into the femoral artery, (B) Placement of microcatheter tip in blood vessels supplying the tumour, (C) Embolisation of the tumour by delivery of microspheres with distal penetration, (D) Reduced tumour size as a result of microsphere occlusion within the feeding blood vessels (images courtesy of Biocompatibles UK Ltd.).

This procedure is common practice for the treatment of the liver cancer hepatocellular carcinoma (HCC) particularly in the intermediate stages of the disease.<sup>29</sup> At the intermediate stage of HCC, the tumours are often too far progressed to be treated by curative methods, such as surgical resection. Liver transplant is a viable option however due to the long transplant list waiting times patients are at an increased risk of further tumour progression whilst waiting for a suitable organ donor. The TAE procedure can be used as a liver transplant bridge therapy.<sup>30</sup> In these cases, embolisation is used to reduce or halt tumour growth whilst a patient is on the transplant waiting list or to reduce tumour size to meet the liver transplant waiting list criteria. Liver transplant bridge therapy offers the opportunity for reduced waiting list dropouts, improved patient outcomes and halted tumour progression.<sup>31</sup>

There are a number of embolic microspheres currently available on the market suitable for the TAE procedure (Table 1.1). The varying properties of the microspheres allow the appropriate embolic material to be selected depending on the disease being treated and the desired clinical

outcome. For example, biodegradable microspheres are utilised in the treatment of gastrointestinal and trauma bleeding in which transient embolisation is required and in the treatments of uterine leiomyomas in which temporary occlusion is beneficial in preserving patient fertility by permitting recanalisation to the embolised vessels.<sup>32</sup> The potential to drug load microspheres such as DC Bead<sup>®</sup> has clinical benefit in the treatment of HCC when loaded with chemotherapeutic agents such as doxorubicin or irinotecan.<sup>33</sup> The use of chemotherapeutic drug in combination with the embolic microspheres in a procedure known as transarterial chemoembolization (TACE) allows for targeted drug delivery at the embolised site thereby reducing the overall systemic toxicity of the chemotherapeutic drug and providing a sustained release of drug at the tumour site. Radiopaque microspheres have the additional advantage of being easily locatable in follow-up imaging.<sup>34</sup> This provides information of whether sufficient volumes of microspheres have been delivered to the targeted vasculature and can also identify any areas of off-target embolisation.<sup>35</sup> Also, during the procedure the precise location of the delivered microspheres is known by real-time fluoroscopy which avoids relying on visualisation of the contrast agent used to create the microsphere suspension which only acts as a surrogate marker for the microspheres and assumes no loss of suspension.

Table 1.1 - Characteristics of commercially available microspheres (data obtained from manufacturers data sheets).

Microsphere Tradename	Manufacturer	Size Ranges	Permanent or Temporary Occlusion	Drug-loadable	Radiopaque	Indications
<b>BeadBlock®</b>	Biocompatibles UK Ltd, a BTG International group company	100-300 µm 300-500 µm 500-700 µm 700-900 µm 900-1200 µm	Permanent	No	No	Hypervascularised tumours including uterine fibroids, AVMs, symptomatic benign prostatic hyperplasia
<b>DC Bead® (LC Bead® in USA)</b>	Biocompatibles UK Ltd, a BTG International group company	70-150 µm 100-300 µm 300-500 µm 500-700 µm	Permanent	Yes - Doxorubicin/ Irinotecan	No	Malignant hypervascularised tumours in the liver, HCC, metastatic colorectal cancer
<b>DC Bead LUMI™ (LC Bead™ LUMI in USA)</b>	Biocompatibles UK Ltd, a BTG International group company	70-150 µm 100-300 µm	Permanent	Yes - Doxorubicin/ Irinotecan	Yes - CT, CBCT and fluoroscopy	Non-malignant hypervascularised tumours, AVMs, malignant hypervascularised tumours in the liver, HCC, metastatic colorectal cancer
<b>EmboGold®</b>	Merit Medical Systems	40-120 µm 100-300 µm 300-500 µm 500-700 µm 700-900 µm 900-1200 µm	Permanent	No	No	Hypervascularised tumours including uterine fibroids and meningiomas, AVMs, benign prostatic hyperplasia
<b>Embosphere®</b>	Merit Medical Systems	50-100 µm 40-120 µm 100-300 µm 300-500 µm 500-700 µm 700-900 µm 900-1200 µm	Permanent	No	No	Hypervascularised tumours including symptomatic uterine fibroids, AVMs, symptomatic benign prostatic hyperplasia

<b>Microsphere Tradename</b>	<b>Manufacturer</b>	<b>Size Ranges</b>	<b>Permanent or Temporary Occlusion</b>	<b>Drug-loadable</b>	<b>Radiopaque</b>	<b>Indications</b>
<b>Embozene™</b>	Varian Medical Systems Inc.	40 ± 10 µm 70 ± 15 µm 100 ± 25 µm 250 ± 50 µm 400 ± 50 µm 500 ± 50 µm 700 ± 50 µm 900 ± 75 µm 1100 ± 75 µm 1300 ± 75 µm	Permanent	No	No	AVMs, hypervascularised tumours including uterine fibroids, symptomatic benign prostatic hyperplasia
<b>Gel-Bead™</b>	Medtronic	100-300 µm 300-500 µm 500-700 µm 700-1000 µm	Temporary	No	No	Hypervascularised tumours
<b>HepaSphere®</b>	Merit Medical Systems	30-60 µm (expands to 120-240 µm) 50-100 µm (expands to 200-400µm) 150-200 µm (expands to 600-800 µm)	Permanent	Yes - Doxorubicin/ Irinotecan	No	Tumours metastasised to the liver, HCC, metastatic colorectal cancer

<b>Microsphere Tradename</b>	<b>Manufacturer</b>	<b>Size Ranges</b>	<b>Permanent or Temporary Occlusion</b>	<b>Drug-loadable</b>	<b>Radiopaque</b>	<b>Indications</b>
<b>HydroPearl®</b>	Terumo Corporation	75 ± 30 µm 200 ± 75 µm 400 ± 75 µm 600 ± 75 µm 800 ± 75 µm 1100 ± 75 µm	Permanent	No	No	Hypervascularised tumours including uterine fibroids, HCC, benign prostatic hyperplasia, peripheral AVMs, tumours of the neck, torso and skeletal system, bleeding, trauma and pre-operative reduction of bleeding
<b>LifePearl®</b>	Terumo Corporation	100 ± 25 µm 200 ± 50 µm 400 ± 50 µm	Permanent	Yes - Doxorubicin/ Irinotecan/ Idarubicin/ Epirubicin	No	Hypervascularised tumours, AVMs
<b>Tandem™ (Oncozene™ in USA)</b>	Varian Medical Systems Inc.	40 ± 10 µm 70 ± 15 µm 100 ± 25 µm	Permanent	No	No	AVMs, hypervascularised tumours, HCC
<b>ResMic®</b>	Guerbet	50-250 µm 100-300 µm 300-500 µm 500-700 µm 700-900 µm 900-1200 µm	Temporary	Yes – Doxorubicin, Irinotecan, Bevacizumab and Sunitinib	No	Benign tumours including uterine fibroids, haemostasis, hypervascularised tumours of the liver and other organs

---

<b>Microsphere Tradename</b>	<b>Manufacturer</b>	<b>Size Ranges</b>	<b>Permanent or Temporary Occlusion</b>	<b>Drug-loadable</b>	<b>Radiopaque</b>	<b>Indications</b>
<b>X-Spheres™</b>	Rembrant Medical	400-600 µm 600-710 µm 710-850 µm	Permanent	No	CT, CBCT and fluoroscopy	Uterine fibroids

---

Some microspheres emerging onto the market include the resorbable OptiSphere™ by Medtronic Inc. and the imageable Easi-Vue™ by ABK. OptiSphere™ consists of gelatin microspheres crosslinked with glutaraldehyde to provide controlled degradation of the microspheres after implantation. The onset of degradation has been reported by Medtronic Inc. to occur approximately 4 weeks after implantation allowing for recanalisation of the vessel following the treatment. In contrast, Easi-Vue™ microspheres are non-degradable but are radiopaque allowing them to be visualised using X-ray techniques. This alleviates the need to rely on contrast agent to act as a surrogate marker for the microspheres during their delivery and allows identification of the location of the microspheres in follow-up scans post-procedure. The wide range of commercially available and emerging microspheres highlights the widespread use of microspheres in the area of transarterial embolisation and requirement to tailor the type of microsphere used for individual treatments.

### ***1.1.3. Sclerosing Agents***

Sclerosing agents are used to penetrate further into smaller blood vessels than particulates, in order to induce tissue infarction in the process of sclerotherapy. These materials function by a different mechanism to mechanical devices and particles as instead of embolising by mechanically blocking the blood flow, sclerosing agents induce inflammation of the blood vessel walls. The resulting inflammation causes the lumen of the blood vessel to constrict, hence reducing and halting the blood flow through the vessel upon injection of the sclerosing agent. The injection of sclerosing agents is often carried out alongside the administration of an anaesthetic due to the pain associated with the induced inflammation.<sup>36</sup>

Embolisation by sclerotherapy is commonly used in the treatment of renal cell carcinoma due to the lack of control of injecting a low viscosity liquid which poses a high risk of distal embolisation downstream from the targeted vasculature<sup>37</sup>. Therefore, the use of sclerosing



agents is limited to treatments where the targeted vasculature does not lead to other organs which could become accidentally embolised, hence its primary use in the kidneys.

Alcohol, such as absolute ethanol, is a cheap and commonly used sclerosing agent. Ethanol functions as a sclerosing agent by inducing immediate thrombosis and inflammation at the levels of small blood vessels and tissue. The high cytotoxicity of absolute ethanol induces severe inflammatory reactions, hence it must be used cautiously to limit the cytotoxic effects and damage to adjacent tissue.<sup>38</sup> The use of absolute ethanol is therefore restricted to cases in which non-target embolisation is unlikely to occur, such as in the kidneys.<sup>39</sup> Similar results can also be achieved by the injection of acetic acid as the sclerosing agent.<sup>40-42</sup>

Polidocanol foam is another commonly used sclerosing agent used in the formulations of Asclera® (Chemische Fabrik Kreussler) and Varithena® (Provensis, a BTG International group company). The foam functions by displacing the blood from the vein being treated and the polidocanol contained in the foam scleroses the endothelium to induce embolisation. The administration of the polidocanol foam is often monitored by ultrasound guidance to allow the progress of the foam within the vasculature to be visualised. Sclerotherapy using polidocanol foam is frequently used for the preoperative embolisation of liver cancers prior to their surgical removal to control the bleeding during their surgical excision.<sup>43</sup> Other sclerosing agents include sodium tetradecyl sulfate marketed as Sotradecol® (Mylan),<sup>44</sup> bleomycin<sup>45</sup> and acetic acid.<sup>46</sup> The various sclerosing agents available allow the interventional radiologist performing the procedure to select the appropriate agent based on the type of disease being treated, personal preference and cost.

## **1.2. Embolisation using Liquid Embolic Agents**

Liquid embolic agents offer an alternative embolisation tool to mechanical devices, particles and sclerosing agents. Liquid embolics function by gelling *in situ* when injected into the vasculature undergoing a solution (sol)-gel transition. The *in situ* formation of a gel enables

the liquid precursors to be easily delivered using a microcatheter provided the material has an appropriate viscosity when in its solution state. Delivery of an embolic material in its solution state circumvents the problem of microcatheter blockage due to aggregation of particles or microspheres.

Once the material undergoes a sol-gel transition, it provides an added advantage over preformed materials, such as coils, in that the produced gel can mould to fill the vasculature into which it is injected along with any irregularities. Hence, the final gel form is unique and ideally suited to the vessel being treated. The gel formed acts to fully occlude the vessel and does not rely on thrombus formation to complete the occlusion. Therefore, liquid embolic materials are advantageous in patients with coagulopathies or patients receiving anti-coagulation therapy in which their ability to form blood clots is impaired.<sup>47,48</sup> Furthermore, the formation of a single solid mass of embolic material at the treatment site also provides the advantage of a lower probability of migration once implanted. This is often a concern with embolic materials, such as particulates, which pose the risk of dislodging once implanted leading to off-target embolisation.

Liquid embolic materials can be spilt into 3 main types; polymerising, precipitating and phase transitioning. Polymerising liquid embolics, such as cyanoacrylate glues, contain monomers or macro-monomers in a carrier solution which polymerise upon contact with a suitable initiator. Often, the initiator is mixed prior to the delivery of the polymerising embolic. Hence, these materials polymerise over a predictable and predetermined gelation time meaning the delivery is restricted to a limited time frame. Therefore, when using a polymerising embolic premixed with an initiator, delivery must be carried out within the predetermined time in order to provide effective embolisation and avoid microcatheter blocking and entrapment. An alternative to this is to deliver polymerising liquid embolics *via* a dual-lumen microcatheter to ensure the reacting components are kept separate during microcatheter delivery until mixing upon exiting the microcatheter at the delivery site. This delivery method relies on a rapid rate

of reaction to prevent wash-out of the embolic material by the blood flow before gelation has occurred.

Precipitating liquid embolics, such as Onyx<sup>®</sup>, are administered as a polymer dissolved in a non-toxic and biocompatible carrier solvent. On contact with a precipitation stimulant, such as a non-solvent or salt present within the blood, precipitation of the previously dissolved polymer chains occurs to form a gel *in situ*. Following gelation, the previously used carrier solvent diffuses away and generally water from the blood replaces it within the polymer matrix. Precipitating polymers offer the advantage that they form gels only when in contact with precipitating stimulus present within physiological fluids and therefore avoid the problem of gelation within the microcatheter which can result in microcatheter blockage. This allows the delivery to be paused during the embolisation procedure in order to prevent escape of material into non-target vessels. There are some disadvantages associated with precipitating liquid embolics in that if the onset of precipitation is not fast enough, the blood flow through the vessel can result in wash-out leading to local or systemic toxicity as a result of the free polymer. Also, a suitable carrier solvent must be selected in order to avoid any toxic effects on injection into the vasculature.

In addition to polymerising and precipitating liquid embolics, polymers which undergo a phase transition from sol-gel in response to external stimuli, such as GPX, have also been demonstrated to be useful in the area of therapeutic embolisation. These materials respond to their surrounding environment due to changes in parameters such as temperature, pH, ion concentrations or electric fields. Hence, phase transitioning polymers can be selected which respond to physiological parameters such as body temperature, blood pH or the salt concentrations in blood. This means phase transitioning systems can be designed to gel under precise conditions which can be tailored to those experienced in an embolisation procedure such as the change in temperature of the injected liquid from room temperature to body temperature as its injected through the microcatheter or the contact with blood and the change in pH and ion concentration as the liquid exits the microcatheter at the delivery site. There is

a limitation for phase transitioning materials that are solely thermo-responsive and gel at temperatures around that of body temperature. This is due to the long lengths of microcatheters used (typically 100-150 cm in length) which can culminate in the injected liquid solution reaching body temperature as it travels along the length of the microcatheter. This poses the risk of microcatheter blockage if the phase transition occurs before exiting the microcatheter.

### ***1.2.1. Current Liquid Embolic Agents***

There are currently three commercially available liquid embolics in widespread use in the clinic; cyanoacrylate glues, Onyx<sup>®</sup> and Lipiodol<sup>®</sup>. The use of Lipiodol<sup>®</sup> is limited to the treatment of HCC.<sup>49</sup> Whereas cyanoacrylate glues and Onyx<sup>®</sup> are used in a range of vascular conditions including in the treatment of AVMs,<sup>50</sup> gastrointestinal bleeding<sup>51</sup> and aneurysms.<sup>52</sup> These liquid embolics are primarily delivered using microcatheters of narrow lumen with hydrophilic coatings to provide lubricity and aid the delivery of the liquids as they pass through the microcatheter lumen during injection. A number of microcatheters are available with side holes to allow the inflation of a small balloon upstream of the delivery site to reduce the blood flow through the vasculature during the delivery of the liquid embolic materials. The balloon is then deflated following embolisation, allowing the microcatheter to be withdrawn from the vasculature. These balloon microcatheters are frequently utilised in the delivery of liquid embolics due to their ability to reduce the flow during the injection of the solidifying liquid thereby providing more control over the delivery process (Figure 1.7).<sup>53</sup>



*Figure 1.7 - Diagram of an inflated balloon microcatheter to reduced blood flow during the delivery of the embolic material.*

### 1.2.1.1. Cyanoacrylate glues

There are a number of glues commercially available including TruFill® (Codman), Histoacryl® (B.Braun) and Glubran® 2 (GEM). The glue formulations are based on the monomer *n*-butyl-2-cyanoacrylate (nBCA), a derivative of superglue. On entering blood vessels, the nBCA monomer rapidly polymerises under the ionic conditions found in blood to form an embolus within the vasculature (Figure 1.8). Care must be taken during the preparation of the glue to prevent premature polymerisation of the monomer on contact with ionic solutions. Prior to the nBCA glue injection, the microcatheter must be flushed with a non-ionic 5% dextrose solution in order to prevent polymerisation within the microcatheter which could result in microcatheter blockage. Delivery of the nBCA glue through a pre-flushed microcatheter ensures that the glue rapidly polymerises on contact with blood upon exiting the tip of the microcatheter at the delivery site. The fast rate of polymerisation is particularly beneficial in cases where rapid embolisation is required such as trauma or gastrointestinal bleeding.

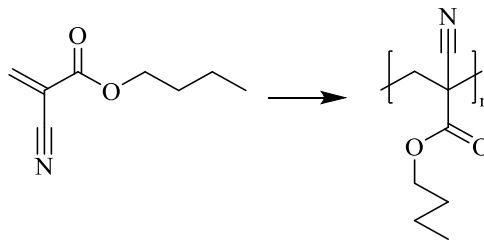


Figure 1.8 - In situ polymerisation of *N*-butyl-2-cyanoacrylate (nBCA).

The low viscosity nature of the nBCA glue results in the formation of a solid cast within the blood vessels with occlusion focused towards the more distal blood vessels.<sup>54</sup> This liquid embolic system provides permanent occlusion of the targeted vessels due to the initiation of an acute inflammatory response in the blood vessel walls and surrounding tissue.<sup>55-57</sup> This leads to fibrosis of the treated area resulting in permanent occlusion of the treated blood vessels.<sup>58</sup>

The rate of polymerisation can be predictably controlled by the use of glacial acetic acid and Lipiodol® (Guerbet Llc.) which act as polymerisation retardants.<sup>59</sup> The addition of these polymerisation retardants to nBCA results in a decrease in the rate of polymerisation due to

the reduced ionic contact of nBCA with blood. This provides the interventional radiologist performing the procedure with a greater flexibility in the working times of the glue.<sup>60</sup> The use of Lipiodol<sup>®</sup> in combination with nBCA increases the overall viscosity of the liquid improving control of the injection and providing less distal embolisation. Additionally, the Lipiodol<sup>®</sup> contrast agent has the advantage of imparting radiopacity to the embolic solution enabling the injection to be monitored by real-time fluoroscopy.

Following the delivery of nBCA it is necessary to immediately withdraw the microcatheter. This is to prevent the entrapment of the microcatheter at the site of administration due to the highly adhesive nature of the material.<sup>61</sup> Gluing of the microcatheter in place may also occur due to excessive degrees of reflux of the material, which is dependent on the volume injected, or early polymerisation. Hence, careful attention must be made to the preparation of the liquid embolic prior to procedure, the delivery technique and the volume of liquid used. Intermittent injection of the polymerising liquid embolic can result in microcatheter blockage which requires the removal and placement of a new microcatheter when this occurs.<sup>62</sup> The occurrence of microcatheter entrapment requires the microcatheter to be broken to leave the distal end in place within the patient.<sup>63</sup> It is generally attempted to keep the remaining microcatheter length as short as possible to avoid the proximal end from blocking or rupturing nearby blood vessels. However if this cannot be achieved then the microcatheter is cut at the point where it enters the artery and is then secured at the site of entry located at either the groin if femoral access was used or the wrist if radial access was used.<sup>64</sup>

In an attempt to overcome some of the problems associated with the nBCA formulation, variations have been trialled using longer alkyl chains<sup>65</sup> (Figure 1.9) and 2-hexyl cyanoacrylate<sup>66</sup> (Figure 1.10). The long chain isostearyl-2-cyanoacrylate formulation proved to be less adhesive in nature than nBCA thereby presenting a reduced risk of microcatheter entrapment.<sup>65</sup> However, the rate of the material's polymerisation was too slow to provide effective and safe embolisation of rapid flow blood vessels and exhibited material wash-out unless used in combination with nBCA. An adhesion study was performed using 2-hexyl

cyanoacrylate in both its pure form and in combination with a polymerisation inhibitor or iodinated oil Ethiodol in comparison to an nBCA control.<sup>67</sup> The study found that when 2-hexyl cyanoacrylate was tested alone or mixed with Ethiodol the adhesion properties of the material were significantly less than for pure nBCA or an equivalent mix of nBCA with Ethiodol. However, when 2-hexyl cyanoacrylate was mixed the polymerisation retardant and contrast the adhesion properties were not significantly different from the adhesion of nBCA mixed with 50% Ethiodol which is commonly used in clinical practice and hence offered no improvement on the current nBCA glue system.

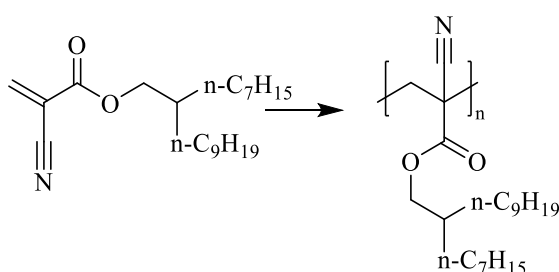


Figure 1.9 - In situ polymerisation of isostearyl-2-cyanoacrylate.

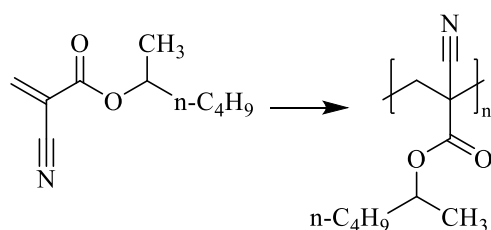


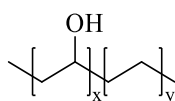
Figure 1.10 - In situ polymerisation of 2-hexyl cyanoacrylate.

An alternative approach to reducing the occurrence of microcatheter entrapment is to instead modify the delivery system rather than the nBCA embolic material itself. Microcatheters with a hydrophilic coating have been shown to reduce the adhesion of nBCA.<sup>68</sup> Additionally, microcatheters are available with detachable tips, such as Apollo™ marketed by Medtronic Inc., which allow a short section of the microcatheter tip to be safely detached and left in place if adhesion to the embolic material were to occur.<sup>69,70</sup> However, the use of these microcatheters in the clinic must be carefully considered due to the resulting higher cost. The risk of microcatheter entrapment is largely dependent on the operator's proficiency and embolic material formulation so specially designed microcatheters have limited benefit. Despite the

risks of microcatheter blocking and entrapment, nBCA is still in widespread clinical use with interventional radiologists that are experienced and proficient in its delivery particularly due to its low cost.

### 1.2.1.2. *Onyx*<sup>®</sup>

*Onyx*<sup>®</sup> (Medtronic Inc.) is a liquid embolic system based on a poly(vinyl alcohol-co-ethylene) copolymer (Figure 1.11) suspended in DMSO with micronised tantalum powder. Prior to delivery, *Onyx*<sup>®</sup> must be agitated for a minimum of 20 minutes on a mixer plate to achieve a uniform suspension of the polymer and tantalum radiopacifying agent in the DMSO carrier solvent.<sup>71</sup> The delivery of the polymer system in the carrier solvent means that the polymer precipitates out of solution on contact with blood due to the aqueous salt conditions which act as a non-solvent for the polymer. The precipitation of the poly(vinyl alcohol-co-ethylene) copolymer results in the entrapment of the suspended tantalum powder and the gradient diffusion of DMSO from the precipitate. Once precipitated, *Onyx*<sup>®</sup> forms a gel with a sponge-like consistency making it ideal for use in the treatment of AVMs as the occluded vessels are soft and easily removed by surgery.<sup>72,73</sup> The contained tantalum within the precipitated gel imparts long-term radiopacity to the material meaning the embolised vessels can be easily located by X-ray and magnetic resonance imaging.



*Figure 1.11 - Poly(vinyl alcohol-co-ethylene).*

*Onyx*<sup>®</sup> is marketed over a range of different viscosities including *Onyx*<sup>®</sup> 18 which is 18 cP, *Onyx*<sup>®</sup> 34 which is 34 cP and *Onyx*<sup>®</sup> 500 which is 500 cP. The different *Onyx*<sup>®</sup> formulations available allow the interventional radiologist performing the procedure to select the appropriate viscosity depending on the disease being treated. For example, the low viscosity *Onyx*<sup>®</sup> 18 is ideal for treatments requiring high degrees of distal penetration such as AVMs as the low viscosity solution can penetrate deep into the vasculature.<sup>74</sup> Whereas, the high



viscosity Onyx<sup>®</sup> 500 is better suited for embolisation of aneurysms particularly of wide necks which are not suitable for surgical clipping as the high viscosity can resist potential wash-out of the material due to the flow of blood past the aneurysm neck.<sup>75</sup>

In contrast to nBCA glue, Onyx<sup>®</sup> does not initiate any significant inflammatory response. However, injection of the organic solvent DMSO necessitates further patient sedation due to the pain caused during the injection. Injection of DMSO can also result in the occurrence of vasospasm due to the cytotoxicity of the solvent in which the blood vessels suddenly constrict causing reduced diameters and blood flow.<sup>76</sup> If this occurs during the procedure then the injection must be halted until vasospasming stops which increases the procedural time and patient risks. Vasospasms can be prevented using slow injection times<sup>77</sup> and hence the recommended injection rate of Onyx<sup>®</sup> is 0.16 mL min<sup>-1</sup>.<sup>71</sup> The use of DMSO in the Onyx<sup>®</sup> formulation also requires the use of specialist syringes and microcatheters due to the degradation by DMSO of commonly used syringes and microcatheters in embolisation procedures.<sup>76</sup> Suitable microcatheters for injection of the DMSO based liquid embolic include Rebar<sup>™</sup> (Medtronic Inc.), Progreat<sup>®</sup> (Terumo) and Apollo<sup>™</sup> (Medtronic Inc.).

This system resolves some of the issues experienced with nBCA glue in that Onyx<sup>®</sup> is non-adhesive in nature so has a reduced risk of microcatheter blockage and entrapment.<sup>78,79</sup> The delivery process can also be carried out using intermitted injections allowing the delivery to be paused to evaluate the progress of the embolus and then continued with further penetration of the embolus into the vasculature. This pushability of the material in paused increments means a single microcatheter can be used for multiple injections during each procedure without the need to place new microcatheters after each injection. Once sufficient material has been delivered into the vasculature, the end-point of the embolisation is determined when the delivered liquid embolic no longer flows within the vasculature due to its solidification as visualised by real-time fluoroscopy.

Despite the less adhesive nature of Onyx<sup>®</sup> in comparison to nBCA glue, the U.S. Food and Drug Administration (FDA) previously released a safety communication relating to the

wording used by the manufacturers of Onyx<sup>®</sup> about the risks of microcatheter entrapment.<sup>80</sup> Some difficulties were encountered when removing microcatheters following injection of Onyx<sup>®</sup> during clinical trials. In all cases the microcatheters were successfully removed but since the launch of Onyx<sup>®</sup> onto the market there have been a number of cases in which it has not been possible to remove the embedded microcatheter. These cases resulted in the microcatheter having to be cut and left in place within the patient. In 9 out of 54 of these cases, the entrapment of the microcatheter was fatal and lead to patient death. For the remaining patients with embedded microcatheters, the microcatheters were removed during the follow-up surgical removal of the occluded blood vessels. The time between Onyx<sup>®</sup> injection and removal of the microcatheter embedded in the Onyx<sup>®</sup> plug left the patients at risk of haemorrhaging or migration of the plug or microcatheter fragment. Also, the patients with entrapped microcatheters were required to take antithrombotic drugs to prevent blood clots forming around the entrapped microcatheter. The Onyx<sup>®</sup> labels now state the risks of microcatheter entrapment and advice on steps to take to minimise the risk of this happening in particular by avoiding excessive degrees of reflux around the microcatheters. Also stated is the need for DMSO-compatible microcatheters along with careful injections of the embolic material to prevent vasospasm and necrosis damage to the majority or all cells of an organ or tissue due to the associated toxicity of the DMSO solvent used.<sup>59</sup> Medtronic Inc. has also developed a specialist DMSO-compatible microcatheter, Apollo<sup>™</sup>, with a detachable tip which can be left in place inside the patient if the microcatheter tip becomes entrapped in the solidified embolic plug during the procedure. This provides a safe and effective method of dealing with microcatheter entrapment if it occurs to reduce patient risk of complication associated with leaving a large length of microcatheter in place.

Following implantation of Onyx<sup>®</sup>, the solidified embolic material can be readily located by X-ray imaging techniques. The embolic is visualised as a dense bright white region due to the high radiopacity imparted by the tantalum radiopacifying agent. However due to the metallic nature of the radiopacifying agent used, Onyx<sup>®</sup> often exhibits a streak artefact under X-ray

imaging as a result of beam hardening and scattering of the X-ray energy used during scanning (Figure 1.12).<sup>81</sup> This imaging artefact can obscure the surrounding anatomy of the treated vascular abnormalities and hinder further diagnosis or monitoring of disease progression. This makes it difficult to assess whether sufficient embolisation has been performed or whether further treatments are required.



*Figure 1.12 - Beam hardening and streak artefact (indicated by white arrow) observed with Onyx<sup>®</sup> in the right hepatic artery by contrast enhanced axial CT (image from Clin. Radiol., 2015, 70, 326–32).*

### **1.2.1.3. Lipiodol<sup>®</sup>**

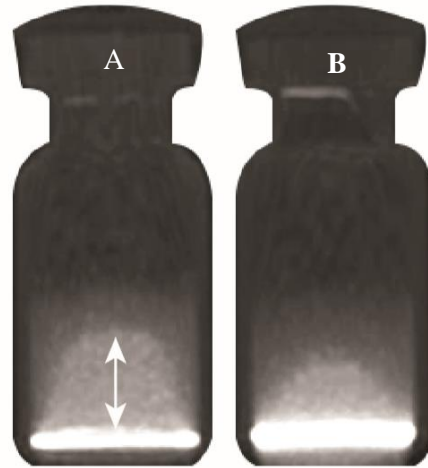
The contrast agent, Lipiodol<sup>®</sup> (Guerbet Llc.), used to aid the delivery of embolic microspheres and particles, may also be classed as a liquid embolic agent. The ethiodised oil is often administered alongside chemotherapeutic drug, such as doxorubicin,<sup>82</sup> in a procedure known as conventional transarterial chemoembolization (cTACE). The contrast agent provides a temporary embolic effect in larger arteries<sup>83</sup> but ultimately accumulates in hypervascularised tumours.<sup>84</sup> The selective uptake and retention of Lipiodol<sup>®</sup> within tumours provides clinical benefit in the treatment of HCC.<sup>49</sup> The treatment of HCC by cTACE is performed in a set of at least two sequential cTACE procedures with significant response often observed as tumour necrosis by the second treatment.<sup>85</sup> Subsequent embolisation of the feeding tumour vessels is

performed using particles or microspheres following the Lipiodol<sup>®</sup> injection. Embolisation in this way has been demonstrated to improve tumour response rates to treatment.<sup>86</sup>

## ***1.2.2. Emerging Liquid Embolic Technologies***

### ***1.2.2.1. Squid<sup>™</sup>***

Squid<sup>™</sup> (Emboflu) is similar to Onyx<sup>®</sup> in that it is a precipitating liquid embolic composed of an ethylene vinyl alcohol copolymer in a DMSO suspension with micronised tantalum powder. In the Squid<sup>™</sup> formulation a smaller grain size of tantalum powder is used which has a slower rate of sedimentation in comparison to Onyx<sup>®</sup> (Figure 1.13).<sup>87</sup> This provides longer working times of the material due to its ability to retain homogeneous suspension over a longer time frame which is particularly useful when using prolonged injection times. Squid<sup>™</sup> is marketed in a range of formulations including Squid<sup>™</sup> 12 and Squid<sup>™</sup> 18 which have viscosities of 12 cP and 18 cP, respectively. This allows the appropriate viscosity to be selected depending on the desired clinical outcome, for example the lower viscosity Squid<sup>™</sup> 12 is ideal for achieving deeper penetration into the vasculature often required with the treatment of AVMs whereas Squid<sup>™</sup> 18 is better suited to the treatment of endoleaks in which there is seepage of blood from the lumen of a vascular graft into the aneurysm sac which the graft was used to repair. This is due to the higher viscosity of Squid<sup>™</sup> 18 and therefore its ability to resist wash out by the blood flow. Squid<sup>™</sup> formulations are also available with 30% less tantalum in the suspension, marketed as Squid<sup>™</sup> 12LD and Squid<sup>™</sup> 18LD.<sup>88</sup> The reduced amount of tantalum in the liquid embolic formulation reduces the imaging artefact of streaking often observed with Onyx<sup>®</sup>. Despite the improved properties over the well-established Onyx<sup>®</sup> treatment, Squid<sup>™</sup> has not found widespread use in clinic likely due to its high cost and requirement of DMSO compatible microcatheters.



*Figure 1.13 - X-ray images showing the longer tantalum suspension time (as indicated by the white arrow) of Squid™ 18 (A) in comparison to Onyx® 18 (B) 15 minutes after agitation (image from Emboflu promotional brochure for Squid™).*

#### **1.2.2.2. PHIL®**

The precipitating hydrophobic injectable liquid PHIL® (MicroVention) is indicated for the embolisation of the peripheral and neurovasculature, including arteriovenous malformations and hypervascular tumours. The liquid embolic is delivered using DMSO as the carrier solvent which on mixing with blood diffuses away as the polymeric material precipitates out of solution on contact with the aqueous environment within the vasculature to form a solid embolus. The polymer is based on a poly(lactide-co-glycolide) and poly(hydroxyethyl methacrylate) copolymer which is non-adhesive in nature so avoids adhesion to the microcatheter during delivery. The radiopacifying agent iodine is covalently bound to the polymer, hence no pre-mixing of materials is required to achieve a homogeneous solution before delivery as is the case for tantalum based radiopacifying agents. Therefore, PHIL® is supplied in pre-loaded syringes which reduces the overall procedural time. It is also marketed in a range of viscosities allowing the interventional radiologist performing the procedure to select the appropriate viscosity for individual treatments depending on the desired level of vascular penetration.

It has been demonstrated that PHIL<sup>®</sup> precipitates with a greater volume of precipitate formed per mL of liquid embolic injection than Onyx<sup>®</sup>,<sup>89</sup> thereby requiring a reduced volume of liquid embolic in the embolisation process potentially reducing materials cost. However, due to the DMSO carrier solvent used in the formulation, PHIL<sup>®</sup> must be used with specialist DMSO compatible connectors and microcatheters, similar to embolisation using Onyx<sup>®</sup> or Squid<sup>™</sup>.

### **1.2.2.3. *Easyx*<sup>™</sup>**

In addition to PHIL<sup>®</sup> another precipitating liquid embolic has recently been developed by Anita Therapeutics. The precipitating liquid embolic Easyx<sup>™</sup> is composed of poly(vinyl alcohol) with iodine containing moieties which are covalently bound to the polymer backbone by ether groups. Similar to Onyx<sup>®</sup>, Squid<sup>™</sup> and PHIL<sup>®</sup> the product is also delivered using DMSO as the carrier solvent which diffuses away from the embolus as the polymer precipitates out of solution on contact with the aqueous blood conditions. This requires the use with DMSO compatible microcatheters to prevent the deterioration of the microcatheters by the solvent. The inherent radiopacity imparted by the covalently bound iodine allows the liquid embolic to be clearly visualised by computed tomography (CT) imaging without the streak artefact observed with the tantalum radiopacify agent used with Onyx<sup>®</sup>. Also, the covalent binding of the radiopaque group alleviates the need to pre-mix the liquid embolic with a radiopacifying agent prior to delivery as the radiopaque materials is supplied in a ready to use solution in DMSO.

Easyx<sup>™</sup> has been developed for the embolisation of hypervascular lesions including tumours and AVMs. The liquid embolic is currently undergoing clinical trials but early data has demonstrated effective embolisation with homogeneous visibility under CT imaging.<sup>90</sup>

#### 1.2.2.4. GPX

GPX (Fluidx Medical Technology) is a biomimetic aqueous based liquid embolic system. The liquid embolic is based on the liquid glue secreted by sandcastle worms to create tubular structures with grains of sand.<sup>91,92</sup> Using the same principal as the sandcastle worms, GPX consists of polyelectrolyte complexes which are stabilised in aqueous solutions of high ionic strength due to charge screening between the polyelectrolytes (Figure 1.14). The stabilised solution can be delivered through the narrow lumens of microcatheters used in embolisation procedures. On exiting the microcatheter at the injection site, complexation of the polyelectrolytes occurs by electrostatic interaction due to the reduction of the ionic strength to physiological strength which removes the charge screening between the oppositely charged polyelectrolytes. This results in polyelectrolyte aggregation to form a gelled embolus within the vasculature with rapid gelation within seconds. Despite the design of GPX based on the liquid glue excreted by sandcastle worms, the embolus formed was found to be none adhesive in nature to the microcatheter used to deliver the embolic material. Embolisation using GPX has been performed in rabbit renal arteries demonstrating a high level of vascular penetration and complete occlusion of the kidney.<sup>93</sup>

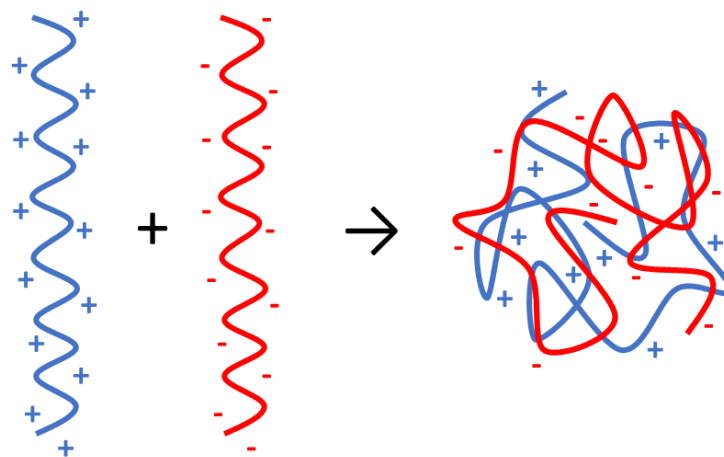


Figure 1.14 - Schematic of the complexation of a polyelectrolyte from polyanions and polycations on reduction of the solution ionic strength.

The aqueous nature of the system alleviates the need to use DMSO compatible microcatheters as required with a number of liquid embolics. However, the material used in the GPX

formulation is not inherently radiopaque so would need to be delivered alongside a contrast agent to enable visualisation of the embolisation procedure. This would likely alter the rate of gelation of the liquid embolic system, hence further testing of GPX is still required.

#### **1.2.2.5. Instylla Hydrogel Embolic System**

Instylla's Hydrogel Embolic System (Incept) is a polyethylene glycol based system which polymerises *in situ* on mixing with an initiator. The low viscosity liquid undergoes rapid gelation to form an embolic gel within the vasculature. The polymeric material is not radiopaque, hence the material must be mixed with contrast agent prior to delivery to monitor the injection.

The product has been tested in animal models in which high vascular penetration was observed likely due to the low viscosity of the liquid embolic. The liquid embolic system has been tested using a range of microcatheters, including balloon microcatheters, and alongside coil embolisation treatments. Successful polymerisation of the gel was also observed in high flow rate tests of 150 mLmin<sup>-1</sup>. Due to the successes demonstrated in early testing of the liquid embolic system, further *in vitro* and *in vivo* testing of Instylla's Hydrogel Embolic System is currently being performed.<sup>94,95</sup>

#### **1.2.2.6. Silk Elastin Protein Polymer (SELP)**

A phase transitioning injectable material has been developed using Silk Elastin Protein Polymer (SELP), a genetically engineered protein polymer. A phase transition of the polymeric material occurs in response to temperature undergoing a sol-gel transition on an increase in temperature from room temperature to body temperature at 37 °C.<sup>96</sup> Feasibility of the material as an injectable material has been demonstrated using an *in vitro* model and animal *in vivo* model.<sup>97,98</sup> The product is currently under further investigation for use as a therapeutic gene delivery system.



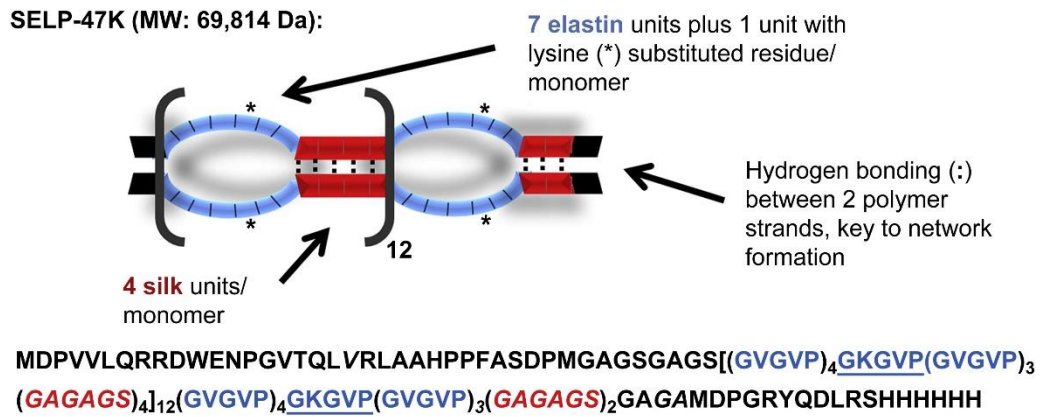


Figure 1.15 - Amino acid composition of a silk elastin protein polymer (SELP-47K)(image adapted from *Biomaterials*, 2015, 57, 142-52).

### 1.2.2.7. Shear Thinning Biomaterials

Shear thinning biomaterials are an attractive approach to liquid embolics as the materials can be injected through microcatheters due to their rheological properties allowing for injection through the narrow lumen of microcatheters. Once the shear stress is removed inside the vasculature the materials return to their gel state and form an embolus *in situ*. Currently under investigation is a shear thinning biomaterial based on a nanocomposite hydrogel containing gelatin and silicate nanoplatelets (Figure 1.16).<sup>98,99</sup> The shear thinning biomaterial demonstrated injectability through a range of microcatheters and needles and formed a sufficient embolus that could withstand physiological pressures without displacement in the vasculature.

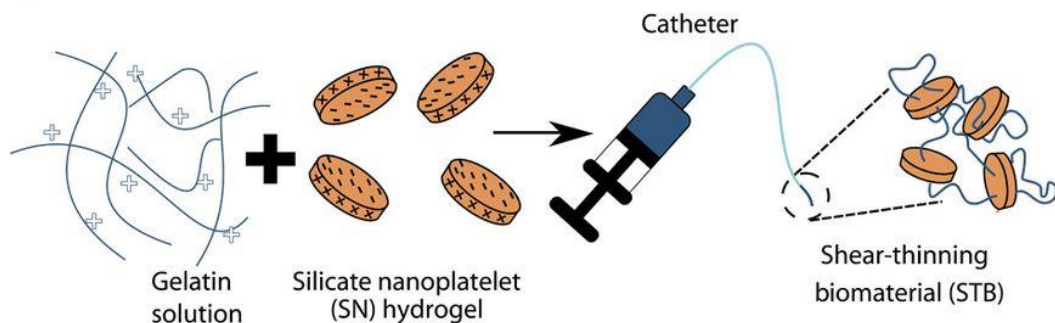


Figure 1.16 - Diagram of shear thinning behaviour of a nanocomposite hydrogel containing gelatin and silicate nanoplatelets (image adapted from *Sci. Transl. Med.*, 2016, 8, 365-77)

The aqueous nanocomposite hydrogel based system alleviates the need for specialist microcatheters. However, the system is not intrinsically radiopaque hence pre-mixing with contrast agents is required to enable monitoring of the injection process. Further testing of the system is currently being carried out using *in vivo* animal models.

### 1.3. Research Aims

Therapeutic embolisation is an already well established treatment with a wide variety of potential materials available on the market. The range of commercially available embolic agents represents the variety of treatments and highlights the need to tailor each embolisation procedure on a case-by-case basis. There are however limitations to these well-established products. For example, microcatheter blocking and off-target embolisations are the primary issues faced. Liquid embolic materials which gel *in situ* offer an attractive alternative to overcome these difficulties and provide additional tools for use in therapeutic embolisation.

This PhD project will further develop the use of PVA as an embolic agent. This particular polymer is ideally suited to use in therapeutic embolisation due to its biocompatibility. Formulations will be developed based on this polymer, investigating the potential *in situ* gelling mechanisms of precipitation and polymerisation. In the precipitation mechanism, formulations will be prepared in which gelation is triggered by contact of the polymer in a carrier solution to stimuli present in the blood, such as aqueous conditions or salt concentrations. This will be achieved by modification of PVA with substituents that respond to conditions in the blood triggering the polymer chains to precipitate from the carrier solvent used to deliver the polymer, thereby forming a gel *in situ*. Formulations developed using the polymerisation mechanism will be based on a polymerising embolic system composed of PVA macromonomer and an initiator that is deliverable *via* a dual-lumen microcatheter. The use of a dual-lumen microcatheter allows the reacting components of the polymerising system to be kept separate during their injection until exiting the microcatheter at the delivery site where

they mix to form a gel *in situ*. This avoids the potential of microcatheter blocking if the components were mixed prior to injection which risks gelation before the materials reach the delivery site. In both gelation systems, the PVA chains will be modified with substituents containing iodine, covalently bound, to impart inherent radiopacity to the materials. This enables the gelled materials to be visualised by X-ray imaging methods both during and after the embolisation procedure.

The modification of the PVA microspheres DC Bead<sup>®</sup> to impart radiopacity has already been demonstrated with development of DC Bead LUMI<sup>™</sup>. The diol backbone of the PVA microspheres was modified with a triiodobenzyl moiety enabling the visualisation of the microspheres in post-procedural scans after the wash-out of contrast agent used to aid delivery of the microspheres.<sup>35</sup> However, the introduction of a highly hydrophobic iodinated aromatic group resulted in altered physical properties of the DC Bead LUMI<sup>™</sup> microspheres in comparison to their previous bland versions DC Bead<sup>®</sup>. The increased hydrophobicity of the microspheres resulted in contraction of bead diameters leading to increased bead density and reduced deformability.<sup>100</sup> Hence, this has resulted in reduced suspension times of the beads in contrast agent during the administration process thereby requiring regular agitation throughout the delivery to ensure a uniform suspension is maintained.<sup>101</sup> A radiopaque *in situ* gelling material based on this system has therefore been proposed to overcome the problems observed along with offering an alternative liquid embolic agent for use within therapeutic embolisation. The development of a new liquid embolic agent would then allow the interventional radiologist performing the procedure to choose the relevant materials for particular treatments.

Other potential uses of radiopaque *in situ* gelling materials include injectable gels which can be used as drug delivery depots or protective spacers. Injectable gels can be delivered alongside therapeutic drugs to provide a drug reservoir capable of eluting the contained drug over a sustained time. This is particularly useful for the treatment of tumours by intratumoural injection to provide a high dose of chemotherapeutic drug directly to the tumour with minimal

systemic toxicity.<sup>102</sup> Injectable gels used as protective spacers are beneficial for use in patients receiving radiotherapy. For example, the degradable SpaceOAR Hydrogel® composed of polyethylene glycol has been successfully used in patients receiving radiotherapy for prostate cancer.<sup>103,104</sup> In these treatments the hydrogel is used as a spacer between the radiated prostate and the rectum in order to shield the rectum from high doses of radiation which can result in a range of complications. These varying applications of *in situ* gelling materials demonstrate their potential in a range of medicinal applications.

### **1.3.1. Important Properties of a Radiopaque Liquid Embolic**

In the development of a radiopaque liquid embolic agent there are a number of aspects to consider including the deliverability of the liquid, function as an embolic material and visibility after implantation.

#### **1.3.1.1. Delivery**

The deliverability of the liquid embolic material relates to the handling and delivery properties as the liquid is injected into the body using a microcatheter and its ability to flow within the vasculature. The deliverability of the injected material will be largely determined by the viscosity possessed by the embolic in its liquid state. Formulations of low viscosity are required to enable the passage of the liquid through the narrow lumen of the needles and microcatheters used in the embolisation procedure. Nevertheless, the injectable embolics must still possess a minimum viscosity in order to prevent wash-out of the material at its injection site from the force exerted by the blood flow within the vessel. Highly viscous solutions need to be avoided as they require the exertion of high injection pressures in order to deliver the material. These high pressures pose the risk of connection adapter breakage and microcatheter rupture which may result in loss of material and off-target embolisation.

However, the ideal viscosity will be determined by the condition being treated as the viscosity of the material determines its distal propagation and how deeply the material can penetrate within the vasculature.<sup>105</sup> Hence, it is desirable to use a low viscosity, slow setting material when penetration into more distal vascular vessels is required. Otherwise, if distal embolisation is not the target of the procedure then a higher viscosity, fast setting material would be more appropriate for the procedure in order to avoid off-target embolisation and other potential complications.

Another factor affecting the delivery of an injectable embolic through a microcatheter is its adhesive properties. Adhesion of cyanoacrylates glues to their delivery systems has been previously discussed. The adhesive nature of these glues can result in the entrapment of the microcatheter, leading to an increased risk of complications for the patient along with increased procedural time and cost. The risk of implant adhesion to the delivery system can be minimised if the procedure is carried out by an experienced radiologist proficient in the art of quickly withdrawing the microcatheter after injection but in a way so not to cause damage to the surrounding vessel walls. However, this cannot always be achieved so it would therefore be more beneficial to use a non-adhesive embolic agent to avoid this problem.

Once injected, the setting mechanism and time become critical factors. The setting mechanism will ultimately be dependent on the type of gelling mechanism used. Liquid embolic prototypes which gel *via* a polymerisation mechanism are likely to set over a predictable time range once the macromonomer comes into contact with the initiating component which is often injected down a separate side of a dual-lumen microcatheter. In contrast, liquid embolic prototypes consisting of precipitating polymers are likely to be more slow setting. Precipitating embolics begin to gel and solidify when they come into contact with the stimuli present within physiologic fluids. Once these materials come into contact with the blood the organic solvent, used to prepare the injectable solution, diffuses away. This results in the formation of skin around the outside of the injected material which first comes into contact with the blood meaning the embolic solidifies from the outside-in. These differences in setting

times may make polymerising and precipitating liquid embolics suitable for different applications depending on the blood flow conditions at the injection site. For example, in the fast flowing conditions of AVMs polymerising embolics would provide more effective occlusion whilst minimizing the risk of distal embolisation. In contrast, precipitating embolics offer vessel occlusion of low flow sites with progression into distal blood vessels to provide optimal occlusion in treatments such as hypervascularised tumours.

The associated side effects of the *in situ* gelling processes are something which must be considered. In liquid embolics which gel by a polymerisation reaction, the reaction must be carefully considered so as not to release toxic by-products or produce local heat spots during the gelling process. Chronic inflammatory reactions have been associated with polymerising embolics due to the toxicities of initiators, cross-linking agents, residual monomers and reaction by-products.<sup>57</sup> Similarly in the case of precipitating liquid embolics, an appropriate carrier solvent must be chosen to prevent any potential local adverse reactions as a result of the injection of the organic solvent into the vasculature.

### **1.3.1.2. Function**

Following the successful delivery of an injectable embolic, the performance and interaction of the material with its surroundings are key to fulfilling its function as an embolic material. The biocompatibility of the implant is dictated by the interaction of the material with its local environment. It is usually best to minimise any tissue reactions by developing materials which are essentially biologically inert. However, there are some embolisation treatments in which a mild to strong inflammatory reaction may be beneficial. For example, in the embolisation of aneurysms a controlled inflammatory response can be useful in stimulating the formation of scar tissue.<sup>106</sup>

Biological activity can be achieved by drug loading the embolic material which is common practice with embolic devices, such as microspheres with chemotherapeutic drugs. *In situ*

gelling materials have a potential for drug loading if the chemotherapeutic drug is mixed with the liquid gel-precursors prior to treatment. Solidification of the embolic-drug mixture would result in entrapment of the drug within the polymer matrix which would then be eluted to the surrounding tissue over time due to concentration gradients.

Implant lifetime and durability are fundamental when selecting the type of material to be used for a particular application. With regards to the use of injectable embolics in therapeutic embolisation, it would be more beneficial to use a material which is non-biodegradable as permanent embolisation is required in the majority of treatment cases. However, in cases where permanent embolisation is not the target, such as in the treatment of uterine fibroids where it is often important to maintain fertility, a non-biodegradable material would not be appropriate as the permanent implant would not allow recanalisation of the treated blood vessel. In cases where embolisation is carried out prior to surgical removal then the degradation and durability of the implant becomes less of a deciding factor in the choice of material as the implant only needs to function as an embolic until surgical removal is carried out.

It is also beneficial to use a material with similar mechanical properties to the surrounding vasculature. Mimicking the stiffness of the material to the surrounding environment helps to reduce mechanical irritation of the solid mass experienced with any potential movement, hence reducing patient discomfort. Similarly, if the implant is not rigid enough then this leaves potential for deformation of the embolus and its movement within the vasculature. This reduces the effectiveness of the embolus and risks off-target embolisation if the implant becomes dislodged from its implanted position.

### **1.3.1.3. Visibility**

During the delivery of any embolic device, visibility is crucial to ensure safe and accurate embolisation. Current embolic materials, such as the vast majority of microspheres, are often

administered alongside a contrast agent to act as a surrogate marker for the location of the material as visualised by real-time fluoroscopy during the procedure. This is due to the organic nature of the microspheres used, composed of elements such as carbon, oxygen and nitrogen, which are not visibly identifiable under X-ray imaging unlike the iodine component typically used in contrast agents. The visibility of the implanted microspheres is lost over time due to wash out of the contrast agent away from the administration site meaning the resulting location of the embolic implant is then unknown following the procedure.

As previously discussed, the method used to impart radiopacity to the otherwise non-radiopaque nBCA glue is to mix the injectable glue with contrast agent to enable visualisation of the injection process. However, this method only imparts temporary radiopacity to the injected glue due to gradual diffusion of the contrast agent away from the treatment site over time. In the case of Onyx<sup>®</sup> radiopacity is achieved by mixing the embolic materials with the heavy metal element tantalum. However, imparting radiopacity by these methods has the limitation that it takes time to mix the materials before they can be administered in the embolisation procedure.

Inherently radiopaque injectable polymer systems can be achieved by reacting non-radiopaque polymers with high atomic mass elements which thereby increase the average electron density and specific gravity of the materials. This imparts inherent radiopacity to the polymers and avoids the leaching of potentially toxic chemicals if the high atomic mass elements are covalently bound to the polymer chains. This process of increasing the average specific gravity of the materials allows visualisation of the implants by methods utilising X-rays such as fluoroscopy and CT imaging. This allows the implanted embolic materials to be visualised during the administration by real-time fluoroscopy and following the procedure by CT or cone beam CT imaging (CBCT).

The proposed method to achieve inherent radiopacity in the PVA liquid embolic systems is by the incorporation of iodine containing groups grafted onto the PVA backbone by cyclic acetal bond linkages. The formation of cyclic acetal bonds allows for permanent retention of



the radiopaque group due to the stability of the linkage to the polymer backbone. Also, the use of iodine based radiopaque groups avoids some of the imaging issues observed with Onyx® of streak artefact due to the heavy metal tantalum being used in the formulation.

In summary, the factors relating to the delivery, function and visibility of a radiopaque liquid embolic material are vital to its performance for use in therapeutic embolisation. Therefore, in this project test methods will be developed to evaluate the performance of the proposed radiopaque liquid embolic systems covering the range of requirements of an embolisation procedure from administration to implantation. They will allow validation as to whether the requirements have been met for the developed liquid embolic systems to perform as suitable embolic agents for use in therapeutic embolisation.

## **Chapter Two**

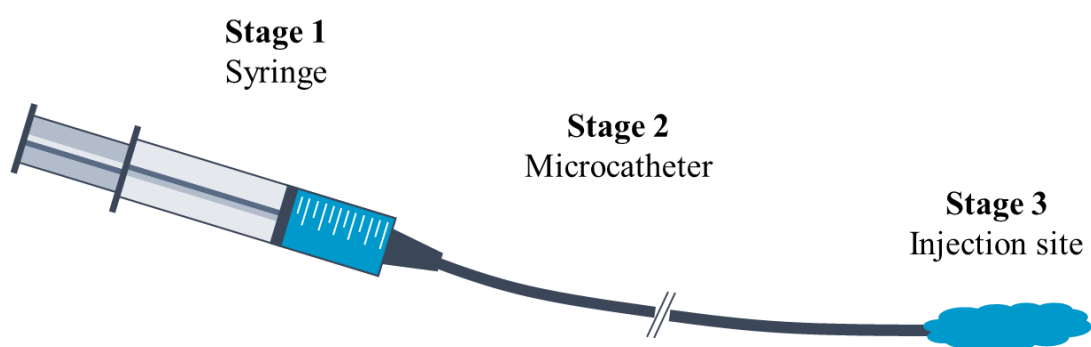
### **2. Development of Characterisation Test Methods**

## 2.1. Introduction

In the development of a radiopaque liquid embolic, a number of criteria need to be met in order to be suitable for use in therapeutic embolisation. There are a number of different requirements for the material at each stage in the process of an embolisation procedure (Figure 2.1). In the first stage of the procedure, there is a desire to have a liquid embolic in a ready to use formulation with a minimal preparation time. The formulation should retain its suspension in solution for the duration of the procedure to enable continuous delivery over the course of the procedure. If the liquid embolic is not packaged in a pre-loaded syringe, then the injected liquid needs to be of suitable viscosity to be easily drawn into a syringe by the interventional radiologist performing the procedure prior to delivery. Similarly, in the next stage of the process, the liquid needs to be of suitable viscosity to be easily deliverable into the vasculature using a microcatheter of narrow diameter. As the liquid enters the vasculature it should flow predictably from the tip of the microcatheter and penetrate the vasculature with a minimal amount of reflux behind the microcatheter. The injected liquid embolic should also fill and embolise a predictable volume of the vasculature for each mL of the liquid injected to provide a gauge of the volume of liquid that needs to be delivered to fill the target vasculature. Importantly, at this stage of the procedure the liquid needs to solidify, reducing the flow in the part of the vasculature it is being injected in order to be able to fulfil its function as an embolic material. Once the targeted area is successfully embolised, it is important that the solidified material does not adhere to the microcatheter used for delivery. Therefore, there is the need to avoid excessive reflux to allow easy withdrawal of the microcatheter following the embolisation procedure.

Once the liquid embolic has been injected into the patient, the characteristics of the solidified material become leading factors in the success of the embolic implant. The implanted material must be biocompatible in nature to avoid adverse effects within the body over long-term implantation. It is vital that the implant has long-term stability at its injection site to avoid migration within the vasculature to non-target vasculature and organs which could pose high

risks to patients. In addition, it is important for the solidified embolic to remain as a solid cohesive mass and not break off or fragment leading to smaller particles which could pose the risk of migrating and embolising elsewhere within the body. Whilst retaining this structural stability, there is also a desire for the liquid embolic to solidify as a soft plug within the vasculature with a compressible nature. This characteristic reduces the likelihood of mechanical irritation with surrounding tissue and also in cases where embolisation is used as aid prior to surgical removal, a compressible implant makes for easier surgical removal.<sup>107</sup>



1) Preparation	2) Delivery	3) Implantation
<ul style="list-style-type: none"> <li>Preparation - minimal time to prepare</li> <li>Deliverability - suitable viscosity to draw into a syringe and deliver using a microcatheter</li> </ul>	<ul style="list-style-type: none"> <li>Injectability - flow proximally with minimal reflux</li> <li>Controllability - able to predictably fill vasculature</li> <li>Adhesiveness - non-adhesive to the microcatheter</li> <li>Predictability - fill a predetermined volume of the vasculature per mL of sample delivered</li> <li>Occlusion - reduces flow through vasculature</li> </ul>	<ul style="list-style-type: none"> <li>Biocompatible - long term biocompatibility</li> <li>Cohesive - remains as solid mass and does not fragment</li> <li>Compressibility - soft plug to avoid mechanical irritation</li> <li>Stability - remains at injection site and does not dislodge</li> </ul>

In the case of radiopaque liquid embolic, there is an additional requirement that the injected liquid is of suitable radiopacity for the delivery to be monitored by fluoroscopy. Then, once solidified, the implanted material must retain long-term radiopacity to be easily located in follow-up scans for the full duration that it is implanted within the patient. The development of suitable test methods is vital to evaluate if the requirements for a liquid embolic can be met

for each stage of the process for an embolisation procedure using developed radiopaque liquid embolic prototypes. Reliable test methods need to be established to replicate the conditions of delivery and implantation to be able to predict *in vivo* behaviour of liquid embolic materials in the development stages.

The development of suitable characterisation test methods will be outlined in this chapter for evaluating the behaviour of a radiopaque liquid embolic prototype based on a radiopaque polymer which precipitates on contact with aqueous conditions when delivered using a carrier solvent of dimethyl sulfoxide (DMSO). The development of an imaging method to determine the radiopacity of the precipitated radiopaque polymer will be discussed in Chapter 3. The characterisation and imaging test methods discussed will be based on a single precipitating radiopaque liquid embolic prototype with further prototypes explored in the proceeding results chapters.

## 2.2. Experimental

### 2.2.1. Statistics

For experiments where the number of replicates was greater than 3, the error associated with the calculated mean was quoted as the standard deviation (Equation 2.1). For experiments where the number of replicates was equal to 3, the error of the calculated mean was quoted as the standard error of the mean (Equation 2.2).

$$\sigma = \sqrt{\frac{\sum(x - \bar{x})^2}{n}}$$

*Equation 2.1 - Standard deviation equation for samples where  $n > 3$ .*

$$\sigma_M = \frac{\sigma}{\sqrt{n}}$$

*Equation 2.2 - Standard error of the mean equation for samples where  $n \leq 3$ .*

Where  $x$  = mean,  $n$  = sample size,  $\sigma$  = standard deviation and  $\sigma_M$  = standard error of the mean.

### ***2.2.2. Nuclear Magnetic Resonance Spectroscopy***

NMR samples were prepared by dissolving 5-25 mg of sample in deuterated solvent (0.7-1.0 mL) and filtering into an NMR tube through a glass wool plug to remove any solid impurities.  $^1\text{H}$  and  $^{13}\text{C}$  NMR spectra were recorded at 400MHz on a Bruker Avance III HD 400 instrument and measured coupling constants are stated in Hz to the nearest decimal place. NMR splitting abbreviations used; s = singlet, d = doublet, t = triplet, q = quartet, quin. = quintet, m = multiplet.

### ***2.2.3. Mass Spectrometry***

Small molecule starting materials used in the synthesis of the liquid embolic samples were analysed by mass spectrometry to confirm the molecular weights of the molecules targeted. Samples were purified typically by column chromatography or recrystallisation and dried in a vacuum desiccator to ensure complete removal of solvent from the samples. Samples were analysed by electrospray mass spectrometry on a Waters LCT Classic LC-MS instrument.

### ***2.2.4. Infrared Spectroscopy***

Fourier-transform infrared spectroscopy (FTIR) was performed for small molecule starting materials used in the synthesis of the liquid embolic samples. This was carried out using a PerkinElmer FT-IR Spectrometer Spectrum Two with Perkin Elmer Spectrum software (version 10.03.07.0112).

### ***2.2.5. Melting Point Analysis***

The melting point of small molecule starting materials used in the synthesis of the liquid embolic samples was determined using an automatic melting point apparatus (Stuart

equipment, SMP50) for replicates of 3. The temperature ramp was started from 24.0 °C and increased with a ramp rate of 1.0 °C min<sup>-1</sup> until melting of the solids was detected.

### **2.2.6. *Elemental Analysis***

Liquid embolic samples were purified by precipitation into a non-solvent and dried in a vacuum oven at 40 °C to ensure complete removal of solvent. At least 50 mg of dried sample was submitted for elemental analysis testing for carbon, hydrogen, nitrogen, and iodine. The combustion analysis was performed on an automated Vario MICRO Cube CHNS analyser.

### **2.2.7. *Size Exclusion Chromatography***

Polymer solutions (2 mg mL<sup>-1</sup>) were prepared in DMF containing 0.1 w/w% lithium bromide and 0.1 w/w% toluene (flow rate marker) and filtered through PTFE membranes (0.45 µm pore size). Size exclusion chromatography of the samples was performed using an Agilent Technologies 1260 Infinity GPC/SEC instrument equipped with an Agilent 1260 Infinity G7800A multi-detector suite (refractive index detector and viscometer). The system was fitted with two PLgel Mixed-C 5 µm columns (300 × 7.5 mm) connected in series and a mobile phase was used of HPLC-grade DMF containing 0.1 w/w% LiBr at a flow rate of 0.1 mL min<sup>-1</sup> at 50 °C. Injection of the samples into the SEC system was performed using an Agilent autosampler with injection volumes of 100 µL. Conventional calibration was completed using a group of poly(methyl methacrylate) standards (Agilent Technologies) ranging from 500 to 1,500,000 g mol<sup>-1</sup>. The molecular weights and dispersity's of the polymer samples were calculated using Agilent GPC/SEC software (version A.02.01).

### 2.2.8. Precipitation Under Flow Conditions

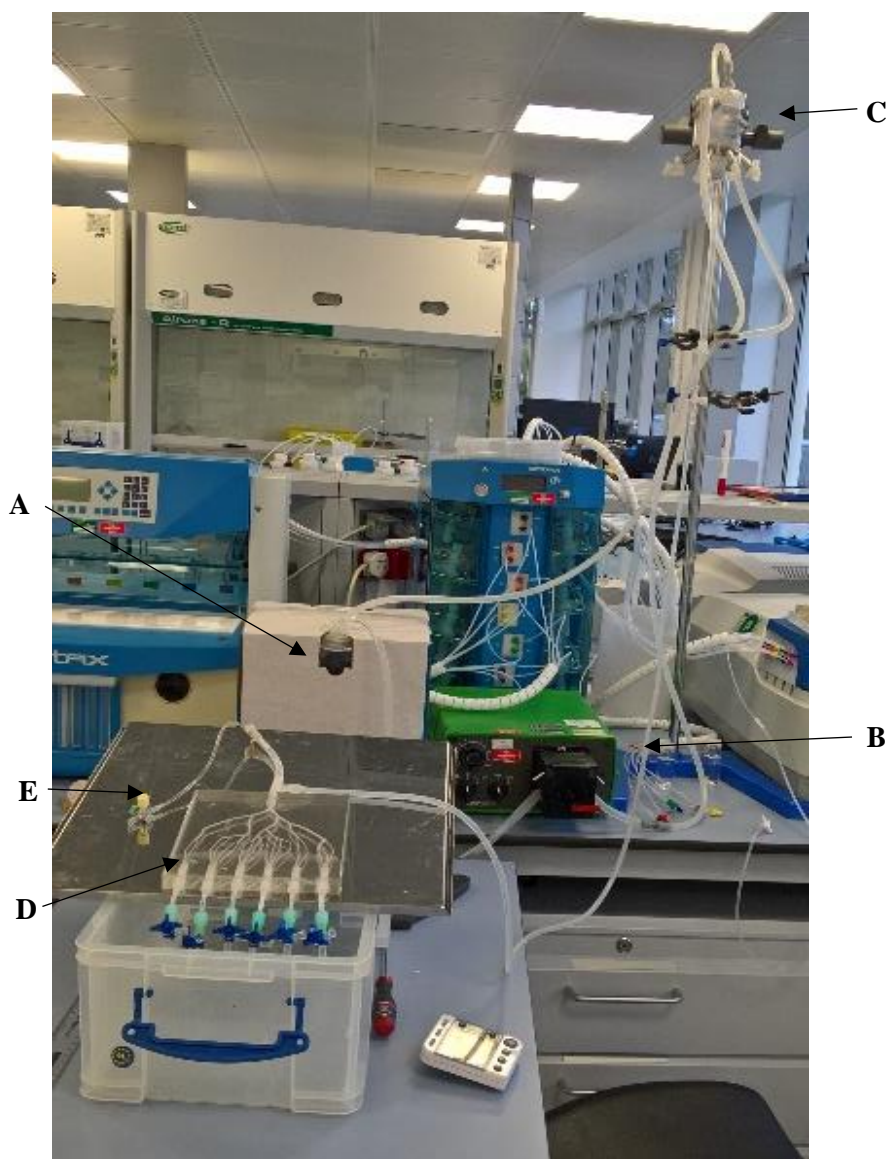


Figure 2.2 - Vascular flow model system set-up; (A) PBS reservoir (B) Peristaltic pump (C) Elevated PBS Reservoir (D) Vascular model (E) Microcatheter inlet.

A flow through system was set up using a peristaltic pump to create flow of phosphate-buffered saline (PBS) feeding into a reservoir elevated to 1.55 m above the point of injection to create pressures similar to that of blood pressure. PBS was flowed at a rate of 20-40 mL  $\text{min}^{-1}$  through a silicone vascular model with a microcatheter inlet.<sup>108</sup> Certified DMSO-compatible microcatheters of 0.57 mm internal diameter and 130 cm in length (Progreat® 2.4 Fr, Terumo or Renegade™ STC 18, Boston Scientific) were fed into the tubing *via* the microcatheter inlet. The liquid embolic samples (0.1 mL) were delivered *via* the microcatheter



from a 3 mL DMSO-compatible syringe and the length of advancement and reflux measured. The flow through the tubing was measured before and after delivery of the samples to allow the rate of occlusion to be inferred from the reduction in flow rate. The microcatheter was removed 5 minutes after delivery of the final portion of the samples and the ease of catheter removal was noted.

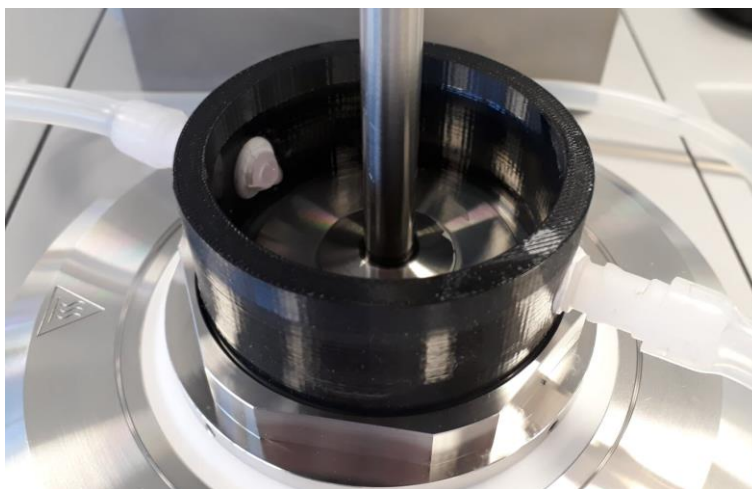
The system set-up was later simplified by replacement of the vascular cast with narrow bore tubing (polythene tubing of 1.67 mm internal diameter, Smiths Medical) to replicate a single vascular channel.

### **2.2.9. Rate of Solidification**

Solidification times of the liquid embolic samples were determined by monitoring the time taken to elute 90% of DMSO released over 1 h. The solidification test was performed using a dissolution bath (USP 2, SOTAX) connected *via* a pump to a UV spectrophotometer (Specord 200 Plus, SOTAX). The dissolution bath was heated to maintain each cell containing 500 mL of PBS at 37.5 °C with a mechanical paddle stirring at 50 rpm. The pump was set to continuously circulate solution from the cells to the UV spectrophotometer and recirculated to the cells in a closed loop system. The UV spectrophotometer was set to measure absorbance at 231 nm over 1 h through an 8-cell sample changer.

Liquid embolic samples (1 mL) were added dropwise into the pre-heated cells *via* delivery ports at staggered 2 minute intervals using a 1 mL micropipette set to reverse pipette (Picus 100, Sartorius) at the slowest rate setting. The elution of DMSO was monitored for 1 h after which the data was exported to Excel and analysed to determine the solidification time: the time taken to reach  $\geq 90\%$  elution of the maximum DMSO release over the monitored time period.

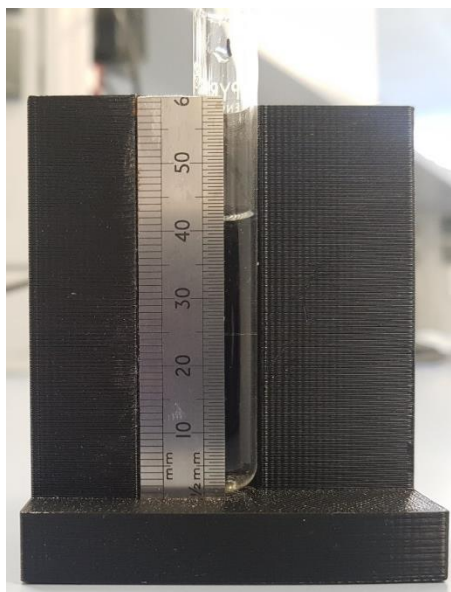
### 2.2.10. Rheometry



*Figure 2.3 - Rheometer experimental set-up with flow of saline through cell.*

The solidification of liquid embolic samples was monitored using a rheometer (Anton Paar, Modular Compact Rheometer 302) with a parallel plate geometry (Anton Paar, 50 mm inset and 25 mm measuring plate) at 37 °C. The base plate of the rheometer was modified with a 3D printed O-ring (approx. 5 cm in height) with an inlet and outlet to allow flow of saline solution across the plate (Figure 2.3). Liquid embolic samples (approx. 0.5 mL) were added to the centre of the base plate and the parallel plate was lowered to a gap of 1.0 mm. The plate was lifted, and further sample was added to ensure complete contact of the sample with the plate. The plate was lowered ensuring a gap of 1.0 mm to the base plate and any excess was removed from the area surrounding the plate using a plastic coated spatula. The viscosity of the liquid sample was monitored at 37 °C at a shear rate,  $\dot{\gamma}$ , of  $0.1 \text{ s}^{-1}$  with measurements taken every second. After 2-3 minutes of viscosity measurements of the liquid, the rheometry cell was flooded with saline solution (0.9% NaCl) pre-heated in a water bath to 40 °C with a peristaltic pump to create flow of saline solution across the rheometry plate. Viscosity measurements were performed for a further 30 minutes after the addition of saline to the rheometry cell with measurements continued every second. Following the test, the data was exported to Excel and analysed for viscosity ( $\eta$ ), storage ( $G'$ ) and loss ( $G''$ ) modulus of the liquid and solidification process.

### ***2.2.11. Precipitate Fill Volume***



*Figure 2.4 - Volume measurement device set-up.*

Liquid embolic samples (0.5 mL) were precipitated into glass petri dishes (10 cm diameter) containing 15 mL of PBS using a 1 mL micropipette set to reverse pipette (Picus 100, Sartorius) at the slowest rate setting. The precipitated samples were allowed to solidify for 30 minutes and then carefully transferred using plastic tweezers onto filter paper to wick surface moisture from the samples ensuring not to compress the samples. The wicked precipitates were then transferred into test tubes filled with approximately 2 mL of PBS. The difference in height of the PBS within the test tube was measured before and after the addition of the precipitates ensuring full submersion and the absence of any air bubbles. The difference in height measurements before and after the addition of the precipitates to PBS was used to determine the volume of precipitates inferred by the volume of PBS displaced within the test tubes.

### ***2.2.12. Fragmentation and Particulate Generation***

Liquid embolic samples (0.5 mL) were precipitated into 50 mL Duran bottles containing 30 mL of PBS from 3 mL DMSO-compatible syringes without needles from a drop height of 12

cm above the surface of PBS. The precipitated samples were allowed to solidify for 30 minutes and then agitated on a shaker plate at 240, 400 or 640 rpm for 30 minutes. Samples of the shaken PBS solutions were transferred to petri dishes using a plastic Pasteur pipette with the narrowed tip removed. The samples were imaged by optical microscopy (BX50 Olympus microscope with a Colorview camera). Images were captured at magnifications of  $\times 10$  to observe particulates and  $\times 4$  to observe fragments. The captured images were analysed, and each sample rated from 1-5 based on the degree of fragmentation and particulate generation.

Fragmentation analysis was carried out by counting the number of fragments over the size of 30 nm and averaged over replicates of 3 for the captured images at each shaker speed. The fragmentation averages were then rated according to the criteria outlined in Table 2.1. The overall fragmentation rating of each sample was taken as the highest fragmentation rating generated across the 3 shaker speeds tested.

*Table 2.1 - Fragmentation rating criteria.*

<b>Fragmentation Rating</b>	<b>Minimum Number of Fragments</b>	<b>Maximum Number of Fragments</b>
<b>1</b>	0	4
<b>2</b>	5	9
<b>3</b>	10	14
<b>4</b>	15	19
<b>5</b>	20	>20

Particulate analysis was carried out by calculating the percentage of the image area covered by particulates and averaged over replicates of 3 for the captured images at each shaker speed. Analysis of the captured images was carried out using ImageJ software (version 1.52) with the following image enhancements; image sharpening, contrast enhancement at 0.3% and noise reduction by despeckling. Analysis of the enhanced images was carried out using manual colour thresholding to highlight the particulates and particle analysis carried out for the selected particulates for sizes of 0.01-infinity pixels and of circularity 0.00-1.00. The calculated percentage area covered by particulates was averaged over 3 images for each sample and at each shaker speed tested. The averaged values were then rated according the

criteria outlined in Table 2.2. The overall particulate generation ranking of each sample was taken as the highest particulate rating generated across the 3 shaker speeds tested.

*Table 2.2 - Particulate rating criteria.*

<b>Particulate Rating</b>	<b>Minimum Particulate Area Coverage (%)</b>	<b>Maximum Particulate Area Coverage (%)</b>
<b>1</b>	0.00	0.99
<b>2</b>	1.00	1.99
<b>3</b>	2.00	2.99
<b>4</b>	3.00	3.99
<b>5</b>	4.00	>4.00

### ***2.2.13. Scanning Electron Microscopy***

The internal structure of I-PVA precipitates was observed by scanning electron microscopy (SEM). Precipitated samples were prepared by the dropwise addition of liquid embolic solutions (0.1 mL) into PBS (15 mL) using 1 mL micropipette set to reverse pipette (Picus 100, Sartorius) at the slowest rate setting. The samples were allowed to fully solidify and then mounted onto metal stubs using an embedding medium (Surgipath FSC 22®, Leica). The embedded samples were frozen using a cryostat (CM1860, Leica) and sliced into 10 µm sections to achieve a cross-sectional slice through the precipitate samples. The cross-sections were mounted onto SEM stubs and gold sputter coated under vacuum (Q150T, Quorum). The coated samples were transferred to the SEM chamber (Sigma FEG, Zeiss), imaged at an accelerated voltage of 10 KeV and the images captured.

### ***2.2.14. Solid Content Study***

The solid content of precipitated liquid embolic samples was measured at 1 h, 24 h, and 7 d following precipitation in PBS. Samples were prepared by precipitation of 0.3 mL of liquid embolic sample as a 40 w/w% solution in DMSO into 20 mL of PBS pre-heated to 37 °C. The sample was precipitated to form a single mass and repeated using 9 vials (corresponding to n=3 for each timepoint taken). The precipitated samples were maintained at 37 °C for the duration of the experiment and removed at timepoints 1 h, 24 h, and 7 d and analysed for their

solid contents. The mass of the ‘wet’ precipitates was measured, and the sample then dried by heating to 150 °C and measuring the ‘dry’ mass once cooled. This was carried out for replicates of 3 for each timepoint and the differences in ‘dry’ and ‘wet’ masses used to determine the solid contents.

## **2.3. Results and Discussion**

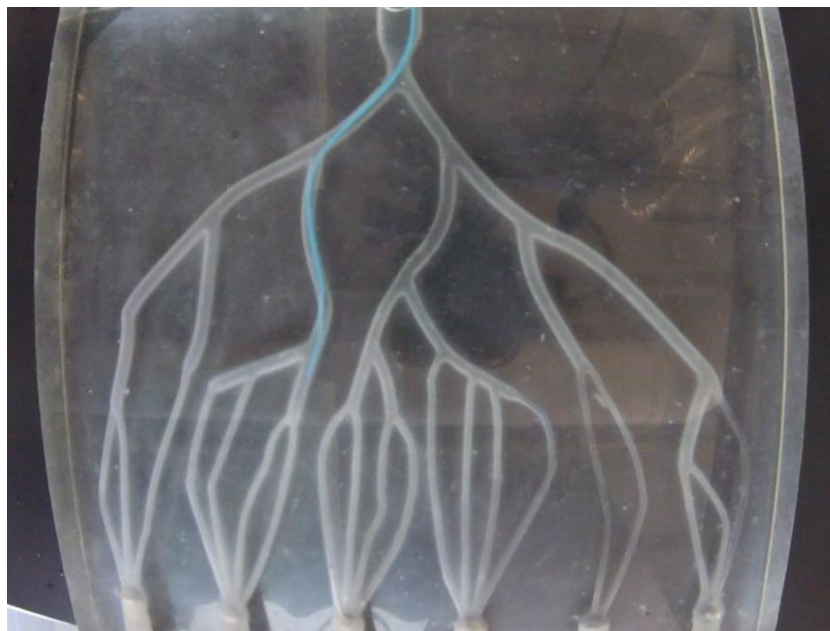
### ***2.3.1. Preparation Time***

A desirable characteristic for a liquid embolic is to have minimal preparation time to allow interventional radiologists to administer the embolic material when needed without adding additional time to the procedure for preparing solutions.<sup>109</sup> The proposed formulation is based on a pre-formulated polymer in a DMSO solution, being supplied ready to use avoiding any additional pre-mixing procedure times. To confirm whether the solution remained stable over long-term storage, photos were taken of the formulations after long-term storage (approximately 1 year) to confirm whether stable solutions were maintained without any sedimentation.

### ***2.3.2. Deliverability Under Flow Conditions***

The delivery properties of the samples were evaluated using a microcatheter to deliver the samples under flow conditions. This allowed insight into the ease of delivery of the liquid sample using a microcatheter, behaviour of the material as it precipitated and the degree of control as to whether embolisation could be achieved and with what amount of reflux if any. Once solidified, the adhesion of the material to the microcatheter was gauged by how difficult or easy it was to remove the microcatheter and whether any sample adhered to the tip of the microcatheter. PBS was chosen to mimic blood plasma due to the similar ion concentrations, osmolarity, and pH to blood plasma whilst also being inexpensive and easily in large quantities prepared as required.

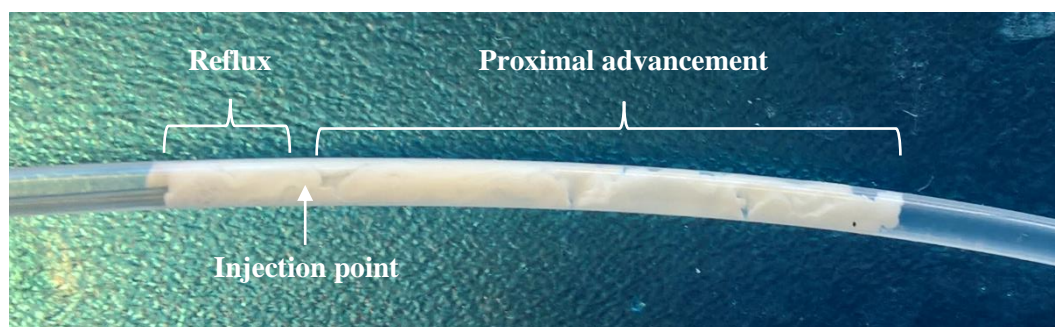
To investigate the delivery of liquid embolic samples, an open flow system was set up using a peristaltic pump creating a flow of PBS *via* a hanging reservoir elevated to a height of 1.55 m to replicate pressures similar to those found in the vasculature. A microcatheter inlet was incorporated into the system to allow the delivery of samples into the system *via* a microcatheter (Progreat® 2.4 Fr, Terumo or Renegade™ STC 18, Boston Scientific). A silicon cast based on vasculature commonly injected during an embolisation procedure was initially used to replicate injection conditions (Figure 2.5). Prior to injection, the flow of PBS through the model was adjusted to a flow rate of 30-40 mL min<sup>-1</sup> through the channel targeted during sample injection. The vascular model included varying sizes of channels along with degrees of branching. Injection into this model allowed insight into how liquid embolic samples performed in varying sizes of channels and the behaviour of the samples around bifurcations at the branching points within the channels. This method provided qualitative analysis of how samples could be expected to behave under embolisation conditions.



*Figure 2.5 - Vascular flow model.*

This method was simplified to instead use narrow bore tubing (1.67 mm internal diameter, approximately 10-15 cm in length) to replicate a single channel vasculature rather than branching and various sized vessels in the silicone cast model. This simplification enabled

reproducible conditions to be created by injecting into the same diameter tubing allowing quantitative analysis of the degree of proximal flow and reflux along with the rates of occlusion (Figure 2.6). The use of tubing meant that the injected sample could then be further analysed following delivery, for example by microCT imaging of the filled tubing to observe the precipitate structure. The liquid embolic samples were injected under the same experimental set-up using the hanging PBS reservoir and delivery through a 2.0 Fr microcatheter. For each injection once the microcatheter was filled with sample, 0.1 mL of liquid embolic was delivered into the system *via* manual injection from the microcatheter under continuous flow of PBS between 20-40 mL min<sup>-1</sup>.



*Figure 2.6 - Liquid embolic injection into tubing under PBS flow.*

Throughout the injection process any observations of the behaviour of the precipitation process were noted, for example the degree of proximal flow before reflux began to occur. The flow rate before and after the delivery of the samples was measured to be able to infer the degree of embolisation from the reduction in flow through the tubing after sample delivery. The lengths of precipitates were measured along with the portions of proximal advancement and reflux to demonstrate the precipitation behaviour of the material. Following delivery of the material, the microcatheter was left in place for 5 minutes with PBS flow remaining. The ease of catheter removal from the solidified samples was then noted (Table 2.3).



Table 2.3 - Delivery results for the tubing method under flow of PBS (n=3).

Replicate	Initial Flow Rate (mL min <sup>-1</sup> )	Final Flow Rate (mL min <sup>-1</sup> )	Reduction in Flow Rate (%)	Length of Precipitate (mm)	Catheter Removal	Delivery Notes
1	32.0	0.0	100.0	39.5	Easy	Refluxed then flowed forward
2	23.0	0.1	99.6	37.0	Easy	Refluxed around microcatheter
3	21.0	0.2	98.8	37.0	Easy	Refluxed then flowed forward

Samples injected during the development of this method were found to dramatically reduce the flow rates of PBS through the tubing by  $99.5 \pm 0.3\%$  after delivery of 0.1 mL of the sample. Flow reduction rates were all found to be greater than 90% indicating high degrees of occlusion of the tubing by the samples demonstrating suitability for use as an embolic agent. Complete blocking of the flow is not necessary for an embolic agent as in the majority of embolisation cases the delivered embolic will act as a mechanical framework for thrombus formation to occur which leads to the complete occlusion of blood vessels.<sup>110</sup> However, high levels of occlusion using an embolic material alone suggest suitability for use in patients with reduced ability to form blood clots such as coagulopathy or in trauma cases where rapid embolisation is required.

### 2.3.3. Rate of Solidification

Predictable solidification times are an essential requirement for liquid embolics as it provides an idea of the working time of the material during its injection. Fast solidification times are required to form an embolus within the vasculature without washout by the blood flow. However, solidification times that are too fast will result in poor penetration into the vasculature reducing the efficiency of embolisation.<sup>111</sup>

The solidification profiles of the liquid embolic solutions were determined by monitoring the release of the carrier solvent (DMSO) as the samples solidified in PBS. This was carried out using a dissolution bath set at 37 °C to replicate body temperature with each test vessel filled with 500 mL of PBS to replicate the aqueous salt conditions of blood. The samples were added dropwise into the vessels with slow mechanical stirring at 50 rpm to allow uniform dissipation of carrier solvent, DMSO, throughout the volume of PBS without destroying the precipitates as they formed. A closed-loop flow of the solution was circulated continuously for 1 h and the UV absorbance of DMSO (231 nm) measured every 10 seconds for each vessel.

The UV data was analysed for the maximum DMSO absorbance, solidification time as measured by the time to elute 90% or higher the total amount of DMSO eluted and time taken to reach the maximum amount of DMSO eluted over the experiment run time (Table 2.4).

*Table 2.4 - Solidification data a liquid embolic prototype (n=3).*

<b>Replicate</b>	<b>Max Absorbance</b>	<b>Solidification Time (<math>\geq</math> 90%) (s)</b>	<b>Max Amount of DMSO Eluted (s)</b>
<b>1</b>	0.3541	364	749
<b>2</b>	0.3478	344	689
<b>3</b>	0.3614	445	1072

There was found to be close agreement between the solidification profiles of each replicate of the liquid embolic sample across the timescale of the test (Figure 2.7). The average solidification time was determined to be 06:24  $\pm$  00:25 for 90% of the total DMSO eluted from the precipitates. This highlights the suitability of this test method for reliably determining the solidification rates of samples solidifying under these conditions.

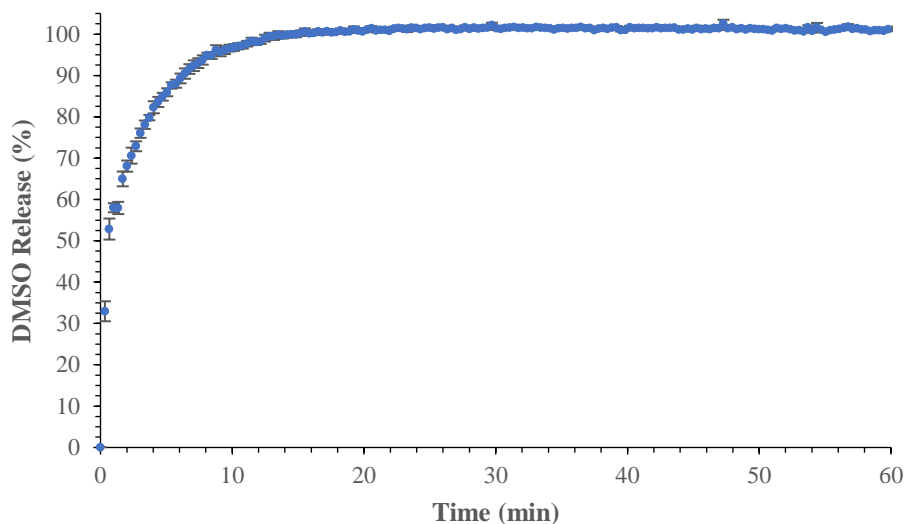


Figure 2.7 - Solidification profile of a liquid embolic prototype ( $n=3$ ).

There is a limitation to determining the rate of solidification for samples that solidify rapidly whilst floating on the surface of PBS (Figure 2.8). This is due to the experimental set-up of the outlet leading to the UV spectrophotometer which is located on the stirrer paddle axis submerged close to the PBS level. Hence, any samples which solidified and floated on the surface of PBS resulted in a higher release of DMSO close to the outlet initially giving rise to a high DMSO absorbance. The DMSO absorbance was then found to reduce over time as the solution was circulated from the UV spectrophotometer into the vessel allowing the dilution of DMSO within the PBS media (Figure 2.9). Hence, this method is not deemed to give a true representation of solidification profiles for samples which solidify rapidly on the surface of PBS adjacent to the UV outlet.



Figure 2.8 - Solidification of a liquid embolic sample on surface of PBS close to the UV outlet.

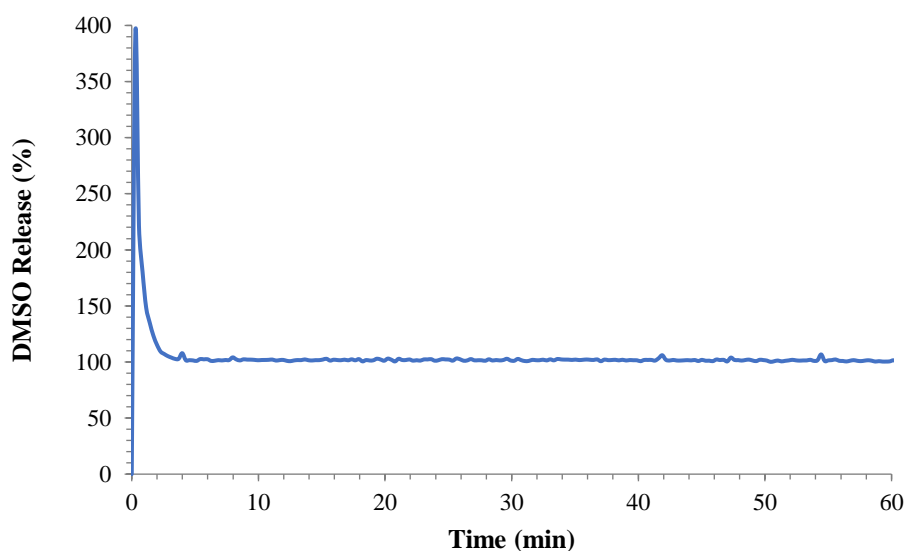


Figure 2.9 - Solidification profile of a rapidly solidifying liquid embolic prototype ( $n=1$ ).

#### 2.3.4. Rheology of Solidification Process

An additional method to characterise the solidification process of the precipitating liquid embolic materials is to use rheometry to monitor the transition from liquid to solid. In the solidification tests, measurements of the liquid sample were initially performed at 37 °C using a parallel plate set-up at a constant shear rate of 0.1 s<sup>-1</sup>. There was found to be high standard

deviations associated with measurements performed on the liquid sample (Figure 2.10, Table 2.5). This was likely due to the geometry of the rheology system used and small plate size.

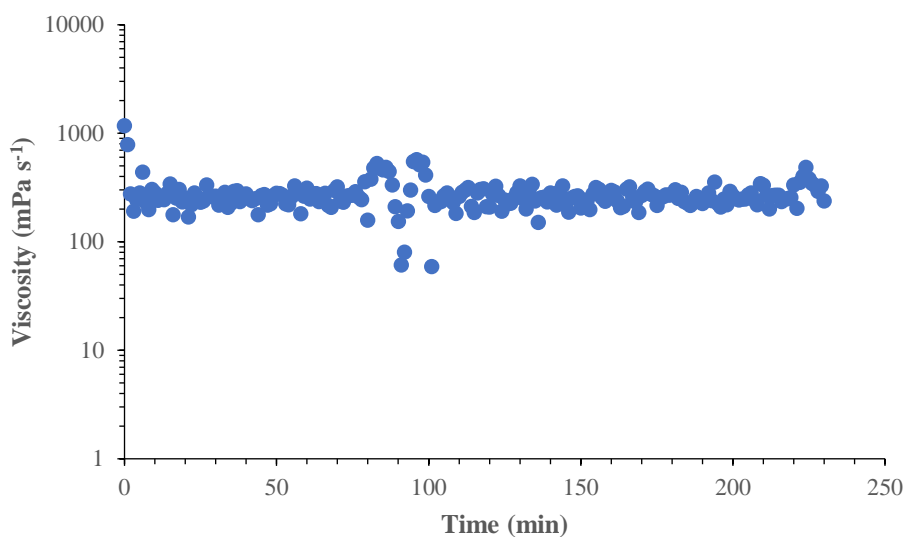


Figure 2.10 - Viscosity of a liquid embolic prototype in DMSO at 37 °C ( $n=1$ ).

Table 2.5 - Rheology data of a liquid embolic prototype in DMSO at 37 °C ( $n=216$ ).

	<b>Mean</b>	<b>Standard Deviation</b>
<b>Viscosity (mPa s<sup>-1</sup>)</b>	275.0	99.2
<b>Storage modulus (Pa)</b>	0.41	0.47
<b>Loss modulus (Pa)</b>	2.68	0.98

Following rheology measurements on the liquid sample, the rheometry cell was then flooded with saline solution (0.9% NaCl) pre-heated to 40 °C to maintain the test temperature of 37 ± 5 °C. On contact of the outer perimeter of the plate with saline solution, there was seen to be a rapid increase in parameters such as the viscosity, storage modulus and loss modulus indicating the onset of solidification (Figure 2.11, Table 2.6). The test was continued for a further 30 minutes after the onset of solidification to monitor the transition to solidified precipitate. Testing the liquid embolic samples under these conditions allows information to be obtained about the properties of the precipitate formed during the solidification process. Initial experiments showed solidification at the outer perimeter of the sample first in contact with PBS but the central region to still be liquid and not solidified (Figure 2.12). Hence, longer

tests would need to be performed to monitor complete solidification, but this method instead provides insight into the onset of solidification.

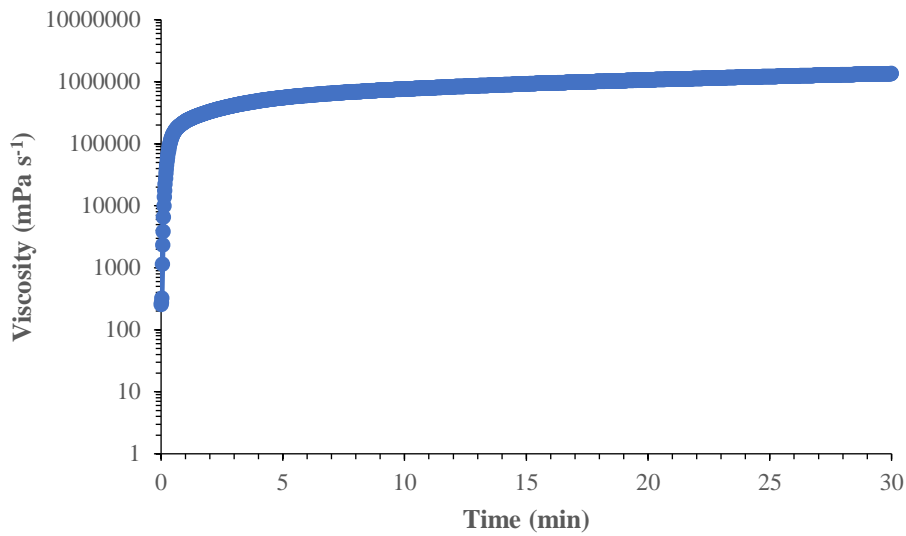


Figure 2.11 - Viscosity profile of the solidification process of a liquid embolic prototype at 37 °C (n=1).

Table 2.6 - Rheology data of the solidification process of the liquid embolic prototype at 37 °C (n=1).

<b>Maximum Viscosity (mPa s<sup>-1</sup>)</b>	<b>Maximum Storage Modulus (Pa)</b>	<b>Maximum Loss Modulus (Pa)</b>
8472700	82257	35032

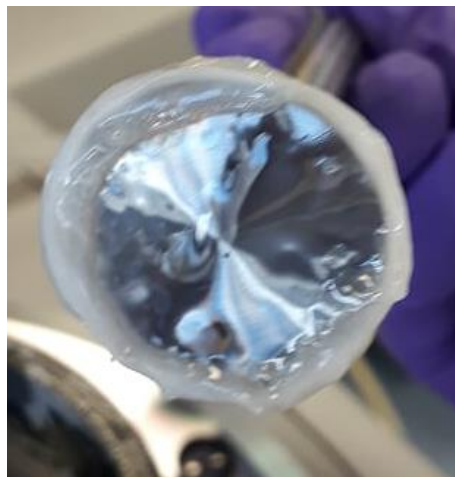


Figure 2.12 - Liquid embolic sample following rheology solidification testing.

### 2.3.5. *Fill Volume After Solidification*

A liquid embolic material should ideally fill the vasculature with a predictable fill volume to allow the interventional radiologist performing the procedure to be able to gauge how much liquid is necessary to fill the targeted vasculature. Therefore, volume measurements of precipitates formed from a known amount of liquid embolic solution were taken to determine the change in volume of the samples on transitioning from liquid to solid.

A volume measurement device was first calibrated using known amounts of PBS accurately dispensed using a micropipette and measured for their heights within a test tube for replicates of 3 for each volume (Table 2.7). The measured heights were then used to create a calibration graph for test tube height against volume (Figure 2.13).

*Table 2.7 - Volume measurement device calibration data (n=3).*

Volume of PBS (mL)	Height of PBS in Tube (mm)			Mean Volume (mL)	Standard Error of Mean
	Replicate 1	Replicate 2	Replicate 3		
<b>0.25</b>	6.5	6.5	6.5	6.5	0.0
<b>0.50</b>	11.5	11.5	11.5	11.5	0.0
<b>0.75</b>	16.0	16.0	16.0	16.0	0.0
<b>1.00</b>	21.0	21.0	21.0	21.0	0.0
<b>1.25</b>	26.0	26.0	26.0	26.0	0.0
<b>1.50</b>	31.0	31.0	31.0	31.0	0.0
<b>1.75</b>	36.0	36.0	36.0	36.0	0.0
<b>2.00</b>	41.0	41.0	41.0	41.0	0.0
<b>2.25</b>	46.0	46.0	46.0	46.0	0.0
<b>2.50</b>	51.0	51.0	51.0	51.0	0.0

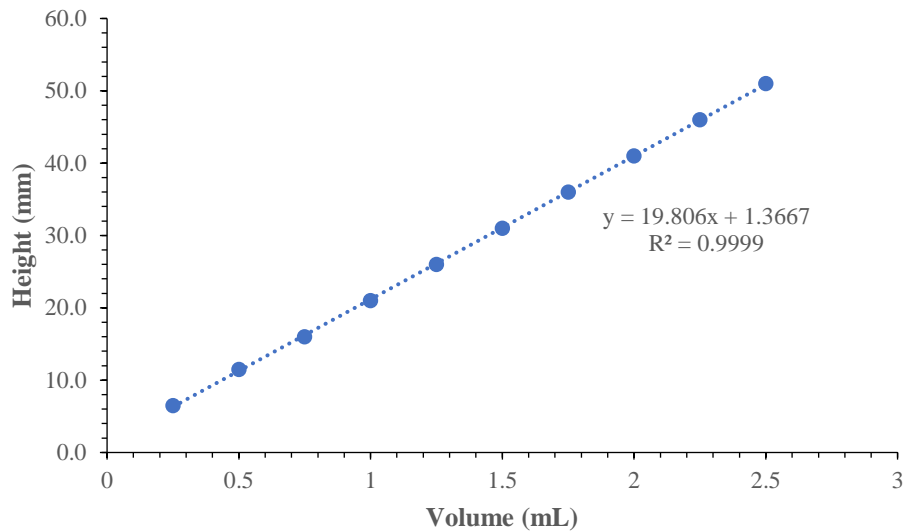


Figure 2.13 - Volume measurement device calibration graph ( $n=3$ ).

During the fill volume test of the liquid embolic samples, 0.5 mL of liquid sample was precipitated dropwise into a glass petri dish containing PBS. The samples were allowed to fully solidify before being wicked of surface moisture and then measured for their volume (Figure 2.14A). Volume measurements were obtained by transferring the precipitates into a test tube containing a known height of PBS (Figure 2.14B). The volume of precipitate was calculated by measuring the displacement of the PBS level within the test tube after the precipitate was submerged.

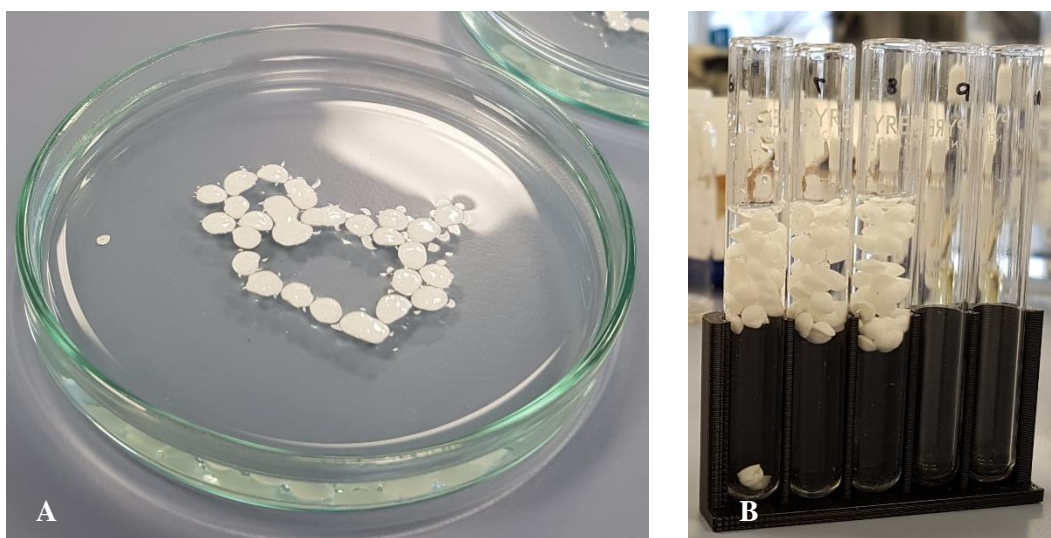


Figure 2.14 - Process of fill volume test; (A) Precipitation of liquid embolic sample. (B) Solidified sample test tube for height measurement in volume measurement device.



The test method was found to produce reproducible measurements for the change in fill volume transitioning from liquid to solid precipitate for replicates of 3 as indicated in Table 2.8. However, this method of producing the solidified sample is unlikely to represent how the samples would precipitate when injected into the vasculature. The method of precipitating the samples dropwise does not replicate the continuous mass of sample formed within the vasculature hence the actual fill volume is likely to vary. However, the test did provide a reproducible method to suggest trends in samples for varying degrees of reduction in volume on transitioning from a liquid to solid.

Table 2.8 - Fill volume data for a liquid embolic prototype (n=3).

Volume of Liquid (mL)	Height of PBS Before Addition (mm)	Height of PBS After Precipitate Addition (mm)	Height of Precipitate (mm)	Volume of Precipitate (mL)	Reduction in Volume (%)	Mean Reduction in Volume (%)	Standard Error of Mean (%)
0.5	43.0	49.5	6.5	0.26	48.1		
0.5	42.0	49.0	7.0	0.28	43.0	43.0	2.4
0.5	42.0	49.5	7.5	0.31	38.0		

### 2.3.6. Fragmentation and Particulate Generation

In order to allow the safe implantation of an embolic material within the vasculature, it is necessary for the material to form a cohesive mass i.e. the material must remain as one solid mass once injected and not break off to form smaller fragments. Any fragments formed pose the risk of becoming dislodged and embolising off-target elsewhere within the body. The cohesiveness of the embolic material can be investigated by examining the likelihood of formation of particulates and fragments when the precipitates are subjected to agitated conditions.

Initial experiments were performed to determine the required drop height to form reproducible precipitates. A drop height was required which was high enough to break the surface tension of the PBS into which the sample was dropped into. A height of 12 cm above the surface of PBS was found to be sufficient to form fully submerged precipitates of fairly uniform spherical shapes, thereby keeping the surface area of the precipitates similar during the agitation process.

The samples were precipitated from the determined drop height of 12 cm above the surface level of PBS (30 mL). The samples were allowed to fully solidify and then agitated on shaker plates at 240, 400, 640 rpm for 30 minutes to replicate low to high agitation conditions. In order to make direct comparisons between samples, the same size and shaped vessels containing PBS were used.

Following agitation, aliquots of the solutions were transferred to petri dishes and observed by optical microscopy. A high magnification was used to observe any particulates and a low magnification was used to observe any fragments that had formed. Analysis of the captured images was carried out to determine the percentage area coverage by particulates and number of fragments generated as observed at high and low magnifications, respectively. The analysis was performed for replicates of 3 images at each shaker speed and rated according to the fragmentation and particulate rating criteria outlined in Table 2.1 and Table 2.2. The fragmentation and particulate generation rating system of 1 to 5 represents minimal generation for samples with a rating of 1 and high amounts of generation for samples with a rating of 5 (Table 2.9 and Table 2.10).

Table 2.9 - Fragmentation data for liquid embolic prototypes (500 µm scale).





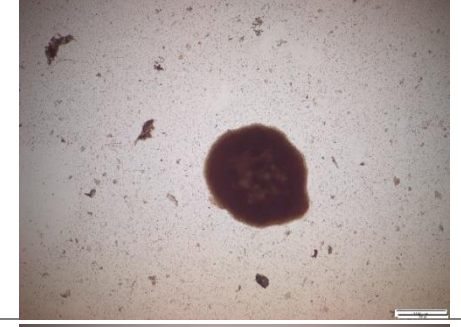






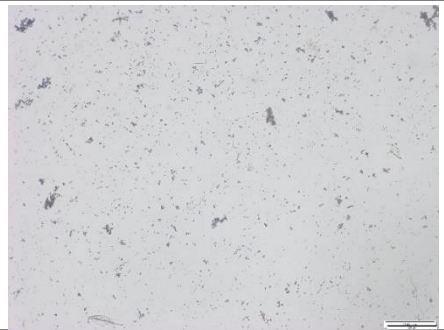

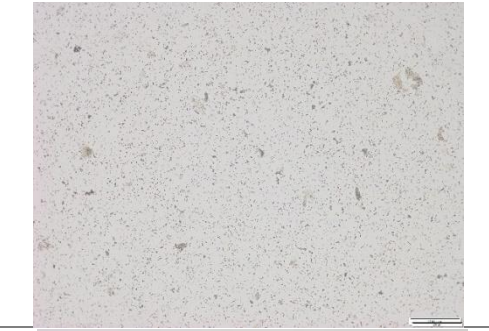

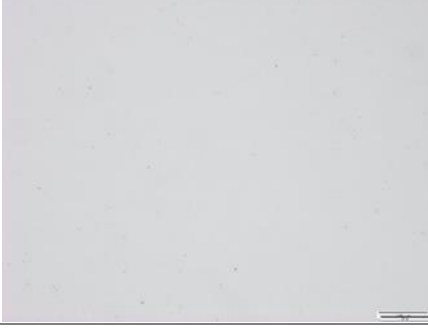

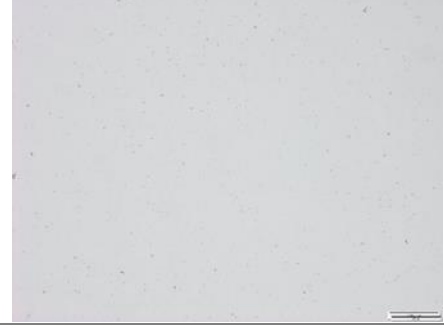
Liquid Embolic Prototype	Slow Shaker Speed (240 rpm)	Medium Shaker Speed (400 rpm)	High Shaker Speed (640 rpm)	Fragmentation Rating
1				3
2				2
3				1

Table 2.10 - Particulate generation data for liquid embolic prototypes (200 µm scale).

Liquid Embolic Prototype	Slow Shaker Speed (240 rpm)	Medium Shaker Speed (400 rpm)	High Shaker Speed (640 rpm)	Particulate Rating
1				5
2				5
3				1

It should be noted that the fragmentation and particulate generation test method used is unlikely to be representative of the conditions found within the vasculature when implanted over a long time period. The high shaker speeds used produced very extreme agitation conditions which are unlikely to be experienced during implantation of the material in the body. In addition, the process of forming the precipitates by the dropwise addition into PBS does not replicate how the embolic would form in the body but instead provides a method of forming uniform precipitates with reproducible surface areas. Due to the smaller size and high number of precipitate spheres formed by this method, there is a much larger surface area of the precipitates and therefore this may result in higher degrees of fragmentation and particulate generation due to the number of precipitates colliding with each other within the vessel as its being shaken. This method instead provides an ideal way of testing and comparing samples in the lab as an indicator of samples which may perform well if they were to be implanted in the body.

### ***2.3.7. Porosity of Internal Structure***

The porosity of the material gives a useful insight into whether the material might be compressible.<sup>112</sup> In addition, any signs of porosity indicate a potential mechanism for eluting drug from the liquid embolic. This would be particularly useful in the embolisation of tumours to provide targeted drug delivery at the tumour site in combination with the embolisation treatment.<sup>113</sup>

The internal porosity of precipitated liquid embolic samples was observed using a scanning electron microscope (SEM). Precipitates formed by dropwise addition into PBS were embedded within an embedding media. The embedded samples were frozen using a Cryostat and then thinly sliced to achieve a cross-section of the precipitate. The cross-section was transferred to an SEM stub and then gold sputter coated prior to observation under SEM.

The internal structure of the samples indicated by SEM provides some insight into how the samples solidify on contact with PBS. Highly porous structures were observed with larger pores located towards the centre of the precipitate with smaller more densely packed pores closer to the surface of the precipitate (Figure 2.15 and Figure 2.16). This corresponds to the initial formation of a skin on contact of the sample with PBS followed by diffusion of the carrier solvent DMSO out of the precipitate as it further solidifies leaving behind pores of varying sizes throughout the sample. This behaviour is often observed with the non-solvent induced phase separation of polymers in the fabrication of membrane structures.<sup>114</sup>

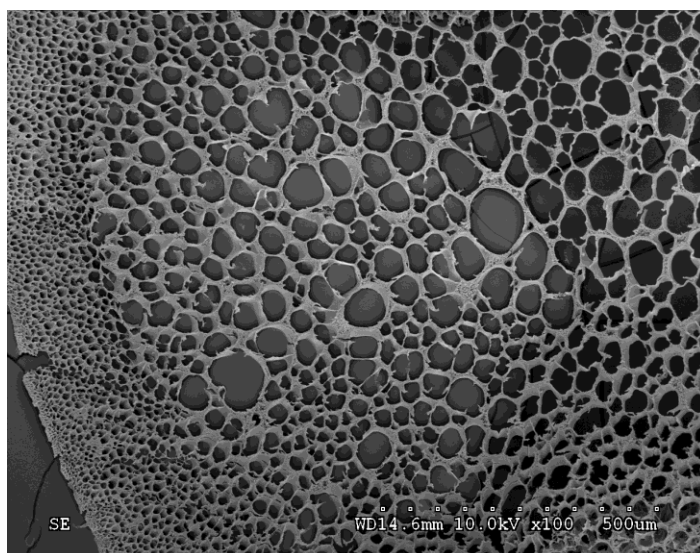


Figure 2.15 - SEM cross-sectional image of a precipitated liquid embolic prototype (500  $\mu\text{m}$  scale).

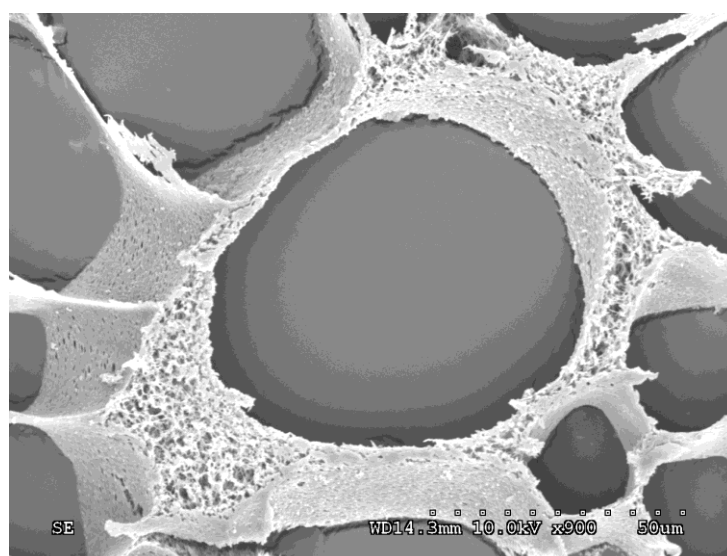


Figure 2.16 - SEM cross-sectional image of a precipitated liquid embolic prototype (50  $\mu\text{m}$  scale).

### 2.3.8. Stability of Precipitate

It is necessary for an implanted embolic material to maintain structural stability to allow the material to remain at its implanted site and avoid migration within the vasculature leading to potentially fatal consequences.<sup>115</sup> Hence, a stability study was performed to gauge any changes in solid content of the precipitated I-PVA following initial injection into PBS to indicate any swelling or contraction over time. Liquid embolic prototypes (0.3 mL) were precipitated into PBS (20 mL) at 37 °C with a replicate number of 3 for each timepoint. The precipitated samples were incubated at 37 °C and timepoints taken at 1 h, 24 h and 7 d to determine the solid content of the samples. This was carried out by taking measurements of the mass when wet and after drying by heating to 150 °C.

The measurements obtained indicated reproducibility between replicates at each time point as indicated by the determined standard errors (Table 2.11). Therefore, the method provides a reproducible method of monitoring changes in solid content of the precipitates over time to indicate any swelling or further hardening of the samples.

Table 2.11 - Solid content measurements over time for a liquid embolic prototype (n=3).

Time Point (h)	Solid Content (%)			Mean Solid Content (%)	Standard Error of Mean (%)
	Replicate 1	Replicate 2	Replicate 3		
1	54.7	36.5	42.9	44.7	4.4
24	44.4	34.5	38.5	39.1	2.3
168	37.7	40.6	34.5	37.6	1.4

### 2.3.9. Biocompatibility

When considering the implantation of materials into the body, it is necessary to fully characterise the chemical compositions to ensure materials are within specification i.e. polymer molecular weights within a suitable range and not containing any potentially toxic starting materials, by-products or residual solvents used in the materials synthesis. Hence, chemical analysis of liquid embolic samples was carried out using standard analytical methods

including proton and carbon NMR spectroscopy to verify the chemical composition of the samples and identify any impurities present. Mass spectroscopy was used to verify the compounds and purities of starting materials used in the synthesis of liquid embolic samples. Elemental analysis was used to verify the incorporation of radiopaque material into the liquid embolic formulations. Finally, gel permeation chromatography was used to verify if the polymer sample remained of a suitable molecular weight distribution after processing and formulation into liquid embolic solutions.

With regards to the cytotoxicity of the materials, the proposed liquid embolic materials have been determined to be biocompatible as outlined in the literature.<sup>34,116</sup> However, the small molecules and solvents used during the synthesis and purification of the liquid embolic prototypes are often toxic in certain quantities. <sup>1</sup>H NMR spectroscopy can be used to observe any residual quantities of small molecule starting material and solvents. By determining the remaining concentration of residuals by NMR spectroscopy these can be compared to toxicology values of the chemicals from literature to determine whether the residual values are within an acceptable range for the delivery of the material into the body when formulated as a liquid embolic.

## **2.4. Conclusions**

A series of test methods were developed to evaluate how potential liquid embolic formulations functioning by a precipitation mechanism might perform if injected into the body. Each stage of the liquid embolic injection was considered from preparation to delivery and implantation as a solidified embolic material. Test methods to evaluate the ease of preparation of the materials comprised of determining the long-term stability in solution by observing the solutions at timepoints of greater than 1 year after formulation into an injectable liquid embolic. Delivery tests encompassed a number of characterisation tests elements including ease of deliverability using a microcatheter, predictability to fill the vasculature,



controllability with regards to advancement and reflux, level of occlusion and adhesiveness once solidified towards the microcatheter. Alongside the deliverability tests, solidification tests also provided insight into the delivery properties of the materials with regards to their working times during injection before complete solidification.

Tests were also developed to evaluate the solidified embolic including analysis of the cohesiveness of materials to remain as a solid mass by fragmentation and particulate generation testing, the stability of precipitate by measuring the solid contents at various timepoints and observation of the internal porosity of the solidified materials.

Finally, chemical analysis of the materials was used to gauge the biocompatibility of the materials by observing and quantifying the presence of any potentially toxic starting materials, by-products and solvents.

## **Chapter Three**

### **3. MicroCT Method Development for Sample Imaging**

### **3.1. Introduction**

In order to evaluate the visibility of the liquid embolic prototypes under X-ray, micro-computed tomography (CT) experiments were conducted. MicroCT provides an ideal method for visualising the radiopaque polymer samples under X-ray and is a useful indicator of the expected visibility of samples *in vivo* as imaged *via* medical CT. The higher resolutions achieved using microCT in comparison to medical CT provides highly detailed 3D imaging of the samples and their internal structures. In the case of the precipitating liquid embolic samples, this offers useful insight into the structural properties and the mechanism by which solidification occurs.

In the microCT process the sample is mounted and secured, then rotated in small increments about a central axis whilst 2D radiographs are recorded using an X-ray source and a series of detectors. Once the scan is complete, radiographs are processed to create a 3D reconstruction of the sample using selected algorithms. The degree of X-ray attenuation is calculated using calibrated software, thereby allowing the radiopacity to be measured and quantified in Hounsfield units (HU).

### **3.2. Experimental**

#### ***3.2.1. Sample Preparation – Free-Formed Structures***

Liquid embolic prototypes were precipitated dropwise into 20 mL of PBS at 37 °C from a 3 mL syringe with a 19-gauge needle submerged under the PBS surface. Precipitated samples were stored in PBS and maintained at 37 °C for 48 h following precipitation.

#### ***3.2.2. Sample Preparation – Tubing Constraints***

Liquid embolic prototypes were injected from a 3 mL syringe *via* a microcatheter of 0.57 mm internal diameter and 130 cm length (Progreat® 2.4 Fr, Terumo) fed into polythene tubing of

1.67 mm internal diameter (Portex, Smiths Medical) through a microcatheter Y-connector. PBS flow was controlled from a PBS reservoir elevated 1.55 m above the delivery point to replicate blood pressure of a hepatic embolisation procedure and adjusted to a rate of 30-40 mL min<sup>-1</sup> for injections under PBS flow or 0 mL min<sup>-1</sup> for injections under no flow of PBS. The prepared samples were stored in PBS at room temperature for 48 h following precipitation.

### ***3.2.3. Sample MicroCT Scan Method***

Solidified liquid embolic samples were radiographed using a Bruker Skyscan 1172  $\mu$ -CT scanner (software version 1.5) with a Hamamatsu 10-megapixel camera using the following scan parameters; 49 kV X-ray voltage, 179  $\mu$ A X-ray current, 0.5 mm aluminium filter, 5.04  $\mu$ m image pixel size, 1000-pixel field width camera resolution, 180 ° tomographic rotation, 0.7 ° rotation step, 2 frame averaging and scan time of 18 min 8 sec.

### ***3.2.4. Reconstruction Parameters of Scan Data***

The scan data was reconstructed using NRecon software (version 1.6.9.4) using the following reconstruction parameters; 205.10 ° reconstruction angular range, 0% smoothing, 10% ring artefact correction, 1 under-sampling factor and 10% beam hardening correction.

### ***3.2.5. Radiopacity Calculations***

The radiopacity of the reconstructed scan images was analysed using CTAn software (version 1.14.4.1). The software was calibrated using the measured attenuation coefficients of a hydroxyapatite (HA) phantom (MicroCT-HA D4.5, QRM) scanned under the parameters outlined in Section 2.1 with the following values; 0.02316 m<sup>-1</sup> for lower phantom of 0.1987 g cm<sup>-3</sup> measured density and 0.08333 m<sup>-1</sup> for upper phantom of 1.2045 g cm<sup>-3</sup>. The calibration

values were normalised for attenuation coefficient values corresponding to density values of 0 and 1 g cm<sup>-3</sup>.

Reconstructed sample scan images were analysed by selecting the 3D volume of interest (VOI) and corresponding datasets. The radiopacity of the selected datasets was calculated using the measured attenuation coefficients with either a manual, automatic or adaptive thresholding method applied.

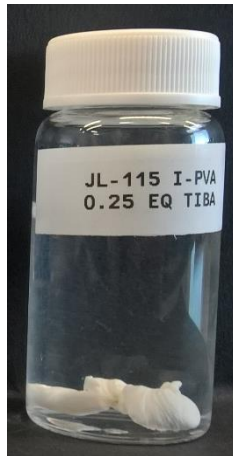
### ***3.2.6. Porosity Calculations***

The porosity of the reconstructed scan images was analysed using CTAn (version 1.14.4.1) by first selecting the 3D volume of interest (VOI) and corresponding datasets. The data was processed using the following functions; global thresholding between the limits of 45-255 grey scale units, removal of white speckles less than 10 voxels over selected 3D image space and 3D analysis selecting all basic values and additional values of number of objects.

## **3.3. Results and Discussion**

### ***3.3.1. Development of MicroCT Scan Method***

Initial sample scans were performed using a solidified liquid embolic sample precipitated by dropwise addition of the sample solution into PBS to produce a free-form structure (Figure 3.1). The precipitate was secured into a sample holder and mounted into the scan chamber. A trial and error method was used to visually select the best scan parameters for the sample with the use of a 0.5 mm aluminium filter found to be optimal for visualising the material alongside the standard operating conditions used to visualise bone samples.<sup>117,118</sup>



*Figure 3.1 – Liquid embolic sample precipitate by the free-form solidification method.*

Upon scanning, the sample was observed to exhibit a brighter region close to the surface. This may be a characteristic of the material or may be a property of the scanning method in which beam hardening is observed. This is a commonly observed imaging artefact arising from the different attenuations of X-rays emitted over a range of energies due to the polychromatic nature of the X-ray source used. X-rays with lower energies are attenuated faster than higher energy X-rays. The result of this is a higher proportion of photons are absorbed at the surface of the sample compared to the internal structures giving rise to the appearance of bright edges.<sup>119</sup>

To verify whether the bright edges observed in the scan images was a characteristic of the material or due to beam hardening artefact; beam hardening corrections were applied over the range of 0-20% (Figure 3.2). From the resulting reconstructed images, it was determined the bright edges could be attributed to an artefact of beam hardening with a 10% beam hardening correction found to be optimal for removing the observed beam hardening effect. The 10% beam hardening correction was subsequently applied to all subsequent liquid embolic prototypes scanned along with the hydroxyapatite (HA) calibrate to ensure accurate calculations of sample radiopacity.

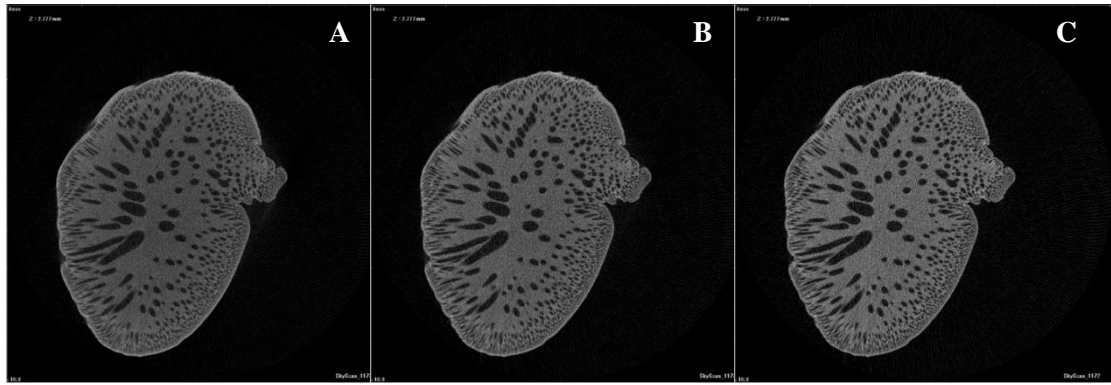


Figure 3.2 - Reconstructed scan images with increasing beam hardening correction applied; (A) 0% (B) 10% (C) 20%.

### 3.3.2. Calibration with Hydroxyapatite Standards

A hydroxyapatite (HA) phantom was used as a calibrate for the radiopacity calculations. The phantom consisted of five enriched HA epoxy resin rods of increasing densities from 0 to 1200  $\text{mg cm}^{-3}$  embedded in an epoxy resin casing. Rods of 200 and 1200  $\text{mg cm}^{-3}$  HA densities were selected as the lower and upper calibration values, respectively, as the radiopacity of the liquid embolic prototypes was anticipated to fall within this region of radiopacity measurements. The calibration calculation was performed using the attenuation coefficients of the two selected rods measured from their reconstructed scan data after the application of a 10% beam hardening image correction (Figure 3.3). These measured values were inputted alongside the accurate HA densities of each rod and the values normalised with respect to HA densities between 0-1000  $\text{mg cm}^{-3}$  (Table 3.1 and Figure 3.4).

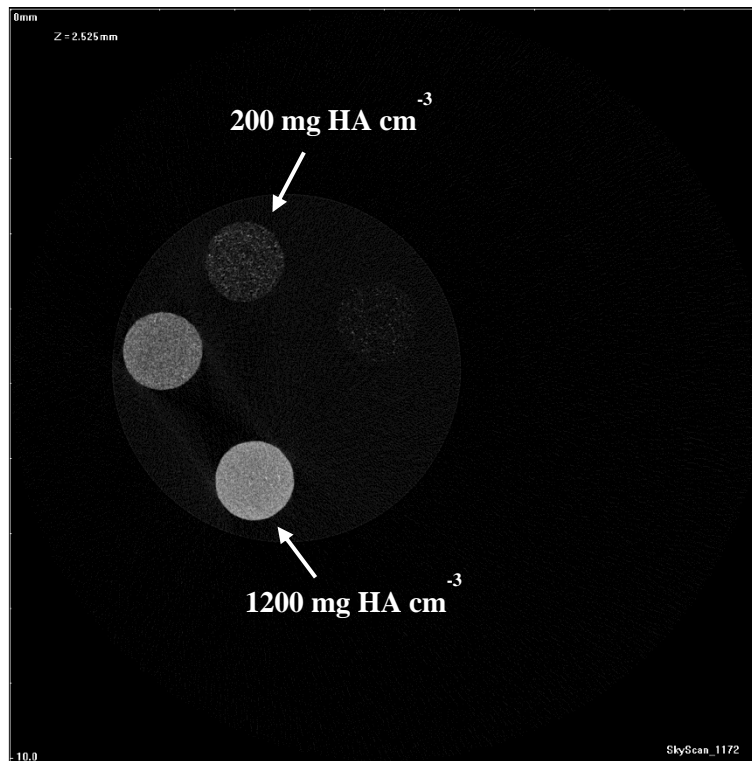


Figure 3.3 - Reconstructed 2D cross-section of HA phantom with selected 200 and 1200 mg HA cm<sup>-3</sup> rods highlighted.

Table 3.1 - HA phantom microCT data (imaging cross-sections, n=198).

HA Phantom (HA mg cm <sup>-3</sup> )	Actual Density (HA mg cm <sup>-3</sup> )	Attenuation Coefficient	Hounsfield Units
0	0.0	0.018	150
50	49.6	0.022	413
200	198.7	0.027	767
800	800.3	0.061	3026
1200	1204.5	0.083	4458



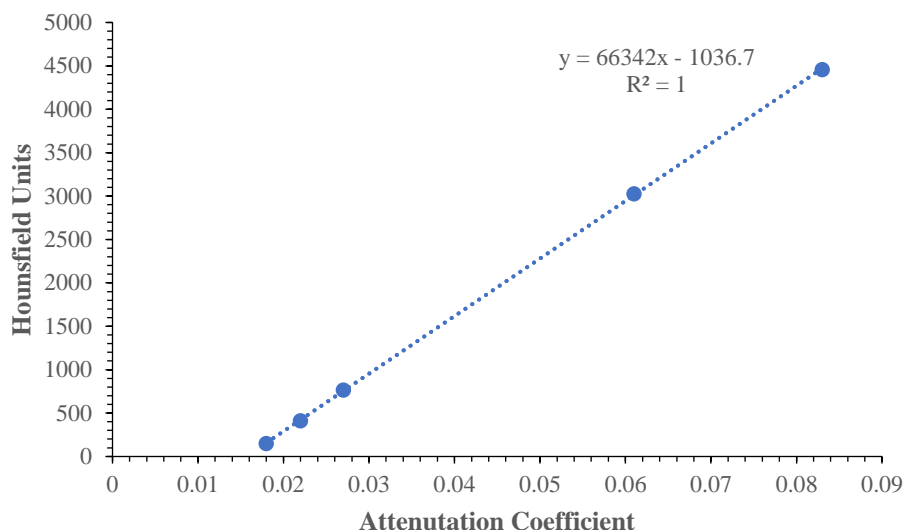


Figure 3.4 - HA phantom radiopacity calibration plot (imaging cross-sections,  $n=198$ ).

### 3.3.3. Scans of Free-Formed Samples

Initial microCT scans in the method development stage were carried out using a single liquid embolic prototype. The scan and reconstruction method developed for this sample was then applied to subsequent liquid embolic prototypes.

The reconstructed images of the different liquid embolic prototypes highlight the porous internal structures of each solidified sample with large pores present towards the centre and many smaller pores close the precipitate surface (Figure 3.5). This is consistent with the diffusion of DMSO out of the materials as they precipitate by initial solidification of the sample at the sample-solvent interface. This solidification process was confirmed visually with a skin first formed around the liquid sample droplet in PBS followed by solidification of the internal structure as indicated by a colour change of the precipitating materials from translucent yellow to opaque white.

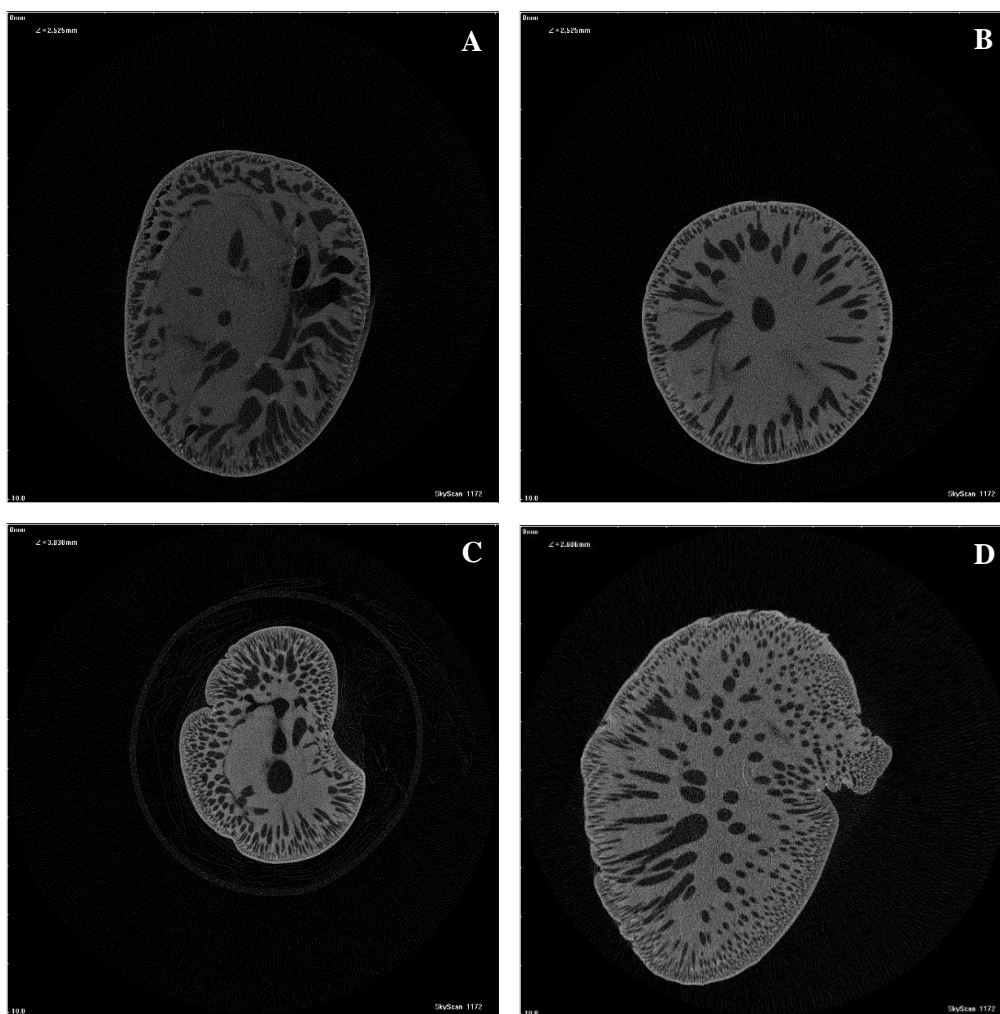


Figure 3.5 - Reconstructed 2D cross-sections of free-form solidified liquid embolic prototypes of varying radiopaque (RO) group concentrations; (A) 0.1 eq RO, (B) 0.15 eq RO, (C) 0.2 eq RO, (D) 0.25 eq RO.

### 3.3.4. Standardising Sample Preparation with Tubing

The microCT scans described thus far were carried out using liquid embolic prototypes solidified as free-formed structures in vials of PBS. However, these conditions are not representative of how the sample would solidify when injected into the vasculature during an embolisation procedure. Therefore, to replicate the conditions of the vasculature, samples were injected into narrow bore tubing from a microcatheter. Tubing with an internal diameter of 1.67 mm and composed of polythene was used making it suitable for use in microCT scans. The liquid embolic prototypes were injected into the tubing using a microcatheter (Progreat® 2.4 Fr, Terumo) which is a certified DMSO compatible microcatheter often used in

embolisation procedures and introduced into the tubing *via* a microcatheter Y-connector. The samples were injected into the tubing under flow of PBS at equivalent pressures to blood pressure using an elevated PBS reservoir calibrated to a height above the base plate to provide the appropriate pressure. The flow rate of PBS was adjusted prior to sample injection to 30-40 mL min<sup>-1</sup> and the initial flow rate recorded in order to give an indication of the degree of embolisation following the injection as determined by the overall reduction in flow rate through the tubing.

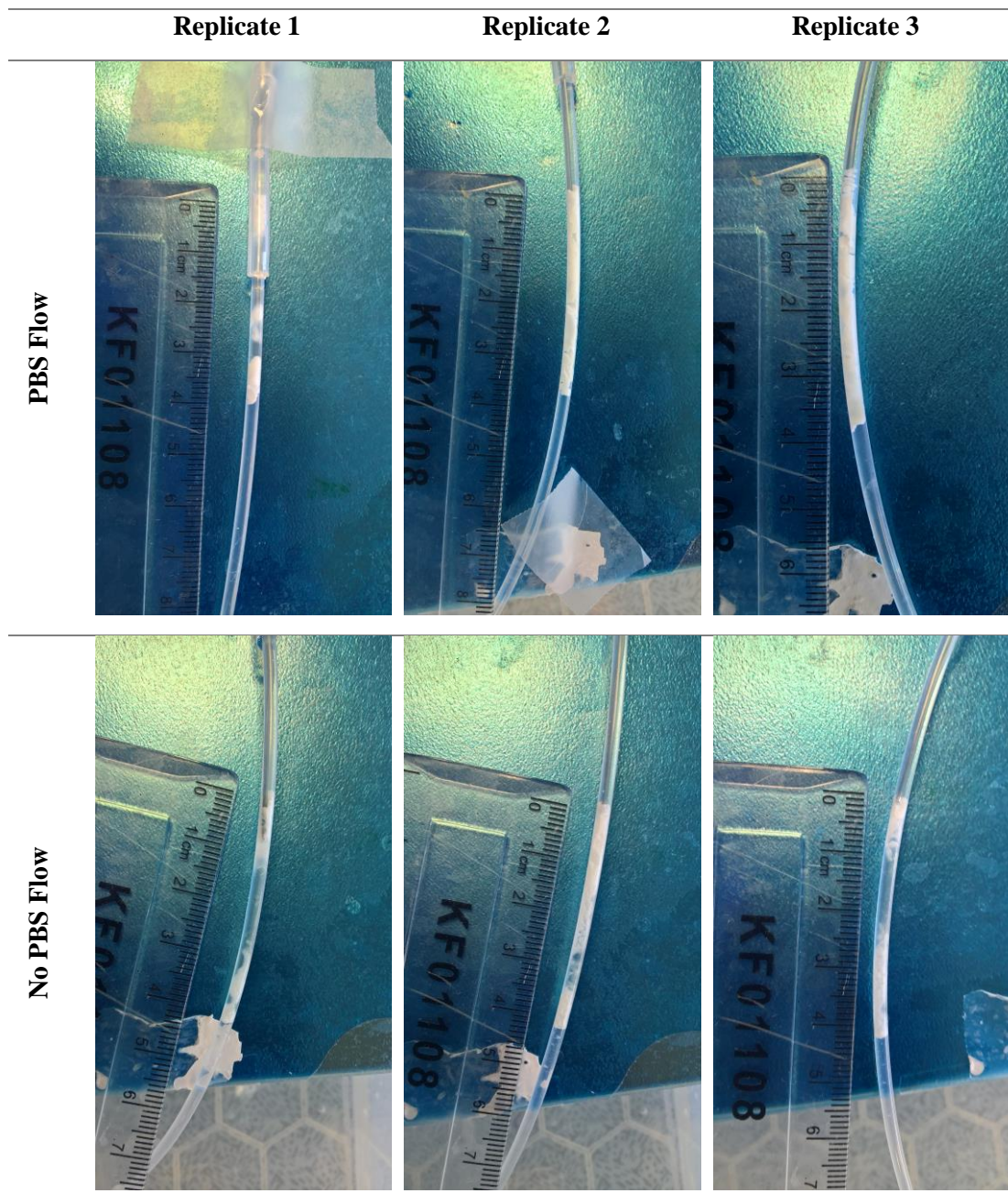
In addition to injection through a standard microcatheter, it is also common practice to utilise a balloon microcatheter to aid the delivery of a liquid embolic. In these procedures a small balloon is inflated around the microcatheter at the injection site resulting in a reduction in blood flow thereby enabling an embolus of liquid embolic to be formed with reduced risk of washout. Therefore, to mimic the conditions of an embolisation procedure carried out using a balloon catheter, injections were performed in which tubing was pre-filled with PBS and the injection carried out without flow through the tubing.

Following delivery, the samples were immersed in PBS for 48 h and the lengths of the precipitates measured at time-points (0, 24 and 48 h) to determine if there were any observable changes in the produced precipitate over time. There was found to be no change in precipitate length after 48 h, suggesting there should be no structural differences over time in the scanned microCT samples once precipitation has occurred. The manual injection method used to prepare the samples was found to produce reproducible precipitate lengths:  $37.8 \pm 0.7$  mm for PBS flow (n=3) and  $40.8 \pm 0.1$  mm for no flow of PBS (n=3) (Table 3.2). The precipitated samples were found to be highly effective at occluding the tubing with occlusion rates of  $99.5 \pm 0.3\%$  (n=3) achieved as determined by the difference in flow rates before and after injection. The microcatheter was also easily removed from the samples 5 minutes after solidification despite the occurrence of a small degree of reflux observed for all samples. This suggests no disturbance of the prepared samples occurred during catheter removal (Table 3.3).

Table 3.2 - Data for sample delivery of a liquid embolic prototype performed under flow and no flow of PBS (n=3).

<b>PBS Conditions</b>	<b>Flow Rate Reduction (%)</b>	<b>Length of Precipitate (mm)</b>	<b>Refluxed?</b>	<b>Ease of Catheter Removal</b>
<b>Under flow</b>	100	39.5	Yes	Easy
	99.6	37.0	Yes	Easy
	98.8	37.0	Yes	Easy
<b>No flow</b>	100	41.0	Yes	Easy
	100	40.5	Yes	Easy
	100	41.0	Yes	Easy

Table 3.3 - Images of a liquid embolic prototype delivered under flow and no flow of PBS (n=3).



### 3.3.5. Standardising Scan Analysis

To be able to accurately compare radiopacities between liquid embolic prototypes, it was necessary to standardise the thresholding method used to set the limits over which radiopacity was measured. During the radiopacity calculation the reconstructed images are binarized over the selected volume of interest (VOI) allowing the removal of noise and background pixels (Figure 3.6). The selected threshold limits determine which pixels are classed as object and

background during the binarization process and therefore directly affect the determined radiopacity. This is particularly the case for the lower threshold value applied.

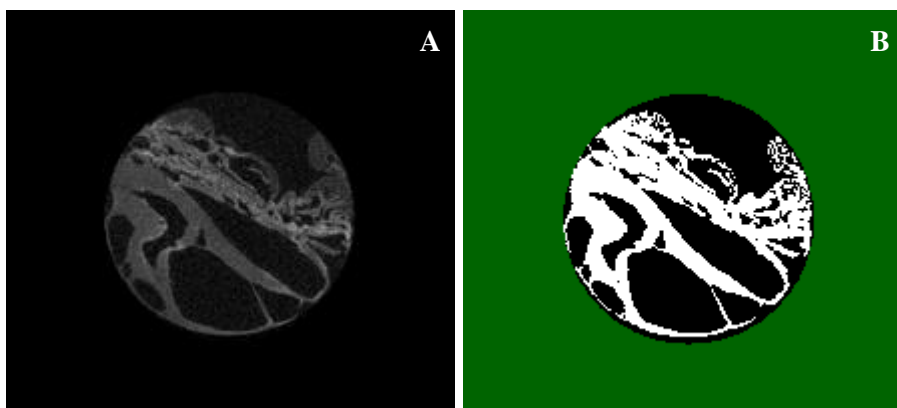


Figure 3.6 – (A) Reconstructed 2D cross-section image (B) Same cross-section image after binarization.

Three thresholding methods were trialled manual, automatic and adaptive. The manual thresholding method required visual comparison of images over a range of lower threshold values to determine the point of optimal noise reduction whilst maintaining image clarity. A limitation of this method is that it can be subjective with varying results between operators and any variations giving rise to variations between the determined radiopacities (Figure 3.7).

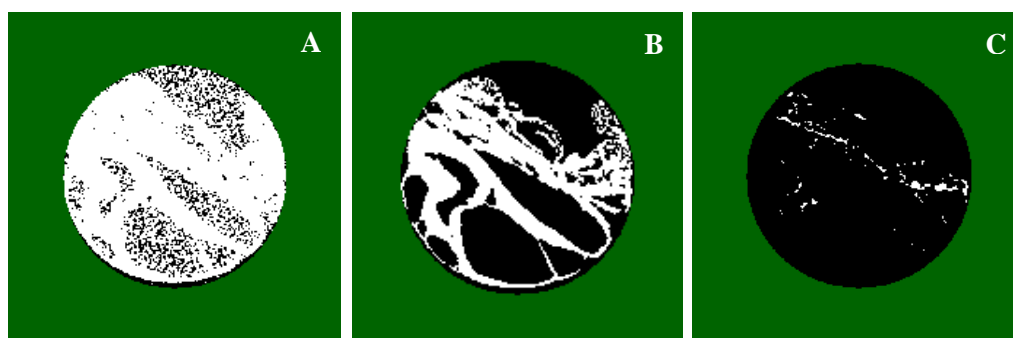


Figure 3.7 – (A) Binarized image with low thresholding (B) Binarized image with optimal thresholding (C) Binarized image with high thresholding.

The second thresholding method applied was the automatic method. This thresholding method utilises Otsu's algorithm in which the weighted in-class variance between the white object pixels and black background pixels is minimised.<sup>120</sup> Hence, low intensity pixels are assumed to be background pixels and are ignored from the radiopacity measurement. This can be

visualised as the point at which the histogram curves for the background and object pixels intersect as the minimum point of variation between the two pixel types (Figure 3.8).

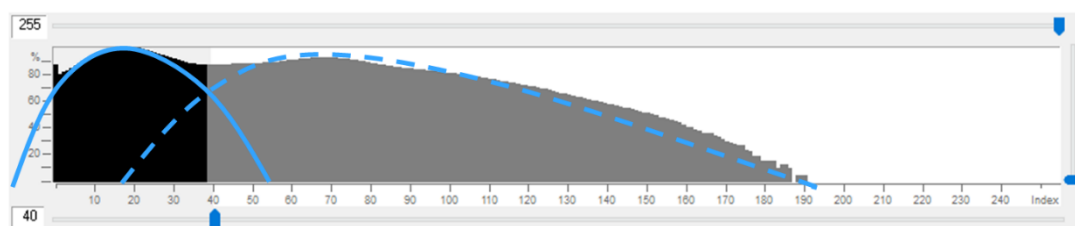


Figure 3.8 - Histogram of background and object pixels with a visual representation of the point of curve intersection used to determine position of automatic threshold.

Both the manual and automatic thresholding methods discussed are forms of global thresholding in that the lower threshold limit determined in the thresholding method is consistently applied across the entire VOI selected. However, it was observed that the structure of the precipitate formed within the tubing consisted of regions of thick and thin precipitate structures. Variation of structure thickness within a sample can give rise to a partial volume effect by which thin structures can appear to have lower X-ray density than thick structures despite the same chemical composition. Therefore, it could be beneficial to apply an adaptive thresholding method. Adaptive thresholding involves the application of a global algorithm calculating the mean for the minimum and maximum values over 3D space, analysing pixel intensity around each pixel within the VOI. This reduces any underestimation of regions of thin structures without over-exaggerating regions of thick structures (Figure 3.9).



Figure 3.9 – (A) Reconstructed 2D cross-section image (B) Binarized cross-section image with global thresholding (C) Binarized cross-section image with adaptive thresholding.

The data presented in Table 3.4 corresponds to liquid embolic samples precipitated *via* the tubing method under flow and no flow of PBS. There was found to be close agreement between the manual and adaptive thresholding methods ( $p=0.89$  as calculated using a two-tailed t-test). This indicates that, despite the presence of thin and thick structures within the samples, an adaptive method offers no benefit over a manual global thresholding method. Despite the subjective nature of the manual method, reliable radiopacity measurements were achieved as indicated by the close agreement with the measurements obtained using the adaptive threshold method. The high radiopacity results obtained using the automatic thresholding method suggest a lower threshold value set too high and therefore not inclusive of less intense object pixels, giving the appearance of a higher radiopacity value (Figure 3.10 and Figure 3.11).

*Table 3.4 - Radiopacity data for manual injections performed under flow and no flow of PBS with thresholding methods; manual, automatic, adaptive (imaging cross-sections,  $n=198$ ).*

Injection Type	Manual Thresholding		Automatic Thresholding		Adaptive Thresholding	
	Mean (HU)	Standard Deviation	Mean (HU)	Standard Deviation	Mean (HU)	Standard Deviation
Under PBS Flow	3052	1769	3094	1763	2819	1829
	5677	4171	11495	1465	5783	4168
	5193	4015	11105	1615	5275	4018
No Flow of PBS	4341	2742	4478	2740	4137	2771
	7260	5720	14619	1510	7564	5737
	6392	5550	14665	736	7140	5656



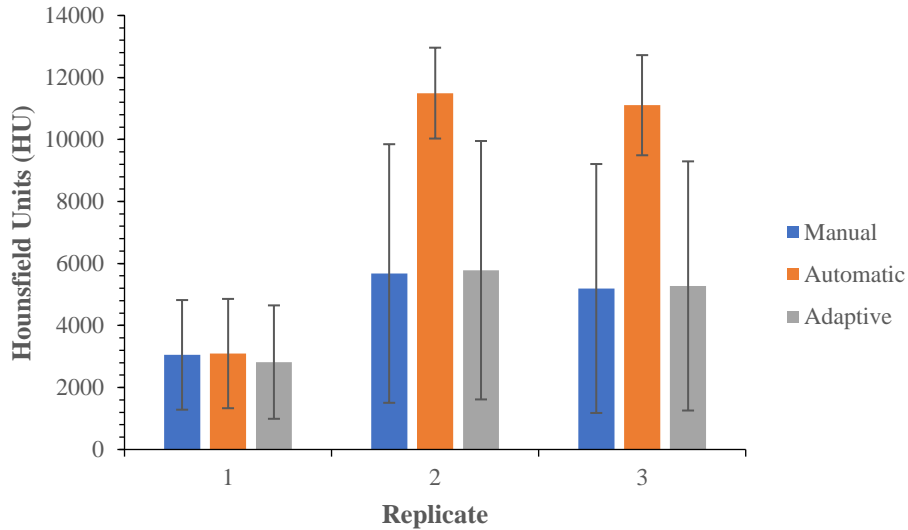


Figure 3.10 - Measured radiopacity of manual injection replicates 1-3 prepared under flow of PBS with thresholding methods of manual, automatic and adaptive (imaging cross-sections,  $n=198$ ).

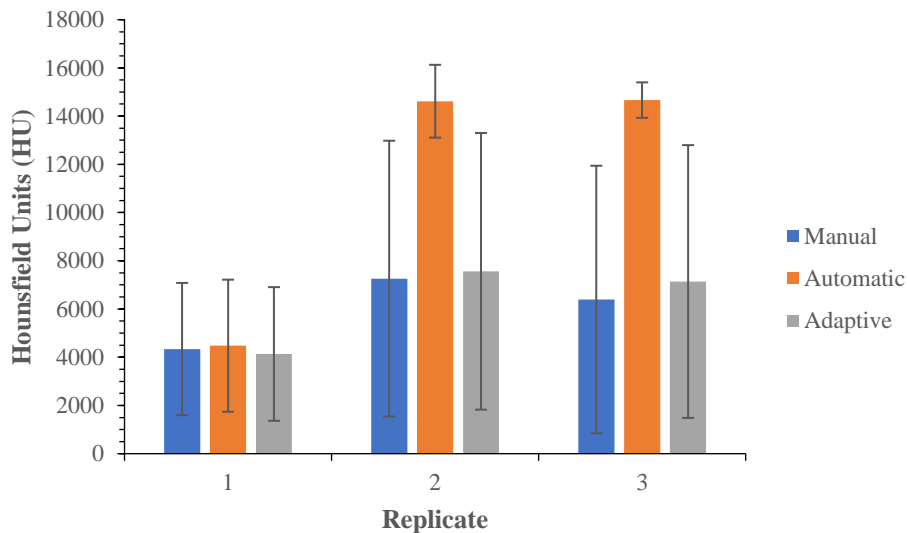


Figure 3.11 - Measured radiopacity of manual injection replicates 1-3 prepared under no flow of PBS with thresholding methods of manual, automatic and adaptive (imaging cross-sections,  $n=198$ ).

An investigation into the length of VOI used for the radiopacity calculations was also carried out to determine whether a short VOI would be a reliable representation of a long VOI. Radiopacity analysis over a short VOI greatly reduces the calculation time thereby streamlining the process. Comparison of the values obtained for long and short VOIs using the same scan sample datasets indicates no statistical difference between analysis carried out over short (1 mm) and long (4 mm) lengths (Table 3.5) ( $p=0.59$  as calculated using a two-

tailed t-test). This justifies that it is suitable to use short VOIs in place of long VOIs enabling a reduction in calculation time whilst maintaining reliable radiopacity measurements.

*Table 3.5 - Radiopacity data for manual injections performed under flow and no flow of PBS analysed over short and long VOIs (imaging cross-sections; n=198 and 792, respectively).*

Injection Type	Short VOI Height (1 mm)		Long VOI Height (4 mm)	
	Mean HU	Standard Deviation	Mean HU	Standard Deviation
<b>Under PBS Flow</b>	3608	2807	2819	1829
<b>No Flow of PBS</b>	4341	2742	4137	2771

A comparison of VOI lengths was also performed for porosity measurements. Similarly, the results indicated no statistical difference between the total porosity measured for short (1 mm) and long (4 mm) VOIs of the same scan sample datasets (Table 3.6) ( $p=0.6$  as calculated by a two-tailed t-test). This again justifies that it is suitable to use short VOIs in preference to long VOIs to reduce porosity calculation time whilst still maintaining reliable porosity measurements.

*Table 3.6 - Porosity data for manual injections performed under flow and no flow of PBS analysed over short and long VOIs (imaging cross-sections; n=198 and 792, respectively).*

Injection Type	Short VOI Height (1 mm)	Long VOI Height (4 mm)
	Porosity (%)	Porosity (%)
<b>Under PBS Flow</b>	48	55
<b>No Flow of PBS</b>	61	64

It is also worth noting the large standard deviations association with all radiopacity measurements. Standard deviations were seen to remain consistently high for each thresholding method tested and with no improvement seen for analysing short rather than long VOIs. This indicates the large standard deviations in radiopacity measurements to be an attribute of the imaging process rather than the sample. This is confirmed by the large standard deviations obtained for the radiopacity measurements of the HA phantoms despite the uniform density of HA for each rod (Table 3.7).

Table 3.7 - Radiopacity data of HA phantoms used for calibration (n=396).

HA Phantom (HA mg/cm <sup>3</sup> )	Hounsfield Units (HU)	Standard Deviation
200	766	651
1200	4460	620

### 3.3.6. Impact of Sample Delivery on Radiopacity Measurements

In order to mimic how the liquid embolic samples might be injected under conditions similar to those in therapeutic embolisation's and therefore replicate the precipitate structure formed, a syringe pump study was performed using a range of injection rates and types. The aim of the study was to observe the impact on precipitate structure and resulting radiopacity when injections were performed using a syringe pump over a range of injection rates and to also observe the differences between continuous and pulsed injections at the same injection rates with different time intervals between injection pulses. These variables were investigated under flow and no flow of PBS to mimic the use of standard microcatheters and balloon microcatheters, respectively.

It was envisaged that by investigating these variables, insight into the precipitate formation by injection techniques commonly used for therapeutic embolisation could be observed. This could help to predict the effect of varying rates and injection consistencies used by the interventional radiologists during the embolisation procedure dependent on their own personal preferences and expertise for liquid embolics.

Rates of syringe pump injection were varied in the range of 0.01-0.5 mL min<sup>-1</sup> with 0.01 mL min<sup>-1</sup> representing a slow cautious liquid embolic injection and 0.5 mL min<sup>-1</sup> representing a rapid injection. Pulse injection times were varied in the range of 10-180 secs to replicate injection pauses commonly used with the current liquid embolics used in the clinic.<sup>74</sup> Initial PBS flow rates were set within the range of 30-40 mL min<sup>-1</sup> or 0 mL min<sup>-1</sup> during the pulsed injection study.

The delivery technique used was found to greatly affect the length of precipitate formed during injection and hence the structure of the precipitate. The greatest lengths of precipitate were formed for samples injected at the highest syringe pump rate of 0.5 mL min<sup>-1</sup> under flow and no flow conditions (Table 3.8). There was no trend in the length of precipitate formed for different pulse injection pauses under both flow and no flow conditions (Table 3.9). Even with the different techniques used for injection, the samples still retained high occlusion rates of 98.8 ± 1.7% (n=6) for those injected using the continuous syringe pump method and 97.6 ± 3.8% (n=5) for those injected using the pulsed syringe pump injection method. Despite the samples having varying degrees of reflux around the microcatheter after injection, the microcatheter could easily be removed from all samples without disturbing the solidified sample thereby preserving the structure of the samples prior to microCT analysis.

*Table 3.8 - Precipitate length data for samples delivered by continuous syringe pump injection method under flow and no flow of PBS (n=1).*

<b>Syringe Pump Injection Rate (mL min<sup>-1</sup>)</b>	<b>Length of Precipitate Formed Under Flow Conditions (mm)</b>	<b>Length of Precipitate Formed Under No Flow Conditions (mm)</b>
<b>0.01</b>	25.5	49.0
<b>0.05</b>	41.5	48.5
<b>0.1</b>	55.0	45.0
<b>0.2</b>	48.0	43.5
<b>0.3</b>	50.0	49.0
<b>0.5</b>	68.0	63.0

*Table 3.9 - Precipitate length data for samples delivered by pulsed syringe pump injection method under flow and no flow of PBS (syringe pump injection rate of  $0.1 \text{ mL min}^{-1}$ )( $n=1$ ).*

<b>Pulsed Injection Interval (s)</b>	<b>Length of Precipitate Formed Under Flow Conditions (mm)</b>	<b>Length of Precipitate Formed Under No Flow Conditions (mm)</b>
<b>0</b>	55.0	45.0
<b>10</b>	40.0	43.0
<b>30</b>	38.0	43.0
<b>60</b>	45.0	44.0
<b>180</b>	36.0	46.0

Despite the use of the same liquid embolic formulation throughout the delivery experiments, the determined radiopacity was found to vary with the different injection conditions used (Table 3.10). For the samples delivered using the continuous syringe pump injection method, the porosity of the produced precipitates was found to increase with increasing injection rates. This is likely to be a contributing factor to the varying radiopacities measured. Visually the samples prepared under PBS flow were observed to be more porous in structure than samples prepared under no flow of PBS, which were seen to contain more areas of uniformly distributed polymer and the presence of less frequent but large voids (Table 3.11 and Table 3.12). These variations in the sample porosity and radiodensity can be clearly seen throughout the scanned sample lengths in Appendices 1-4 which show 3D cross-sectional videos of the samples delivered at  $0.01$  and  $0.5 \text{ mL min}^{-1}$  for both flow and no flow conditions to highlight the impact of different injection rates and flow conditions on the structure of the precipitated sample.

Table 3.10 - Radiopacity and porosity data for continuous syringe pump injections performed under PBS flow and no flow (imaging cross-sections, n=198).

<b>PBS Flow</b>	<b>Syringe Pump Rate of Injection (mL min<sup>-1</sup>)</b>	<b>Mean Hounsfield Units (HU)</b>	<b>Standard Deviation</b>	<b>Porosity (%)</b>
<b>Flow</b>	0.01	5388	4125	60
	0.05	5541	4059	58
	0.1	6628	4513	78
	0.2	4478	3128	71
	0.3	4548	3268	70
	0.5	5129	3767	70
<b>No Flow</b>	0.01	3545	2801	55
	0.05	2787	2024	44
	0.1	2706	1757	46
	0.2	5877	4836	65
	0.3	5486	4331	62
	0.5	8781	5317	79

Table 3.11 - X-ray shadowgraphs and reconstructed 2D cross-sectional images of continuous syringe pump injected liquid embolic sample prepared under flow of PBS.

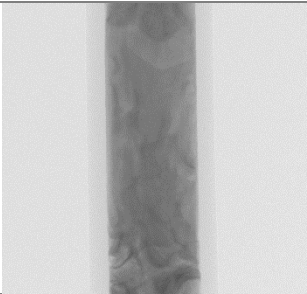
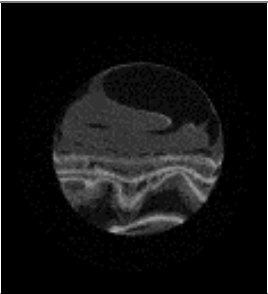
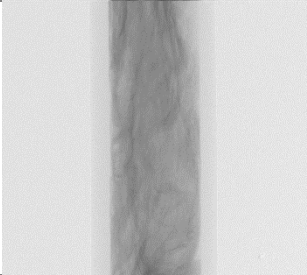

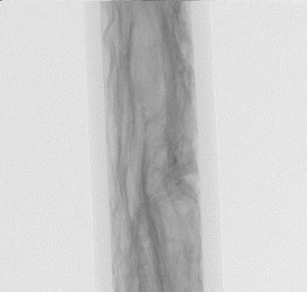
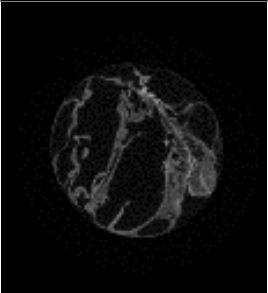
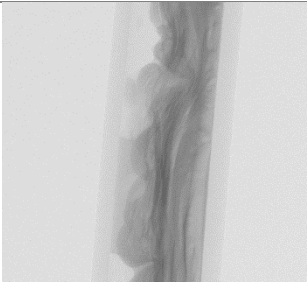
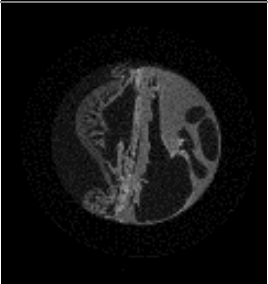
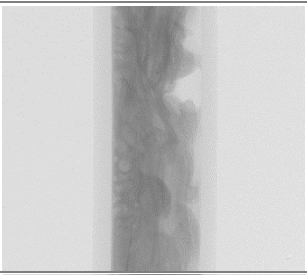

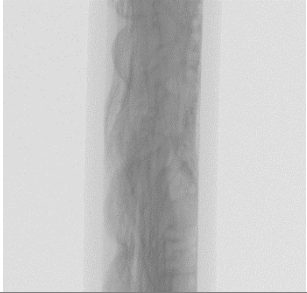
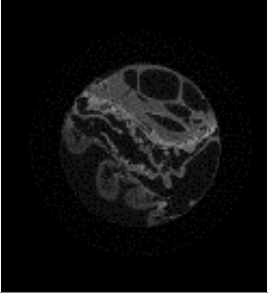
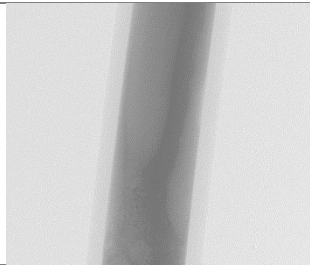
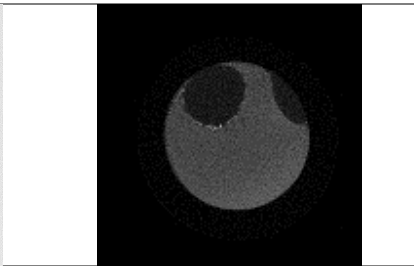
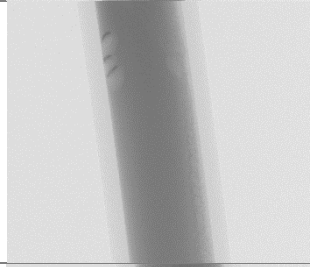
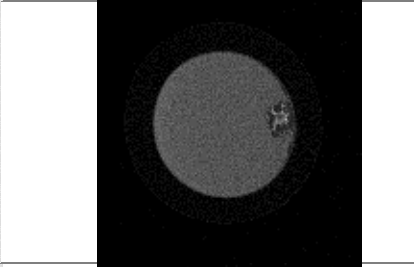
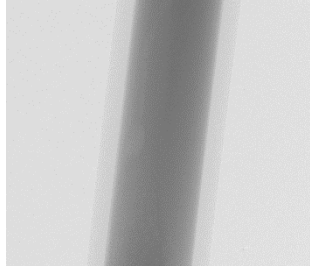
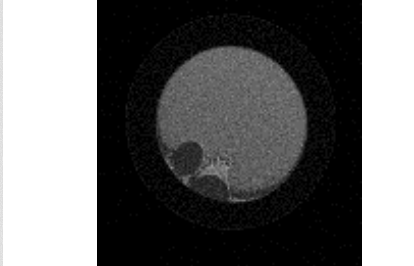
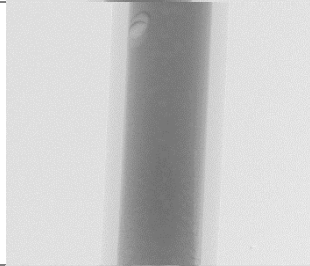
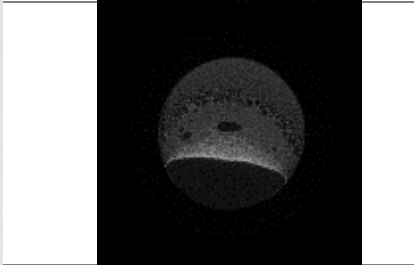
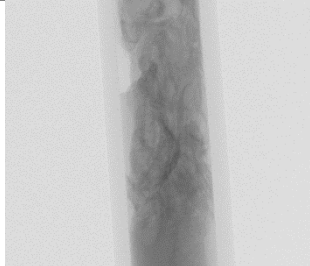
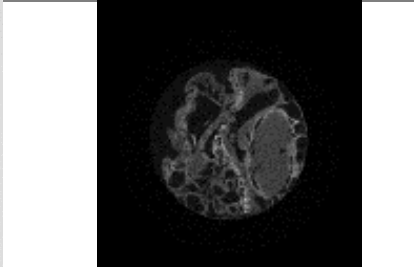

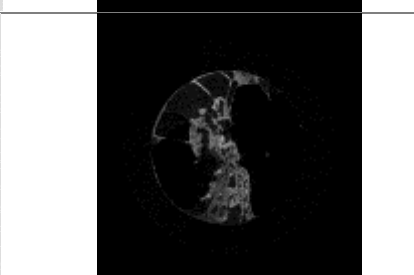
Syringe Pump Injection Rate (mL min <sup>-1</sup> )	X-ray Shadowgraph	Reconstructed 2D Cross-Section
0.01		
0.05		
0.1		
0.2		
0.3		
0.5		

Table 3.12 - X-ray shadowgraphs and reconstructed 2D cross-sectional images of continuous syringe pump injected liquid embolic sample prepared under no flow of PBS.

Syringe Pump Injection Rate (mL min <sup>-1</sup> )	X-ray Shadowgraph	Reconstructed 2D Cross-Section
0.01		
0.05		
0.1		
0.2		
0.3		
0.5		



For samples delivered by the pulsed syringe pump method, there was found to be a slight trend towards reduced radiopacity and porosity for samples delivered using longer pulse injection intervals (Table 3.13). The pulsed injection method visually formed disjointed precipitates but each region of the segments produced in each pulsed injection had approximately uniform structures, which were less porous and hence more compact than for continuous injections particularly under flow of PBS (Table 3.14 and Table 3.15). This is perhaps due to the pressure front generated by the initial injection meaning that resulting injections had to overcome this solidified front to form a precipitate in the direction in which it was being injected. There was noticeably more reflux observed for samples injected by a pulsed injection method in comparison to those injected by a continuous pump method.

*Table 3.13 - Radiopacity and porosity data for pulsed syringe pump injections performed under PBS flow and no flow (imaging cross-sections, n=198).*

<b>PBS Flow</b>	<b>Pulsed Injection Interval (s)</b>	<b>Mean Hounsfield Units (HU)</b>	<b>Standard Deviation</b>	<b>Porosity (%)</b>
<b>Flow</b>	0	6628	4513	78
	10	2395	992	66
	30	2531	857	66
	60	3041	1236	65
	180	2535	876	57
<b>No Flow</b>	0	2706	1757	46
	10	2669	846	73
	30	2487	820	68
	60	1846	443	53
	180	2105	458	54

Table 3.14 - X-ray shadowgraphs and reconstructed 2D cross-sectional images of pulsed syringe pump injected liquid embolic sample prepared under PBS flow ( $0.1 \text{ mL min}^{-1}$  injection rates).

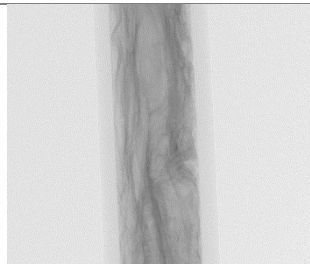
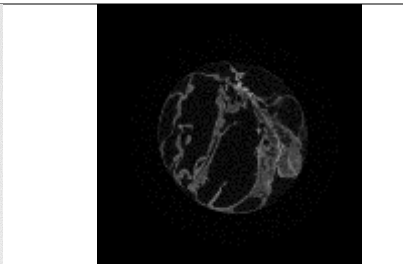
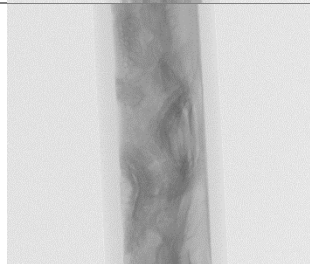
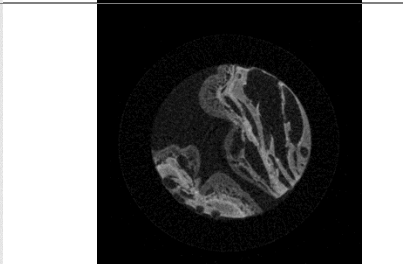
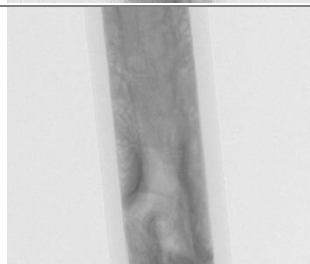
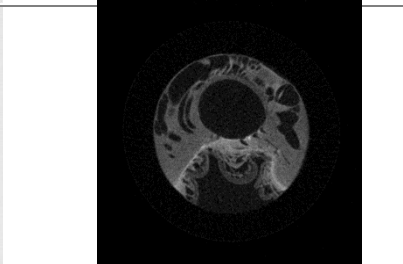
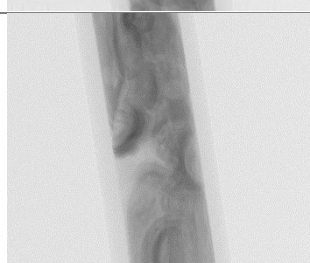
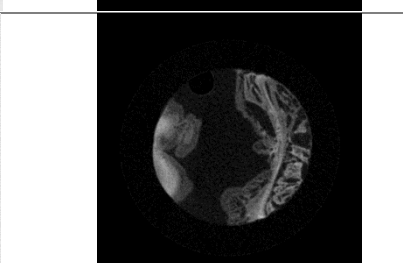

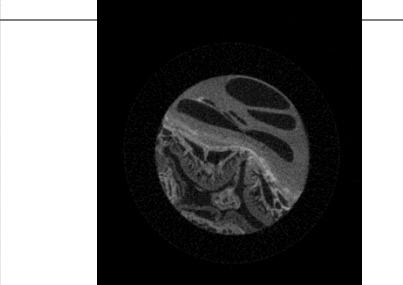
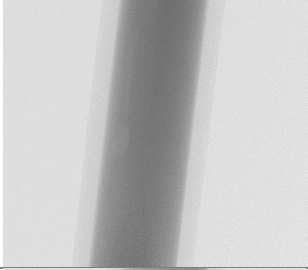
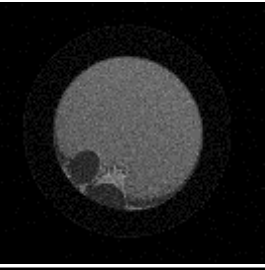
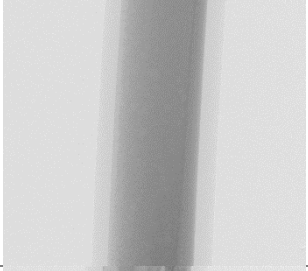
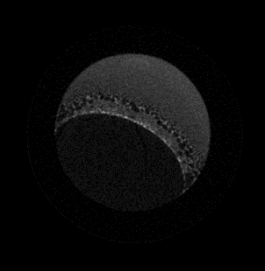
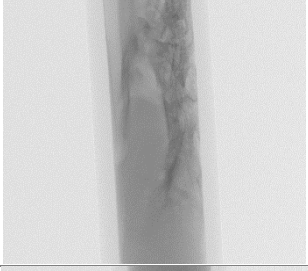
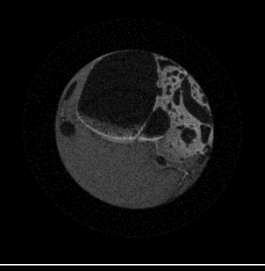
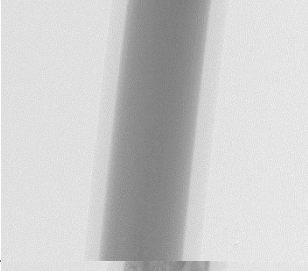
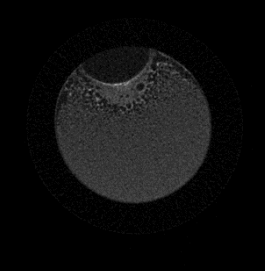
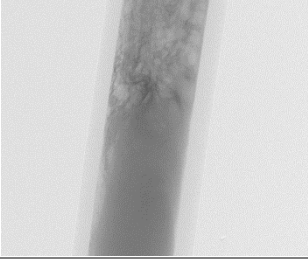
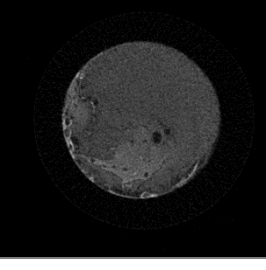
Pulsed Injection Interval (s)	X-ray Shadowgraph	Reconstructed 2D Cross-Section
0		
10		
30		
60		
180		

Table 3.15 - X-ray shadowgraphs and reconstructed 2D cross-sectional images of pulsed syringe pump injected liquid embolic sample prepared under no flow of PBS ( $0.1 \text{ mL min}^{-1}$  injection rates).

Pulsed Injection Interval (s)	X-ray Shadowgraph	Reconstructed 2D Cross-Section
0		
10		
30		
60		
180		

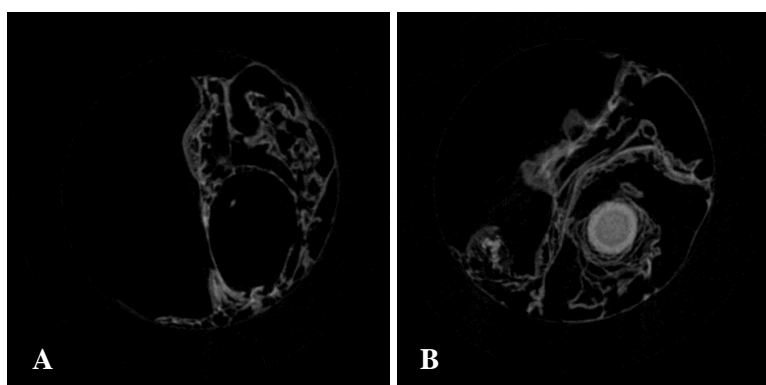
The variation in porosity and radio-density for these samples delivered by a pulsed technique can be visually confirmed in 3D cross-sectional videos of the scanned samples. Videos depicting samples delivered by a pulse injection with pulse intervals of 10 and 180 seconds under PBS flow and no flow conditions can be found in Appendices 5-8.

### 3.3.7. Scans Across Whole Precipitate Lengths

Thus far the microCT scans discussed were performed within the section of the samples where the precipitate was visually determined to have most fully distributed inside the tubing. The scanned area is limited to a height of 4.7 mm due to the limits of the microCT scanner. However, it is not known how representative this selected point is of the whole sample.

Scans were performed on a selection of samples prepared *via* manual injection, syringe pump injection, pulsed injection, under PBS flow and no flow at multiple points through each sample to understand how the precipitate structure changes over the length of injection. Five points equally spaced throughout each sample were chosen to incorporate areas of reflux, catheter injection site, bulk of proximal flow and furthest point of proximal.

The microcatheter injection site within the samples could be easily located due to the presence of a cylindrical hole throughout a short portion of the precipitate corresponding to the diameter of the microcatheter used. This led to the identification of areas of reflux behind the microcatheter. It was also noted that there was a bright region of precipitate immediately proximal to the hole where the microcatheter was removed. This suggests the formation of a dense region of precipitate is formed as the liquid embolic flows from the tip of the microcatheter (Figure 3.12).



*Figure 3.12 - Reconstructed 2D cross sections of liquid embolic sample delivered by continuous syringe pump method under PBS flow (A) hollow remaining after removal of microcatheter (B) bright region immediately proximal to the catheter hollow.*


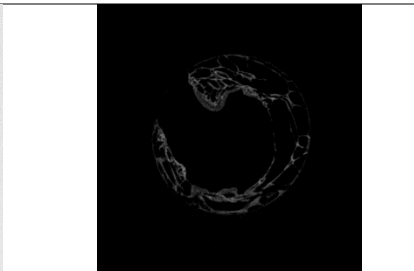
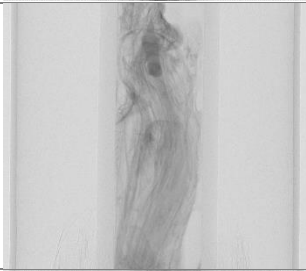
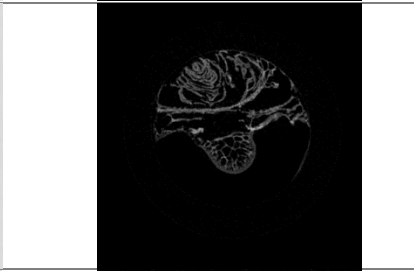
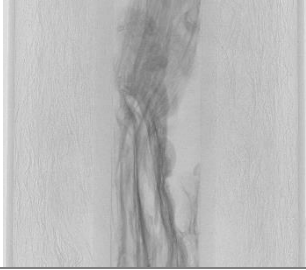

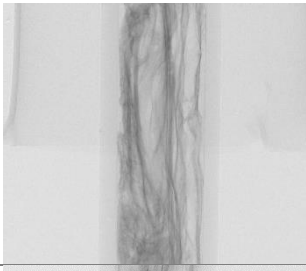
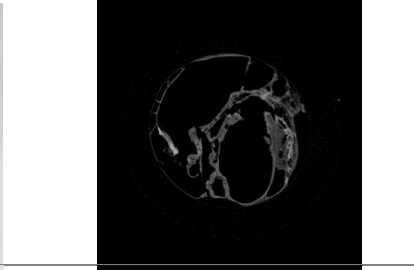

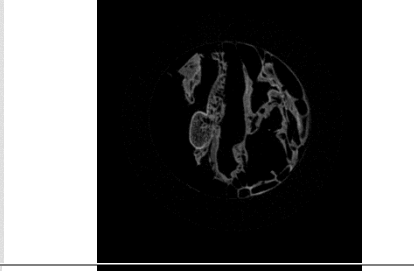
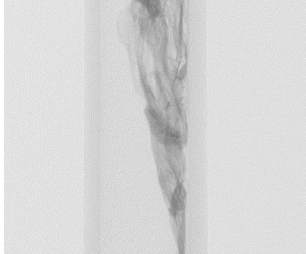
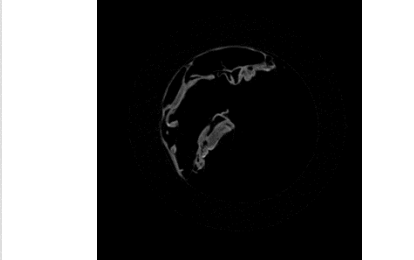
In the case of the sample prepared by continuous syringe pump injection at  $0.1 \text{ mL min}^{-1}$  under flow of PBS, the radiopacity of the precipitate remained fairly consistent throughout with a

mean radiopacity of  $4286 \pm 332$  HU (n=6). The porosity was found to fluctuate throughout the length of sample with the regions of highest porosity found in the areas of reflux and furthest proximal point where the precipitate structure was less uniform. The regions of lowest porosity were located within the centre of the sample proximal to the injection point suggesting these regions were more densely packed (Table 3.16 and Table 3.17).

*Table 3.16 - Radiopacity and porosity data across length of liquid embolic sample prepared by continuous syringe pump injection ( $0.1 \text{ mL min}^{-1}$ ) under PBS flow (imaging cross-sections, n=198).*

<b>Position Through Sample</b>	<b>Mean Hounsfield Units (HU)</b>	<b>Standard Deviation</b>	<b>Porosity (%)</b>
<b>Reflux</b>	4945	1566	91
<b>Injection Site</b>	4283	1574	81
<b>Proximal Region (1)</b>	4374	1204	84
<b>Proximal Region (2)</b>	4021	1380	78
<b>Proximal Region (3)</b>	3911	1198	82
<b>Furthest Point of Proximal Flow</b>	4184	1301	91

Table 3.17 - X-ray shadowgraphs and reconstructed 2D cross-sectional images across length of liquid embolic sample prepared by continuous syringe pump injection ( $0.1 \text{ mL min}^{-1}$ ) under PBS flow.

Position Through Sample	X-ray Shadowgraph	Reconstructed 2D Cross-Section
<b>Reflux</b>		
<b>Injection Site</b>		
<b>Proximal Region (1)</b>		
<b>Proximal Region (2)</b>		
<b>Proximal Region (3)</b>		
<b>Furthest Point of Proximal Flow</b>		

Comparing the radiopacity data of the samples prepared by pulsed injections at  $0.1 \text{ mL min}^{-1}$  injection rates with intervals of 30 seconds performed under PBS flow and no flow, the measured radiopacity was found to be slightly reduced within the central sections of the sample proximal to the injection site compared to the regions of reflux and the furthest point of proximal flow (Table 3.18). The higher radiopacity found at the edges could be attributed to the bright lineation observed in the regions of reflux and furthest regions of proximal flow along the walls of the sample which would likely have been in contact with PBS during the precipitation process (Table 3.19 and Table 3.20). The porosity of the samples throughout their lengths was found to be similar, irrelevant of whether the sample was formed under flow or no flow of PBS ( $p=0.87$  as calculated using a two-tailed t-test).

*Table 3.18 - Radiopacity and porosity data across length of liquid embolic sample prepared by pulsed syringe pump injection ( $0.1 \text{ mL min}^{-1}$ ) with 30 sec intervals under PBS flow and no flow (imaging cross-sections,  $n=198$ ).*

<b>PBS Flow</b>	<b>Position Through Sample</b>	<b>Mean Hounsfield Units (HU)</b>	<b>Standard Deviation</b>	<b>Porosity (%)</b>
<b>Flow</b>	Reflux	4630	2124	74
	Injection Site	4573	1863	76
	Proximal Region (1)	4229	1780	74
	Proximal Region (2)	4117	1793	66
	Furthest Point of Proximal Flow	4432	1919	74
<b>No Flow</b>	Reflux	4140	1444	77
	Injection Site	4062	1459	75
	Proximal Region (1)	3141	1042	87
	Proximal Region (2)	3122	1016	68
	Furthest Point of Proximal Flow	4624	1339	61

Table 3.19 - X-ray shadowgraphs and reconstructed 2D cross-sectional images across length of liquid embolic sample prepared by pulsed syringe pump injection ( $0.1 \text{ mL min}^{-1}$ ) with 30 sec intervals under PBS flow.

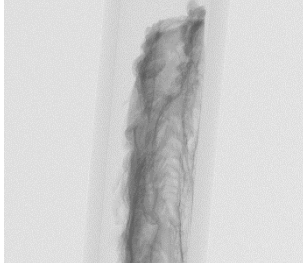
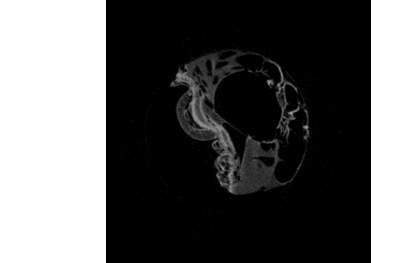

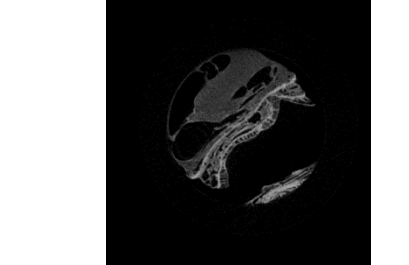

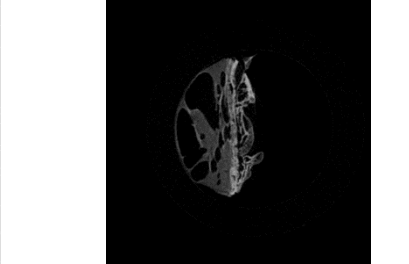


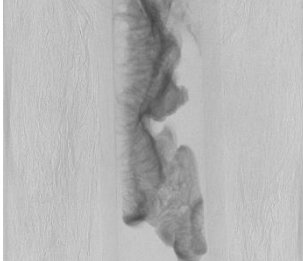

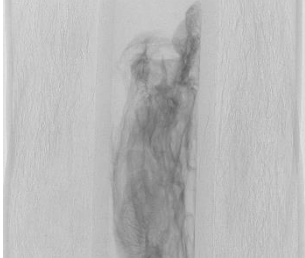
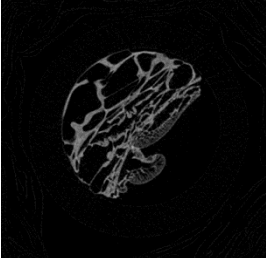
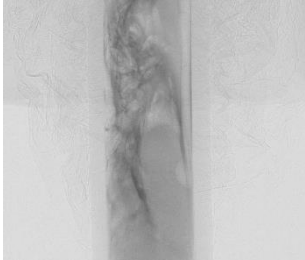
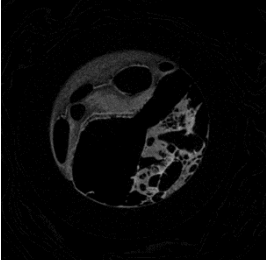
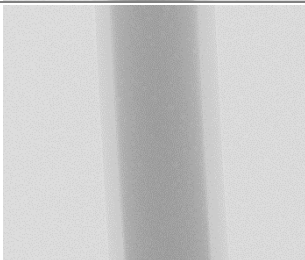
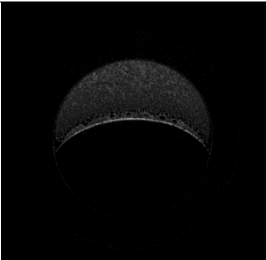
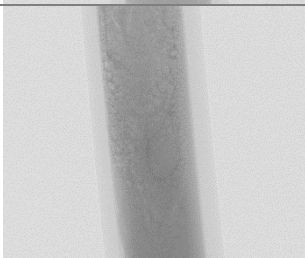
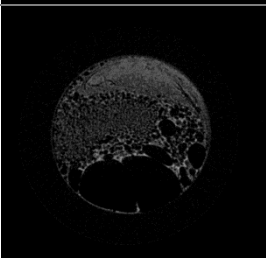
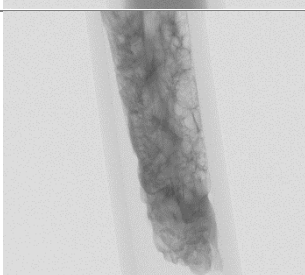
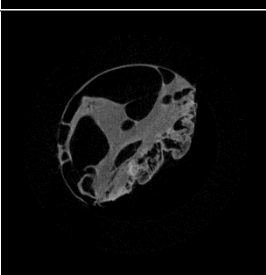
Position Through Sample	X-ray Shadowgraph	Reconstructed 2D Cross-Section
<b>Reflux</b>		
<b>Injection Point</b>		
<b>Proximal Region (1)</b>		
<b>Proximal Region (2)</b>		
<b>Furthest Point of Proximal Flow</b>		



Table 3.20 - X-ray shadowgraphs and reconstructed 2D cross-sectional images across length of liquid embolic sample prepared by pulsed syringe pump injection ( $0.1 \text{ mL min}^{-1}$ ) with 30 sec intervals without PBS flow.

Position Through Sample	X-ray Shadowgraph	Reconstructed 2D Cross-Section
<b>Reflux</b>		
<b>Injection Point</b>		
<b>Proximal Region (1)</b>		
<b>Proximal Region (2)</b>		
<b>Furthest Point of Proximal Flow</b>		

These large variations of precipitate structure and subsequent determined radiopacity across the length of a single sample indicate that scanning at a point where the precipitate appears to best fill the tubing is not representative of the whole sample length. It would be more

representative to scan at a number of positions throughout the injection length and average the radiopacity and porosity measurements across the scanned sections.

### **3.4. Conclusions**

MicroCT experiments have been used to determine the radiopacity and internal porosity of solidified liquid embolic prototypes. Scan reconstruction parameters were optimised for the precipitated materials in which it was found that a beam hardening correction was necessary to obtain accurate images. The processing of the reconstructed data by different thresholding methods to set the limits of binarization was investigated in which a local manual thresholding method was found to be sufficient for retaining high image resolution and accurately determining the radiopacity. Calculation of radiopacity and porosity over VOIs 1 mm in length were found to have close agreement to results calculated over VOIs 4 mm in length indicating that analysis carried out over short sections was sufficient to represent whole scan sections.

The radiopacity of solidified liquid embolic prototypes was found to vary depending on the type of injection method used to prepare the samples, despite the use of the same liquid embolic formulation throughout the sample preparation investigation. Similarly, the porosity of the precipitates was found to vary depending not only on the type of injection but also on whether the injection was carried out under flow or no flow of PBS. Hence, it is important to standardise the sample preparation method to accurately compare radiopacity and porosity measurements of different liquid embolic formulations in order to observe differences in radiopacity and precipitate structure. Likewise, it is necessary to compare the same area of each sample as the radiopacity and porosity was observed to vary depending on the site analysed within the same sample over five different points.

The development of a suitable microCT scan method alongside an understanding of how sample preparation effects the determined radiopacity, provides an ideal method for measuring the radiopacity of liquid embolic prototypes in order to gauge their visibility when implanted

in vivo. An additional feature of this method is the measurement of the precipitate porosity allowing structural information to be obtained about the liquid embolic materials once solidified.

## **Chapter Four**

### **4. Synthesis and Characterisation of a Precipitating Liquid Embolic**

## 4.1. Introduction

Precipitating materials are an attractive approach to the formation of an *in situ* embolus. Phase inversion can be designed to be triggered upon contact with physiological fluids. As the polymer chains precipitate out of solution, the solubilising solvent utilised to aid delivery diffuses away to leave a solid embolus.

This approach for a liquid embolic system is already established in the area of therapeutic embolisation. The use of Onyx<sup>®</sup> (Medtronic Inc) in AVMs and neurovascular indications is well documented.<sup>121–123</sup> Onyx<sup>®</sup> is delivered into the vasculature as a dimethyl sulfoxide (DMSO) solution of ethylene vinyl alcohol copolymer containing a suspension of micronized tantalum powder to impart radiopacity to the injected material. In order to obtain a uniform suspension of the polymer solution with the radiopacifying agent agitation of the product is required prior to delivery. Slow injection of Onyx<sup>®</sup> results in a solid cast of the vasculature being formed at the delivery site due to precipitation of the polymer on contact with the aqueous conditions found in blood.

Embolisation using Onyx<sup>®</sup> provides highly effective occlusion of the target site with easy delivery using narrow lumen microcatheters. However, one limitation is the required preparation time (a minimum of 20 minutes) with regards to the agitation prior to injection to achieve a uniform suspension of the high density tantalum. In addition to the challenges of density, the radiodense metallic nature of the radiopacifying agent often results in streak artefact observed by X-ray imaging.<sup>81</sup> These streak artefacts may obscure the anatomy around the treatment site making monitoring of disease progression difficult in follow up imaging. Also, in cases where Onyx<sup>®</sup> is used as a tool prior to surgical removal, there is a risk of sparking of the material due to combustion during surgical resection.<sup>124</sup> A further drawback to the use of Onyx<sup>®</sup> is in treatment of diseases which are located close to the surface of the skin as tantalum can be seen to have a tattooing effect under the skin.<sup>125</sup> This is likely to be unaesthetically pleasing to the patients receiving treatment.

In an attempt to overcome these issues, there are currently iodine-based systems undergoing clinical trials including Easyx™ (Antia Therapeutics) and PHIL™ (Microvention-Terumo).<sup>126,127</sup> Both systems function by the same mechanism as Onyx® and precipitate on contact with an aqueous environment. Easyx™ is based on a polyvinyl alcohol ether copolymer with covalently bound iodine. Similarly, PHIL™ is based on a copolymer of polylactide-co-glycolide and polyhydroxyethylmethacrylate with covalently bound iodine. Both systems are formulated as DMSO solutions which allows safe injection into the vasculature provided the liquid embolic formulations are injected at slow rates to prevent vasospasm from DMSO injection.<sup>74</sup> However, a product recall was recently issued for PHIL™ due to metallic contamination and Easyx™ is still undergoing clinical trials and therefore not available on the market.<sup>128</sup>

The work proposed here is based on poly(vinyl alcohol) (PVA) modified with a triiodinated aromatic group which has dual functionality (Figure 4.1). The hydrophobicity imparted by the triiodinated aromatic group allows the previously water soluble PVA to undergo phase inversion and precipitate on contact with an aqueous environment. The triiodinated aromatic group has a second function of imparting radiopacity to the material with a high density of the radiopaque iodine element incorporated for each aromatic group grafted onto the PVA backbone. The previously demonstrated biocompatibility of similar polymer compositions in the literature makes it an ideal starting point for the development of a ready to use liquid embolic material.<sup>116,129</sup>

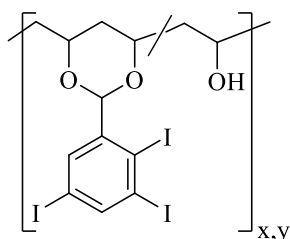


Figure 4.1 - Proposed structure of a precipitating radiopaque embolic liquid.

The radiopaque precursor 2,3,5-triiodobenzaldehyde (TIBA) was chosen as the radiopaque moiety to be covalently bound to the PVA backbone *via* a cyclic acetal bond.<sup>100</sup> This is likely

to be highly stable under physiological conditions thereby imparting permanent radiopacity to the implanted embolic.<sup>129</sup> This ensures the material remains visible and easily locatable in post-procedural scans.

The radiopaque moiety renders the polymer insoluble in water due to the hydrophobic nature of the triiodinated aromatic group. This provides an ideal mechanism for a liquid embolic, which functions by a phase inversion mechanism as the radiopaque polymer can be delivered as a solution in DMSO which then precipitates on contact with an aqueous environment, in theory forming a solid embolus when introduced into the vasculature.

The covalent binding of the radiopaque moiety to the PVA backbone allows the material to be delivered as a ready to use formulation if pre-formulated in DMSO. This offers an advantage over the currently used Onyx<sup>®</sup> liquid embolic system, which requires a 20 minute agitation of the solution before use to ensure uniform suspension the radiopaque tantalum additive thereby increasing the overall procedural time.

A number of variables will be investigated to determine the impact on the performance of the formulations for suitable behaviour as liquid embolic materials under the test methods previously developed in Chapter 2. The variables investigated will include the number of TIBA radiopaque group equivalents targeted, polymer molecular weight used and the concentration of the radiopaque polymer in the carrier solvent.

## 4.2. Experimental

The following chemicals were used as supplied from their manufacturers; anhydrous DMSO (99.7%,) from Acros Organics, HCl (0.1 N) from Acros Organics, methanesulfonic acid ( $\geq 99.0\%$ ) from Sigma Aldrich, Mowiol<sup>®</sup> 4-88 ( $\sim 31,000 \text{ g mol}^{-1}$ , 86.7-88.7 mol% hydrolysed) from Sigma Aldrich, Mowiol<sup>®</sup> 8-88 ( $\sim 67,000 \text{ g mol}^{-1}$ , 86.7-88.7 mol% hydrolysed) from Sigma Aldrich, Mowiol<sup>®</sup> 18-88 ( $130,000 \text{ g mol}^{-1}$ , 86.7-88.7 mol% hydrolysed) from Sigma Aldrich, oxalyl chloride (98%) from Acros Organics, propylphosphonic anhydride (50 w/w%

in ethyl acetate) from Fluorochem, triethylamine ( $\geq 99.0\%$ ) from Sigma Aldrich, 2,3,5-triiodobenzaldehyde (99.5%) from Aldlab and 2,3,5-triiodobenzyl alcohol (97%) from Sigma Aldrich. The removal of solvent was carried out under reduced pressure using a rotary evaporator.  $^1\text{H}$  and  $^{13}\text{C}$  NMR spectra were recorded at 400 MHz on a Bruker Avance III HD 400 instrument and measured coupling constants were stated in Hz to the nearest decimal place. NMR splitting abbreviations used; s = singlet, d = doublet, t = triplet, q = quartet, quin. = quintet, m = multiplet. Electrospray mass spectrometry was recorded on a Water LCT instrument.

#### 4.2.1. Synthesis of 2,3,5-Triiodobenzaldehyde (TIBA)

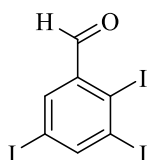


Figure 4.2 - 2,3,5-triiodobenzaldehyde (TIBA).

#### Preparation using Propylphosphonic Anhydride (T3P):

A 50 w/w% solution of T3P in ethyl acetate (3.0 mL, 1.6 g, 5.0 mmol) was added dropwise over 5 minutes at room temperature to a solution of 2,3,5-triiodobenzyl alcohol (2.43 g, 5.0 mmol) in anhydrous DMSO (25 mL) under  $\text{N}_2$  flow with magnetic stirring. The reaction mixture was stirred at room temperature for 4 hours and then poured into deionised water (25 mL). The precipitate was filtered and washed with the mother liquors and deionised water (20 mL). The cake was slurried with ethyl acetate (20 mL), filtered and washed again with ethyl acetate (20 mL). The product was then dried in vacuum desiccator. Yield = 37%;  $\delta_{\text{H}}$  (400 MHz, d-DMSO) 8.08 (1H, s, ArCH), 8.46 (1H, s, ArCH), 9.89 (1H, s, COH);  $R_f = 0.70$  [40-60 petroleum ether/ethyl acetate (9:1)].

#### Preparation using Oxalyl Chloride:



A solution of anhydrous DMSO (0.8 mL, 0.84 g, 10.8 mmol) in THF (4.0 mL) was added dropwise over 5 minutes to a solution of oxalyl chloride (3.1 mL, 1.1 g, 6.2 mmol) in THF (40 mL) under N<sub>2</sub> flow with magnetic stirring at -78 °C. The solution was stirred for 5 minutes before the dropwise addition of 2,3,5-triodobenzyl alcohol (2.5 g, 5.15 mmol) in THF (4.0 mL). The reaction mixture was stirred for 30 minutes at -78 °C. Triethylamine (3.6 mL, 2.6 g, 26 mmol) was then added dropwise, the solution warmed to room temperature and stirred for 3 hours. Deionised water (25 mL) was added and the pH adjusted to neutral using 0.1 M HCl solution. The aqueous layer was extracted with DCM (3 × 25 mL). The organic layers were combined and washed with deionised water (25 mL), 10% HCl in deionised water (3 × 25 mL), deionised water (25 mL), 10% NaOH in deionised water (3 × 25 mL), deionised water (25 mL), saturated brine (2 × 25 mL). The collected sample was then dried over MgSO<sub>4</sub>, filtered and the solvent removed under reduced pressure. The product was then dried in a vacuum desiccator. Yield = 59%; found C 17.57%, H 0.86%, I 71.6%, C<sub>7</sub>H<sub>3</sub>I<sub>3</sub>O; FT-IR  $\nu$  cm<sup>-1</sup> 2849 and 2734 (C-H, aldehyde), 1729 (C=O, aldehyde), 1677 (C=C, aromatic), 524 (C-I, iodide);  $\delta_{\text{H}}$  (400 MHz, d-DMSO) 8.08 (1H, s, ArCH), 8.46 (1H, s, ArCH), 9.89 (1H, s, COH);  $\delta_{\text{C}}$  (400 MHz, d-DMSO) 96.7 (ArCI), 137.5 (ArCH), 151.2 (ArCH), 197.1 (COH); m/z (EI) 483.7 (89%, M<sup>+</sup>); mp 142 °C; R<sub>f</sub> = 0.70 [40-60 petroleum ether/ethyl acetate (9:1)].

#### 4.2.2. Synthesis of Iodinated PVA (I-PVA)

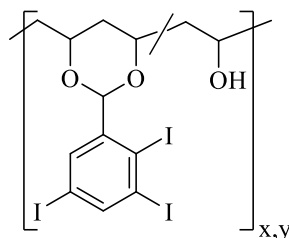


Figure 4.3 - Iodinated PVA (I-PVA).

Mowiol® 4-88, Mowiol® 8-88 or Mowiol® 18-88 (10 g) was dissolved in anhydrous DMSO (320 mL) and mechanically stirred at 350 rpm for 2 hours at 50 ± 9 °C with N<sub>2</sub> flow in a flat

flange reaction vessel. A solution of 2,3,5-triiodobenzaldehyde (0.55-13.7 g, 1.1-28.4 mmol) in anhydrous DMSO (30 mL) was degassed for 10 minutes and then added dropwise to the PVA solution. After 5 minutes, methane sulfonic acid (22 mL, 32.6 g, 339 mmol) was added dropwise and the reaction mixture stirred at  $50 \pm 9$  °C for 24 hours. Once cooled to room temperature, the polymer was precipitated twice from THF ( $2 \times 750$  mL) and the collected precipitate washed with further THF (50mL). The product was collected by centrifugation and then dried in a vacuum oven at 40 °C. Yield = 79%;  $\delta_{\text{H}}$  (400 MHz, d-DMSO) 1.26-1.56 (m), 1.92-2.02 (m), 3.56-3.69 (m), 3.73-3.95 (m), 4.21-4.30 (m), 4.45-4.54 (m), 4.66-4.74 (m), 5.08-5.17 (m), 7.67-7.70 (s broad, aromatic), 8.29-8.26 (s broad, aromatic). Details of each reaction performed are provided in Table 4.1.

Table 4.1 - Reaction quantities used in the synthesis of iodinated PVA samples.

Mowiol®	Molecular Weight (kDa)	TIBA (Eq to PVA Diol Groups)	Mass of TIBA (g)	Moles of TIBA (mmol)	Yield (%)
<b>8-88</b>	67	0.01	0.55	1.1	73
<b>8-88</b>	67	0.05	2.75	5.7	67
<b>8-88</b>	67	0.10	5.49	11.4	85
<b>8-88</b>	67	0.15	8.24	17.0	73
<b>8-88</b>	67	0.20	10.98	22.7	86
<b>8-88</b>	67	0.25	13.73	28.4	88
<b>4-88</b>	31	0.10	5.49	11.4	89
<b>4-88</b>	31	0.25	13.73	28.4	82
<b>18-88</b>	130	0.10	5.49	11.4	98
<b>18-88</b>	130	0.25	13.73	28.4	96

#### 4.2.3. Water Solubility Test

Water solubility testing of iodinated PVA samples synthesised using Mowiol® 8-88 and 0.01-0.25 equivalents of TIBA was carried out by accurately weighing between 0.2-0.3 g of sample. Deionised water (5.00 mL) was added to the sample and the solution heated at 50 °C for 2 hours with regular agitation. Upon cooling, the solution was removed and any remaining solids dried in a vacuum desiccator for 48 hours. The dried precipitate was weighed, and the water solubility of the sample calculated. The process was repeated for 3 replicates of each sample along with PVA control of Mowiol® 8-88.

#### 4.2.4. Preparation of I-PVA Liquid Embolic Prototypes

Liquid embolic prototypes were prepared using I-PVA synthesised samples in section 4.2.2 by dissolving in anhydrous DMSO to formulate solutions in the range of 8-12 w/w% in solution (Table 4.2).

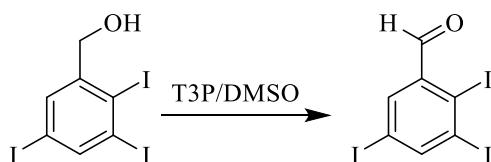
Table 4.2 – Formulations of liquid embolic prototypes.

Prototype	TIBA (Eq to PVA Diol Groups)	PVA Molecular Weight (kDa)	Concentration in DMSO (w/w%)
1.1	0.1	67	8
1.2	0.1	67	12
1.3	0.1	67	20
1.4	0.15	67	8
1.5	0.15	67	12
1.6	0.15	67	20
1.7	0.20	67	8
1.8	0.20	67	12
1.9	0.20	67	20
1.10	0.25	67	8
1.11	0.25	67	12
1.12	0.25	67	20
1.13	0.1	31	20
1.14	0.1	130	20
1.15	0.25	31	20
1.16	0.25	130	20

### 4.3. Results and Discussion

#### 4.3.1. Preparation of a Radiopaque Substituent

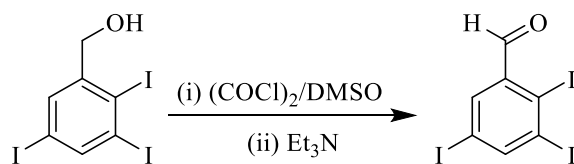
2,3,5-triiodobenzaldehyde (TIBA) was prepared *via* Swern oxidation of 2,3,5-triiodobenzyl alcohol. Initially, this was carried out using propylphosphonic anhydride (T3P, 50% in ethyl acetate) (Scheme 4.1).<sup>130</sup> The first trial of the reaction gave a crude yield of 63%. However, analysis by <sup>1</sup>H NMR spectroscopy indicated a large amount of 2,3,5-triiodobenzyl alcohol starting material remaining, approximately 40% of the crude mass obtained. The use of a higher equivalent of T3P reagent, 1.2 equivalents instead of 1.0, was found to reduce the amount of starting material isolated in the crude product to approximately 10%.



Scheme 4.1 - Synthesis of 2,3,5-triodobenzaldehyde (TIBA) using T3P.

Recrystallisation of the crude material was trialled in a variety of solvents and solvent mixtures including; acetone, ethyl acetate, dichloromethane and hexane. However, the majority of these experiments did not yield crystals and the few successful experiments which produced crystals were shown by <sup>1</sup>H NMR spectroscopy to still contain a significant amount of the 2,3,5-triodobenzyl alcohol starting material. This indicates a small purification of the crude product by recrystallisation, however clean separation of the aldehyde and alcohol materials was not possible using the solvents trialled. This is likely to be due to the similar polarities of the two materials. A small amount of sample was successfully separated using flash column chromatography using a solvent system of 80:20 ethyl acetate:petroleum ether yielding enough product for full characterisation.

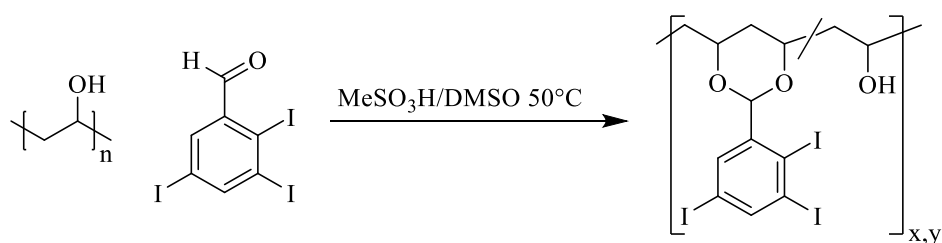
In order to produce larger quantities of 2,3,5-triodobenzaldehyde with higher conversions of the starting materials, the synthesis was trialled using a different reagent. The reaction was carried out using oxalyl chloride in DMSO followed by the addition of triethylamine (Scheme 4.2).<sup>131</sup> Following work-up of the reaction mixture and purification of the product, analysis by <sup>1</sup>H NMR spectroscopy of the dried product indicated the clean isolation of product with a yield of 66%. The product was synthesised in sufficient amounts for initial feasibility tests as a radiopaque moiety grafted onto PVA, after which 2,3,5-triodobenzaldehyde was commercially sourced from Aldlab Chemicals (99.5% purity).



Scheme 4.2 - Synthesis of 2,3,5-triodobenzaldehyde (TIBA) using oxalyl chloride.

### 4.3.2. Preparation of Iodinated PVA

Iodinated PVA (I-PVA) was prepared by an acid catalysed acetalisation reaction of PVA with TIBA (Scheme 4.3).<sup>130</sup> The reaction was carried out for 24 hours at 50 °C then precipitated twice from an anti-solvent, such as tetrahydrofuran (THF), in order to remove any unreacted TIBA starting material and isolate the I-PVA product. The product was then manually drawn into pieces before drying in a vacuum oven at 40 °C. The acetalisation reaction of PVA was confirmed by <sup>1</sup>H NMR spectroscopy analysis due to the presence and shifting of the aromatic peaks upfield.



Scheme 4.3 - Synthesis of iodinated PVA (I-PVA).

I-PVA samples were synthesised over a range of different TIBA equivalents to PVA diol groups between 0.01 to 0.25 equivalents. Samples were prepared over this range of TIBA equivalents in order to study the effect the incorporation of varying amounts of the radiopaque substituent had on the materials visibility under X-ray and liquid embolic properties. The grafting of varying equivalents of TIBA onto PVA is reflected in the increasing iodine content of the samples with increasing equivalents of TIBA used in the acetalisation reaction (Table 4.3).

Table 4.3 - I-PVA theoretical and determined iodine contents by elemental analysis ( $n=2$ ).

TIBA (Eq to PVA Diol Groups)	Targeted Iodine Content (%)	Iodine Content by Elemental Analysis (%)
0.01	4.1	1.6
0.05	17.7	14.5
0.10	28.3	27.1
0.15	36.1	36.3
0.20	42.0	41.7
0.25	46.5	42.9

### 4.3.3. Feasibility Testing

In order to assess the potential of the produced radiopaque polymers to behave as liquid embolic materials as a solution in DMSO, a number of feasibility tests were performed. These were carried out using radiopaque I-PVA polymers synthesised using Mowiol® 8-88 over varying equivalents of TIBA to determine how the radiopaque group content affected the ability of the materials to function as embolic materials by a precipitation mechanism from DMSO under aqueous conditions.

#### 4.3.3.1. Solubility in Water

The water solubility of the I-PVA samples was determined to observe the impact of coupling a hydrophobic group to the PVA backbone. There was found to be a large reduction in water solubility of the I-PVA samples with increasing number of TIBA equivalents (Table 4.4 and Figure 4.4). This is as expected and can be rationalised by the increasing hydrophobicity imparted by the incorporated TIBA into the I-PVA samples resulting in a switch from water soluble to insoluble.<sup>132</sup> This highlights the potential for the materials to undergo a phase inversion in the presence of an aqueous environment to form a solid precipitate when solubilised in a suitable solvent such as DMSO.

Table 4.4 - Water solubility data of I-PVA samples ( $n=3$  for I-PVA samples and  $n=15$  for PVA control).

Sample	TIBA (Eq to PVA Diol Groups)	Mean Water Solubility (mg mL <sup>-1</sup> )	Standard Error of Mean (mg mL <sup>-1</sup> )
PVA control	0.00	46.8	8.4
I-PVA	0.01	35.5	0.9
I-PVA	0.05	0.1	0.0
I-PVA	0.10	2.6	0.1
I-PVA	0.15	4.0	0.0
I-PVA	0.20	2.1	0.5
I-PVA	0.25	5.3	0.4

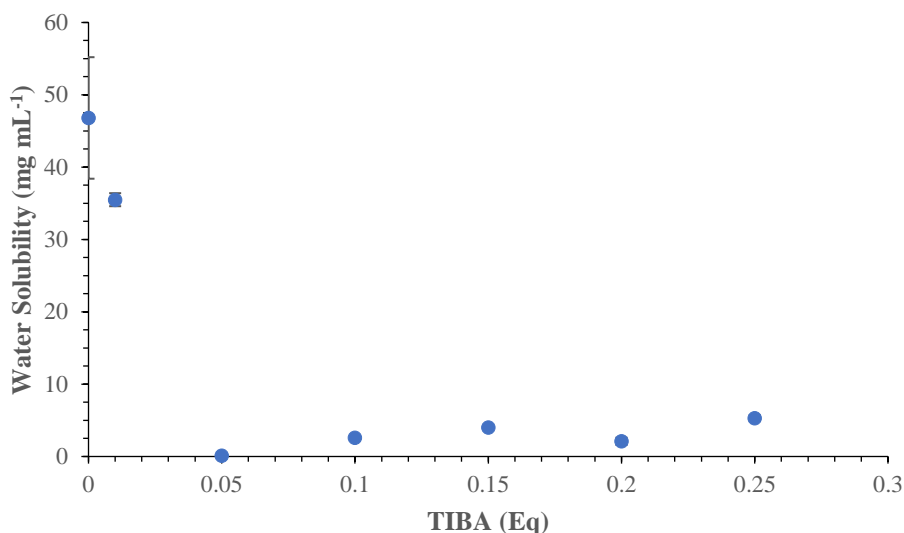


Figure 4.4 - Water solubility results of I-PVA samples ( $n=3$  for I-PVA samples and  $n=15$  for PVA control).

A control of PVA, Mowiol® 8-88, was carried out for each time the water solubility test was performed totalling 15 replicates. Hence, this average considers any variation in water purity, vacuum strength and variation in lab temperature leading to significantly higher standard errors of the mean than the individual I-PVA tests due to the higher number of samples involved compared to the standard 3 replicates.

#### 4.3.3.2. *Precipitation under Aqueous Conditions*

Precipitation tests were carried out to determine the feasibility of the prepared I-PVA samples behaving as precipitating embolic agents as indicated by their poor water solubility. The I-PVA samples synthesised using 0.01-0.25 equivalents of TIBA were formulated as solutions in DMSO. Due to the hardening of the samples and drying as large solid masses, it was not possible to produce samples of equal concentrations. Instead, solutions were prepared in the range of 4-30 w/w% depending on the samples affinity to be solubilised by DMSO. Hence, the results obtained were not directly comparable but gave a crude indication of the sample's ability to form a precipitate upon contact with PBS.

The precipitation tests were carried out by initially pre-heating vials of PBS (25 mL) in a water bath to 37 °C. The I-PVA solutions (1 mL) were then injected into the pre-heated PBS and the samples observed for any precipitation. All samples tested, with the exception of the I-PVA sample synthesised using the lowest equivalent of TIBA at 0.01, were seen to precipitate in PBS to some extent (Table 4.5 and Figure 4.5). The I-PVA sample synthesised using the highest equivalent of TIBA, 0.25 eq per PVA diol group, was seen to be the least soluble in PBS and precipitated almost instantly upon contact with the solution forming a solid mass. The precipitated polymer mass was initially soft but gradually hardened over time indicating the progressive solidification as the DMSO diffused out of the solidifying mass. The varying concentrations of solutions used meant it was not possible to directly compare the degree of precipitation between samples but did demonstrate the ability of I-PVA samples to undergo phase inversion in aqueous environments.

*Table 4.5 - Data of I-PVA precipitation test in PBS at 37 °C (n=1).*

<b>TIBA (Eq to PVA Diol Groups)</b>	<b>Concentration in DMSO (w/w%)</b>	<b>Precipitation in PBS?</b>
<b>0.01</b>	4	No
<b>0.05</b>	4	Yes
<b>0.10</b>	20	Yes
<b>0.15</b>	20	Yes
<b>0.20</b>	4	Yes
<b>0.25</b>	30	Yes



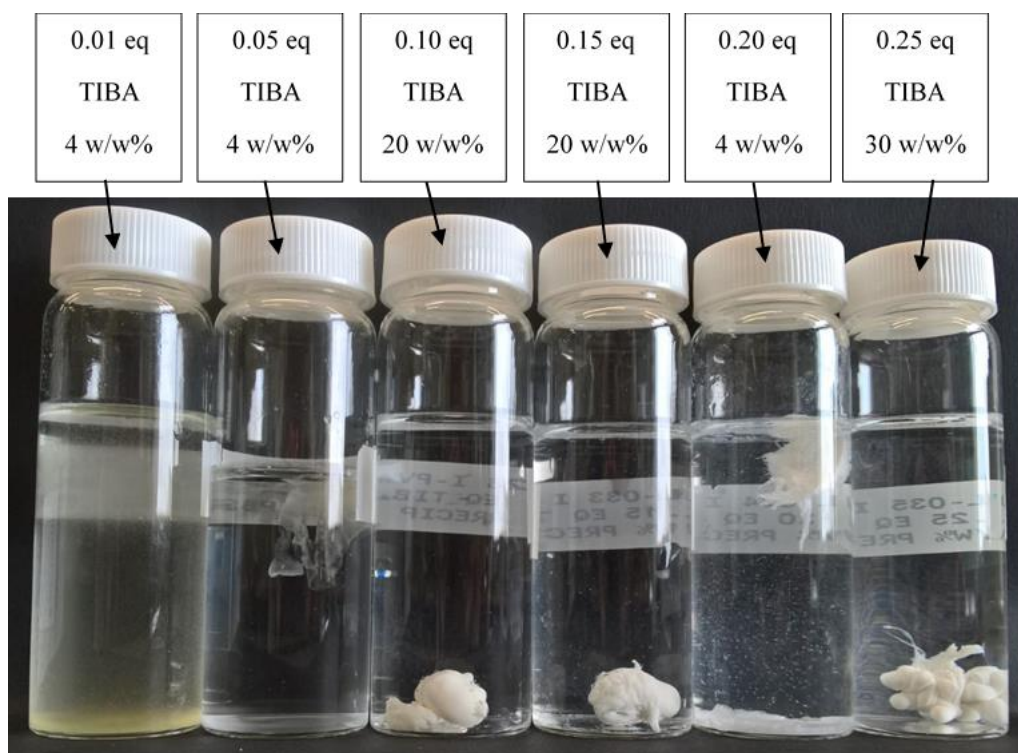


Figure 4.5 - Photo of I-PVA precipitation test.

#### 4.3.3.3. Precipitation under Flow Conditions

Due to the favourable precipitation properties exhibited by the I-PVA sample synthesised using 0.25 equivalent of TIBA, this sample was chosen for further testing under aqueous flow conditions. The precipitation test was carried out under varying flow rates of PBS to mimic the flow conditions found within the vasculature during embolisation procedures.

A 40 w/w% solution of the I-PVA sample in DMSO was injected into a basic flow model using a wide bore tubing and a peristaltic pump set at varying PBS flow rates of 100-500 mL min<sup>-1</sup>. The sample was found to precipitate under all flow rates tested (Table 4.6 and Figure 4.6). The injection carried out at 500 mL min<sup>-1</sup> of PBS flow was found to completely block the flow through the tubing demonstrating the potential for occlusion under rapid flow rates.

Table 4.6 - Results of precipitation test of I-PVA synthesised at 0.25 equivalents of TIBA under varying flow rates of PBS (n=1).

Flow Rate (mL min <sup>-1</sup> )	Precipitation under PBS flow?
100	Yes
200	Yes
300	Yes
400	Yes
500	Yes

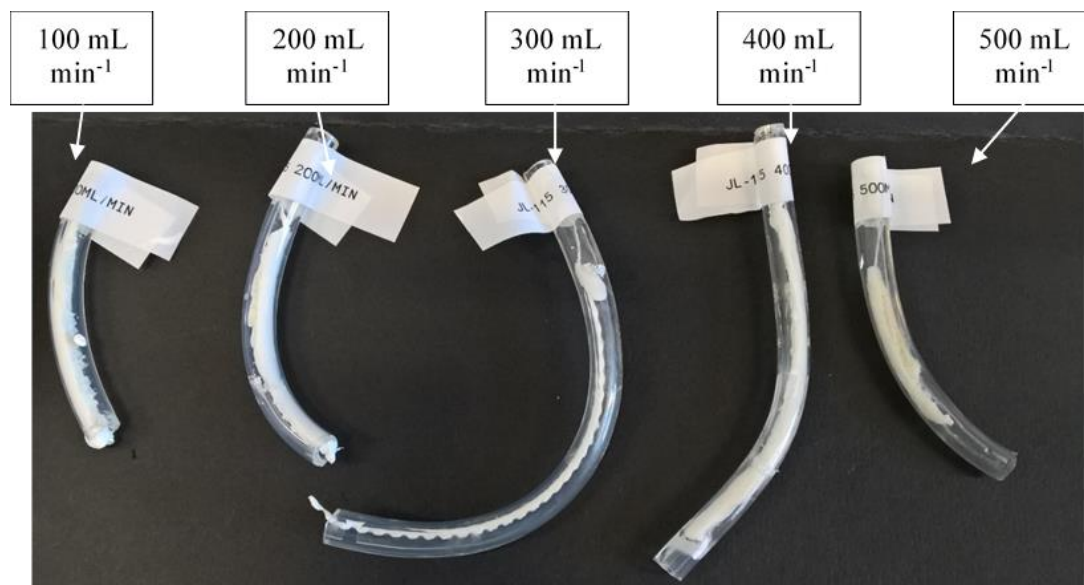


Figure 4.6 - Photo of precipitation test of I-PVA synthesised at 0.25 equivalents of TIBA under varying flow rates of PBS.

The ability of the sample to precipitate under flow conditions was further examined using a vascular flow model in which the sample was injected into a vasculature cast under PBS flow conditions replicating blood flow. In the test, a 20 w/w% solution of the I-PVA sample in DMSO was used to investigate the precipitation properties of a more dilute and hence lower viscosity polymer solution. The 20 w/w% I-PVA solution (1 mL) was injected into the vascular model using a microcatheter (Progreat® 2.4 Fr, Terumo) to replicate the delivery method of an embolisation procedure. The sample was delivered using different injection techniques (Table 4.7) and at different vascular positions within the model (Table 4.8) to gauge the ability of the sample to function as a liquid embolic material and occlude channels when subjected to a range of conditions as indicated by the reduction in flow rate through the injected channel. In each variation of the vascular flow model test, the I-PVA sample was

found to demonstrate embolic properties as indicated by the substantial reduction in flow through the channels injected.

*Table 4.7 - Results of precipitation in vascular flow model using varying injection techniques (n=1).*

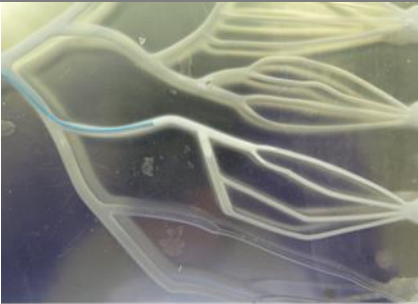
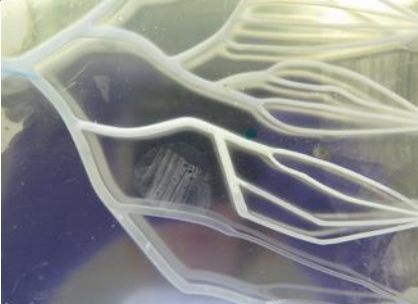
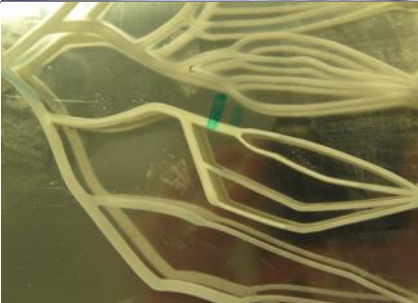
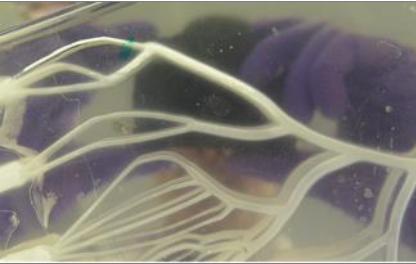
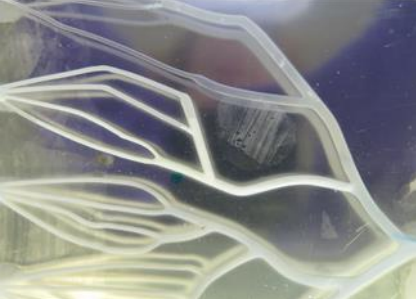
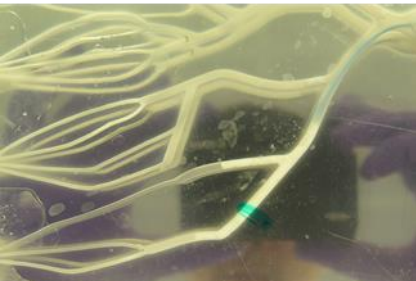
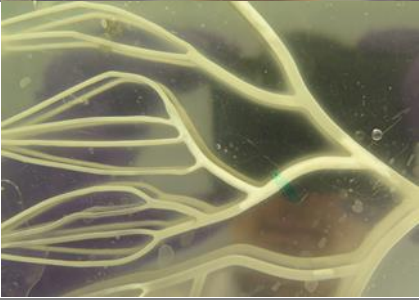
<b>Injection Type</b>	<b>Initial Flow Rate (mL min<sup>-1</sup>)</b>	<b>Final Flow Rate (mL min<sup>-1</sup>)</b>	<b>Reduction in Flow Rate (%)</b>	<b>Injection Photo</b>
<b>Pulsed with 10 s intervals</b>	59.0	10.0	83.1	
<b>Pulsed with 60 s intervals</b>	49.0	2.5	94.9	
<b>Continuous</b>	48.0	1.0	97.9	

Table 4.8 - Results of precipitation in vascular flow model at different delivery sites (n=1).

<b>Injection Location</b>	<b>Initial Flow Rate (mL min<sup>-1</sup>)</b>	<b>Final Flow Rate (mL min<sup>-1</sup>)</b>	<b>Reduction in Flow Rate (%)</b>	<b>Injection Photo</b>
<b>Small Channel - Straight</b>	98.0	0.5	99.5	
<b>Small Channel - Bifurcation</b>	49.0	2.5	94.9	
<b>Large Channel - Straight</b>	66.0	14.0	78.8	
<b>Large Channel - Bifurcation</b>	76.0	5.0	93.4	

Due to the demonstrated suitability of the I-PVA prototype over a range of feasibility tests, the material was further investigated in a series of characterisation tests to evaluate the potential as a liquid embolic material. The characterisation tests were performed using I-PVA samples synthesised using a range of TIBA equivalents between 0.1-0.25 and formulated as DMSO solutions ranging from 8-20 w/w% concentrations. In addition to I-PVA samples prepared using Mowiol 8-88 ( $M_w \sim 67$  kDa), the study was also extended to I-PVA samples

synthesised using varying molecular weights of PVA based on Mowiol<sup>®</sup> 4-88 ( $M_w \sim 31$  kDa) and Mowiol<sup>®</sup> 18-88 ( $M_w \sim 130$  kDa) in order to investigate the impact of polymer molecular weight on the liquid embolic properties alongside the TIBA equivalents and concentration in DMSO (Table 4.2).

#### **4.3.4. Preparation Time**

A minimal preparation time is an ideal property for a liquid embolic material as this can help to reduce the overall procedural time. The liquid embolic prototypes discussed in this chapter were all formulated in DMSO. Therefore, they do not require additional preparation time to mix solutions due to the materials already being in solution ready to use. A consideration should to be given as to how the solutions would be provided. This could be done either in vials which would require the solutions to be withdrawn into syringes before starting the procedure or in ready to use syringes which would be ideal where rapid treatment is required. However, any packaging would be required to be DMSO compatible in order to avoid any degradation of the packaging material whilst the solution is stored prior to use.

To ensure the liquid embolic prototypes maintained a stable solution in DMSO without any sedimentation, visual observations were made following approximately one year after formulation in DMSO. All liquid embolic prototypes prepared were seen to have retained their solution in DMSO without any sedimentation, which would indicate suitability for long-term storage over the time period tested (Table 4.9).

Table 4.9 - Results of long-term solution stability of liquid embolic prototypes 1 year after formulation in DMSO (n=1).

Prototype	TIBA (Eq to PVA Diol Groups)	PVA Molecular Weight (kDa)	Concentration in DMSO (w/w%)	Retained Stable Solution without Sedimentation?
1.1	0.1	67	8	Yes
1.2	0.1	67	12	Yes
1.3	0.1	67	20	Yes
1.4	0.15	67	8	Yes
1.5	0.15	67	12	Yes
1.6	0.15	67	20	Yes
1.7	0.20	67	8	Yes
1.8	0.20	67	12	Yes
1.9	0.20	67	20	Yes
1.10	0.25	67	8	Yes
1.11	0.25	67	12	Yes
1.12	0.25	67	20	Yes
1.13	0.1	31	20	Yes
1.14	0.1	130	20	Yes
1.15	0.25	31	20	Yes
1.16	0.25	130	20	Yes

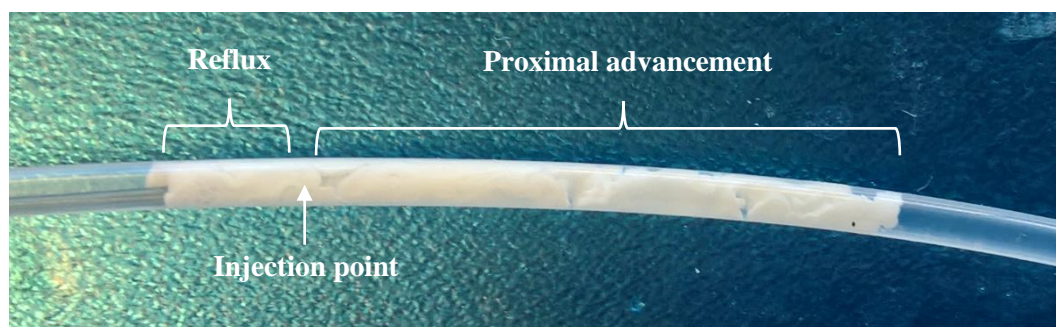
The maintained long-term stable solution of the liquid embolic materials in DMSO without any sedimentation is an improvement on the suspension times of Onyx<sup>®</sup>. Due to the tantalum powder used in the formulation of Onyx<sup>®</sup>, the liquid embolic system has a limited suspension time following agitation.<sup>133</sup> The long-term retention of stable liquid embolic solutions prepared here is beneficial in reducing the preparation time of an embolisation procedure due to no pre-mixing of the materials being required to achieve a uniform suspension.

#### 4.3.5. Deliverability Under Flow Conditions

It is vital to gain an understanding of how the developed liquid embolic prototypes are likely to perform when injected under conditions replicating an embolisation procedure. In order to replicate the embolisation conditions whilst maintaining repeatability, a flow model was used consisting of narrow bore tubing replicating single channelled blood vessels with PBS flow to replicate blood flow. The samples were delivered into the flow model using a commercially

available DMSO-compatible microcatheter (Progreat® 2.4 Fr, Terumo or Renegade™ STC 18, Boston Scientific) to further replicate the delivery of a liquid embolic material.

During the test, a number of observations were made in order to evaluate the delivery of each liquid embolic prototype. The flow rate prior to delivery was noted in order to achieve a comparison for the flow rate before and after delivery, allowing the degree of occlusion of the tubing to be inferred. The delivery of the liquid solutions using a commonly used microcatheter diameter of 2.4 Fr (0.67 mm internal diameter) allowed the suitability of this size of microcatheter to deliver the samples to be gauged. Observations were also made for how the material behaved during the delivery, measuring the degree of proximal flow along with the degree of reflux (Figure 4.7).



*Figure 4.7 - Areas of reflux and proximal flow of the liquid embolic with respect to the injection point during deliverability test.*

As seen in Table 4.10 and Table 4.11, all samples were successfully delivered using the 2.4 Fr microcatheters indicating suitability for delivery by this method. All solidified liquid embolic prototypes resulted in high reductions in the flow rate of PBS through the tubing with a minimum of 93% indicating high levels of occlusion, fulfilling the function of an embolic material. Initial formation of filaments as the solutions exited the tip of the microcatheter into the flow model were noted for a number of liquid embolic prototypes, particularly those prepared at low concentrations in DMSO and also low TIBA equivalents (Table 4.10).

The molecular weight of the polymer component used was not found to impact the likelihood of initial filament formation (Table 4.11). In cases where the filaments remained attached, such as prototypes 1.3 and 1.6, this does not pose a problem as further injection of liquid

embolic material solidified around the initial filament. However, samples which formed filaments which became detached and washed out of the model could pose a risk in an embolisation procedure as this could lead to off-target embolisation elsewhere in the body. Hence, prototypes in which this occurred should be avoided for use within patients.



Table 4.10 - Delivery results of liquid embolic prototypes over a range of TIBA equivalents and DMSO concentrations (n=1).

Prototype	TIBA (Eq to PVA Diol Groups)	Concentration in DMSO (w/w%)	Length of Precipitate (mm)	Length of Proximal Advancement (mm)	Length of Reflux (mm)	Reduction in Flow Rate (%)	Catheter Withdrawal	Delivery Notes
<b>1.1</b>	0.1	8	40.0	40.0	0.0	94.4	Easy	Filaments wash out initially
<b>1.2</b>	0.1	12	41.0	41.0	0.0	98.9	Easy	Filaments wash out initially
<b>1.3</b>	0.1	20	25.0	23.0	2.0	93.2	Easy	Filaments - stayed attached
<b>1.4</b>	0.15	8	32.0	31.0	2.0	95.6	Easy	Filaments wash out initially
<b>1.5</b>	0.15	12	42.0	40.0	2.0	98.7	Easy	Small amount of wash out
<b>1.6</b>	0.15	20	24.0	21.0	3.0	96.4	Easy	Filaments - stayed attached
<b>1.7</b>	0.2	8	32.0	29.0	3.0	99.4	Easy	Filaments wash out initially
<b>1.8</b>	0.2	12	38.0	35.0	3.0	98.7	Easy	Small amount of wash out
<b>1.9</b>	0.2	20	36.0	21.0	15.0	100.0	Easy	No filaments
<b>1.10</b>	0.25	8	37.0	34.0	3.0	99.4	Easy	Filaments wash out initially
<b>1.11</b>	0.25	12	27.0	22.0	5.0	99.4	Easy	No filaments
<b>1.12</b>	0.25	20	30.0	21.0	9.0	97.6	Easy	No filaments

Table 4.11 - Delivery results of liquid embolic prototypes over a range of polymer molecular weights at 0.1 and 0.25 equivalents of TIBA (n=1).

Prototype	TIBA (Eq to PVA Diol Groups)	PVA Molecular Weight (kDa)	Length of Precipitate (mm)	Length of Proximal Advancement (mm)	Length of Reflux (mm)	Reduction in Flow Rate (%)	Catheter Withdrawal	Delivery Notes
<b>1.13</b>	0.1	31	39.0	33.0	6.0	100.0	Some sample removed	No filaments
<b>1.3</b>	0.1	67	25.0	23.0	2.0	93.2	Easy	Filaments - stayed attached
<b>1.14</b>	0.1	130	28.0	17.5	10.5	100.0	Some sample removed	No filaments
<b>1.15</b>	0.25	31	33.0	23.0	10.0	100.0	Easy	No filaments
<b>1.12</b>	0.25	67	30.0	21.0	9.0	97.6	Easy	No filaments
<b>1.16</b>	0.25	130	40.0	34.0	6.0	100.0	Easy	No filaments

With regards to the degree of proximal flow, it is beneficial that the liquid embolic flows with a large portion of proximal flow and minimal reflux to ensure sufficient penetration into the vasculature and with a minimal degree of reflux to avoid entrapment of the microcatheter used to deliver the material during the procedure.<sup>134</sup> Comparison of the percentage of proximal flow over the whole length of the solidified samples against the number of TIBA equivalents generally indicated high portions of proximal flow highlighting minimal degrees of reflux (Figure 4.8). There was seen to be lower degrees of proximal flow for the two highest TIBA equivalents (0.2 and 0.25) formulated at 20 w/w% in DMSO indicating a higher portion of reflux which would pose a risk of microcatheter entrapment. However, it was noted that, even when these samples with high degrees of reflux had solidified, it was still relatively easy to remove the microcatheters without any removal of sample highlighting catheter entrapment was not experienced despite the higher risk posed by these samples (Table 4.10).

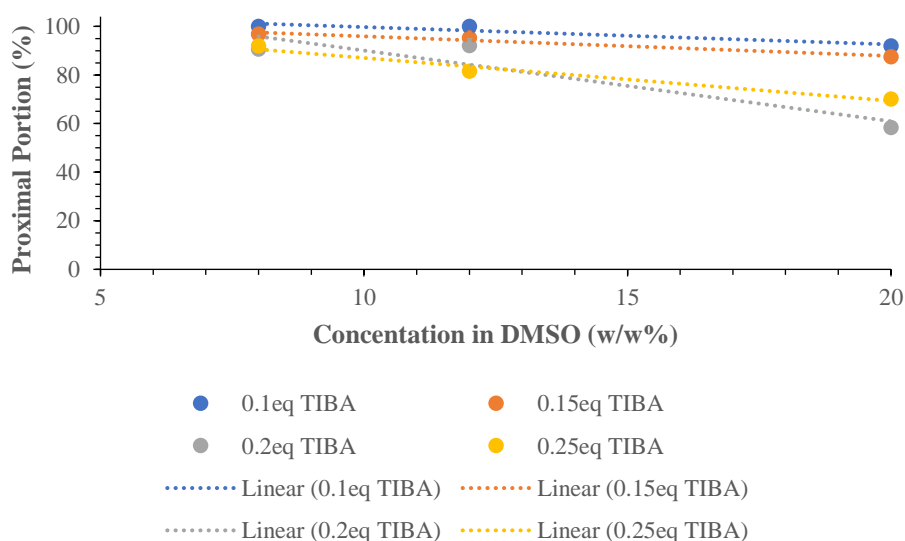


Figure 4.8 - Percentage of proximal flow of solidified liquid embolic prototypes over a range of equivalents of TIBA and concentrations in DMSO ( $n=1$ ).

Comparison of the percentage of proximal flow against the molecular weights of polymer used in the liquid embolic prototypes indicated no trend across the molecular weight range tested (Figure 4.9). However, in the case of the liquid embolic prototypes of 0.1 equivalents of TIBA and 31 and 130 kDa of polymer molecular weight, it was noted that following solidification of the samples and removal of the microcatheter that some sample remained attached to the

tip of the microcatheter (Table 4.11). This is likely due to the lower hydrophobicity of the 0.1 equivalent prototypes resulting in some surface interactions with the microcatheter coating. If this was to occur during an embolisation procedure, it could pose the risk of dislodging the embolic material from the delivery site or dislodgment of the attached polymer as the microcatheter is being withdrawn posing the risk of off-target embolisation elsewhere in the body.

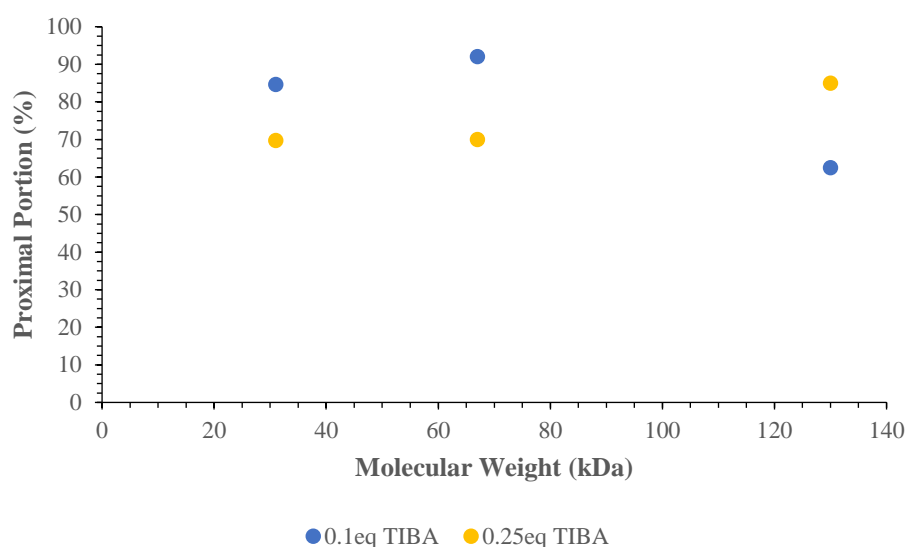


Figure 4.9 - Percentage of proximal flow of solidified liquid embolic prototypes over a range of polymer molecular weights ( $n=1$ ).

The length of the precipitate produced, including the proximal and reflux portions, was not found to correlate with the equivalents of TIBA, concentration in DMSO or polymer molecular weight used. However, small volumes of liquid embolic prototypes were used in the delivery test (0.1 mL) which might not be sufficient to detect any noticeable trends between samples. It must also be noted that due to the manual method used to inject the samples through the microcatheters, this is likely to have introduced variation into the delivery of the materials (as established in Chapter 3). However, the manual injection method used does help to replicate the variability of injections carried out by interventional radiologists during embolisation procedures. The flow model in this test does not accurately replicate the conditions of an embolisation procedure as the vasculature would be composed of a series of blood vessels, diameters and branching points. Instead, the use of narrow bore tubing

replicates a single channel straight blood vessel as an initial indicator of how the liquid embolic prototypes could be expected to behave if injected under similar conditions *in vivo*. The majority of liquid embolic prototypes tested in this model were found to exhibit suitable behaviour during the delivery test. However, prototypes with initial filament formation and excessive degrees of reflux would not be optimal for injection into the body.

The deliverability of the commercially available liquid embolic product Onyx<sup>®</sup> 18 was determined by a slightly altered version of the test using an 18 gauge needle to deliver the sample into the tubing under PBS instead of the use of a microcatheter. This was to prevent contamination of microcatheters used to deliver the liquid embolic prototypes with the tantalum present in Onyx<sup>®</sup>. The other test method parameters including the PBS flow rate, tubing diameter, sample volume and injection technique were all kept constant in order for comparisons to be made between the deliverability results of the liquid embolic prototypes and Onyx<sup>®</sup>. The results obtained for the delivery of Onyx<sup>®</sup> 18 were similar to those obtained using the liquid embolic prototypes including a large length of proximal flow and complete reduction in PBS flow through the tubing (Table 4.12). It was noted that during the delivery of Onyx<sup>®</sup> a filament was formed initially which remained attached throughout the delivery of the sample. The formation of filaments was also observed for a number of liquid embolic prototypes suggesting that in cases where the filaments remain attached to the delivered embolus that the filaments should not pose a problem if used in therapeutic embolisation. There was also seen to be some solidified Onyx<sup>®</sup> sample which remained attached to the needle as it was withdrawn from the solidified sample. However, this is likely to be attributable to the differences in surface interaction of the solidified Onyx<sup>®</sup> with the needle in comparison to the microcatheters with hydrophilic coatings used for Onyx<sup>®</sup> delivery in embolisation procedures.

Table 4.12 - Delivery results of Onyx® 18 (n=1).

Sample	Length of Precipitate (mm)	Length of Proximal Advancement (mm)	Length of Reflux (mm)	Reduction in Flow Rate (%)	Needle Withdrawal	Delivery Notes
Onyx® 18	44.0	37.0	7.0	100.0	Easy but some sample dislodged	Filament – stayed attached

#### 4.3.6. Rate of Solidification

It is important to have an idea of the working time of a liquid embolic i.e. the time taken for the material to fully solidify. This provides a gauge of the timescale over which the injection can be performed and the length of any potential pauses during delivery. The rate of solidification of the liquid embolic prototypes was measured by the dropwise precipitation of the materials into a large volume of PBS (500 mL) which was slowly mechanically stirred (50 rpm) to allow dispersion of the eluted DMSO into the vessel of PBS. The DMSO eluted as the samples solidified was monitored by UV spectroscopy. The solidification time was calculated as the time taken for the samples to elute 90% of the total DMSO eluted over the test time (1 hour) (Table 4.13 and Table 4.14).

Table 4.13 - Solidification data of liquid embolic prototypes over a range of TIBA equivalents and concentrations in DMSO (n=1).

Prototype	TIBA (Eq to PVA Diol Groups)	Concentration in DMSO (w/w%)	Solidification Time (>90%) (s)
1.1	0.1	8	20
1.2	0.1	12	40
1.3	0.1	20	40
1.4	0.15	8	17
1.5	0.15	12	17
1.6	0.15	20	486
1.7	0.2	8	51
1.8	0.2	12	376
1.9	0.2	20	335
1.10	0.25	8	20
1.11	0.25	12	40
1.12	0.25	20	445

Table 4.14 - Solidification data of liquid embolic prototypes over a range of polymer molecular weights at 0.1 and 0.25 equivalents of TIBA ( $n=1$ ).

Prototype	TIBA (Eq to PVA Diol Groups)	PVA Molecular Weight (kDa)	Solidification Time (>90%) (s)
<b>1.13</b>	0.1	31	611
<b>1.3</b>	0.1	67	40
<b>1.14</b>	0.1	130	2051
<b>1.15</b>	0.25	31	506
<b>1.12</b>	0.25	67	445
<b>1.16</b>	0.25	130	61

The results indicated a trend towards longer solidification times for the higher concentrations in DMSO and higher equivalents of TIBA (Figure 4.10). In particular, for the 20 w/w% solutions in DMSO were observed to have reduced rates of solidification in comparison to 8 and 12 w/w% solutions (Figure 4.11). This can be rationalised by the higher polymer content at the polymer/PBS interface which reduces the diffusion of DMSO out of the precipitating material hence reducing the rate of solidification.<sup>135</sup>

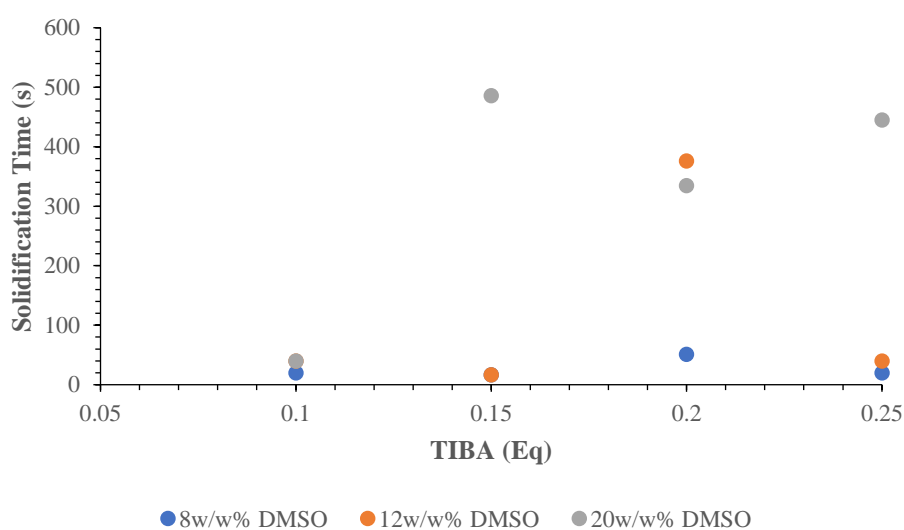


Figure 4.10 - Solidification results of liquid embolic prototypes over a range of TIBA equivalents and concentrations in DMSO ( $n=1$ ).

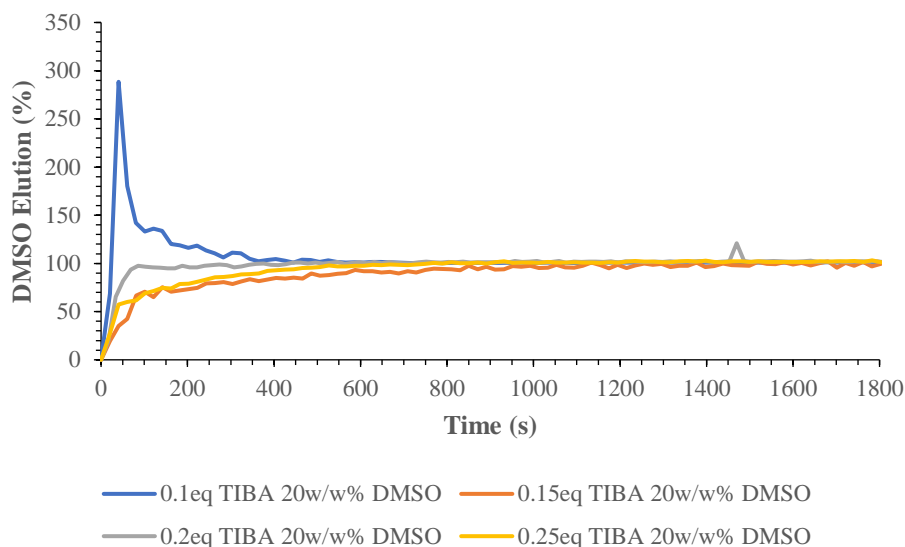


Figure 4.11 - Solidification profiles of liquid embolic prototypes over a range of TIBA equivalents at 20 w/w% solutions in DMSO ( $n=1$ ).

Rapid rates of solidification ( $\leq 1$  minute) were observed for all samples prepared as 8 w/w% solutions in DMSO irrelevant of the number of TIBA equivalents used. For the liquid embolic prototypes prepared using 0.1 equivalents of TIBA, fast rates of solidification were measured across all DMSO concentrations tested with the burst release effects observed for each formulation (Figure 4.12). This supports the theory of lower polymer contents at the phase inversion interface allowing for diffusion of DMSO out of the precipitating materials more freely than for prototypes of higher polymer concentration in DMSO.<sup>135</sup>



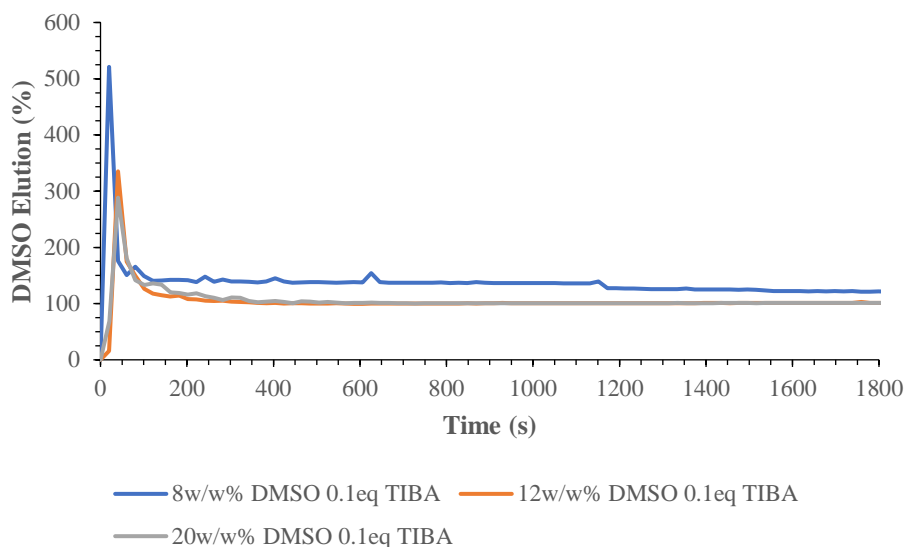


Figure 4.12 - Solidification profiles of liquid embolic prototypes over a range of concentrations in DMSO at 0.1 equivalents of TIBA ( $n=1$ ).

The solidification time of liquid embolic prototypes prepared over a range of polymer molecular weights were seen to exhibit a trend towards faster solidification times with increasing polymer molecular weights (Figure 4.13). In particular, for liquid embolic samples prepared at the highest polymer molecular weights of 130 kDa, a burst release effect of DMSO was observed as the samples precipitated close to the outlet leading to the UV spectrophotometer.

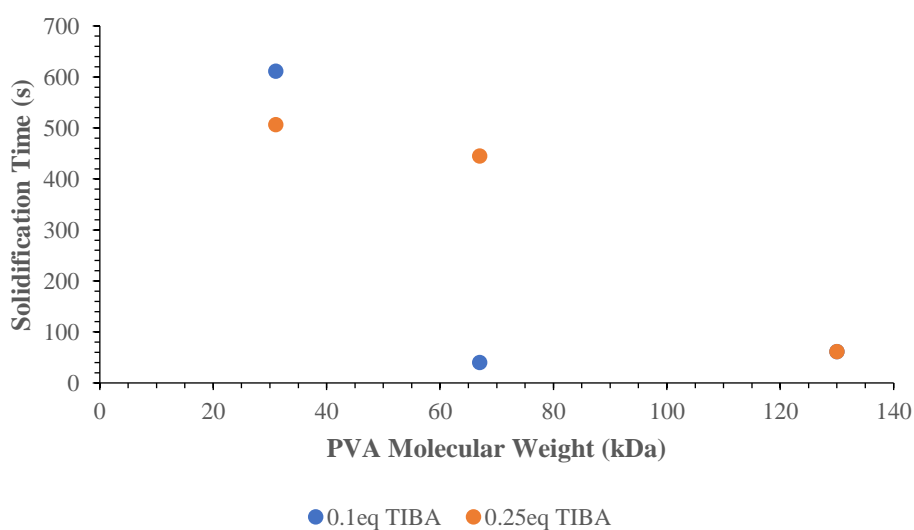


Figure 4.13 - Solidification results of liquid embolic prototypes over a range of polymer molecular weights at 0.1 and 0.25 equivalents of TIBA ( $n=1$ ).

Burst release effects were observed for 0.1 equivalent TIBA samples of medium and high polymer molecular weights due to precipitation at the surface of PBS close to the UV outlet likely due to the low density of the materials (Figure 4.14). A slower solidification profile was observed for the lower molecular weight formulation suggesting the occurrence of a skinning effect in which the outer perimeter of the sample droplet solidifies first followed by the gradual solidification of the contained material by gradient diffusion of DMSO. This reduces the rate of elution of DMSO out of the solidifying material as observed by UV spectroscopy.

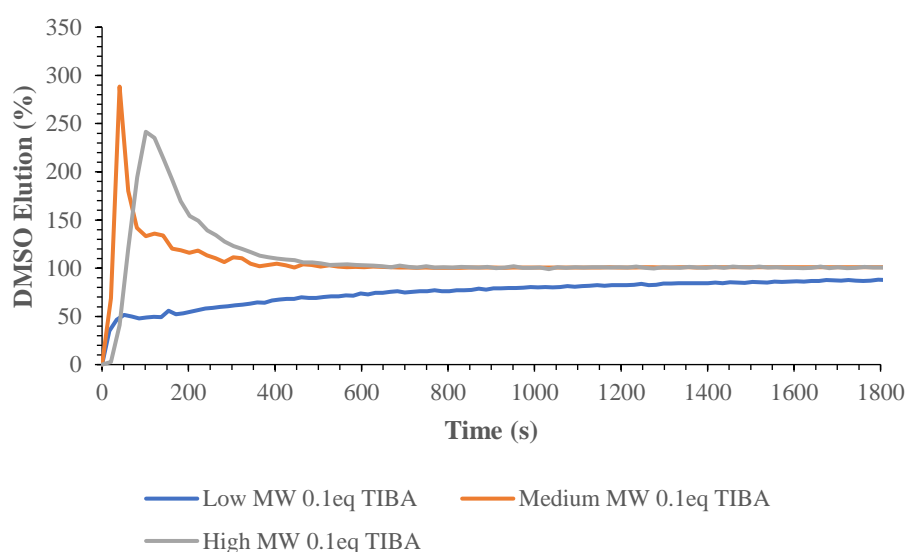


Figure 4.14 - Solidification profiles of liquid embolic prototypes over a range of molecular weights at 0.1 equivalents of TIBA ( $n=1$ ).

A similar trend was observed for the solidification profiles of liquid embolic prototypes tested at 0.25 equivalents of TIBA over a range a polymer molecular weights. Slower solidification profiles were observed for decreasing polymer molecular weights consistent with the theory of higher TIBA density polymers exhibiting a skinning effect during precipitation thereby reducing the rate of solidification (Figure 4.15).

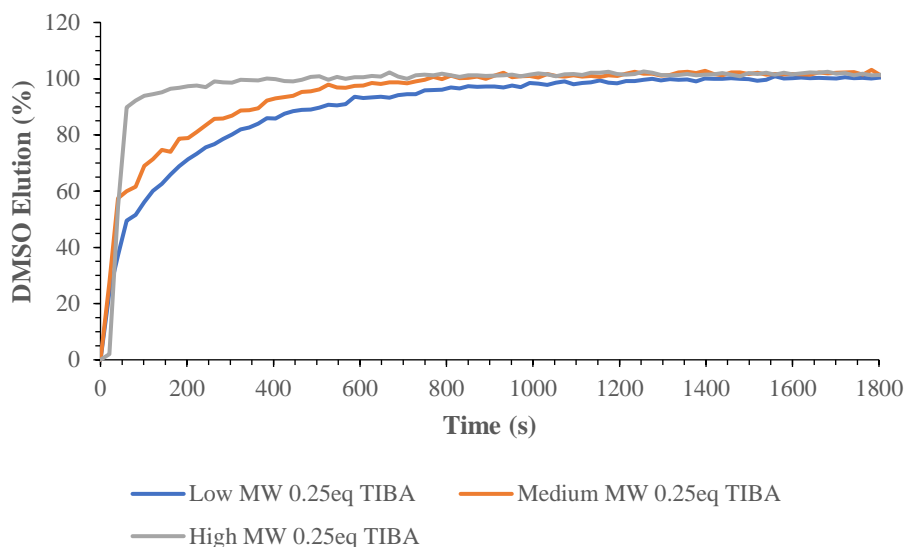


Figure 4.15 - Solidification profiles of liquid embolic prototypes over a range of molecular weights at 0.25 equivalents of TIBA ( $n=1$ ).

It should be noted that this test method is likely to indicate faster solidification times than would be expected if injected into the vasculature. This is due to the dropwise precipitation method used which gave rise to much smaller droplet volumes and hence larger surface areas for the elution of DMSO out of the solidifying materials. A limitation of this method is that very fast solidification times are unable to be accurately determined due to the time required to pump the solutions to the UV spectrophotometer. Similarly, samples which precipitated directly on the surface of PBS close to the outlet feeding the UV spectrophotometer were found to obscure the measured rate of solidification due to the initial spike in DMSO release. The concentration of DMSO was then reduced as the solvent mixture was pumped in the closed loop between the UV spectrophotometer and PBS vessel allowing the eluted DMSO to be dissipated in the volume of PBS.

Despite the limitations of this test method, comparison of the results attained for the liquid embolic prototypes to Onyx<sup>®</sup> 18 tested using the same solidification method allows conclusions to be drawn as to whether a suitable solidification time is being targeted. The rate of solidification of Onyx<sup>®</sup> 18 (Table 4.15) was found to be in the range of a number of the liquid embolic prototypes discussed here. The investigation of the liquid embolic prototypes over a range of parameters has demonstrated that the rate of solidification can be tuned

depending on the number of TIBA equivalents and concentration in DMSO used during the preparation of the materials. The solidification rate of the liquid embolic prototypes was also found to increase with increasing polymer molecular weight used between the range tested of 31 to 130 kDa. This therefore demonstrates the ability to modify the rate of solidification to suit the required working time of liquid embolic materials in varying embolisation treatments.

*Table 4.15 - Solidification data of Onyx®18 (n=1).*

<b>Sample</b>	<b>Solidification Time (&gt;90%) (s)</b>
<b>Onyx® 18</b>	81

#### **4.3.7. Rheology of Precipitation Process**

Rheology tests were used to quantify the changes in a number of factors including complex viscosity, storage modulus and loss modulus, to indicate the delivery behaviour of the liquid embolic prototypes. The complex viscosity of the samples, resistance to flow under oscillating shear stress, gives an indication of injectability of the materials in their liquid state through a microcatheter with lower complex viscosities being preferable as these would require less force for injection. The change in complex viscosity as phase inversion occurs can be used to monitor the precipitation process as the solidifying material becomes more resistant to flow during solidification. Measurement of the storage modulus of the samples allows insight to be gained into the rigidity of the samples that is attributable to elastic deformation. It is expected that an increase in this value will be observed as phase inversion occurs and the liquid embolic materials solidify under aqueous conditions. Similarly, an increase in loss modulus is likely to be observed during the precipitation process as the rigidity of the sample that is attributable to viscous flow increases.

The rheology test method provides a useful indication into how the various parameters change with the onset of precipitation. The rheology precipitation tests were performed using a parallel plate geometry onto which the liquid embolic prototypes were loaded. Rheology measurements were performed using the prototypes in their liquid states at a shear rate of 0.1 s<sup>-1</sup> to determine the initial rheological properties of the samples. After sufficient measurements

were taken of the prototypes in their liquid form, the rheology cell was flooded with saline solution heated to 37 °C to mimic the aqueous salt conditions of blood as the liquid embolic material enters the blood vessels. Further measurements were taken to monitor the precipitation process for a total of 30 minutes. An example of the precipitation profile is given below for the liquid embolic prototype 1.9 in Figure 4.16 and Figure 4.17.

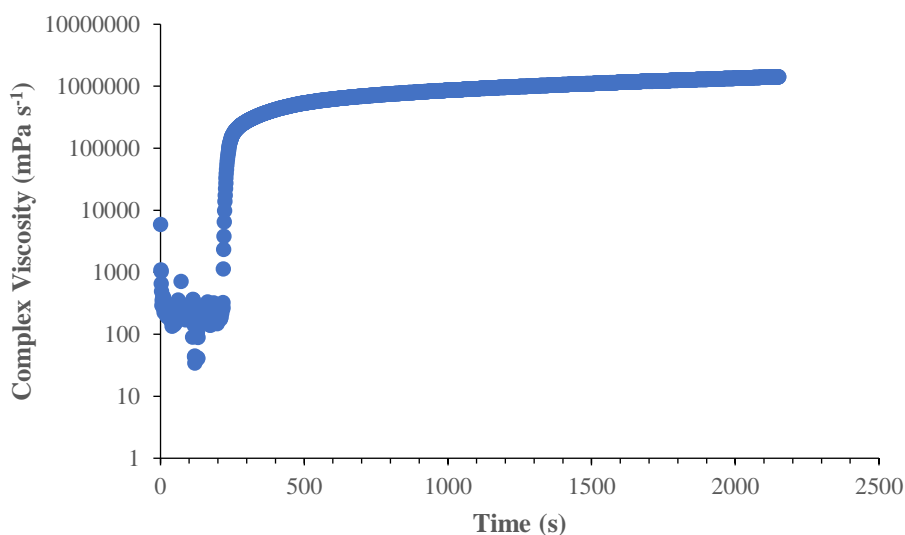


Figure 4.16 - Complex viscosity profile of precipitation process for liquid embolic prototype 1.9 of 0.2 equivalents of TIBA for 67 kDa PVA at 20 w/w% in DMSO (onset of precipitation at 3.5 mins) ( $n=1$ ).

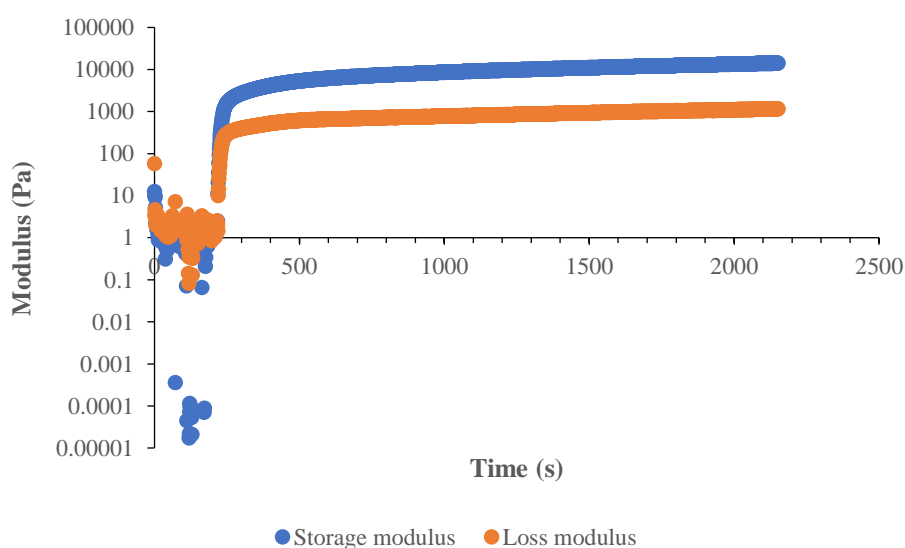


Figure 4.17 - Storage and loss modulus profiles of precipitation process for liquid embolic prototype 1.9 of 0.2 equivalents of TIBA for 67 kDa PVA at 20 w/w% in DMSO (onset of precipitation at 3.5 mins) ( $n=1$ ).

The rheology precipitation test was performed for a number of liquid embolic prototypes chosen to investigate trends of TIBA equivalents, concentration in DMSO and polymer molecular weight (Table 4.16 and Table 4.17). Measurements were obtained for the complex viscosity, storage modulus and loss modulus of the liquid embolic prototypes in their liquid and precipitate states.

Table 4.16 - Rheology data of liquid embolic prototypes in liquid states for a range of TIBA equivalents, polymer molecular weights and concentrations in DMSO ( $n=1$ ).

Prototype	TIBA (Eq to PVA Diol Groups)	PVA Molecular Weight (kDa)	Concentration in DMSO (w/w%)	Mean Storage Modulus (Pa)	Standard Deviation (Pa)	Mean Loss Modulus (Pa)	Standard Deviation (Pa)	Mean Complex Viscosity ( $\text{mPa s}^{-1}$ )	Standard Deviation ( $\text{mPa s}^{-1}$ )
<b>1.7</b>	0.2	67	8	0.64	1.35	1.62	2.75	196	293
<b>1.8</b>	0.2	67	12	0.62	0.55	1.38	0.66	160	67.8
<b>1.9</b>	0.2	67	20	0.41	0.47	2.68	0.98	275	99.2
<b>1.13</b>	0.1	31	20	1.60	0.83	2.02	0.76	269	79.8
<b>1.14</b>	0.1	130	20	0.09	0.41	18.70	0.84	1870	84.9
<b>1.15</b>	0.25	31	20	0.04	0.11	1.24	0.41	125	41.4
<b>1.16</b>	0.25	130	20	1.04	0.64	6.63	0.67	674	65.7

Table 4.17 - Rheology data of liquid embolic prototypes in precipitate states for a range of TIBA equivalents, polymer molecular weights and concentrations in DMSO ( $n=1$ ).

Prototype	TIBA (Eq to PVA Diol Groups)	PVA Molecular Weight (kDa)	Concentration in DMSO (w/w%)	Max Storage Modulus (Pa)	Max Loss Modulus (Pa)	Max Complex Viscosity ( $\text{mPa s}^{-1}$ )
<b>1.7</b>	0.2	67	8	39172	4623	3943300
<b>1.8</b>	0.2	67	12	101680	11591	10233000
<b>1.9</b>	0.2	67	20	82257	35032	8472700
<b>1.13</b>	0.1	31	20	9671	5553	1115200
<b>1.14</b>	0.1	130	20	9842	20776	2077600
<b>1.15</b>	0.25	31	20	371600	39458	37322000
<b>1.16</b>	0.25	130	20	158490	65902	17110000

Comparison of liquid embolic prototypes synthesised at TIBA equivalents of 0.1 and 0.25 show a trend for higher maximum viscosities attained in the precipitate states with an increase in TIBA equivalents across both molecular weights tested of 31 and 130 kDa (Figure 4.18). An increase in TIBA equivalents from 0.1 to 0.25 resulted in complex viscosities of ten-fold higher for the liquid embolic prototypes in their precipitate states. The molecular weight of the polymer used was also found to have an impact on the complex viscosity of prototypes in their liquid states with higher complex viscosities observed for the prototypes prepared using the higher PVA molecular weight of 130 kDa which is consistent with the literature data for higher molecular weight polymer solutions.<sup>136</sup> The same trend for an increase in storage and loss modulus of these liquid embolic prototypes was observed with an increase in TIBA equivalents, again with variation depending on the polymer molecular weight used (Figure 4.19 and Figure 4.20). This suggests the number of equivalents of TIBA used in the formulations to have a strong impact on the rheological properties of prototypes in their liquid and precipitate states.

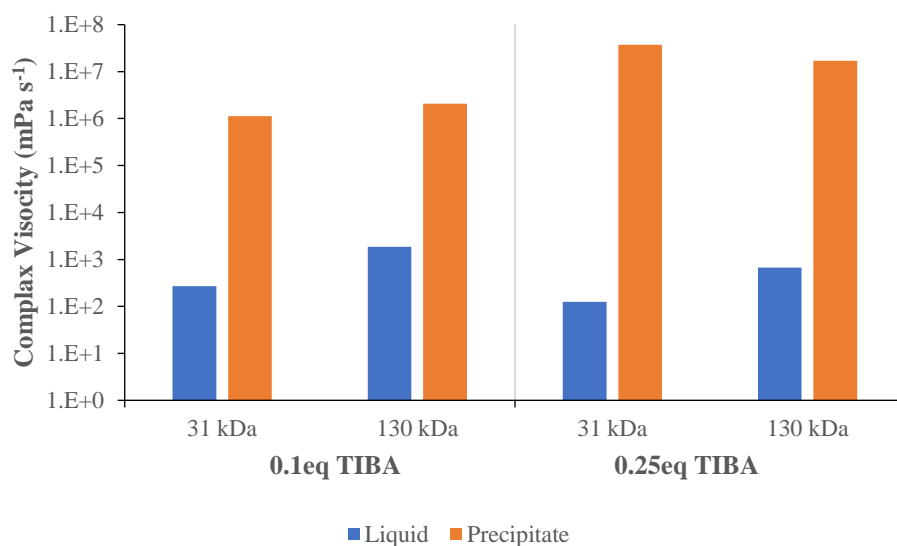


Figure 4.18 - Complex viscosity results of liquid embolic prototypes for low and high molecular weights at 0.1 and 0.25 equivalents of TIBA in liquid and precipitate states ( $n=1$ ).



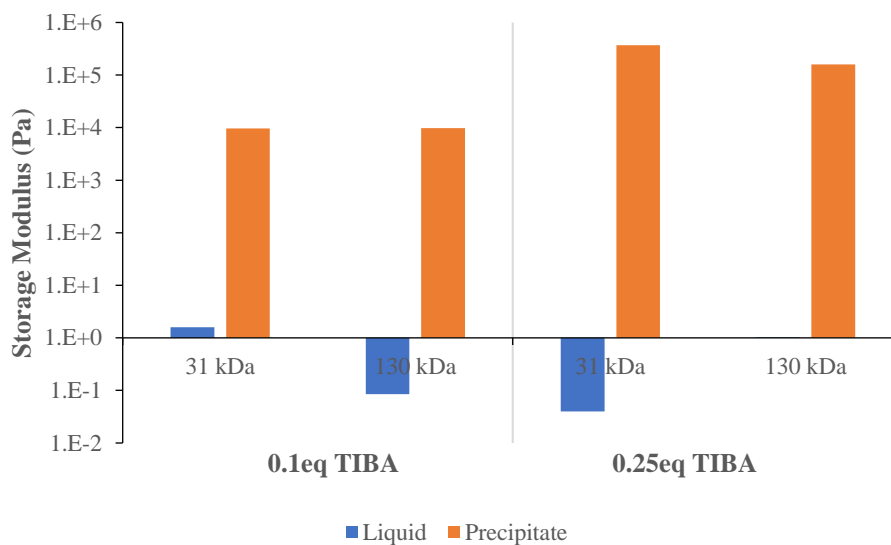


Figure 4.19 - Storage modulus results of liquid embolic prototypes for low and high molecular weights at 0.1 and 0.25 equivalents of TIBA in liquid and precipitate states ( $n=1$ ).

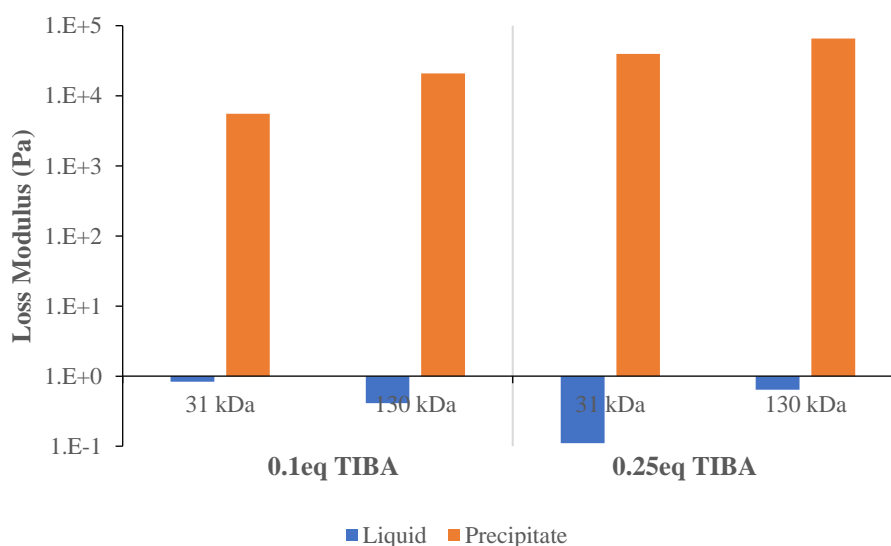


Figure 4.20 - Loss modulus results of liquid embolic prototypes for low and high molecular weights at 0.1 and 0.25 equivalents of TIBA in liquid and precipitate states ( $n=1$ ).

Comparison of liquid embolic prototypes prepared at the same TIBA equivalents and formulated over a range of concentrations in DMSO indicated a less marked change in complex viscosity than observed with an increase in TIBA equivalents (Figure 4.21). The complex viscosity of the liquid embolic prototypes was of similar viscosities in their liquid and precipitate states. This suggests that the concentration of radiopaque polymer in DMSO has less of an impact on the materials rheological properties than the composition of the

radiopaque polymer itself. Similar results were seen for the samples of varying DMSO concentrations for their storage and loss modulus in both their liquid and precipitated states (Figure 4.22 and Figure 4.23).

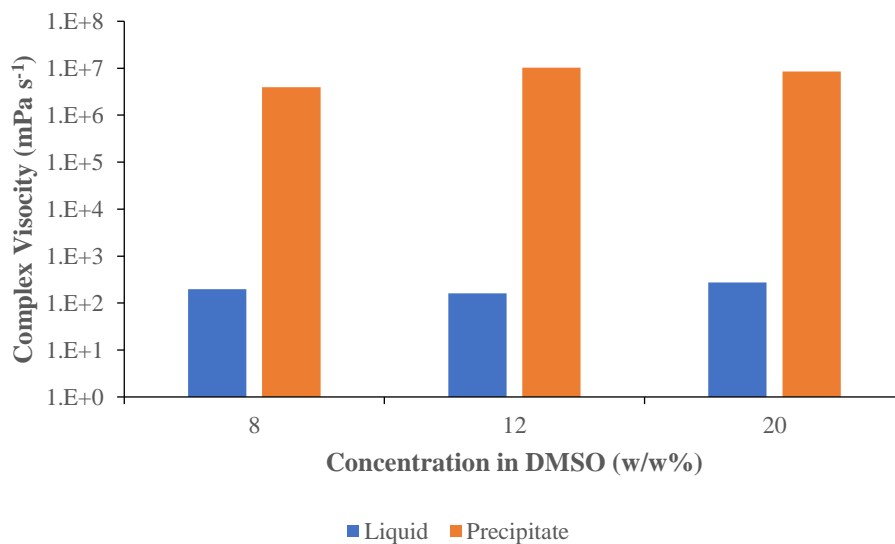


Figure 4.21 - Complex viscosity results of liquid embolic prototypes at 0.2 equivalents of TIBA over a range of concentrations in DMSO in liquid and precipitate states (n=1).

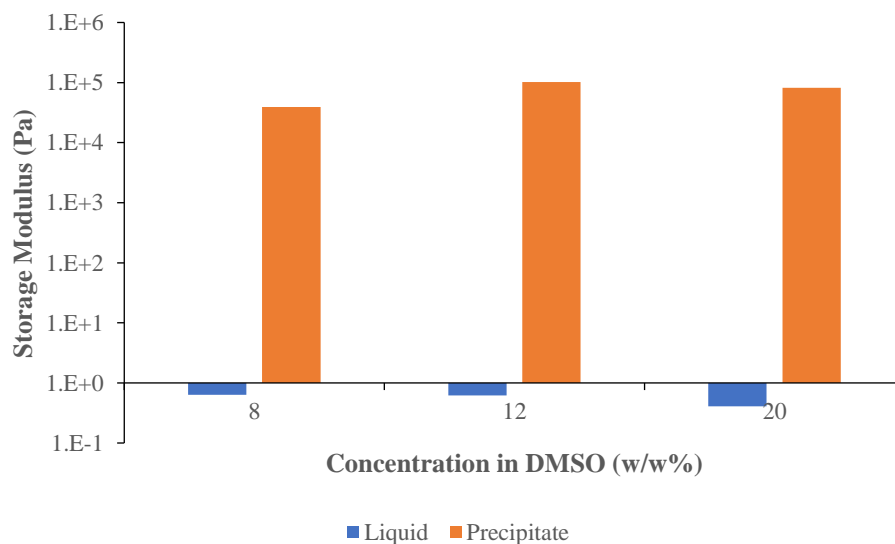


Figure 4.22 - Storage modulus results of liquid embolic prototypes at 0.2 equivalents of TIBA over a range of concentrations in DMSO in liquid and precipitate states (n=1).

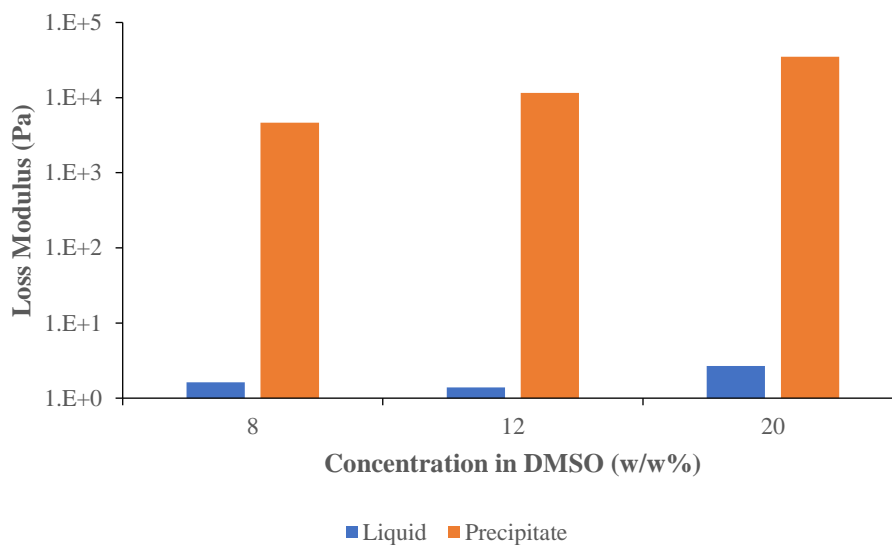


Figure 4.23 - Loss modulus results of liquid embolic prototypes at 0.2 equivalents of TIBA over a range of concentrations in DMSO in liquid and precipitate states ( $n=1$ ).

The rheology precipitate test results outlined in this section give a useful indicator as to the changes in complex viscosity, storage and loss modulus of the liquid embolic prototypes with regards to the TIBA equivalents, concentration in DMSO and polymer molecular weight during precipitation. It should be noted that the values quoted for the materials in their precipitated state are unlikely to be the final measurements of the materials once fully solidified. The test was carried out for 30 minutes following the addition of saline solution to the rheology cell. However due to the geometry of the parallel plate set-up used, precipitation first occurred at the outer perimeters of the samples. This initial skin formation resulted in saline not fully penetrating through to the centre of the samples within the 30 minute test time meaning the centre of the samples had not yet fully solidified. Further tests should be undertaken until complete precipitation is observed to obtain the true values of the prototypes in their fully solidified states. The method used does however, provide a comparison of the maximum values of complex viscosity, storage modulus and loss modulus reached 30 minutes after onset of precipitation for each sample.

Comparison of the complex viscosities determined for the liquid embolic prototypes measured in this test can be made with currently used liquid embolic materials of Onyx<sup>®</sup> formulations. Conversion of the measured complex viscosities can be converted to viscosities at the shear

rate of  $0.1 \text{ s}^{-1}$ . This gives the range of viscosities for the prototypes tested of 1250-18700 mPa. The Onyx<sup>®</sup> formulations of Onyx<sup>®</sup> 18 and Onyx<sup>®</sup> 34 have viscosities of 18 and 34 mPa, respectively.<sup>71</sup> Therefore, the liquid embolic prototypes tested are of much higher viscosities than the Onyx<sup>®</sup> formulations already currently available on the market. This suggests larger injection pressures would be required to deliver the proposed liquid embolic prototypes using narrow lumen microcatheters in comparison to Onyx<sup>®</sup>. It should be noted that the relative viscosity may vary with different shear rates meaning these values are unlikely to be a true comparison but instead provide a gauge of the higher measured viscosities of the liquid embolic prototypes.

#### ***4.3.8. Fill Volume After Solidification***

During an embolisation procedure, it is beneficial for the interventional radiologist performing the injection to have an idea of how much liquid needs to be delivered to fill the targeted volume of the vasculature. In order to gain an understanding of the expected fill volumes of the liquid embolic prototypes, a known volume of liquid embolic sample was precipitated dropwise in PBS and the volume of the solidified material determined (Table 4.18 and Table 4.19). It should be noted that, due to the dropwise method used for precipitation, this is not representative of how the materials would solidify within the body but instead provides a method of forming reproducible precipitates. This allows insight into any trends in volume changes between liquid embolic prototypes rather than their true fill volumes if implanted within the body.

## Chapter 4: Synthesis and Characterisation of a Precipitating Liquid Embolic

Table 4.18 - Fill volume data of liquid embolic prototypes over a range of TIBA equivalents and concentrations in DMSO (n=3).

Prototype	TIBA (Eq to PVA Diol Groups)	Concentration in DMSO (w/w%)	Initial Liquid Volume (ml)	Height of Precipitate (mm)	Volume of Precipitate (ml)	Mean Reduction in Volume (%)	Standard Error of Mean (%)
<b>1.1</b>	0.1	8	0.5	2.0	0.03	95.3	1.4
			0.5	1.5	0.01		
			0.5	2.0	0.03		
<b>1.2</b>	0.1	12	0.5	2.5	0.06	85.2	2.8
			0.5	3.5	0.11		
			0.5	2.5	0.06		
<b>1.3</b>	0.1	20	0.5	5.5	0.21	58.2	2.4
			0.5	6.0	0.23		
			0.5	5.0	0.18		
<b>1.4</b>	0.15	8	0.5	3.5	0.11	86.9	3.6
			0.5	2.0	0.03		
			0.5	2.5	0.06		
<b>1.5</b>	0.15	12	0.5	3.5	0.11	80.1	1.4
			0.5	3.0	0.08		
			0.5	3.5	0.11		
<b>1.6</b>	0.15	20	0.5	6.5	0.26	46.4	1.4
			0.5	7.0	0.28		
			0.5	6.5	0.26		
<b>1.7</b>	0.2	8	0.5	2.5	0.06	86.9	1.4
			0.5	3.0	0.08		
			0.5	4.5	0.16		
<b>1.8</b>	0.2	12	0.5	4.0	0.13	66.6	3.6
			0.5	5.5	0.21		
			0.5	8.0	0.34		
<b>1.9</b>	0.2	20	0.5	8.5	0.36	29.6	1.4
			0.5	8.5	0.36		
			0.5	3.0	0.08		
<b>1.10</b>	0.25	8	0.5	3.0	0.08	83.5	0.0
			0.5	3.0	0.08		
			0.5	3.0	0.08		
<b>1.11</b>	0.25	12	0.5	3.0	0.08	81.8	1.4
			0.5	3.5	0.11		
			0.5	6.5	0.26		
<b>1.12</b>	0.25	20	0.5	7.0	0.28	43.0	2.4
			0.5	7.5	0.31		
			0.5	7.5	0.31		

Table 4.19 - Fill volume data of liquid embolic prototypes over a range of polymer molecular weights at 0.1 and 0.25 equivalents of TIBA ( $n=3$ ).

Prototype	TIBA (Eq to PVA Diol Groups)	PVA Molecular Weight (kDa)	Initial Liquid Volume (ml)	Height of Precipitate (mm)	Volume of Precipitate (ml)	Mean Reduction in Volume (%)	Standard Error of Mean (%)
1.13	0.1	31	0.5	9.0	0.39	19.5	2.8
			0.5	10.0	0.44		
			0.5	9.0	0.39		
1.3	0.1	67	0.5	5.5	0.21	58.2	2.4
			0.5	6.0	0.23		
			0.5	5.0	0.18		
1.14	0.1	130	0.5	7.5	0.31	39.7	1.4
			0.5	7.0	0.28		
			0.5	7.5	0.31		
1.15	0.25	31	0.5	7.0	0.28	41.4	1.4
			0.5	7.5	0.31		
			0.5	7.0	0.28		
1.12	0.25	67	0.5	6.5	0.26	43.0	2.4
			0.5	7.0	0.28		
			0.5	7.5	0.31		
1.16	0.25	130	0.5	8.5	0.36	24.5	1.4
			0.5	9.0	0.39		
			0.5	9.0	0.39		

There was found to be a correlation between the concentration of polymeric material in DMSO and the resulting fill volume of the solidified material (Figure 4.24). Samples precipitated as solutions of lower concentration in DMSO (8 w/w%) were found to undergo a much higher reduction in volume than those samples precipitated from solutions of higher concentrations in DMSO (20 w/w%). This is as expected due to the lower polymer content of the more dilute solutions giving rise to high volume reductions as the DMSO diffuses out of the precipitating material.

There was also seen to be a trend for the equivalents of TIBA used and the resulting volume of the solidified material (Figure 4.24). Liquid embolic prototypes prepared using a higher equivalents of TIBA to PVA diol groups were found to undergo a lower volume reduction on

solidification than those prepared using a lower equivalents of TIBA. This can be rationalised by the initial formation of a skin which was observed visually as the higher TIBA equivalents samples solidified. This formation of an initial skin allowed the materials to retain a spherical shape compared to a flat disk shape observed with the lower TIBA content samples. The formation of a more spherical shape is likely to have resulted in a higher retention of DMSO trapped within voids of the precipitated samples in comparison to the samples of a flatter disk shape giving rise to the lower fill volume reductions observed.<sup>114</sup>

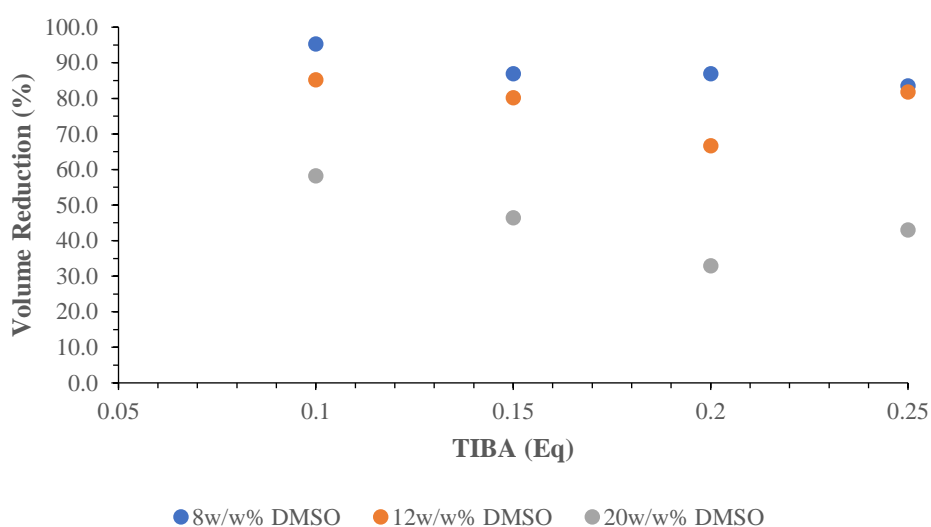


Figure 4.24 - Fill volume results of liquid embolic prototypes over a range of TIBA equivalents and concentrations in DMSO ( $n=3$ ).

Comparison of the fill volume data for liquid embolic prototypes prepared over a range of polymer molecular weights at 0.1 and 0.25 equivalents of TIBA to PVA diol groups, indicated no trend in the fill volume (Figure 4.25). This suggests that the molecular weight of the polymer used in the liquid embolic formulation does not impact the resulting fill volume of the solidified material over the range of molecular weights tested (31-130 kDa).

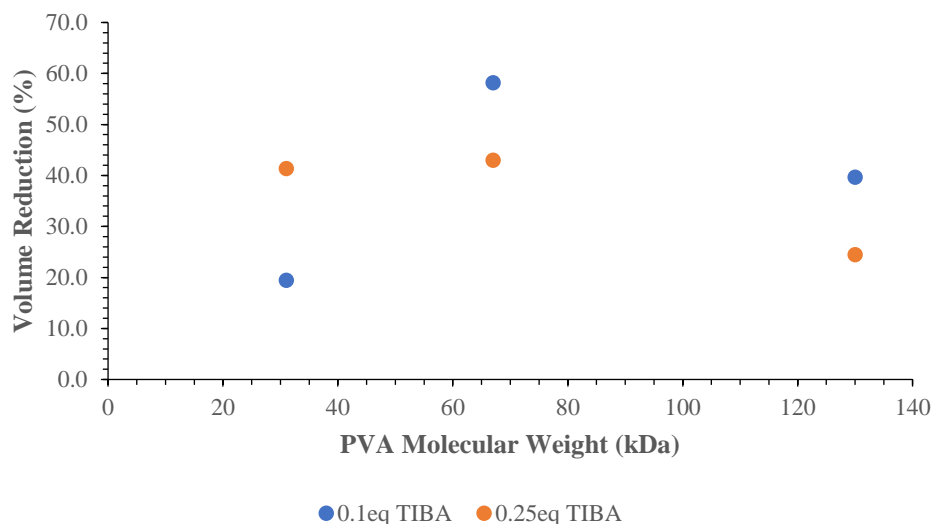


Figure 4.25 - Fill volume results of liquid embolic prototypes over a range of polymer molecular weights at 0.1 and 0.25 equivalents of TIBA ( $n=3$ ).

Although it is not a requirement to have a high fill volume per mL of liquid injected, samples with very high reductions in fill volume are less favourable. The more important factor is the knowledge of how much solid volume will be obtained from the volume of liquid injected. Liquid embolic prototypes with a lower volume reduction, such as prototype 1.12 (synthesised at 0.25 equivalents of TIBA using 67 kDa PVA and formulated at 20 w/w% in DMSO), will allow for a larger area of the targeted vasculature to be embolised during the procedure, thereby being more cost effective. Comparison of the fill volumes attained for the liquid embolic prototypes to Onyx<sup>®</sup> 18 (Table 4.20) indicate that an approximate 50% reduction of fill volume on transition from liquid to solid is already tolerated for commercially available liquid embolics. Hence, it would be preferable for new liquid embolic materials to possess a similar or improved fill volume per mL of injected liquid.

Table 4.20 - Fill volume data of Onyx<sup>®</sup> 18 ( $n=1$ ).

Sample	Initial Liquid Volume (ml)	Height of Precipitate (mm)	Volume of Precipitate (ml)	Reduction in Volume (%)
Onyx <sup>®</sup> 18	1.0	11.0	0.49	51.3



### 4.3.9. Fragmentation and Particulate Generation

It is necessary for an implanted embolic material to remain as a complete solid mass when delivered into the vasculature as any formation of fragments could pose the risk of dislodging leading to off-target embolisation elsewhere within the body. This can pose serious complications in which healthy tissue or organs become unintentionally embolised.<sup>14,15</sup> To reduce the risk of these complications the proposed implanted embolic materials must be subjected to stresses which are likely to be exhibited in the body to determine the ability of the material to remain as a solid mass. This was carried out using a fragmentation and particulate generation test in which liquid embolic prototypes were precipitated dropwise into PBS and shaken at various speeds (240-600 rpm) for 30 minutes to replicate agitation after implantation. Solutions of the agitated samples were then removed and observed under optical microscope at different magnifications ( $\times 4$  and  $\times 10$ ) to observe the formation of any particulates and fragments. The captured images were analysed for the number of fragments formed and percentage surface area covered by particulates then each sample was attributed a rating of 1-5 with 1 being minimal and 5 being high generation of particulates and fragments (Table 4.21, Table 4.22, Table 4.23 and Table 4.24).

Table 4.21 - Fragmentation data of liquid embolic prototypes over a range of TIBA equivalents and concentrations in DMSO ( $n=3$ ).

Prototype	TIBA (Eq to PVA Diol Groups)	Concentration in DMSO (w/w%)	Highest Number of Fragments	Standard Error of Mean	Fragmentation Rating
1.1	0.1	8	17	1	4
1.2	0.1	12	27	1	5
1.3	0.1	20	17	1	4
1.4	0.15	8	16	1	4
1.5	0.15	12	21	1	5
1.6	0.15	20	8	1	2
1.7	0.2	8	7	1	2
1.8	0.2	12	3	0	1
1.9	0.2	20	8	1	2
1.1	0.25	8	14	1	3
1.11	0.25	12	7	1	2
1.12	0.25	20	3	0	1

Table 4.22 - Particulate generation data of liquid embolic prototypes over a range of TIBA equivalents and concentrations in DMSO (n=3).

Prototype	TIBA (Eq to PVA Diol Groups)	Concentration in DMSO (w/w%)	Highest Area Coverage by Particulates (%)	Standard Error of Mean	Particulate Rating
1.1	0.1	8	4.47	0.29	5
1.2	0.1	12	3.29	0.15	4
1.3	0.1	20	1.79	0.15	2
1.4	0.15	8	7.78	0.70	5
1.5	0.15	12	5.82	0.33	5
1.6	0.15	20	3.12	0.35	4
1.7	0.2	8	5.17	0.30	5
1.8	0.2	12	3.93	0.27	4
1.9	0.2	20	0.19	0.06	1
1.1	0.25	8	30.63	0.51	5
1.11	0.25	12	6.21	0.34	5
1.12	0.25	20	0.33	0.02	1

Table 4.23 - Fragmentation data for liquid embolic prototypes over a range of polymer molecular weights at 0.1 and 0.25 equivalents of TIBA (n=3).

Prototype	TIBA (Eq to PVA Diol Groups)	PVA Molecular Weight (kDa)	Highest Number of Fragments	Standard Error of Mean	Fragmentation Rating
1.13	0.1	31	18	1	4
1.3	0.1	67	17	1	4
1.14	0.1	130	16	1	4
1.15	0.25	31	6	1	2
1.12	0.25	67	3	0	1
1.16	0.25	130	4	1	1

Table 4.24 - Particulate generation data for liquid embolic prototypes over a range of polymer molecular weights at 0.1 and 0.25 equivalents of TIBA (n=3).

Prototype	TIBA (Eq to PVA Diol Groups)	PVA Molecular Weight (kDa)	Highest Area Coverage by Particulates (%)	Standard Error of Mean	Particulate Rating
1.13	0.1	31	2.72	0.23	3
1.3	0.1	67	1.79	0.15	2
1.14	0.1	130	0.26	0.03	1
1.15	0.25	31	0.21	0.01	1
1.12	0.25	67	0.33	0.02	1
1.16	0.25	130	0.06	0.01	1

In general, it was found that liquid embolic prototypes formulated as a higher concentration in DMSO tended to exhibit lower degrees of fragmentation and particulate generation (Figure 4.26 and Figure 4.27). The equivalents of TIBA used to prepare the liquid embolic prototypes was also found to influence the likelihood for the solidified materials to generate particulates and fragments under agitated conditions. Lower equivalents of TIBA were associated with higher rates of fragmentation and particulate generation, irrelevant of the concentration in DMSO. This is likely due to the reduced structural strength of the precipitates as a result of less opportunity for  $\pi$ - $\pi$  stacking between aromatic groups due to the lower percentage of TIBA used the formulation.<sup>135</sup>

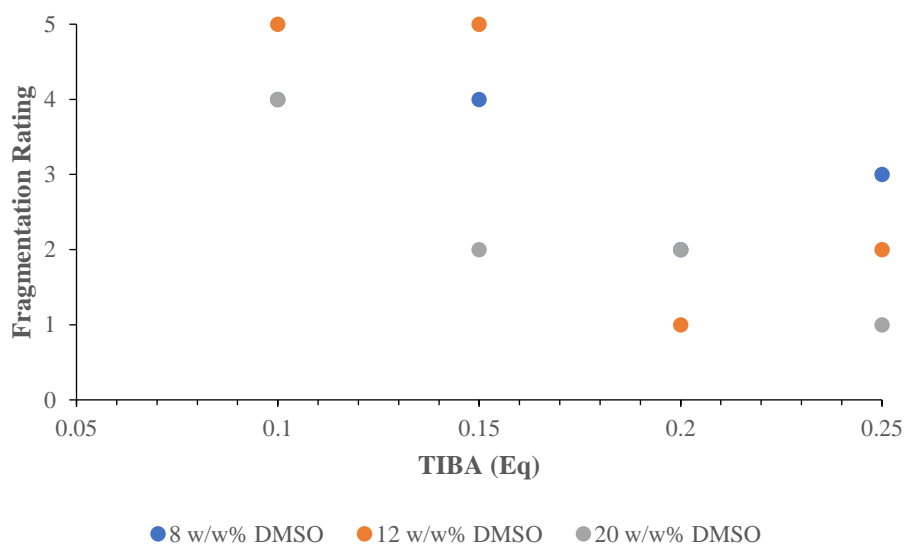


Figure 4.26 - Fragmentation ratings of liquid embolic prototypes of a range of DMSO concentrations and TIBA equivalents ( $n=3$ ).

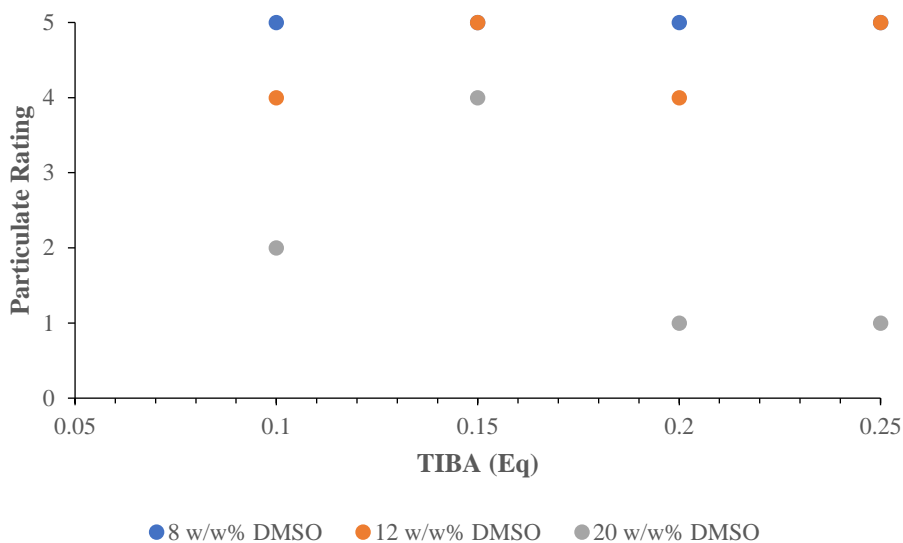


Figure 4.27 - Particulate ratings of liquid embolic prototypes of a range of DMSO concentrations and TIBA equivalents (n=3).

The molecular weight of PVA used in the preparation of the liquid embolic prototypes was not found to affect the fragmentation and particulate generation of the solidified materials (Figure 4.28 and Figure 4.29). There was no trend observed for the fragmentation or particulate rating across all the polymer molecular weights tested (31-130 kDa). The trend for prototypes prepared using a lower equivalents of TIBA exhibiting higher rates of fragmentation was consistent across all molecular weights tested.

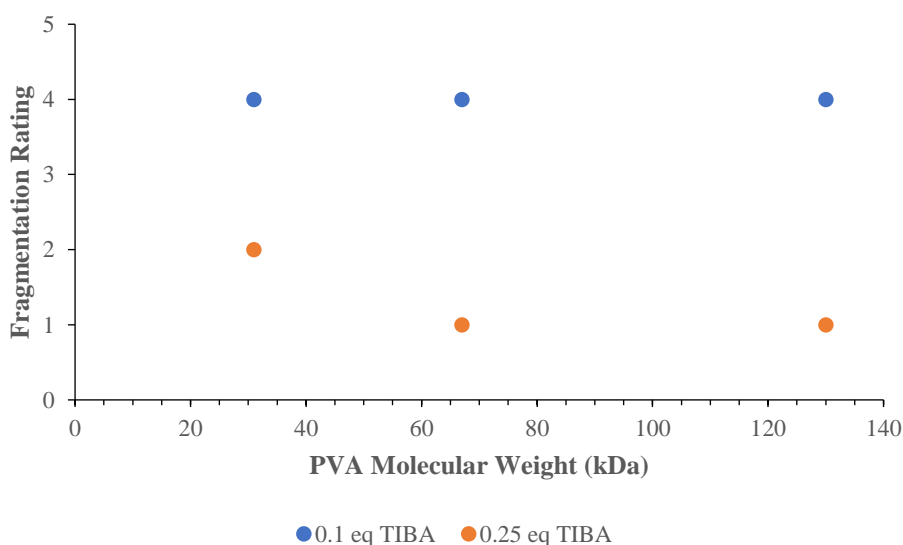


Figure 4.28 - Fragmentation ratings of liquid embolic prototypes of a range of polymer molecular weights at 0.1 and 0.25 equivalents of TIBA (n=3).

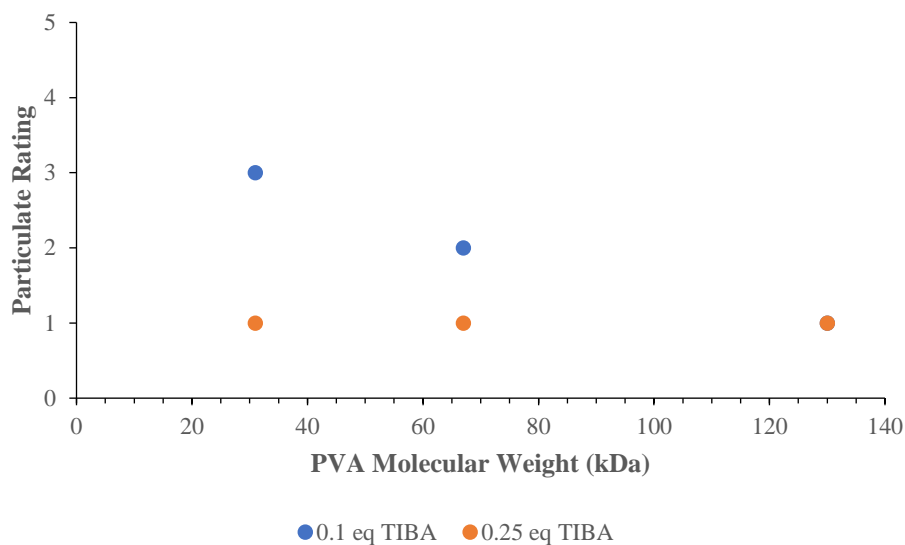


Figure 4.29 - Particulate ratings of liquid embolic prototypes of a range of polymer molecular weights at 0.1 and 0.25 equivalents of TIBA ( $n=3$ ).

The results of the fragmentation and particulate generation tests suggest that the molecular weight of the polymer used in the formulation could be changed in the range of 31-130 kDa without impacting on the risk of fragmentation and particulate generation. Formulations of higher concentrations in DMSO and at a higher equivalents of TIBA were found to be less likely to pose a risk of fragmentation and particulate generation once solidified within the vasculature. This correlates with the literature of electrospinning as uniform fibres are observed for polymers electrospun using higher polymer concentrations whereas lower polymer concentrations are associated with irregular shaped and sized particles formed.<sup>137</sup>

Determination of the fragmentation and particulate ratings of the currently used liquid embolic, Onyx<sup>®</sup> 18, under the same test method conditions suggest a current benchmark for fragmentation and particulate generation to be 4 and 2, respectively (

Table 4.25 and Table 4.26). Hence, an aim for new liquid embolic materials would be to exhibit similar or lower rates of particulate generation which has been determined for a number of the liquid embolic prototypes tested.

Table 4.25 - Fragmentation data for Onyx<sup>®</sup> 18 (n=3).

<b>Prototype</b>	<b>Highest Number of Fragments</b>	<b>Standard Error of Mean</b>	<b>Fragmentation Rating</b>
<b>Onyx<sup>®</sup> 18</b>	15	1	4

Table 4.26 - Particulate generation data for Onyx<sup>®</sup> 18 (n=3).

<b>Prototype</b>	<b>Highest Area Coverage by Particulates (%)</b>	<b>Standard Error of Mean</b>	<b>Particulate Rating</b>
<b>Onyx<sup>®</sup> 18</b>	2.80	0.15	2

#### ***4.3.10. Stability of Precipitate***

The retention of structural stability once the implanted material has solidified is important for allowing the delivered embolic to retain its position at the implantation site. Any shrinkage of the material over time could pose the risk of the embolic material becoming dislodged from its site and embolising off-target elsewhere within the body. A stability study therefore was carried out to monitor the solid content of the precipitated liquid embolic prototypes at 1 hour, 24 hours and 7 days after solidification (Table 4.27).

Table 4.27 - Solid content data for liquid embolic prototypes of different TIBA equivalents (n=3).

Prototype	TIBA (Eq to PVA Diol Groups)	Replicate	Timepoint (h)	Wet Weight (g)	Dry Weight (g)	Solid Content			
						Solid Content (%)	Mean (%)	Standard Error of Mean (%)	
1.3	0.1	1	1	0.353	0.119	33.8	33.6	0.1	
		2		0.336	0.113	33.6			
		3		0.229	0.076	33.3			
		1	24	1	0.150	0.042	27.7	32.3	1.9
		2		0.200	0.069	34.3			
		3		0.389	0.136	34.9			
		1	168	1	0.164	0.054	32.8	30.5	1.1
		2		0.222	0.068	30.6			
		3		0.385	0.108	28.2			
1.6	0.15	1	1	0.308	0.131	42.7	37.9	2.9	
		2		0.383	0.118	30.9			
		3		0.301	0.121	40.0			
		1	24	1	0.299	0.126	42.1	39.2	1.2
		2		0.348	0.133	38.1			
		3		0.312	0.117	37.5			
		1	168	1	0.390	0.121	31.1	35.8	2.4
		2		0.305	0.126	41.4			
		3		0.331	0.116	35.0			
1.9	0.2	1	1	0.382	0.158	41.5	43.4	2.3	
		2		0.369	0.147	39.8			
		3		0.257	0.126	49.0			
		1	24	1	0.413	0.231	56.0	51.5	2.8
		2		0.418	0.224	53.7			
		3		0.218	0.098	44.8			
		1	168	1	0.339	0.171	50.4	50.9	0.7
		2		0.289	0.143	49.6			
		3		0.355	0.186	52.5			
1.12	0.25	1	1	0.116	0.064	54.7	44.7	4.3	
		2		0.517	0.189	36.5			
		3		0.302	0.130	42.9			
		1	24	1	0.223	0.099	44.4	39.2	2.3
		2		0.364	0.126	34.5			
		3		0.343	0.132	38.5			
		1	168	1	0.279	0.105	37.7	37.6	1.4
		2		0.339	0.138	40.6			
		3		0.403	0.139	34.5			



Liquid embolic prototypes prepared using higher equivalents of TIBA to PVA diol groups were found to have higher solid contents across all the timepoints measured (Figure 4.30). This is likely to be due to the higher incorporation of the hydrophobic TIBA group giving rise to further solidification of the materials in the presence of aqueous PBS conditions.

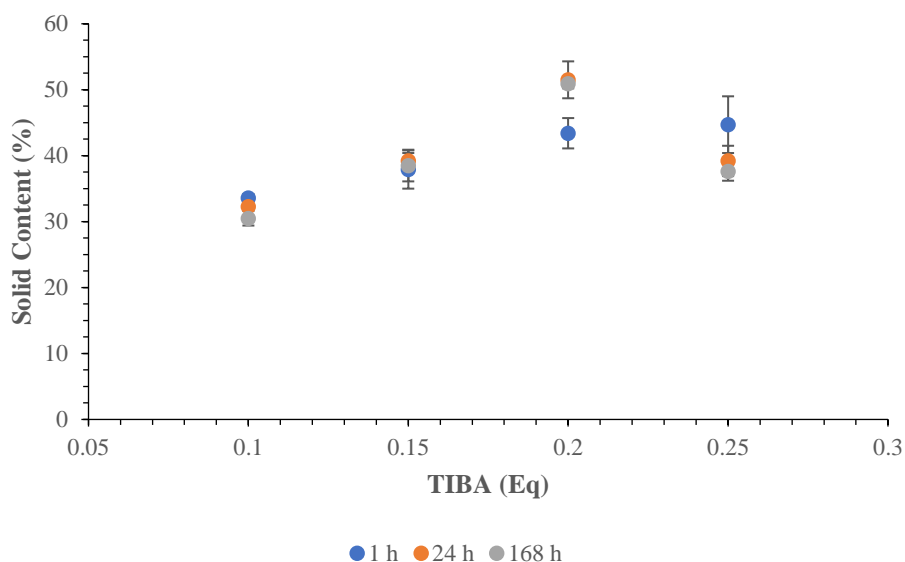


Figure 4.30 - Solid content results for liquid embolic prototypes of different TIBA equivalents ( $n=3$ ).

There was found to be a slight decrease in the solid content of the samples over the test time monitored (Figure 4.31). This could be due to further elution of DMSO from the precipitated samples over time in PBS. This suggests a potential for structural changes over time but would need to be tested against any changes in volume to confirm whether a reduction in solid content of the materials would result in any volume shrinkage. This would require further tests to be taken over a longer timeframe.

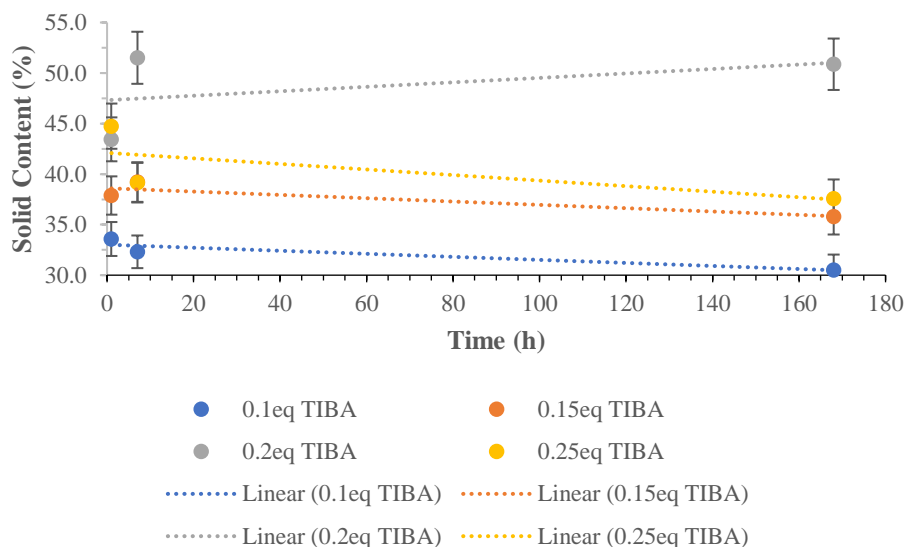


Figure 4.31 - Solid content results over time of liquid embolic prototypes over a range of TIBA equivalents ( $n=3$ ).

#### 4.3.11. Biocompatibility

The radiopaque polymer composition similar to those used in the liquid embolic prototype formulations have already been deemed biocompatible as determined in cytotoxicity tests outlined in the literature.<sup>34,116</sup> The synthesised radiopaque polymer was formulated as a solution in DMSO as the solvent has been shown to be safe for injection provided it is carried out at a slow controlled rate in order to prevent vasospasms of the blood vessels being treated.<sup>74</sup>

In order to ensure the biocompatibility of the liquid embolic prototypes, the samples must be analysed to ensure removal of any potentially toxic small molecule starting materials. This includes the TIBA starting material used as the binding group to impart radiopacity to PVA. Proton NMR spectroscopy was used to confirm the removal of any unreacted TIBA following the purification of the modified polymers (Table 4.28).

Table 4.28 - Residual reactant traces as determined from  $^1\text{H}$  NMR spectra of liquid embolic prototypes ( $n=1$ ).

Prototype	TIBA (Eq to PVA Diol Groups)	PVA Molecular Weight (kDa)	Concentration in DMSO (w/w%)	Residual Traces of TIBA Reactant Detected
<b>1.1</b>	0.1	67	8	
<b>1.2</b>	0.1	67	12	None
<b>1.3</b>	0.1	67	20	
<b>1.4</b>	0.15	67	8	
<b>1.5</b>	0.15	67	12	None
<b>1.6</b>	0.15	67	20	
<b>1.7</b>	0.20	67	8	
<b>1.8</b>	0.20	67	12	None
<b>1.9</b>	0.20	67	20	
<b>1.10</b>	0.25	67	8	
<b>1.11</b>	0.25	67	12	None
<b>1.12</b>	0.25	67	20	
<b>1.13</b>	0.1	31	20	None
<b>1.14</b>	0.1	130	20	None
<b>1.15</b>	0.25	31	20	None
<b>1.16</b>	0.25	130	20	None

In order to ensure the retention of polymer chain length throughout the processing of the liquid embolic samples, size exclusion chromatography was carried out (Table 4.29). The results of the determined number average molecular weights indicate the retention of the polymer structures with no observed fragmentation of the polymers as indicated by the smooth bell curves observed.

Table 4.29 - Results of molecular weights determined by SEC for liquid embolic prototypes ( $n=1$ ).

Prototype	TIBA (Eq to PVA Diol Groups)	PVA Molecular Weight (kDa)	Concentration in DMSO (w/w%)	Number Average Molecular Weight (kDa)	Dispersity
1.1	0.1	67	8		
1.2	0.1	67	12	107	2.22
1.3	0.1	67	20		
1.4	0.15	67	8		
1.5	0.15	67	12	97.4	2.08
1.6	0.15	67	20		
1.7	0.2	67	8		
1.8	0.2	67	12	88.5	2.33
1.9	0.2	67	20		
1.1	0.25	67	8		
1.11	0.25	67	12	76.1	2.33
1.12	0.25	67	20		
1.13	0.1	31	20	35.8	2.16
1.14	0.1	130	20	111	2.09
1.15	0.25	31	20	40.8	2.01
1.16	0.25	130	20	121	2.28

Overall the chemical analysis of the liquid embolics outlined here suggests suitability for injection into the body due to the absence of toxic starting materials and low molecular weight polymer fragments. Due to this it is theorised that the liquid embolic prototypes are unlikely to cause toxicity effects if injected *in vivo*.

#### 4.3.12. Radiopacity

Sample analysis by microCT was used to determine the radiopacity of the various radiopaque liquid embolic formulations. The samples were prepared for microCT by manually injecting the liquid solutions into narrow bore tubing (1.67 mm internal diameter) and allowing 0.1 mL of each sample to solidify under PBS flow (30-40 mL min<sup>-1</sup>). The scan method and reconstruction parameters developed in Chapter 3 were used and the radiopacity calculated against the hydroxyapatite controls (Table 4.30 and Table 4.31). It must be noted that, due to the high associated standard deviations with the radiopacity measurements, the determined

radiopacities may not be the true value for the precipitated materials but instead can offer a gauge of any trends between different formulations.

*Table 4.30 - MicroCT data for I-PVA samples over a range of TIBA equivalents and DMSO concentrations synthesised using 67 kDa PVA (imaging cross-sections, n=198).*

Sample	TIBA (Eq to PVA Diol Groups)	Concentration in DMSO (w/w%)	Radiopacity (HU)	Standard Deviation (HU)
1.1	0.1	8	715	417
1.2	0.1	12	512	357
1.3	0.1	20	777	416
1.4	0.15	8	817	513
1.5	0.15	12	1200	556
1.6	0.15	20	2434	905
1.7	0.2	8	1827	816
1.8	0.2	12	2096	926
1.9	0.2	20	2776	1058
1.10	0.25	8	1925	828
1.11	0.25	12	2037	941
1.12	0.25	20	3267	1085

*Table 4.31 - MicroCT data for I-PVA samples over a range of polymer molecular weights at 0.1 and 0.25 equivalents of TIBA (imaging cross-sections, n=198).*

Sample	TIBA (Eq to PVA Diol Groups)	PVA Molecular Weight (kDa)	Radiopacity (HU)	Standard Deviation (HU)
1.13	0.1	31	1783	867
1.3	0.1	67	777	416
1.14	0.1	130	2013	1020
1.15	0.25	31	3921	1377
1.12	0.25	67	3267	1085
1.16	0.25	130	3077	1012

Formulations with higher equivalents of TIBA to PVA diol groups were found to have higher radiopacities (Figure 4.32). This is as expected due to the increased incorporation of iodine, the element imparting a high radiodensity to the material, with higher equivalents of TIBA grafted onto the PVA polymer backbone. Higher radiopacities were also found to be associated with formulations delivered as more concentrated solutions in DMSO.

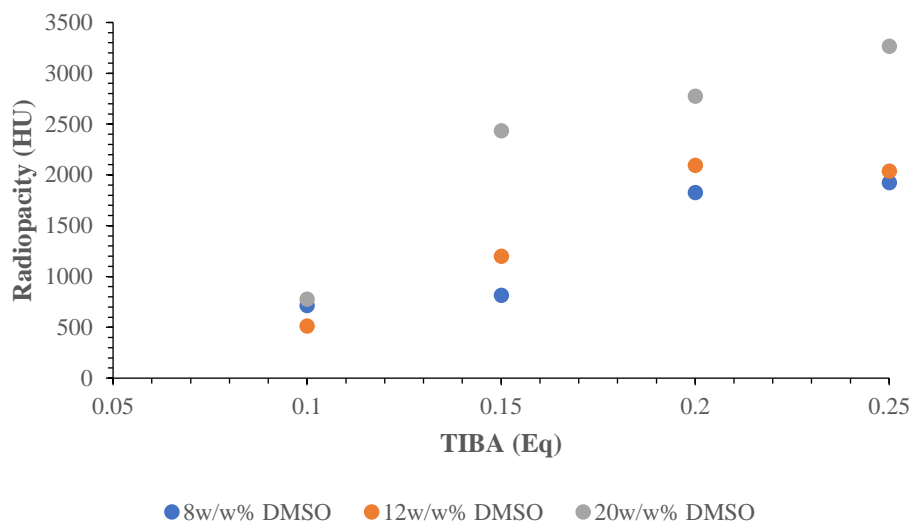


Figure 4.32 - MicroCT results for I-PVA samples over a range of TIBA equivalents and DMSO concentrations synthesised using 67 kDa PVA (imaging cross-sections, n=198).

There was found to be no trend in the radiopacity for the polymer molecular weight used for the preparation of the liquid embolic prototypes (Figure 4.33). There was variation in the radiopacity measurements but this was not found to be statistically different due to the high standard deviations associated with the measurements. These variations are likely to be due to the manual preparation of the samples and variation across individual samples as was found in the microCT method development outlined in Chapter 3.

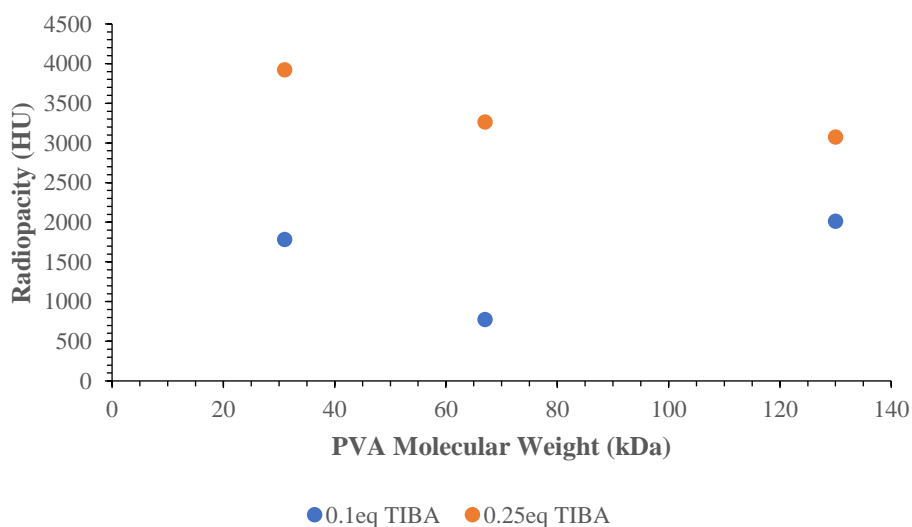


Figure 4.33 - MicroCT results for I-PVA samples over a range of polymer molecular weights at 0.1 and 0.25 equivalents of TIBA (imaging cross-sections, n=198).

Appropriate radiopacity of the liquid embolic prototypes is vital in the visualisation of the materials once implanted within the body. In order to gauge whether the developed prototypes were of sufficient radiopacity to be visualised, such as by CT imaging, when implanted *in vivo*, the radiopacity of a commercially used contrast agent was measured by the same microCT method used for the sample analysis. The contrast agent Histodenz, marketed as Omnipaque™, was prepared over a range of concentrations increasing in 60 mg mL<sup>-1</sup> of iodine increments starting from 0 mg mL<sup>-1</sup> iodine (water blank) to 300 mg mL<sup>-1</sup> iodine. The higher iodine concentrations tested of 180, 240 and 300 mg mL<sup>-1</sup> are representative of the contrast agent formulations used in medical imaging of Omnipaque™ 180, 240 and 300, respectively (Figure 4.34).<sup>138</sup>

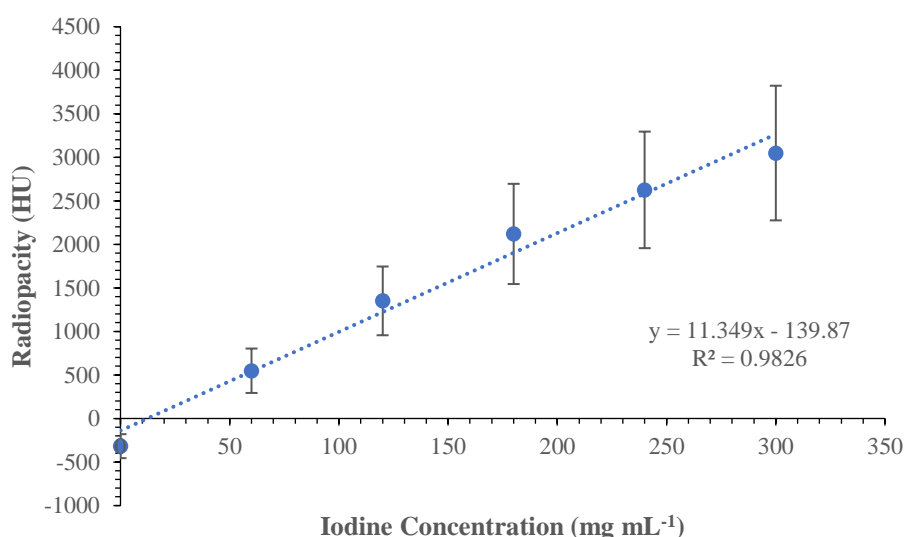


Figure 4.34 - Measured radiopacity of Histodenz controls (imaging cross-sections,  $n=198$ ).

Histodenz is frequently used as the Omnipaque™ formulations of 180, 240 and 300 mg mL<sup>-1</sup>,<sup>139</sup> hence it can be assumed that a radiopacity of 2120 HU (corresponding to 180 mg mL<sup>-1</sup>) or higher is sufficiently radio-dense to be visualised *in vivo* by CT imaging. Comparing the radiopacity measurements of the liquid embolic prototypes in their solidified states shows the samples delivered as 20 w/w% solutions in DMSO are generally of radiopacity higher than 2120 HU across the TIBA equivalents tested (Table 4.32). Therefore, it is predicted that if an I-PVA formulation of 20 w/w% in DMSO was injected into the vasculature it would be of

optimal radiodensity to be easily visualised by conventional CT imaging once solidified within the vasculature.

Table 4.32 - Comparison of radiopacity values of liquid embolic prototypes against Omnipaque™ 180 (imaging cross-sections, n=198).

Prototype	TIBA (Eq to PVA Diol Groups)	PVA Molecular Weight (kDa)	Concentration in DMSO (w/w%)	Mean Radiopacity (HU)	Sufficient Radiopacity?
1.1	0.1	67	8	715	No
1.2	0.1	67	12	512	No
1.3	0.1	67	20	777	No
1.4	0.15	67	8	817	No
1.5	0.15	67	12	1200	No
1.6	0.15	67	20	2434	Yes
1.7	0.2	67	8	1827	No
1.8	0.2	67	12	2096	Yes
1.9	0.2	67	20	2776	Yes
1.10	0.25	67	8	1925	No
1.11	0.25	67	12	2037	No
1.12	0.25	67	20	3267	Yes
1.13	0.1	31	20	1783	No
1.14	0.1	130	20	2013	Yes
1.15	0.25	31	20	3921	Yes
1.16	0.25	130	20	3077	Yes

Comparison of the I-PVA radiopacity measurements to Onyx® 18 indicate that I-PVA liquid embolic prototypes are much less radiopaque than Onyx® 18 (Figure 4.35 and Table 4.33). This avoids the issues of streak artefact observed with Onyx® delivery, which hinders diagnostic imaging particularly in follow-up scans. Therefore, the I-PVA formulations of 20 w/w% in DMSO appear to be of optimal radiopacity for visualisation but not of a radiopacity high enough to cause streak artefact. This makes the I-PVA formulation an ideal candidate as a radiopaque liquid embolic with respect to its radiopacity following precipitation.



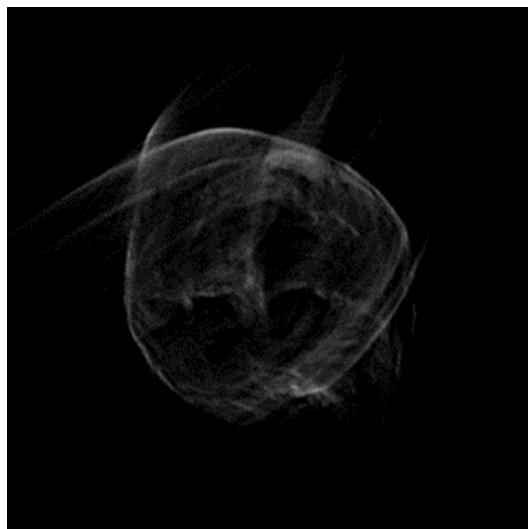


Figure 4.35 - Reconstructed 2D cross section of Onyx<sup>®</sup> sample.

Table 4.33 - Radiopacity data of solidified Onyx<sup>®</sup> (imaging cross-sections, n=198).

Sample	Radiopacity (HU)	Standard Deviation (HU)
Onyx <sup>®</sup> 18	27411	9146

#### 4.3.13. Porosity

There is no specification for porosity for a solidified liquid embolic material. However, a material which solidifies with a degree porosity is likely to have potential for compression. Compressibility is beneficial for the long-term implantation of an embolic material as it allows for the movement of the vasculature whilst still maintaining the implanted position. Compression testing was trialled using a Lloyd PF Plus Compression and Tension Testing Machine but due to the small size of the precipitates, results varied greatly between precipitates of the same liquid embolic prototype. Hence, the likelihood towards compressibility was instead inferred from the porosity of the precipitated samples as calculated from samples scanned by microCT. The porosity of the scanned liquid embolic prototypes was calculated over a section of the material precipitated within tubing with a height of 1 mm and diameter of 1.6 mm (Table 4.34 and Table 4.35).

Table 4.34 - Porosity data for I-PVA samples over a range of TIBA equivalents and DMSO concentrations synthesised using 67 kDa PVA (imaging cross-sections, n=198).

Prototype	TIBA (Eq to PVA Diol Groups)	Concentration in DMSO (w/w%)	Porosity (%)
1.1	0.1	8	56.9
1.2	0.1	12	51.6
1.3	0.1	20	58.5
1.4	0.15	8	52.1
1.5	0.15	12	53.6
1.6	0.15	20	63.2
1.7	0.2	8	53.3
1.8	0.2	12	62.3
1.9	0.2	20	54.3
1.10	0.25	8	79.8
1.11	0.25	12	74.0
1.12	0.25	20	74.0

Table 4.35 - Porosity data for I-PVA samples over a range of polymer molecular weights at 0.1 and 0.25 equivalents of TIBA (imaging cross-sections, n=198).

Prototype	TIBA (Eq to PVA Diol Groups)	PVA Molecular Weight (kDa)	Porosity (%)
1.13	0.1	31	19.0
1.3	0.1	67	58.5
1.14	0.1	130	30.8
1.15	0.25	31	22.5
1.12	0.25	67	74.0
1.16	0.25	130	36.8

There was found to be a slight trend for increasing porosity as the TIBA content of the liquid embolic formulation increased, particularly at the higher TIBA equivalents used of 0.25 (Figure 4.36). This suggests more distinct regions are formed for higher TIBA equivalents samples with regions of polymer and pores in the network. No correlation was observed between the concentration of the sample in DMSO used to prepare the microCT samples and the calculated porosity of the precipitated samples.

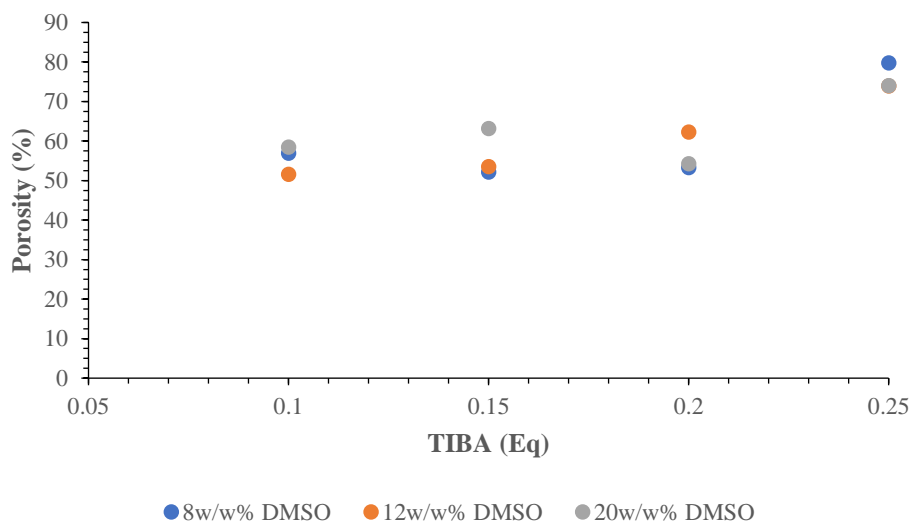


Figure 4.36 - Porosity results for I-PVA samples over a range of TIBA equivalents and DMSO concentrations synthesised using 67 kDa PVA (imaging cross-sections,  $n=198$ ).

Investigation of the porosity for liquid embolic prototypes of 0.1 and 0.25 equivalents of TIBA over a range of polymer molecular weights confirmed the trends observed previously for samples of higher TIBA equivalents resulting in higher porosity which was consistent across all the polymer molecular weights tested (Figure 4.37). No trend in porosity was found for an increasing molecular weight across the range tested (31-130 kDa). Instead the highest porosity observed was for the median molecular weight of 67 kDa for both TIBA equivalents tested.

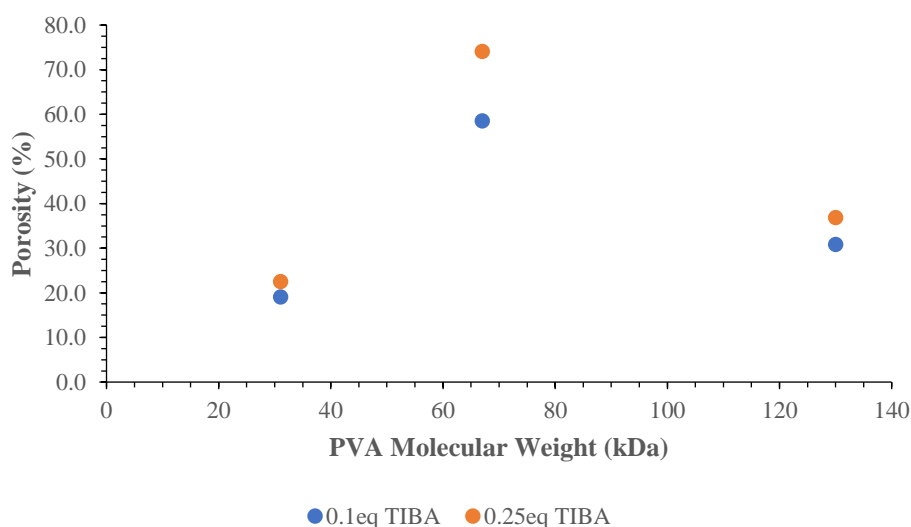


Figure 4.37 - Porosity results for I-PVA samples over a range of polymer molecular weights at 0.1 and 0.25 equivalents of TIBA (imaging cross-sections,  $n=198$ ).

The measurement of sample porosity by this method provided a useful insight into the trends between liquid embolic prototypes and information into how the materials precipitate to form a porous mass. These porosity values provided an indication into potential towards compression but do not explicitly provide data towards compressibility. There is also likely to be a large variation of porosity across the entire length of the precipitated liquid embolic material as established in Chapter 3. Hence, the values provided here are a snapshot of porosity at a short section of the precipitated sample and do not represent the entire length of precipitated material. Also, as was observed in Chapter 3, the injection method used to prepare the microCT samples was found to impact the calculated radiopacity. The manual injection method used to prepare the samples during this test was therefore likely to have introduced variation into the porosity measurements. Thus, the porosity measurements given here simply indicate any trends between different liquid embolic prototypes.

The porosity of Onyx<sup>®</sup> 18 was also determined by the same method used for the liquid embolic prototypes (Table 4.36). The calculated porosity of 76.9% demonstrated Onyx<sup>®</sup> 18 to have a high internal porosity of a similar value to a number of the liquid embolic prototypes. This highlights the similarities in the solidification process of Onyx<sup>®</sup> and the I-PVA liquid embolic prototypes with their precipitation to form structures with a degree of internal porosity.

*Table 4.36 - Porosity data of Onyx<sup>®</sup> 18 and Onyx<sup>®</sup> 34 (imaging cross-sections, n=198).*

<b>Sample</b>	<b>Porosity (%)</b>
<b>Onyx<sup>®</sup> 18</b>	76.9

#### **4.4. Conclusions**

This chapter has highlighted the potential for an iodinated polymer formulated as a solution in DMSO to demonstrate suitable properties as a liquid embolic agent. During the I-PVA synthesis it was found that the iodination levels of the produced polymers could be easily controlled by varying the concentration of TIBA used during the grafting reaction. The incorporation of increasing amounts of the radiopaque group precursor was observed to have

a dramatic effect on the polymer's water solubility. This was attributed to the hydrophobic effect of the iodinated aromatic ring greatly reducing the I-PVA samples affinity for water allowing phase inversion of the polymer on contact with an aqueous environment.

The number of equivalents of TIBA used during the synthesis of the liquid embolic prototypes was found to impact multiple properties including the solidification times, rheologic properties and imageability under X-ray. The concentration of the radiopaque polymer formulated in DMSO was also found to greatly influence the liquid embolic properties measured. Conversely, variation of the polymer molecular weight used in the liquid embolic formulations was found to have minimal impact on the behaviour of the materials during the characterisation tests perform. The results of the characterisation tests discussed in this chapter show how the performance of the liquid embolic materials can be tuned by controlling various parameters, in particular radiopaque group content and concentration in the DMSO carrier solvent. Due to the demonstration of suitable properties for a radiopaque liquid embolic material, the data discussed here has formed the basis of a patent application filed by Biocompatibles UK Ltd. entitled "Radiopaque Polymers" (filed 2018-06-29, GB201810784).

## **Chapter Five**

### **5. Synthesis and Characterisation of a Precipitating Liquid Embolic with Alternative Radiopaque Groups**

## 5.1. Introduction

In Chapter 4, the formulation of PVA modified with the radiopaque group TIBA as delivered in a solution of DMSO was demonstrated to possess suitable properties as a potential precipitating liquid embolic agent. In order to further modify the properties of the liquid embolic material allowing tailoring to the varying types of embolisation treatments, formulations were prepared using varying ratios of alternative radiopaque groups in combination with TIBA to observe the impact of changing the precipitating materials hydrophobicity on the liquid embolic properties including the delivery and precipitate properties.

The first alternative radiopaque group chosen was 3-(2,4,6-triiodo-5-formylphenoxy)-1-propanesulfonic acid (S-TIBA). This group was selected for its ability to impart the same level of iodination as TIBA due to the tri-iodination of the aromatic ring whilst also having a degree of hydrophilicity due to the pendent sulfonic acid group. The sulfonic acid end-group also enables the polymer to behave as a polyanion due to the negative ionic charge imparted. This allows chelation of the ionic end-group with cations presence in PBS thereby further influencing the solidification behaviour.

The second radiopaque group chosen was 3-iodobenzaldehyde (IBA) which has a lower degree of hydrophobicity than TIBA due the mono-iodination of the aromatic ring rather than tri-iodination. As a result of the lower iodination of the aromatic group, IBA is unable able to impart the same level of radiopacity as TIBA so needs to be used in combination with TIBA in order to retain sufficient radiopacity. The chosen radiopaque groups allow insight into the effects of using TIBA in combination with varying ratios of the more hydrophilic group of S-TIBA and the less hydrophobic group of IBA (Figure 5.1).

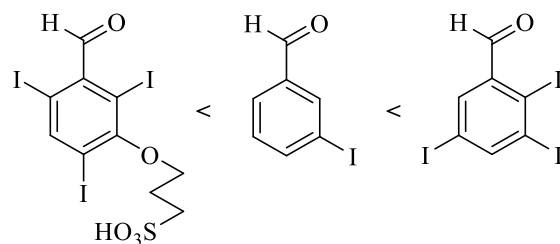


Figure 5.1 - Hydrophobicity difference of S-TIBA, IBA and TIBA.

The liquid embolic prototypes were prepared over a range of ratios of S-TIBA:TIBA and IBA:TIBA all targeting the same total equivalents of 20% of the PVA diol groups modified. The synthesised radiopaque polymers were formulated in DMSO as 20 w/w% solutions and characterised using the developed test methods outlined in Chapters 2 and 3.

## 5.2. Experimental

The following chemicals were used as supplied from their manufacturers; anhydrous DMSO (99.7%) from Acros Organics, 3-hydroxy-triiodobenzaldehyde (99%) from Biocompatibles UK Ltd., 3-iodobenzaldehyde (98%) from Alfa Aesar, methanesulfonic acid ( $\geq 99.0\%$ ) from Sigma Aldrich, Mowiol<sup>®</sup> 8-88 ( $\sim 67,000 \text{ g mol}^{-1}$ , 86.7-88.7 mol% hydrolysis) from Sigma Aldrich, potassium *tert*-butoxide (97%) from Alfa Aesar, 1,3-propanesultone (99%) from Alfa Aesar and 2,3,5-triiodobenzaldehyde (99.5%) from Aldlab. The removal of solvent was carried out under reduced pressure using a rotary evaporator.  $^1\text{H}$  and  $^{13}\text{C}$  NMR spectra were recorded at 400 MHz on a Bruker Avance III HD 400 instrument and measured coupling constants were stated in Hz to the nearest decimal place. NMR splitting abbreviations used; s = singlet, d = doublet, t = triplet, q = quartet, quin. = quintet, m = multiplet. Electrospray mass spectrometry was recorded on a Water LCT instrument.



### 5.2.1. Synthesis of *S-TIBA*

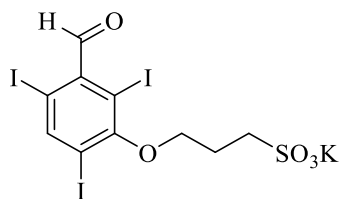


Figure 5.2 - 3-(2,4,6-triiodo-5-formylphenoxy)-1-propanesulfonic acid (*S-TIBA*).

3-hydroxy-triiodobenzaldehyde (10.0 g, 20.0 mmol) was dissolved in THF (5 mL) with magnetic stirring at 300 rpm at room temperature. A suspension of potassium *tert*-butoxide (2.4 g, 21.4 mmol) in THF (20 mL) was degassed for 10 minutes and then slowly added to the 3-hydroxy-triiodobenzaldehyde solution with constant stirring. The reaction mixture was heated to 40 °C and a solution of 1,3-propanesultone (15.0 g, 123 mmol) dissolved in THF (15 mL) was slowly added resulting in precipitation. The reaction was stirred for 3 hours at 40 °C under N<sub>2</sub> flow. The reaction mixture was then poured into ethyl acetate (500 mL) and the precipitated product collected then washed with further ethyl acetate (100 mL). The product was recrystallised from ethanol and dried in a vacuum oven with no heating. Yield = 63%; found C 18.28%, H 2.02%, S 6.12%, I 41.5%, C<sub>10</sub>H<sub>9</sub>I<sub>3</sub>O<sub>5</sub>S; FT-IR  $\nu$  cm<sup>-1</sup> 2851 and 2738 (C-H, aldehyde), 1734 (C=O, aldehyde), 1687 (C=C, aromatic), 1184 (C-O, ether), 1044 (S=O, sulfoxide), 613 (C-I, iodide);  $\delta_{\text{H}}$  (400 MHz, d-DMSO) 2.67 (2H, quin., *J* 6.4, CH<sub>2</sub>), 3.42 (2H, t, *J* 6.4, CH<sub>2</sub>), 3.96 (2H, t, *J* 6.4, CH<sub>2</sub>), 8.46 (1H, s, ArCH), 9.58 (1H, s, COH);  $\delta_{\text{C}}$  (400 MHz, d-DMSO) 26.5 (CH<sub>2</sub>), 49.0 (CH<sub>2</sub>), 60.9 (CH<sub>2</sub>SO<sub>3</sub>H), 91.6 (ArCI), 96.5 (ArCI), 98.9 (ArCI), 140.5 (ArCH), 150.0 (ArC), 159.0 (ArCO), 196.8 (CHO); *m/z* (ES) 621 (54%, M<sup>+</sup>); mp 256 °C.

### 5.2.2. Modification of PVA with S-TIBA and TIBA

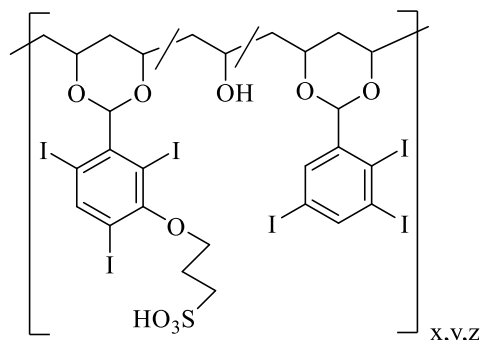


Figure 5.3 - PVA modified with S-TIBA and TIBA.

Mowiol® 8-88 (2 g) was dissolved in anhydrous DMSO (50 mL) and stirred at 350 rpm for 2 hours at  $50 \pm 9$  °C with  $N_2$  flow in a round bottom flask (Table 5.1). A solution of 2,3,5-triodobenzaldehyde (0.55-1.65 g, 1.1-3.4 mmol) in anhydrous DMSO (10 mL) was degassed for 10 minutes and then added dropwise to the PVA solution. This was immediately followed by the dropwise addition of a degassed solution of 3-(2,4,6-triiodo-5-formylphenoxy)-1-propanesulfonic acid (0.71-2.82 g, 1.1-4.5 mmol) in anhydrous DMSO (10 mL). After 5 minutes, methane sulfonic acid (4.4 mL, 6.52 g, 68 mmol) was added dropwise and the reaction mixture stirred at  $50 \pm 9$  °C for 24 hours. Once cooled to room temperature, the polymer was precipitated twice into THF ( $2 \times 500$  mL) and the collected precipitate washed with further THF (30 mL). The product was collected by centrifugation and then dried in a vacuum oven at 40 °C. Yield = 85-98%;  $\delta_H$  (400 MHz, d-DMSO) 1.24-1.54 (m), 1.94-1.99 (m), 3.76-3.94 (m), 4.17-4.24 (m), 4.43-4.49 (m), 4.64-4.69 (m), 7.69-7.72 (s broad, aromatic), 8.26-8.29 (s broad, aromatic), 8.31-8.34 (s broad, aromatic).

Table 5.1 - Reaction quantities used in the modification of PVA with S-TIBA and TIBA.

TIBA (Eq to PVA Diol Groups)	Mass of TIBA (g)	Moles of TIBA (mmol)	S-TIBA (Eq to PVA Diol Groups)	Mass of S-TIBA (g)	Moles of S-TIBA (mmol)	Yield (%)
<b>0.15</b>	1.65	3.4	<b>0.05</b>	0.71	1.1	92
<b>0.10</b>	1.10	2.3	<b>0.10</b>	1.41	2.3	85
<b>0.05</b>	0.55	1.1	<b>0.15</b>	2.12	3.4	97
-	-	-	<b>0.20</b>	2.82	4.5	98

### 5.2.3. Modification of PVA with IBA and TIBA

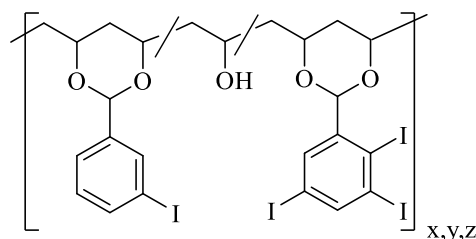


Figure 5.4 - PVA modified with IBA and TIBA.

Mowiol® 8-88 (6 g) was dissolved in anhydrous DMSO (180 mL) and mechanically stirred at 350 rpm for 2 hours at  $50 \pm 9$  °C with N<sub>2</sub> flow in a flat flange reaction vessel (Table 5.2). A solution of 2,3,5-triiodobenzaldehyde (1.65-4.94 g, 3.4-10.2 mmol) in anhydrous DMSO (15 mL) was degassed for 10 minutes and then added dropwise to the PVA solution. This was immediately followed by the dropwise addition of a degassed solution of 3-iodobenzaldehyde (0.79-2.37 g, 3.4-10.2 mmol) in anhydrous DMSO (15 mL). After 5 minutes, methane sulfonic acid (13.2 mL, 19.6 g, 203 mmol) was added dropwise and the reaction mixture stirred at  $50 \pm 9$  °C for 24 hours. Once cooled to room temperature, the polymer was precipitated twice into THF (2 × 750 mL) and the collected precipitate washed with further THF (50 mL). The product was collected by centrifugation and then dried in a vacuum oven at 40 °C. Yield = 88-93%;  $\delta_H$  (400 MHz, d-DMSO) 1.22-1.66 (m), 1.91-1.99 (m), 3.32-3.36 (m), 3.99-4.09 (m), 4.19-4.24 (m), 4.36-4.40 (m), 4.65-4.70 (m), 5.45-5.50 (m), 7.15-7.21 (s broad, aromatic), 7.40-7.46 (s broad, aromatic), 7.67-7.77 (s broad, aromatic), 8.26-8.29 (s broad, aromatic).

Table 5.2 - Reaction quantities used in the modification of PVA with IBA and TIBA.

TIBA (Eq to PVA Diol Groups)	Mass of TIBA (g)	Moles of TIBA (mmol)	IBA (Eq to PVA Diol Groups)	Mass of IBA (g)	Moles of IBA (mmol)	Yield (%)
0.15	4.94	10.2	0.05	0.79	3.4	88
0.10	3.29	6.8	0.10	1.58	6.8	93
0.05	1.65	3.4	0.15	2.37	10.2	89
-	-	-	0.20	3.16	13.6	89

### 5.2.4. Formulation as Solutions in DMSO

The synthesised radiopaque polymer samples were formulated as 20 w/w% solutions in DMSO for characterisation testing as liquid embolic materials (Table 5.3).

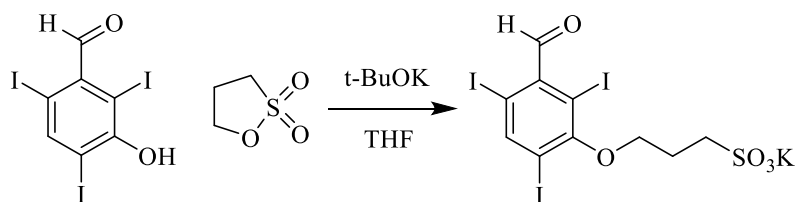
Table 5.3 - Formulations of liquid embolic prototypes modified with combinations of S-TIBA, IBA and TIBA.

Prototype	TIBA (Eq to PVA Diol Groups)	S-TIBA (Eq to PVA Diol Group)	IBA (Eq to PVA Diol Groups)	PVA Molecular Weight (kDa)	Concentration in DMSO (w/w%)
1.9	0.20	-	-	67	20
2.1	0.15	0.05	-	67	20
2.2	0.10	0.10	-	67	20
2.3	0.05	0.15	-	67	20
2.4	-	0.20	-	67	20
2.5	0.15	-	0.05	67	20
2.6	0.10	-	0.10	67	20
2.7	0.05	-	0.15	67	20
2.8	-	-	0.2	67	20

## 5.3. Results and Discussion

### 5.3.1. Iodinated PVA in Combination S-TIBA

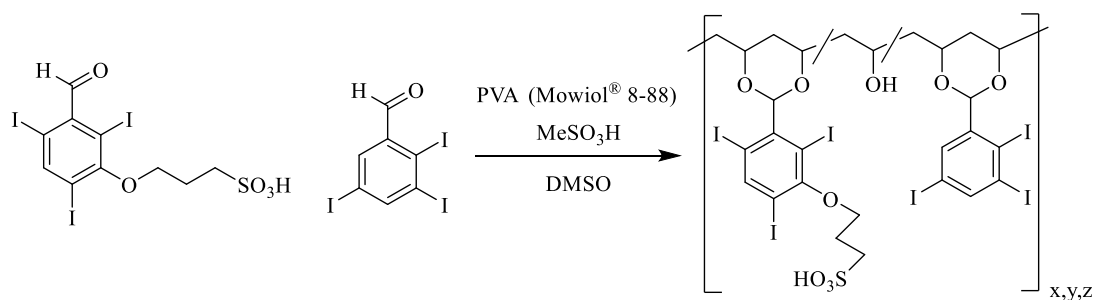
S-TIBA was prepared from 3-hydroxy-triiodobenzaldehyde by initial deprotonation of the hydroxyl group using potassium *tert*-butoxide followed by reaction with 1,3-propanesultone to impart the pendent sulfonic acid group (Scheme 5.1). Recrystallisation of the product from ethanol gave the purified product with a yield of 66%.



Scheme 5.1 - Synthesis of 3-(2,4,6-triiodo-5-formylphenoxy)-1-propanesulfonic acid (S-TIBA).

The product was then used in combination with TIBA in the modification of PVA at a polymer molecular weight of 67 kDa. This was performed by a one-pot acid catalysed acetalisation reaction using varying ratios of S-TIBA and TIBA targeting a total modification of 0.2 equivalents of PVA diol groups (i.e. 20% of diol groups modified with a radiopaque group) (Scheme 5.2). The liquid embolic prototype 1.9 synthesised in Chapter 4 was used as a

comparison for PVA modified with 100% TIBA at 0.2 equivalents. Following purification of the modified polymers by precipitation into an anti-solvent, the polymers were analysed by  $^1\text{H}$  NMR spectroscopy analysis and elemental analysis. The obtained polymers were then formulated in DMSO at 20 w/w%.



*Scheme 5.2 - Modification of PVA with varying ratios of S-TIBA and TIBA.*

The results of elemental analysis confirm the binding of the radiopaque groups used in the acetalisation reaction (

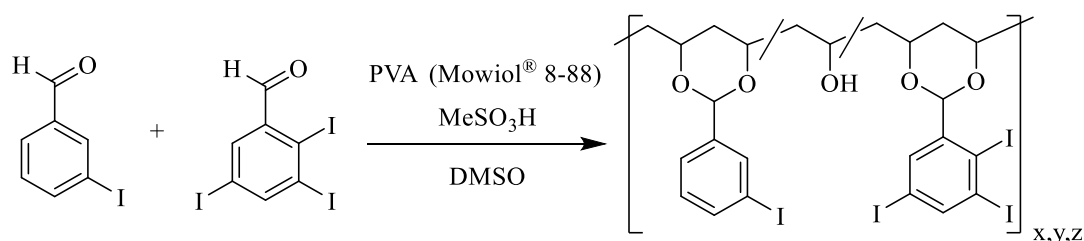
Table 5.4). However, there are large discrepancies between the theoretical iodine content targeted and the actual iodine content measured of the prototypes. Lower iodine contents than expected are likely due to remaining solvent within the precipitated samples, as was noted by  $^1\text{H}$  NMR spectroscopy, despite extended drying periods in a vacuum oven prior to elemental analysis. The lower iodine contents attained may also be an indicator of incomplete binding of the TIBA and S-TIBA groups during the reaction thereby resulting in the reduced iodine contents. The close agreement of targeted and measured iodine content for the prototype 1.9 synthesised using TIBA alone suggests incomplete binding is more likely of the S-TIBA group than TIBA. Prototype 2.1 was observed to have a higher iodine content than expected by 5.7%, this was due to a mis-calculation in the addition of S-TIBA in the reaction.

Table 5.4 - Liquid embolic samples synthesised using S-TIBA and TIBA theoretical and determined iodine contents by elemental analysis (n=2).

Prototype	TIBA (Eq to PVA Diol Groups)	S-TIBA (Eq to PVA Diol Groups)	Targeted Iodine Content (%)	Iodine Content by Elemental Analysis (%)
1.9	0.2	-	42.0	41.7
2.1	0.15	0.05	39.5	45.2
2.2	0.10	0.10	39.0	31.8
2.3	0.05	0.15	36.9	28.8
2.4	-	0.20	36.5	24.0

### 5.3.2. Iodinated PVA in Combination with IBA

PVA with a molecular weight of 67 kDa was modified using varying ratios of IBA and TIBA targeting a total equivalents of 0.2 of the PVA diol groups modified. The modification of PVA was carried out using a one-pot reaction acid catalysed acetalisation reaction with controlled amounts of IBA and TIBA in DMSO at 50 °C to target varying ratios of the radiopaque group combinations (Scheme 5.3). The modified polymers were purified by precipitation into an anti-solvent then isolated and dried prior to analysis by <sup>1</sup>H NMR spectroscopy analysis and elemental analysis. The purified polymers were then formulated as 20 w/w% solutions in DMSO for testing as liquid embolic materials.



Scheme 5.3 - Modification of PVA with varying ratios of IBA and TIBA.

Modification of PVA with the radiopaque groups TIBA and IBA was confirmed by elemental analysis of the prototypes (Table 5.5). The small discrepancies between the targeted and measured iodine contents suggests a high efficiency for binding of the radiopaque groups during the acetalisation reaction. All measured iodine contents are slightly lower than expected by between 0.3-4.7% which is likely due to a combination of incomplete reaction of

the radiopaque groups and remaining solvent in the precipitated samples which was confirmed by <sup>1</sup>H NMR spectroscopy.

*Table 5.5 - Liquid embolic samples synthesised using IBA and TIBA theoretical and determined iodine contents by elemental analysis (n=2).*

<b>Prototype</b>	<b>TIBA (Eq to PVA Diol Groups)</b>	<b>IBA (Eq to PVA Diol Groups)</b>	<b>Targeted Iodine Content (%)</b>	<b>Iodine Content by Elemental Analysis (%)</b>
<b>1.9</b>	0.2	-	42.0	41.7
<b>2.1</b>	0.15	0.05	36.7	35.7
<b>2.2</b>	0.10	0.10	32.5	29.3
<b>2.3</b>	0.05	0.15	25.7	24.8
<b>2.4</b>	-	0.20	19.4	14.6

### **5.3.3. Preparation Time**

It was demonstrated in Chapter 4 that liquid embolic prototypes prepared using PVA modified with TIBA maintain their solution in DMSO without any sedimentation across all TIBA equivalents, polymer molecular weights and DMSO concentrations tested. In order to assess whether the liquid embolic prototypes maintained long-term stable solutions in DMSO without any sedimentation when prepared using different combinations of radiopaque groups, the liquid embolic prototypes were visually observed approximately 6-12 months after their formulation in DMSO. All of the liquid embolic prototypes prepared using the varying combinations of radiopaque group were found to have maintained stable solutions without any visible sedimentation (



Table 5.6). This highlights the ability of the materials to retain a stable formulation for long-term stability as a ready to use material in an embolisation procedure.

Table 5.6 - Results of long-term solution stability of liquid embolic prototypes 6-12 months after formulation in DMSO (n=1).

Prototype	TIBA (Eq to PVA Diol Groups)	S- TIBA (Eq to PVA Diol Group)	IBA (Eq to PVA Diol Groups)	PVA Molecular Weight (kDa)	Conc in DMSO (w/w%)	Retained Stable Solution without Sedimentation?
1.9	0.20	-	-	67	20	Yes
2.1	0.15	0.05	-	67	20	Yes
2.2	0.10	0.10	-	67	20	Yes
2.3	0.05	0.15	-	67	20	Yes
2.4	-	0.20	-	67	20	Yes
2.5	0.15	-	0.05	67	20	Yes
2.6	0.10	-	0.10	67	20	Yes
2.7	0.05	-	0.15	67	20	Yes
2.8	-	-	0.2	67	20	Yes

#### 5.3.4. Deliverability Under Flow Conditions

Evaluation of the delivery properties of the liquid embolic prototypes was carried out using a single channelled delivery model under continuous flow of PBS at a rate of 30-40 mL min<sup>-1</sup>. The same total volume of injected liquid embolic was maintained at 0.1 mL following complete filling of the dead space of the microcatheter. This allowed comparisons to be drawn on the deliverability of the prototypes for a number of measurements including the length of precipitate formed, length of proximal flow, length of reflux and reduction in PBS flow through the tubing. Measurement of these parameters allowed insight into the behaviour of the liquid embolic prototypes as they solidify under aqueous flow conditions and their ability to occlude vessels as they solidify to form a solid mass. The ease of removal of the microcatheter (Renegade™ STC 18, Boston Scientific) used to deliver the liquid embolic prototypes was also noted to evaluate whether or not the materials were adhesive in nature (Table 5.7 and Table 5.8).

Table 5.7 - Delivery results of liquid embolic prototypes prepared using combinations of S-TIBA and TIBA (n=1).

Prototype	TIBA (Eq to PVA Diol Groups)	S-TIBA (Eq to PVA Diol Groups)	Length of Precipitate (mm)	Length of Proximal Advancement (mm)	Length of Reflux (mm)	Reduction in Flow Rate (%)	Catheter Withdrawal	Delivery Notes
1.9	0.2	-	36.0	21.0	15.0	100.0	Easy	Filament - stayed attached
2.1	0.15	0.05	41.0	31.0	10.0	100.0	Some sample removed	Initial wash out
2.2	0.1	0.1	40.0	38.0	2.0	99.3	Some sample removed	Initial wash out
2.3	0.05	0.15	-	-	-	0.0	-	Complete wash out
2.4	-	0.2	-	-	-	0.0	-	Complete wash out

Table 5.8 - Delivery results of liquid embolic prototypes prepared using combinations of IBA and TIBA (n=1).

Prototype	TIBA (Eq to PVA Diol Groups)	IBA (Eq to PVA Diol Groups)	Length of Precipitate (mm)	Length of Proximal Advancement (mm)	Length of Reflux (mm)	Reduction in Flow Rate (%)	Catheter Withdrawal	Delivery Notes
1.9	0.2	-	36.0	21.0	15.0	100.0	Easy	Filament - stayed attached
2.5	0.15	0.05	30.0	18.0	12.0	100.0	Some sample removed	Filament - stayed attached
2.6	0.1	0.1	38.5	38.5	0.0	25.7	Easy	Filament - stayed attached
2.7	0.05	0.15	38.5	27.5	11.0	98.6	Easy	Viscous - difficult to inject
2.8	-	0.2	N/A	N/A	N/A	N/A	N/A	Too viscous for injection

Liquid embolic prototypes prepared using a combination of S-TIBA and TIBA were found to exhibit poor deliverability properties when increasing the portion of S-TIBA in the formulation (Table 5.7). The prototypes prepared using higher portions of S-TIBA of 75% and 100% failed to form solid emboli when injected into the flow model resulting in complete washout from the model. It was also noted that the addition of S-TIBA in combination with TIBA at 25% and 50% led to the occurrence of initial wash out of the injected material before a solid embolus was formed which poses the risk of off-target embolisation if injected *in vivo*. For these prototypes there was also observed to be a small amount of the precipitated materials which remained attached to the microcatheter as it was withdrawn. The adhesion of these samples to the microcatheter could pose a risk of dislodging the embolic plug or off-target embolisation if the adhered material was to become dislodged from the microcatheter during withdrawal from the patient.

In the case of the liquid embolic prototypes prepared using combinations of IBA and TIBA, the majority of the prototypes were found to form filaments early in the injection process which remained attached therefore not posing a risk of off-target embolisation (Table 5.8). The microcatheter could be easily removed from all solidified samples with the exception of the liquid embolic prototype prepared using 25% IBA which removed a small amount of the solidified sample at the tip of the microcatheter. The delivery of the liquid embolic prototype prepared using the highest portions of IBA at 75% and 100% were found to be highly viscous in nature making delivery using the microcatheter difficult due to the requirement of a high amount of force for injection. This is likely due to the higher portion of IBA groups bound to the PVA backbone which have lower steric hindrance in comparison to TIBA thereby allowing increased  $\pi$ - $\pi$  interactions resulting in an increase in viscosity of the polymer solutions. The high injection pressure required to deliver these samples would not be suitable during an embolisation procedure as it could result in uncontrolled delivery of the material or the surpassing of microcatheter burst release pressures.<sup>140</sup>

The portion of proximal flow was found to increase with higher portions of the hydrophilic group S-TIBA and less hydrophobic group IBA (Figure 5.5). The increase in proximal flow for samples prepared with higher amounts of the alternative radiopaque groups suggests a characteristic for higher penetration into the vasculature during an embolisation procedure. It should be noted that these results are disregarding the liquid embolic prototypes prepared at S-TIBA portions of 75% and above as these samples failed to solidify under aqueous flow suggesting the loss of hydrophobicity required to sufficiently precipitate on contact with aqueous conditions.

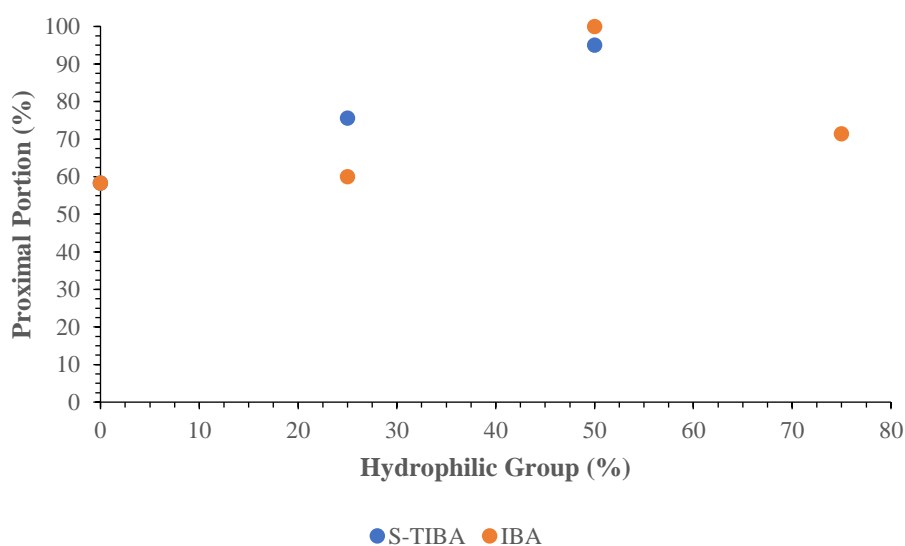


Figure 5.5 - Percentage of proximal flow of solidified liquid embolic prototypes prepared using combinations of S-TIBA, IBA and TIBA (n=1).

### 5.3.5. Rate of Solidification

In order to gauge the working time of the liquid embolic prototypes, the rate of solidification was determined by measuring the elution of DMSO from the samples during the solidification process. This was carried out by the dropwise addition of the prototypes in their liquid states (1 mL) into a large volume of PBS (500 mL). The solution into which the liquid embolic samples were precipitated was continuously circulated on a closed loop system to a UV spectrophotometer with UV measurements taken at the wavelength corresponding to DMSO

for 1 hour. The rate of solidification of the samples was calculated for the time at which 90% of the total DMSO eluted was released over the test time of 1 hour (Table 5.9).

*Table 5.9 - Solidification data of liquid embolic prototypes prepared using combinations of S-TIBA, IBA and TIBA (n=1).*

<b>Prototype</b>	<b>TIBA (Eq to PVA Diol Groups)</b>	<b>S-TIBA (Eq to PVA Diol Group)</b>	<b>IBA (Eq to PVA Diol Groups)</b>	<b>PVA Molecular Weight (kDa)</b>	<b>Concentration in DMSO (w/w%)</b>	<b>Solidification Time (&gt;90%) (s)</b>
<b>1.9</b>	0.20	-	-	67	20	335
<b>2.1</b>	0.15	0.05	-	67	20	608
<b>2.2</b>	0.10	0.10	-	67	20	61
<b>2.3</b>	0.05	0.15	-	67	20	41
<b>2.4</b>	-	0.20	-	67	20	81
<b>2.5</b>	0.15	-	0.05	67	20	485
<b>2.6</b>	0.10	-	0.10	67	20	68
<b>2.7</b>	0.05	-	0.15	67	20	34
<b>2.8</b>	-	-	0.2	67	20	77

Liquid embolic samples prepared using 50% or higher of the alternative radiopaque groups were observed to have rapid solidification times (Figure 5.6). Whereas comparison of the solidification results of liquid embolic prototypes prepared using TIBA alone and a combination with a low amount of the S-TIBA or IBA groups at 25%, indicated an increase in the solidification time for samples on addition of the alternative radiopaque groups. The slower solidification profiles observed for the prototypes prepared using 25% of the alternative radiopaque groups is likely to be due to the initial formation of a skin to form a spherical droplet which was observed visually during the solidification of the materials. The initial formation of a skin around the solidifying droplets is likely to have reduced the rate of diffusion of DMSO out of the solidifying materials giving rise to a slower rate of solidification. In contrast, the samples prepared using 50% or higher of the alternative radiopaque group in combination with TIBA, did not form an initial skin around solidifying materials. Instead, these prototypes formed more string like masses on contact with PBS which remained close to the outlet for the UV spectrophotometer giving rise to the rapid solidification times measured (Figure 5.7).

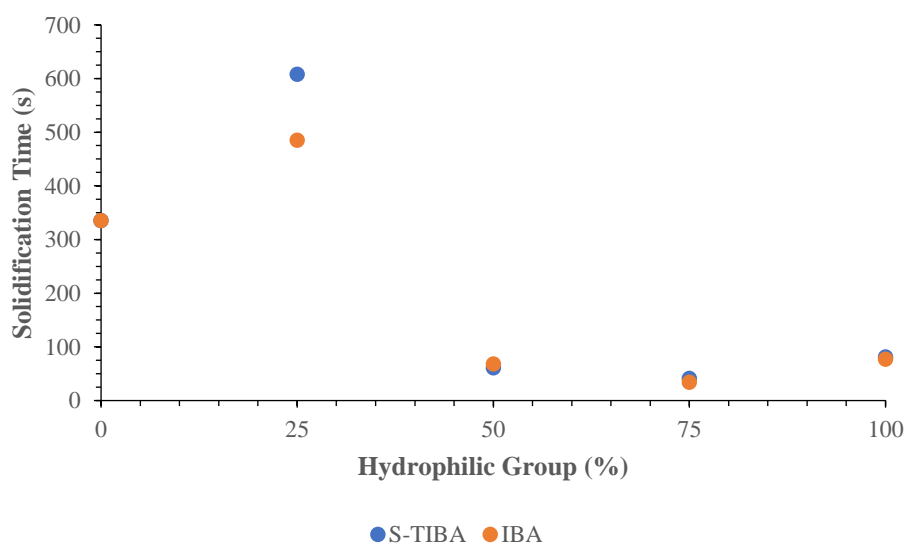


Figure 5.6 - Solidification results of liquid embolic prototypes prepared using combinations of S-TIBA, IBA and TIBA (n=1).



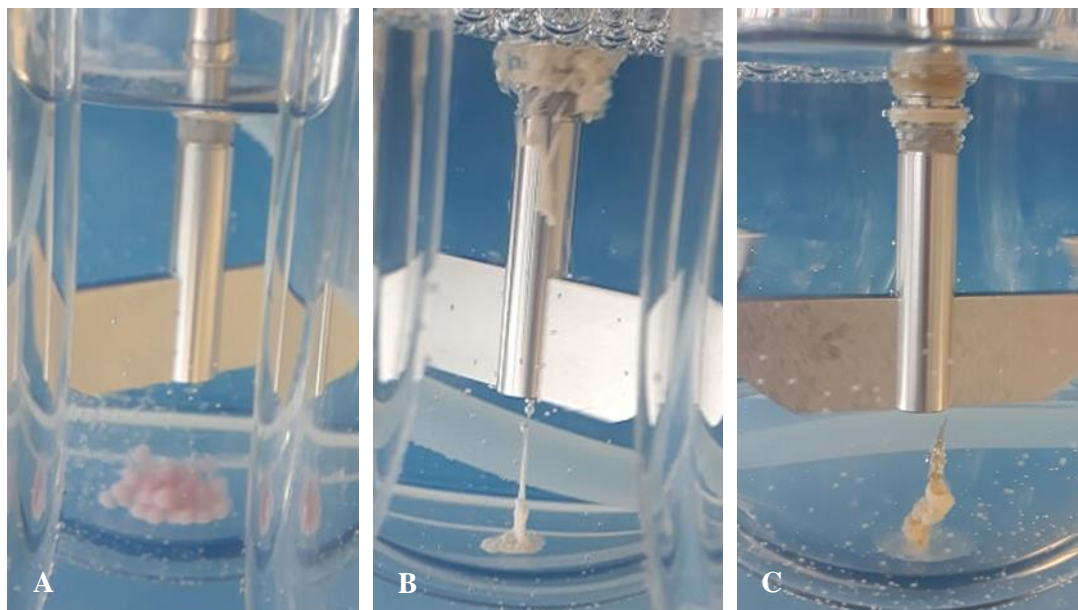


Figure 5.7 - Images of liquid embolic prototypes during solidification test; (A) 25% S-TIBA (B) 50% IBA (C) 50% S-TIBA.

Variation in the rate of solidification with the addition of 25% S-TIBA and IBA in comparison to TIBA alone can be observed in their measured solidification profiles (Figure 5.8). A faster solidification profile was observed for the prototype prepared using TIBA alone, the most hydrophobic formulation. Reduction of the hydrophobicity of the material by utilising 25% IBA was observed to reduce the solidification rate and the solidification rate was reduced further still by the use of 25% of the hydrophilic group S-TIBA. This demonstrates the influence of hydrophobicity on the phase inversion properties of the solidifying polymers with higher hydrophobicities resulting in increased rates of solidification on contact with water.<sup>135</sup>

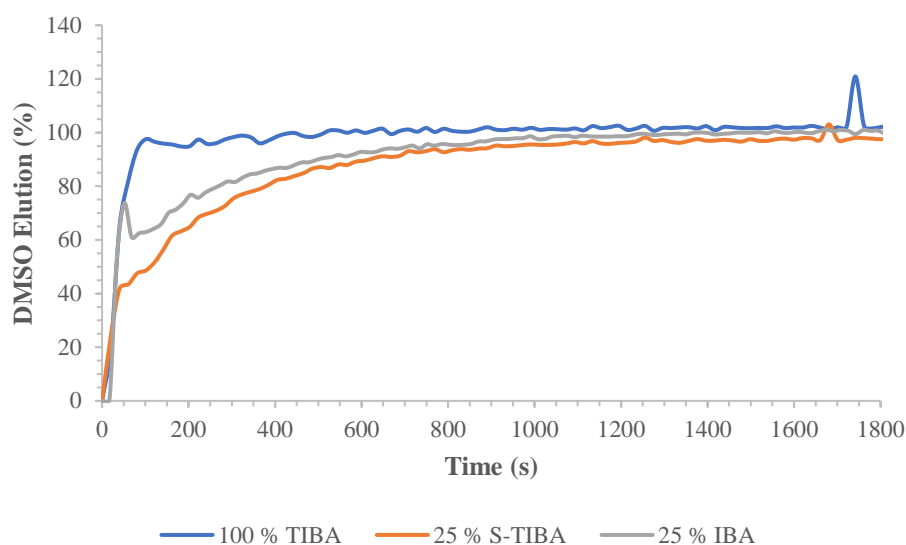


Figure 5.8 - Solidification profiles of liquid embolic prototypes prepared using combinations of S-TIBA, IBA and TIBA ( $n=1$ ).

### 5.3.6. Rheology of Precipitation Process

Rheology measurements were used to gain insight into the delivery and solidification of the liquid embolic prototypes with regards to their complex viscosities, loss modulus and storage modulus in both the liquid and precipitate states. This was carried out using a rheometer with a parallel plate geometry. Measurements of the liquid samples were taken before and after flooding the cell with saline flow across the plate to monitor the rheological properties of the liquid and its precipitation process at an oscillating shear stress of  $0.1 \text{ s}^{-1}$ . These measurements were all performed at  $37 \text{ }^\circ\text{C}$  in order to replicate the conditions of injection into the body. Tests were performed using liquid embolic prototypes prepared with 100% TIBA and 25% S-TIBA and 25% IBA in combination with TIBA in order to gauge the impact of using a small amount of alternative radiopaque in combination with TIBA (Table 5.10).

Table 5.10 - Rheology data of precipitation process for liquid embolic prototypes prepared combinations of S-TIBA, IBA and TIBA (n=1).

Prototype	TIBA (Eq to PVA Diol Groups)	S-TIBA (Eq to PVA Diol Groups)	IBA (Eq to PVA Diol Groups)	Liquid						Precipitate		
				Mean Storage Modulus (Pa)	Standard Deviation (Pa)	Mean Loss Modulus (Pa)	Standard Deviation (Pa)	Mean Complex Viscosity (mPa s <sup>-1</sup> )	Standard Deviation (mPa s <sup>-1</sup> )	Max Storage Modulus (Pa)	Max Loss Modulus (Pa)	Max Complex Viscosity (mPa s <sup>-1</sup> )
1.9	0.2	-	-	0.41	0.47	2.68	0.98	275	99	82257	35032	8472700
2.1	0.15	0.05	-	1.26	1.03	1.86	0.76	233	111	14178	1158	1422500
2.5	0.15	-	0.05	0.91	0.36	2.20	0.41	241	40	297550	58922	30332000

Similar complex viscosities were found for all of the prototypes tested in their liquid states (Figure 5.9). Variations in the complex viscosity measurements were observed for the prototypes in their precipitate states. The prototype prepared using a combination of TIBA with 25% IBA demonstrated the highest maximum complex viscosity of  $3.03 \times 10^7$  mPa s<sup>-1</sup>. In contrast the prototype prepared using a combination of TIBA with 25% S-TIBA exhibited the lowest complex viscosity in its precipitate state of  $1.42 \times 10^7$  mPa s<sup>-1</sup>. This could perhaps be attributed to the facilitation of increased interaction of the TIBA groups with the smaller sized and less sterically hindered IBA groups by  $\pi$ - $\pi$  stacking between the aromatic rings. The increased interaction between the radiopaque groups is likely to result in a higher viscosity of the polymer solution during the precipitation process. In contrast, the larger steric hindrance imparted by the pendent sulfonic acid group of S-TIBA is likely to have hindered any  $\pi$ - $\pi$  stacking between the aromatic rings of S-TIBA and TIBA. Another contributing factor is likely to be electrostatic repulsion between the deprotonated S-TIBA groups of the polyanions as indicated by the end-group pK<sub>a</sub> value of 1.6 in DMSO.<sup>141</sup> Hence, the lower maximum complex viscosity measured of the 25% S-TIBA sample following 30 minutes after the initial onset of phase inversion.

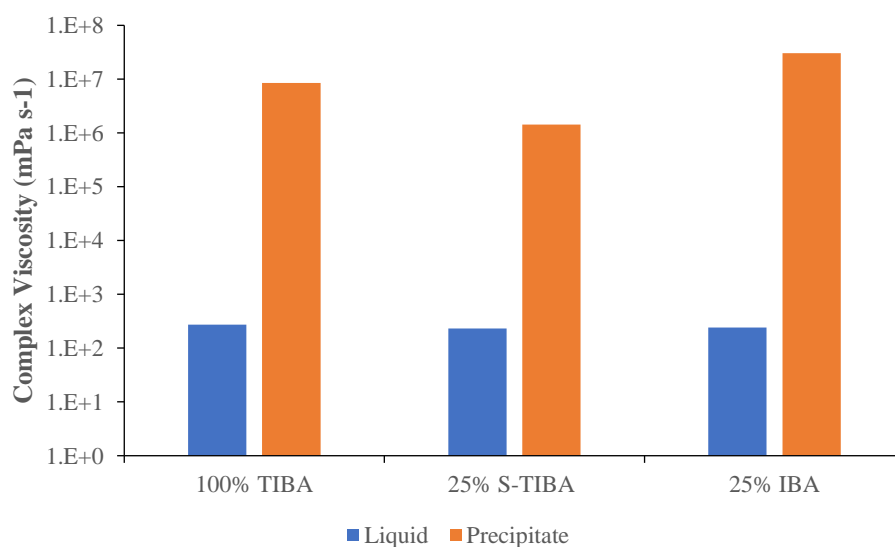


Figure 5.9 - Complex viscosity results of liquid embolic prototypes prepared using combinations of S-TIBA, IBA and TIBA in their liquid and precipitate states (n=1).

Similar trends were observed for the storage and loss moduli of the prototypes with similar values across all prototypes in their liquid states and the same trends in variation in their precipitate states (Figure 5.10 and Figure 5.11). The lowest storage and loss modulus' were exhibited for the prototype prepared using a combination of TIBA with 25% S-TIBA. This suggests the use of the sterically hindered charged S-TIBA group to inhibit the interactions between polymer chains in comparison to TIBA alone, resulting in reduced rigidity of the precipitating material due to elastic deformation and viscous flow respectively.

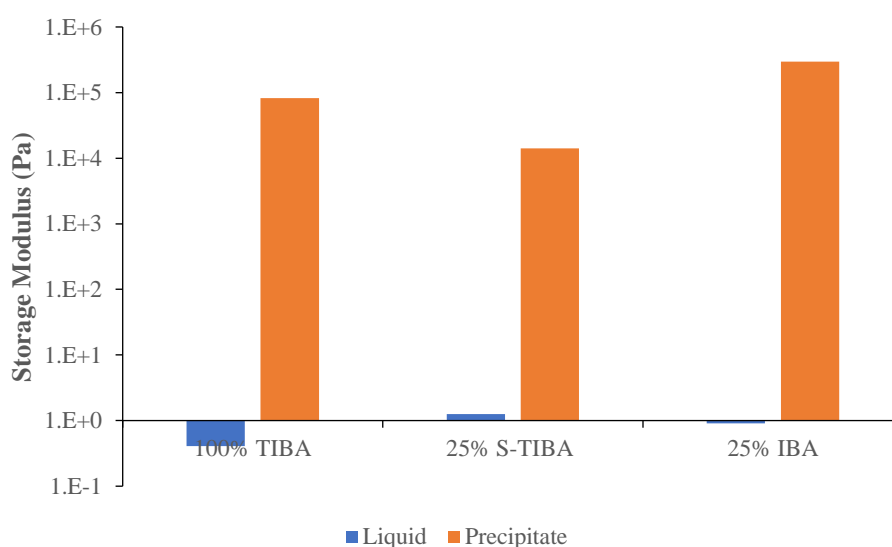


Figure 5.10 - Storage modulus results of liquid embolic prototypes prepared using combinations of S-TIBA, IBA and TIBA in their liquid and precipitate states (n=1).

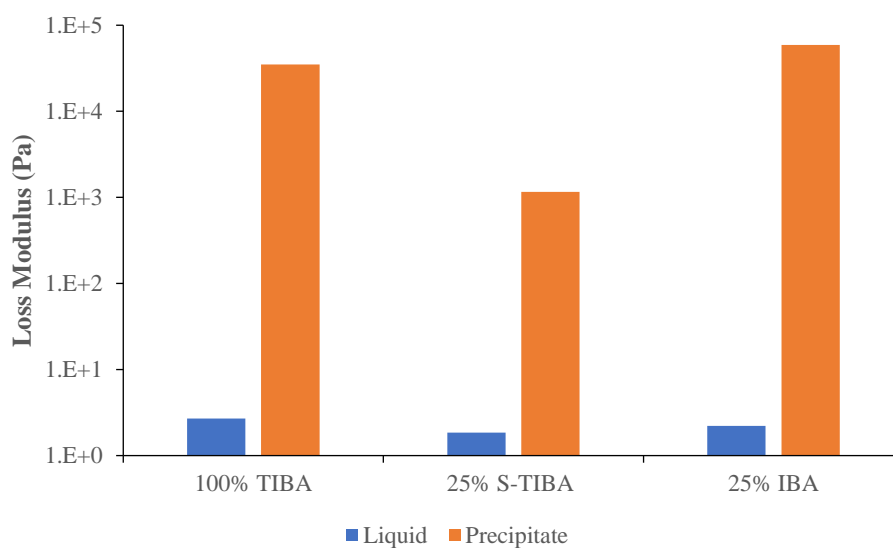


Figure 5.11 - Loss modulus results of liquid embolic prototypes prepared using combinations of S-TIBA, IBA and TIBA in their liquid and precipitate states ( $n=1$ ).

### 5.3.7. Fill Volume after Solidification

Fill volume measurements were performed in order to gain an idea of the expected change in volume of the liquid embolic prototypes on transitioning from liquid to solid states. This was carried out by precipitating a set volume of liquid sample (0.5 mL) into PBS (15 mL). The samples were allowed to fully solidify before being transferred to a volume measurement device in which the volume of the solid precipitates was calculated using the volume of PBS displaced within the volume measurement device (Table 5.11 and Table 5.12).

Table 5.11 - Fill volume data of liquid embolic prototypes prepared using combinations of S-TIBA and TIBA (n=3).

Prototype	TIBA (Eq to PVA Diol Groups)	S-TIBA (Eq to PVA Diol Groups)	Initial Liquid Volume (mL)	Height of Precipitate (mm)	Volume of Precipitate (mL)	Mean Reduction in Volume (%)	Standard Error of Mean (%)
<b>1.9</b>	0.2	-	0.50	8.0	0.34	30	1.4
			0.50	8.5	0.36		
			0.50	8.5	0.36		
<b>2.1</b>	0.15	0.05	0.50	8.5	0.36	25	2.8
			0.50	9.5	0.41		
			0.50	8.5	0.36		
<b>2.2</b>	0.1	0.1	0.50	15.5	0.71	66	6.3
			0.50	16.0	0.74		
			0.50	13.5	0.61		
<b>2.3</b>	0.05	0.15	0.50	7.5	0.31	33	2.4
			0.50	8.0	0.34		
			0.50	8.5	0.36		
<b>2.4</b>	-	0.2	0.50	5.5	0.21	55	2.8
			0.50	6.5	0.26		
			0.50	5.5	0.21		

Table 5.12 - Fill volume data of liquid embolic prototypes prepared using combinations of IBA and TIBA (n=3).

Prototype	TIBA (Eq to PVA Diol Groups)	IBA (Eq to PVA Diol Groups)	Initial Liquid Volume (mL)	Height of Precipitate (mm)	Volume of Precipitate (mL)	Mean Reduction in Volume (%)	Standard Error of Mean (%)
<b>1.9</b>	0.2	-	0.5	8.0	0.34	30	1.4
			0.5	8.5	0.36		
			0.5	8.5	0.36		
<b>2.5</b>	0.15	0.05	0.5	7.0	0.28	41	1.4
			0.5	7.5	0.31		
			0.5	7.0	0.28		
<b>2.6</b>	0.1	0.1	0.5	7.5	0.31	35	1.4
			0.5	8.0	0.34		
			0.5	8.0	0.34		
<b>2.7</b>	0.05	0.15	0.5	8.5	0.36	28	0.0
			0.5	8.5	0.36		
			0.5	7.5	0.31		
<b>2.8</b>	-	0.2	0.5	7.5	0.31	40	1.4
			0.5	7.5	0.31		
			0.5	7.0	0.29		

All liquid embolic prototypes were seen to undergo a reduction in volume upon solidification (Figure 5.12). Liquid embolic samples prepared using varying ratios of IBA:TIBA were found to undergo fill volume reductions ranging from 28 to 40%. The portion of IBA used in the formulation was not found to influence the magnitude of reduction in fill volume on transition to a solid. In contrast, fill volume reductions measured for the prototypes prepared using varying ratios of S-TIBA:TIBA were observed to vary with increasing ratios of S-TIBA:TIBA. Prototypes prepared using S-TIBA portions of 50% or above were found to undergo higher reductions in fill volumes with the highest reduction exhibited for the prototype prepared using 50% S-TIBA. These prototypes were observed to form flat disk-like precipitates in comparison to the spherical precipitates produced for prototypes of S-TIBA contents below 50%. The flat disk shapes produced by the prototypes of S-TIBA contents of 50% or above are expected to have been of lower volume than the spherical precipitates which



would have likely still contained some of the DMSO carrier solvent giving rise to a lower reduction in fill volume.

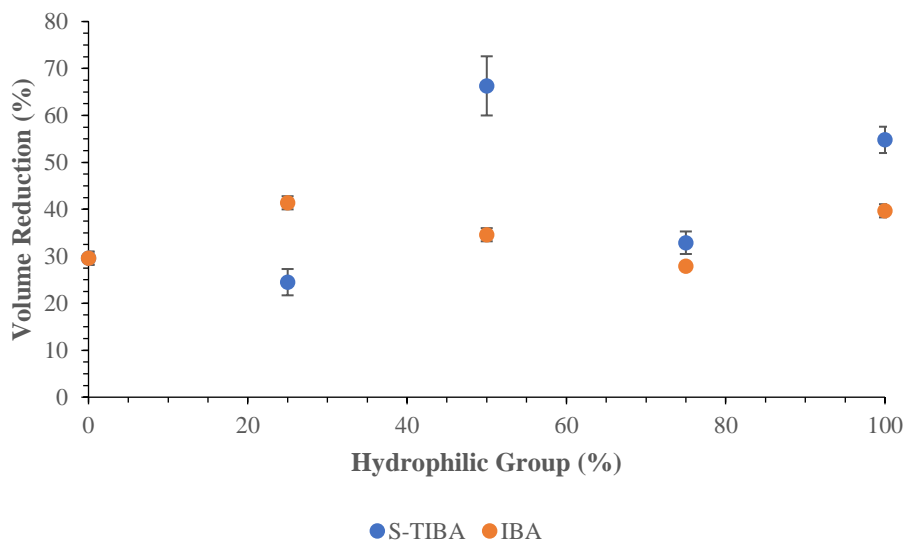


Figure 5.12 - Fill volume results of liquid embolic prototypes prepared using combinations of S-TIBA, IBA and TIBA ( $n=3$ ).

### 5.3.8. Fragmentation and Particulate Generation

To assess the cohesiveness of the liquid embolic prototypes once solidified, fragmentation and particulate generation tests were performed. This was carried out by precipitating the liquid embolic prototypes (0.5 mL) into PBS (30 mL) in a set geometry using the same shaped Duran bottle for each sample. The samples were allowed to fully solidify before being agitated at shaker plate speeds of 240, 400 and 640 rpm for 30 minutes. Aliquots of the agitated solutions were then observed under optical microscopy using magnifications of  $\times 4$  to observe any fragments formed and  $\times 10$  to observe any particulates formed. Images were captured and analysed for the number of fragments formed and percentage area covered by particulates ( $n=3$ ) at each shaker speed. The samples were rated for their formation of particulates and fragments based on the highest generation observed across the 3 shaker speeds. Ratings were used in which a value of 1 represents minimal generation and a value of 5 represents high fragmentation and particulate generation (Table 5.13 and Table 5.14).

Table 5.13 - Fragmentation and particulate generation of liquid embolic prototypes prepared using combinations of S-TIBA and TIBA (n=3).

Prototype	TIBA (Eq to PVA Diol Group)	S-TIBA (Eq to PVA Diol Group)	Fragmentation Rating	Particulate Rating
1.9	0.20	-	2	1
2.1	0.15	0.05	3	4
2.2	0.10	0.10	5	5
2.3	0.05	0.15	5	5
2.4	-	0.20	1	1

Table 5.14 - Fragmentation and particulate generation of liquid embolic prototypes prepared using combinations of IBA and TIBA (n=3).

Prototype	TIBA (Eq to PVA Diol Group)	IBA (Eq to PVA Diol Group)	Fragmentation Rating	Particulate Rating
1.9	0.20	-	2	1
2.5	0.15	0.05	1	1
2.6	0.10	0.10	3	1
2.7	0.05	0.15	1	1
2.8	-	0.20	3	1

Low degrees of fragmentation and particulate generation were observed for liquid embolic prototypes prepared using combinations of IBA:TIBA (Figure 5.13 and Figure 5.14). Fragmentation ratings of these samples fluctuated in the range of 1 to 3, whereas a minimal degree of particulate generation was observed across all IBA:TIBA combinations with a rating of 1. This suggests the ratio of IBA:TIBA has minimal influence on the cohesive nature of the solidified embolic prototypes.

The use of S-TIBA in combination with TIBA was noted to give rise to higher degrees of fragmentation and particulate generation than formulations prepared using TIBA or S-TIBA alone (Figure 5.13 and Figure 5.14). This suggests the use of S-TIBA in combination with TIBA gives rise to samples that are less cohesive in nature when solidified possibly due to the polyanion nature of the polymer imparted by the charged S-TIBA group. The reduced cohesive nature is something which should be avoided when considering a material for use as an embolic agent as fragmentation and particulate generation could pose the risk of off-target embolisation or migration from the delivery site if the sample does not remain as a solid cohesive mass.

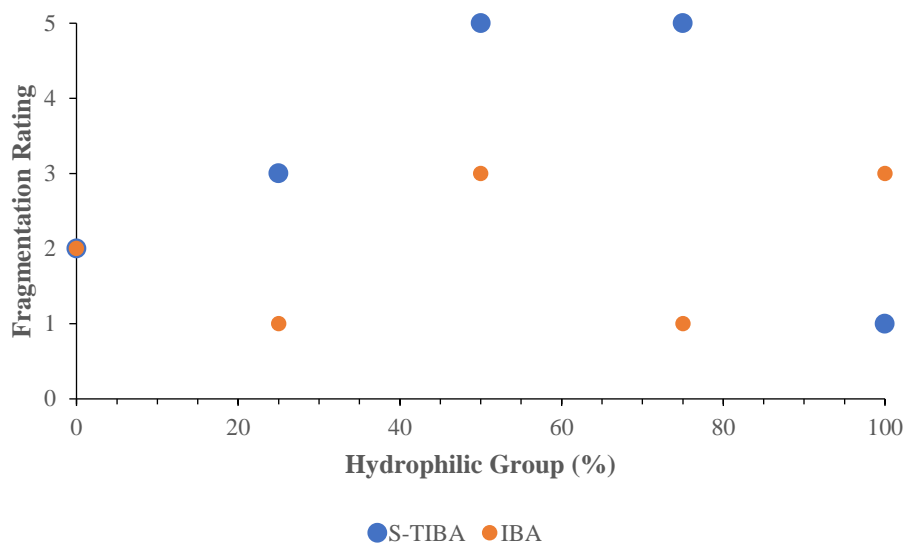


Figure 5.13 - Fragmentation ratings of liquid embolic prototypes prepared using combinations of S-TIBA, IBA and TIBA ( $n=3$ ).

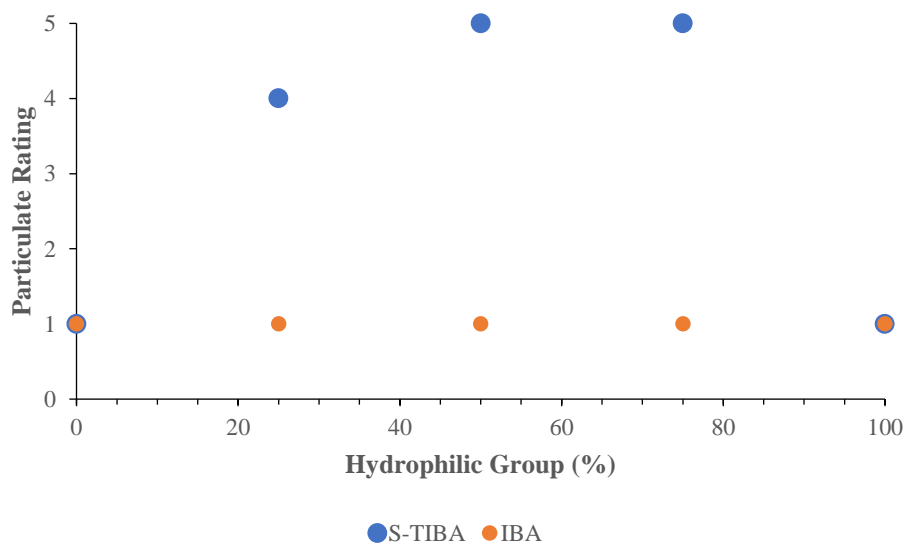


Figure 5.14 - Particulate ratings of liquid embolic prototypes prepared using combinations of S-TIBA, IBA and TIBA ( $n=3$ ).

### 5.3.9. Biocompatibility

The biocompatibility of similar structures of PVA modified with TIBA has already been established,<sup>116,129</sup> however the biocompatibility PVA modified with S-TIBA and IBA groups is currently untested. It is theorised that covalent binding of these groups to the PVA backbone

would maintain the biocompatibility of PVA as the radiopaque groups would be permanently bound to the polymer backbone by stable cyclic acetal bonds and therefore not able to leach into surrounding tissue. However, cytotoxicity tests would be required if these materials were to be used *in vivo*.

To ensure biocompatibility of the liquid embolic prototypes, the formulations should be free from any unbound radiopaque groups as these small molecules are likely to be toxic.<sup>142</sup> The purity of the IBA and S-TIBA radiopaque groups themselves was confirmed prior to use in the modification of PVA by a range of techniques including; <sup>1</sup>H NMR spectroscopy, <sup>13</sup>C NMR spectroscopy and elemental analysis. Analysis of the <sup>1</sup>H NMR spectra of radiopaque polymers prepared using combinations of S-TIBA:TIBA and IBA:TIBA confirmed purification of the polymers from any small molecule starting materials suggesting no issues of cytotoxicity with respect to unbound radiopaque groups (Table 5.15).

Table 5.15 - Residual reactant traces as determined from <sup>1</sup>H NMR spectra of liquid embolic prototypes (n=1).

Prototype	TIBA (Eq to PVA Diol Groups)	S-TIBA (Eq to PVA Diol Group)	IBA (Eq to PVA Diol Groups)	PVA Molecular Weight (kDa)	Concentration in DMSO (w/w%)	Residual Traces of TIBA/S-TIBA/IBA
1.9	0.20	-	-	67	20	None
2.1	0.15	0.05	-	67	20	None
2.2	0.10	0.10	-	67	20	None
2.3	0.05	0.15	-	67	20	None
2.4	-	0.20	-	67	20	None
2.5	0.15	-	0.05	67	20	None
2.6	0.10	-	0.10	67	20	None
2.7	0.05	-	0.15	67	20	None
2.8	-	-	0.2	67	20	None

Analysis of the molecular weights of the liquid embolic prototypes was also performed to confirm the retention of polymer molecular weight throughout the processing of the liquid embolic prototypes. The results of size exclusion chromatography confirms the retention of polymer molecular weight as indicated by the number average molecular weights and

dispersities measured. This suggests safe injection of the liquid embolic prototypes *in vivo* without injection of short polymer chain fragments that could cause toxic effects (Table 5.16).

Table 5.16 - Results of molecular weights determined by SEC for liquid embolic prototypes ( $n=1$ ).

Prototype	TIBA (Eq to PVA Diol Groups)	S-TIBA (Eq to PVA Diol Group)	IBA (Eq to PVA Diol Groups)	PVA Molecular Weight (kDa)	Concentration in DMSO (w/w%)	Number Average Molecular Weight (kDa)	Dispersity
1.9	0.2	-	-	67	20	88.5	2.33
2.1	0.15	0.05	-	67	20	99.3	2.04
2.2	0.1	0.1	-	67	20	97.0	3.28
2.3	0.05	0.15	-	67	20	110	3.66
2.4	-	0.2	-	67	20	85.6	4.58
2.5	0.15	-	0.05	67	20	106	1.90
2.6	0.1	-	0.1	67	20	104	2.03
2.7	0.05	-	0.15	67	20	133	1.79
2.8	-	-	0.2	67	20	157	1.60

### 5.3.10. Radiopacity

The radiopacity of the liquid embolic prototypes was measured using microCT analysis. The samples were analysed using the solidified samples produced in the deliverability test (Section 5.3.4). The samples were prepared by delivery of the liquid embolic prototypes (0.1 mL) into narrow bore tubing (1.67 mm internal diameter) under PBS flow conditions and allowed to solidify. The tubing containing the solidified samples was scanned using the microCT scan and reconstruction parameters developed in Chapter 3 to determine the radiopacity of the samples as measured in Hounsfield units (Table 5.17).

Table 5.17 - MicroCT data for liquid embolic samples prepared using combinations of S-TIBA, IBA and TIBA (imaging cross-sections, n=198).

<b>Prototype</b>	<b>TIBA (Eq to PVA Diol Groups)</b>	<b>S-TIBA (Eq to PVA Diol Groups)</b>	<b>IBA (Eq to PVA Diol Group)</b>	<b>Radiopacity (HU)</b>	<b>Standard Deviation (HU)</b>
<b>1.9</b>	0.2	-	-	2776	1058
<b>2.1</b>	0.15	0.05	-	3669	1808
<b>2.2</b>	0.1	0.1	-	5981	1307
<b>2.3</b>	0.05	0.15	-	1778	547
<b>2.4</b>	-	0.2	-	3758	1373
<b>2.5</b>	0.15	-	0.05	2815	1082
<b>2.6</b>	0.1	-	0.1	4071	1225
<b>2.7</b>	0.05	-	0.15	1400	617
<b>2.8</b>	-	-	0.2	1091	531

There were no observed clear trends in the data for the radiopacity measured with varying ratios of S-TIBA:TIBA and IBA:TIBA (Figure 5.15). This is likely due to the large standard deviations associated with the measurements as established in Chapter 3. In theory for the S-TIBA:TIBA prototypes, the measured radiopacity should be consistent across increasing portions of S-TIBA due to the tri-iodination of both S-TIBA and TIBA. Whereas, the radiopacity of the IBA:TIBA samples should reduce on increasing the portion of IBA due to the mono-iodination of IBA in comparison to the tri-iodination of TIBA thereby imparting less radiopacity to the material.

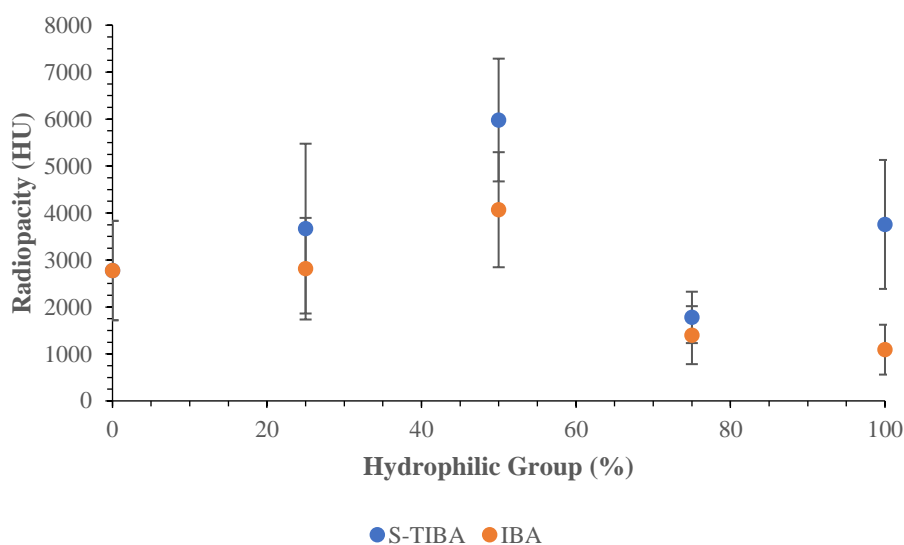


Figure 5.15 - MicroCT results for liquid embolic samples prepared using combinations of S-TIBA, IBA and TIBA (imaging cross-sections,  $n=198$ ).

Comparing the radiopacity values measured for the liquid embolic prototypes to the lowest concentration of commercially used contrast agent for CT imaging of Omnipaque™ 180 at 2120 HU, it can be assumed that samples with measured radiopacity greater than this should be sufficiently radio-dense to be visualised if implanted within the body. The majority of the liquid embolic prototypes were determined to be of sufficient radiopacity with the exception of the prototypes prepared using 75% S-TIBA:TIBA, 75% IBA:TIBA and 100% IBA:TIBA (Table 5.18). In the case of the 75% S-TIBA:TIBA sample this is likely due to the large standard deviations associated with the measurements as in theory, the iodination level should be equivalent to the other samples in the S-TIBA:TIBA sample set due to the same total equivalents of PVA diol groups targeted of 20%. Whilst in the cases of the 75% and 100% IBA:TIBA prototypes, the lower radiopacities are expected due to the reduced iodination levels by the use of a higher portion of IBA:TIBA than the previous samples in the same sample set.

Table 5.18 - Comparison of radiopacity values of liquid embolic prototypes against Omnipaque™ 180 (imaging cross-sections, n=198).

Prototype	TIBA (Eq to PVA Diol Groups)	S-TIBA (Eq to PVA Diol Groups)	IBA (Eq to PVA Diol Group)	Mean Radiopacity (HU)	Sufficient Radiopacity?
<b>1.9</b>	0.20	-	-	2776	Yes
<b>2.1</b>	0.15	0.05	-	3669	Yes
<b>2.2</b>	0.10	0.10	-	5981	Yes
<b>2.3</b>	0.05	0.15	-	1778	No
<b>2.4</b>	-	0.20	-	3758	Yes
<b>2.5</b>	0.15	-	0.05	2815	Yes
<b>2.6</b>	0.10	-	0.10	4071	Yes
<b>2.7</b>	0.05	-	0.15	1400	No
<b>2.8</b>	-	-	0.20	1091	No

### 5.3.11. Porosity

Materials which solidify with some degree of porosity suggest possibility for a compressible nature which is beneficial for maintaining the position at the implantation site if any compression of the vasculature were to occur. Hence, porosity measurements were used to infer whether the solidified liquid embolic prototypes may have potential for compression. Porosity measurements were obtained from the reconstructed scan data of microCT imaging (Section 5.3.10). The porosity of the solidified liquid embolic prototypes within the tubing was calculated across a 3D cross-sectional area of 1.6 mm in diameter and 1 mm in height (Table 5.19).



Table 5.19 - Porosity data for liquid embolic prototypes prepared using combinations of S-TIBA, IBA and TIBA (imaging cross-sections, n=198).

Prototype	TIBA (Eq to PVA Diol Groups)	S-TIBA (Eq to PVA Diol Groups)	IBA (Eq to PVA Diol Groups)	Porosity (%)
1.9	0.2	-	-	54.3
2.1	0.15	0.05	-	55.1
2.2	0.1	0.1	-	72.8
2.3	0.05	0.15	-	5.9
2.4	-	0.2	-	94.8
2.5	0.15	-	0.05	24.8
2.6	0.1	-	0.1	78.9
2.7	0.05	-	0.15	35.0
2.8	-	-	0.2	26.4

There was not observed to be any significant trends in porosity for increasing ratios of S-TIBA:TIBA and IBA:TIBA (Figure 5.16). This is likely to be due to the small cross-section used which only provides a snapshot of the porosity of the sample at a particular point. In Chapter 3 it was determined that the porosity of a sample varies greatly across its whole length hence it is not possible to accurately determine an average porosity representative of the whole sample length.

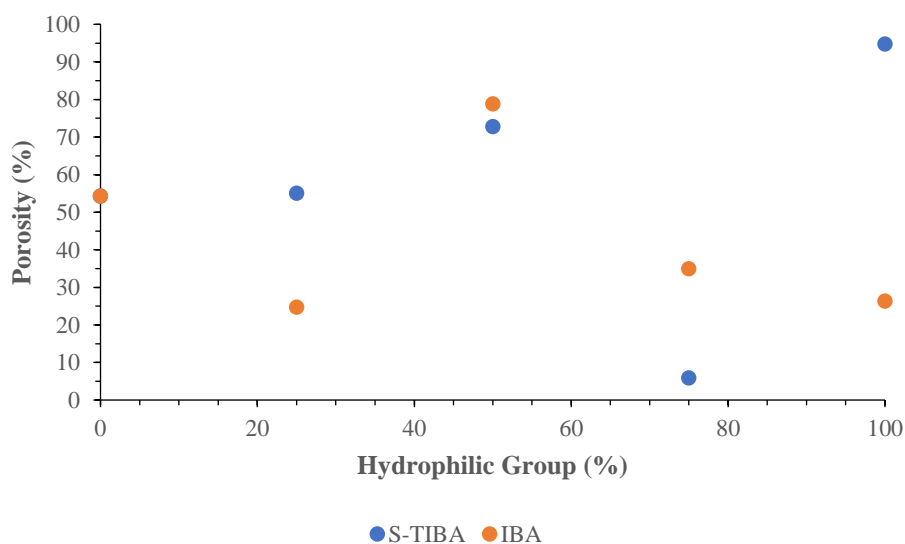


Figure 5.16 - Porosity results for liquid embolic samples prepared using combinations of S-TIBA, IBA and TIBA (imaging cross-sections, n=198).

## 5.4. Conclusions

Liquid embolic prototypes were prepared using varying combinations of S-TIBA:TIBA and IBA:TIBA to investigate the impact of using a hydrophilic group and a less hydrophobic group in combination with TIBA. These groups were found to have a large influence on the characteristics of the liquid embolic materials. Modification using a ratio of 50% or higher of the S-TIBA radiopaque group was found to have a negative effect on the liquid embolic properties with poor deliverability, rapid solidification rates, large reductions in fill volumes and high degrees of fragmentation and particulate generation. The same trend was observed for liquid embolic prototypes prepared using a ratio of 50% or higher of the IBA radiopaque group but with a less dramatic effect.

Modification using 25% of the S-TIBA radiopaque group was found to be optimal for increasing the portion of proximal flow, increasing the rate of solidification and reducing the fill volume reduction. However, an increase in fragmentation and particulate generation was observed in comparison to using TIBA alone in the formulation. Use of 25% of IBA in the formulation was found to also increase the rate of solidification whilst retaining similar deliverability, fill volume reduction and fragmentation and particulate generation. This indicates the ability to tune the properties of the liquid embolic materials by utilising small amounts of alternative radiopaque groups in combination with TIBA.

The polyanionic nature of the prototypes prepared using combinations of TIBA with S-TIBA was not investigated in this chapter. However, further investigations would be warranted to determine the influence of the sulfonic acid group on the phase inversion of the polyanions in aqueous ionic environments. This should include solidification and deliverability tests in aqueous solutions of varying ionic strength to observe the effects of varying salt concentrations on the solidification behaviour of these materials.

## **Chapter Six**

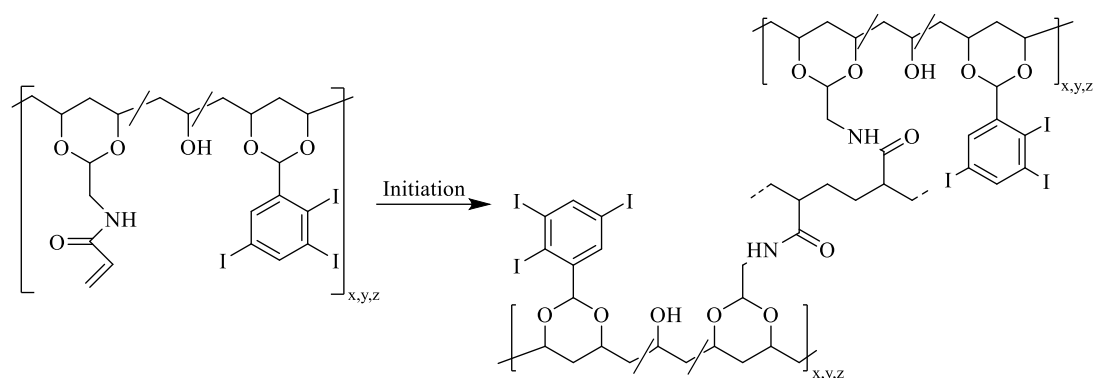
### **6. Synthesis and Characterisation of Aqueous-Based Liquid Embolics**

## 6.1. Introduction

The current liquid embolic system in widespread clinical use, Onyx<sup>®</sup>, is a solvent-based system utilising DMSO as a carrier solvent for the precipitating polymer. However, there is a drive towards solvent-free systems which avoid the complications associated with the injection of solvents into the vasculature. The elimination of DMSO from liquid embolic formulations eliminates the risk of vasospasms induced by the rapid injection of DMSO.<sup>74</sup>

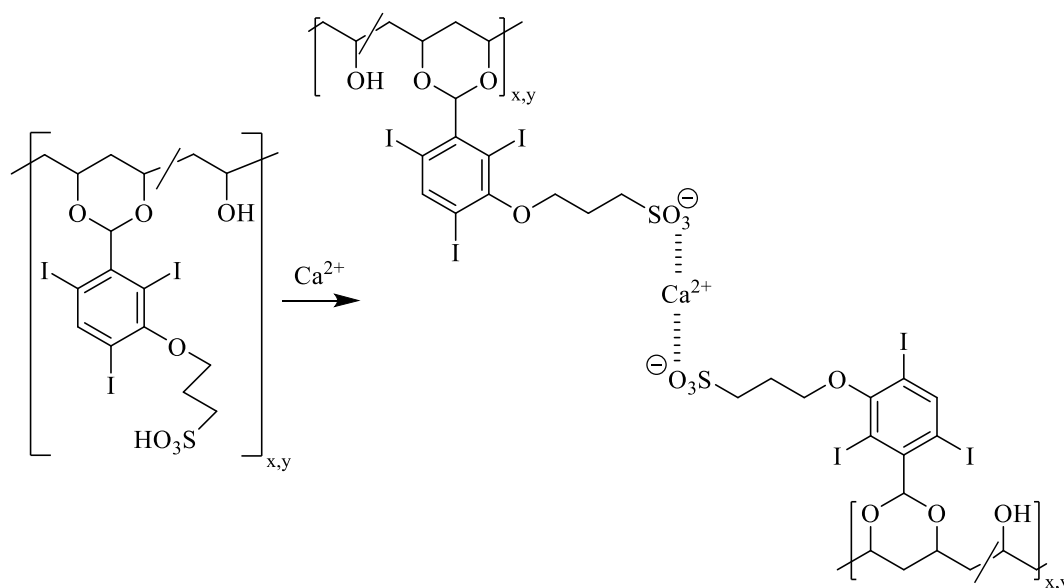
A solvent-free liquid embolic which is currently undergoing investigation is GPX by Fluidx Medical Technology. The proposed system consists of polyelectrolyte complexes which aggregate when injected into the vasculature due to the reduced ionic strength of blood in comparison to the high salt concentration of the aqueous carrier solution.<sup>91,92</sup> This reduction in ionic strength removes the charge screening between the polyelectrolytes resulting in aggregation of the polyelectrolyte complexes to form a gel *in situ* to rapidly occlude blood vessels. However, due to the organic nature of the polymer used in the formulation, GPX must be mixed with tantalum to enable visualisation of the injection process. This presents the same issues faced by Onyx<sup>®</sup> with the requirement of agitation prior to injection and the occurrence of streak artefact on imaging.<sup>81</sup>

Two distinct approaches are discussed in this chapter in an attempt to formulate a solvent-free radiopaque liquid embolic. The first approach outlined is an aqueous-based liquid embolic system which utilises a polymerising mechanism. The polymerising system is based on a PVA macromonomer delivered as an aqueous solution which polymerises on contact with an initiator. In order to impart radiopacity to the polymerising material, the PVA macromonomer will be modified with the radiopacifying agent TIBA used in Chapters 4 and 5 (Scheme 6.1).



*Scheme 6.1 - Gelation of radiopaque PVA macromonomer.*

The second approach to producing a solvent-free radiopaque embolic system is based on a precipitating mechanism. In contrast to formulations discussed in Chapters 4 and 5, the precipitating polymer will be delivered using water as the carrier solvent. Therefore, an alternative stimulus to initiate precipitation must be used instead of water. The proposed precipitation stimuli are ionic salts present in the blood. It is anticipated that contact of the aqueous-based polymer system with these ionic salts will result in precipitation of the polymer from the aqueous carrier solvent due to interaction with the ions present. The radiopaque component responsible for triggering the precipitation will be S-TIBA (previously used in Chapter 5) which will be covalently bound to PVA to produce a polyanion. It is theorised that the pendent sulfonic acid group of S-TIBA will chelate with cations, such as  $\text{Ca}^{2+}$ ,<sup>143</sup> enabling the precipitation of the radiopaque polymer to form a solid embolus (Scheme 6.2).



Scheme 6.2 - Gelation of radiopaque PVA on contact with  $\text{Ca}^{2+}$  ions.

## 6.2. Experimental

The following chemicals were used as supplied from their manufacturers; *N*-acryloyl aminoacetaldehyde dimethyl acetal (99%) from Biocompatibles UK Ltd., 2-aminoethylphosphonic acid (99%) from Sigma Aldrich, anhydrous DMSO (99.7%) from Acros Organics, ascorbic acid ( $\geq 99.0\%$ ) from Sigma Aldrich, 2,2'-azobis(2-methylpropionamide) dihydrochloride (97%) from Sigma Aldrich, 2,2-dimethoxyethylamine (99%) from Fluorochem, glycine ( $\geq 99\%$ ) from Sigma, hydrochloric acid (35% concentration) from VWR Chemicals, hydrogen peroxide (30 w/w% in  $\text{H}_2\text{O}$ ) from VWR Chemicals, iron gluconate dihydrate (94%) from Fluka Analytical, 2-mercaptoethanesulfonic acid (96%) from Alfa Aesar, methanesulfonic acid ( $\geq 99.0\%$ ) from Sigma Aldrich, 3-mercaptopropionic acid (99%) from Alfa Aesar, Mowiol® 4-88 ( $\sim 31,000 \text{ g mol}^{-1}$ , 86.7-88.7 mol% hydrolysed) from Sigma Aldrich, Mowiol® 8-88 ( $\sim 67,000 \text{ g mol}^{-1}$ , 86.7-88.7 mol% hydrolysed) from Sigma Aldrich, taurine (99%) from Alfa Aesar, triethylamine ( $\geq 99.0\%$ ) from Sigma Aldrich and 2,3,5-triiodobenzaldehyde (99.5%) from Aldlab. Acryloyl chloride ( $\geq 97\%$ , Sigma Aldrich) was distilled prior to use with hydroquinone at atmospheric pressure. The removal of solvent

was carried out under reduced pressure using a rotary evaporator.  $^1\text{H}$  and  $^{13}\text{C}$  NMR spectra were recorded at 400 MHz on a Bruker Avance III HD 400 instrument and measured coupling constants were stated in Hz to the nearest decimal place. NMR splitting abbreviations used; s = singlet, d = doublet, t = triplet, q = quartet, quin. = quintent, m = multiplet. Electrospray mass spectrometry was recorded on a Water LCT instrument.

### 6.2.1. *N*-Acryloyl aminoacetaldehyde dimethyl acetal (NAAADA)

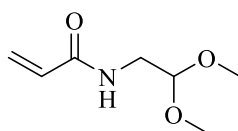


Figure 6.1 - *N*-Acryloyl aminoacetaldehyde dimethyl acetal (NAAADA).

A 20% v/v solution of acryloyl chloride (5.4 mL, 6.0 g, 66.0 mmol) in diethyl ether (27 mL) was added dropwise over 5 minutes at 0 °C to a 20% v/v solution of 2,2-dimethoxyethylamine (7.2 mL, 6.9 g, 66.0 mmol) in diethyl ether (36 mL) with triethylamine (9.2 mL, 6.7 g, 66.0 mmol) under  $\text{N}_2$  flow with magnetic stirring at 250 rpm. The reaction mixture was allowed to warm to room temperature and stirred for 2 hours. The solution was then filtered, and the collected precipitate washed with diethyl ether ( $2 \times 50$  mL). The ether solvent was removed from the filtrate in small aliquots ( $\sim 30$  mL) under reduced pressure. The product was dried overnight in vacuum desiccator. Yield = 94.0%; FT-IR  $\nu$   $\text{cm}^{-1}$  3289 and 1543 (N-H, amide), 3075 and 806 (C-H alkene), 1659 and 1626 (C=O, amide), 1543 (C=C, aromatic), 1447 and 1367 (C-H,  $\text{CH}_3$ ), 1129 (C-O, ether);  $\delta_{\text{H}}$  (400 MHz, d-DMSO) 3.38 (6H, s,  $\text{CH}_3$  alkane), 3.40 (2H, d,  $J$  5.2,  $\text{CH}_2$  alkane), 4.41 (1H, t,  $J$  5.3, CH alkane), 5.64 (1H, d of d,  $J$  10.1, CH alkene), 6.10 (1H, d,  $J$  10.1,  $\text{CH}_2$  alkene), 6.14 (1H, d,  $J$  10.1,  $\text{CH}_2$  alkene), 6.26 (1H, s, NH);  $\delta_{\text{C}}$  (400 MHz, d-DMSO) 41.0 (2  $\text{CH}_3$ ), 54.5 ( $\text{CH}(\text{OR})_2$ ), 102.6 ( $\text{CH}_2\text{NH}$ ), 126.7 (CH alkene), 130.6 ( $\text{CH}_2$  alkene), 165.0 (C=O);  $m/z$  (ES) 182.1 (40%,  $\text{MNa}^+$ );  $R_f = 0.33$  [ethyl acetate/40-60 petroleum ether (3:2)].

### 6.2.2. PVA Macromonomer

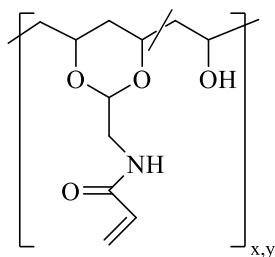


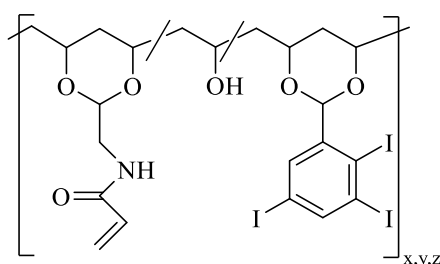
Figure 6.2 - PVA macromonomer.

Mowiol<sup>®</sup> 4-88, Mowiol<sup>®</sup> 8-88 or Mowiol<sup>®</sup> 18-88 (20.0 g) was dissolved in deionised water (140 mL) and stirred at 400 rpm using an overhead stirrer at  $50 \pm 9$  °C with N<sub>2</sub> flow in a flange reaction vessel until fully dissolved. The PVA solution was allowed to cool and once at room temperature NAAADA (0.33-6.47 g, 2.1-40.6 mmol, see Table 6.1) was added followed by the dropwise addition of concentrated HCl (11.0 mL, 13.0 g, 106 mmol). The solution was stirred at room temperature for 18 hours then adjusted to pH 7 using 2.5 M NaOH solution. The product was then purified and concentrated via tangential flow filtration (Sartorius Vivaflow 50). Yield = 67.1%;  $\delta_{\text{H}}$  (400 MHz, D<sub>2</sub>O) 1.72-1.44 (m), 1.98-2.05 (m), 3.86-4.02 (m), 4.63-4.81 (m), 5.68-5.73 (m), 6.10-6.26 (m).

Table 6.1 - Experimental details of PVA macromonomer synthesis.

Prototype	PVA Molecular Weight (kDa)	NAAADA (Eq per PVA Chain)	Mass of NAAADA (g)	Moles of NAAADA (mmol)
<b>3.1</b>		7	0.72	4.5
<b>3.2</b>	31	21	2.16	13.5
<b>3.3</b>		63	6.47	40.6
<b>3.4</b>		7	0.33	2.1
<b>3.5</b>	67	21	1.00	6.3
<b>3.6</b>		63	2.99	18.8



6.2.3. *I*-PVA MacromonomerFigure 6.3 - *I*-PVA macromonomer.

Dried PVA macromonomer (2.0 g, synthesised using parameters outline in Section 6.2.2) was dissolved in anhydrous DMSO (70 mL) and stirred at 350 rpm at  $50 \pm 9$  °C with  $N_2$  flow until fully dissolved. A solution of 2,3,5-triodobenzaldehyde (0.11 g, 0.23 mmol or 1.10 g, 2.27 mmol)(Table 6.2) in anhydrous DMSO (10 mL) was added to the PVA solution followed by methanesulfonic acid (4.4 mL, 6.5 g, 67.8 mmol). The reaction mixture was stirred at  $50 \pm 9$  °C under  $N_2$  flow for 24 hours after which the cooled solution was precipitated twice from THF ( $2 \times 500$  mL) with magnetic stirring at 600 rpm. The purified polymer was isolated and dried in a vacuum oven at 40 °C. Yield = 68-89%;  $\delta_H$  (400 MHz, d-DMSO) 1.23-1.73 (m), 1.90-2.01 (m), 3.58-3.69 (m), 3.76-3.95 (m), 3.99-4.12 (m), 4.49-4.98 (m), 5.08-5.16 (m), 5.45-5.52 (m), 5.59 (d of d,  $J$  10.7, CH alkene), 5.74-5.83 (m), 6.12 (br s, NH), 6.26 (d,  $J$  10.7,  $CH_2$  alkene), 6.30 (d,  $J$  10.7,  $CH_2$  alkene), 7.70 (s, aromatic), 8.28 (s, aromatic).

Table 6.2 - Experimental details of *I*-PVA macromonomer synthesis.

Prototype	PVA Molecular Weight (kDa)	NAAADA (Eq per PVA Chain)	TIBA (Eq per PVA Diol Group)	Yield (%)
3.7	31	7	0.01	82
3.8		21		69
3.9		63		88
3.10		7	0.1	77
3.11		21		73
3.12		63		85
3.13	67	7	0.01	80
3.14		21		82
3.15		63		89
3.16		7	0.1	84
3.17		21		75
3.18		63		73

### 6.2.4. PVA Macromonomer with Pendent Groups

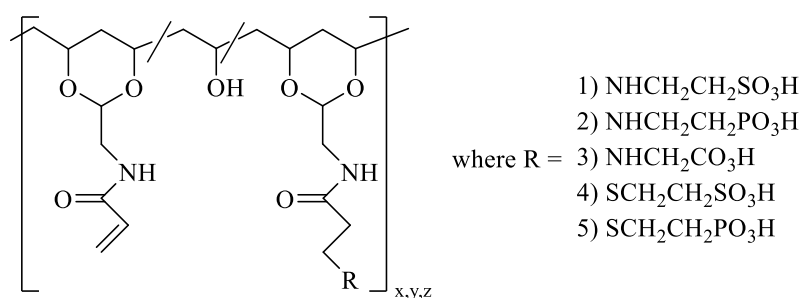


Figure 6.4 - PVA macromonomer modified with pendent groups.

PVA macromonomer (1.0 g) was dissolved in deionised water (30 mL) and magnetically stirred at 400 rpm at  $60 \pm 5$  °C with  $\text{N}_2$  flow. The polymer solution was stirred for 2 hours to ensure complete dissolution of the PVA macromonomer then the pendent group in deionised water (10 mL) was added dropwise (quantities outlined in Table 6.3). The reaction mixture was stirred at  $60 \pm 5$  °C for 24 hours. Once cooled to room temperature, the product was purified and concentrated by tangential flow filtration (Sartorius Vivaflow 50) and then precipitated twice from MeOH ( $2 \times 350$  mL) with stirring at 600 rpm. The product was isolated and dried in a vacuum desiccator.

Table 6.3 - Reaction quantities used in the modification of PVA macromonomer with hydrophilic pendent groups.

Prototype	Pendent Group	Pendent Groups (Eq to NAAADA Double Bonds)	Mass of Pendent Group (g)	Moles of Pendent Group (mmol)	Yield (%)
3.19	Taurine	10	2.54	20.3	97.1
3.21	2-aminoethylphosphonic acid	4	0.50	4.0	96.8
3.22	Glycine	10	1.50	20.0	97.8
3.20	2-mercaptoethanesulfonic acid	1	0.25	1.5	92.7
3.23	3-mercaptopropionic acid	1	0.25	2.4	89.0

### **6.2.5. Water Solubility Test**

Water solubility testing was carried out by precisely weighing between 0.2-0.3 g of PVA/I-PVA macromonomer sample. Deionised water (5.0 mL) was added to the sample and the solution heated at 50 °C for 2 hours. Upon cooling, the solution was removed and any remaining solids dried in a vacuum desiccator for 48 hours. The dried precipitate was weighed and the water solubility of the sample calculated. The process was repeated for 3 replicates of each samples along with PVA control of Mowiol® 4-88 or Mowiol® 8-88.

### **6.2.6. Gelation Test using an Azo Initiator**

PVA macromonomer (1.0 g) was dissolved in deionised water (1.4 mL) and degassed for 5 minutes under N<sub>2</sub> flow with magnetic stirring. The initiator 2,2'-azobis(2-methylpropionamide) dihydrochloride (8 mg, 0.03 mmol) was added and the solution stirred at room temperature until gelation was observed.

### **6.2.7. Gelation Test using Redox Initiators**

A polymer solution was prepared by dissolving PVA macromonomer in deionised water (2-20 w/w%). Stock solutions were prepared using iron gluconate dihydrate (0.2 g, 0.4 mmol), ascorbic acid (0.73 g, 4.1 mmol) and hydrogen peroxide (4.2 mL, 4.7 g, 3.7 mmol) in deionised water (10 mL each). A reductant solution was prepared by the addition of iron gluconate dihydrate (40 µL) and ascorbic acid (32 µL) to an aliquot of the PVA macromonomer solution (0.75 mL). An oxidant solution was prepared by the addition of 4.15 M hydrogen peroxide (32 µL) to a separate aliquot of the PVA macromonomer solution (0.75 mL). The reductant and oxidant solutions were drawn into two 1 mL syringes and connected by a 3-way connector. The syringe plungers pushed back and forth for 5 minutes or until gelation occurred.

### 6.2.8. PVA Modified with S-TIBA

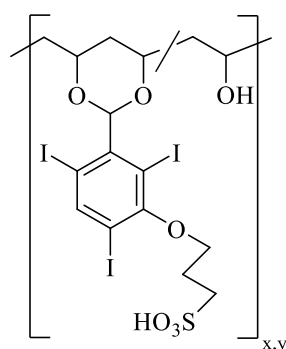


Figure 6.5 - PVA macromonomer modified with S-TIBA.

Mowiol® 8-88 (4 g) was dissolved in anhydrous DMSO (120 mL) in a flange reaction vessel and stirred at 350 rpm using an overhead stirrer for at  $50 \pm 9$  °C with  $N_2$  flow until fully dissolved. A solution of 3-(2,4,6-triiodo-5-formylphenoxy)-1-propanesulfonic acid (0.71-2.82 g, 1.1-4.5 mmol) in anhydrous DMSO (20 mL) was degassed for 10 minutes and then added dropwise to the PVA solution. After 5 minutes, methanesulfonic acid (8.8 mL, 13.0 g, 136 mmol) was added dropwise and the reaction mixture stirred at  $50 \pm 9$  °C for 24 hours. Once cooled to room temperature, the polymer was precipitated twice into ethyl acetate ( $2 \times 500$  mL) and the collected precipitate washed with further ethyl acetate (30mL). The product was collected by centrifugation and then dried in a vacuum oven at 40 °C. Yield = 91%;  $\delta_H$  (400 MHz, d-DMSO) 1.27-1.74 (m), 1.93-2.00 (m), 3.75-3.94 (m), 4.15-4.24 (m), 4.41-4.49 (m), 4.63-4.69 (m), 8.28 (s, aromatic).

### 6.2.9. Precipitation Test with $Ca^{2+}$

Ringer's solutions was prepared by dissolving sodium chloride (7.2 g, 123 mmol), potassium chloride (0.37 g, 4.9 mmol) and calcium chloride (0.17 g, 1.5 mmol) in deionised water (1 L) and the pH adjusted to 7.4. The polymer sample synthesised in Section 6.2.8 was dissolved in deionised water (20 w/w%). The sample (0.5 mL) was added to Ringer's solution (60 mL) and stirred at room temperature with magnetic stirring at 250 rpm. Calcium chloride was added to

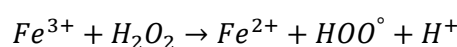
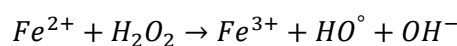
the solution until precipitation of the polymer was observed and the mass of calcium chloride used was recorded.

### 6.3. Results and Discussion

#### 6.3.1. Approach 1: In Situ Polymerising Embolic

Liquid embolics functioning by a polymerising mechanism are an attractive approach due to the ability to tailor the polymerisation time to suit the timeframe required to form a solid embolus *in situ*. Polymerising systems can be delivered by first pre-mixing the polymerising component with an initiator prior to delivery with a microcatheter. However, this limits the time over which the liquid embolic can be delivered and poses the risk of microcatheter blockage if the embolic is not delivered into the vasculature before polymerisation occurs. Another delivery method that can be used is a dual-lumen microcatheter which allows the separation of the reacting components until exiting the microcatheter where they are permitted to mix and polymerise *in situ* within the vasculature.

LiquiGel™ is a non-toxic polymerising system in the Biocompatibles UK Ltd. portfolio developed for use as a liquid embolic.<sup>144</sup> The polymerising system consists of Nelfilcon™, a PVA macromonomer, which polymerises under the redox conditions of the Fenton reaction by the generation of highly reactive hydroxyl and hydroperoxyl radicals (Equation 6.1). The macromonomer solution can be delivered as an aqueous solution using a dual-lumen microcatheter allowing the oxidant and reductant reacting components to be kept separate during delivery. Upon delivery into the vasculature the reactive components mix to initiate *in situ* polymerisation of the macromonomer (Figure 6.6).



Equation 6.1 - Radical formation in redox driven superoxide Fenton reaction.

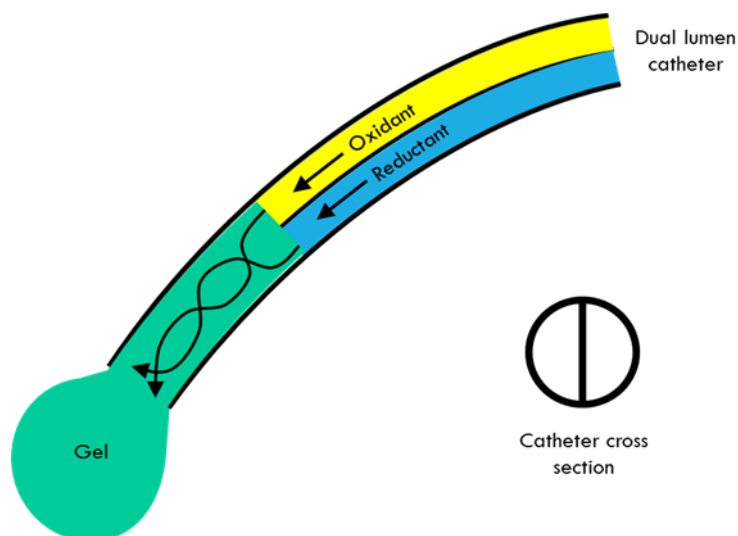


Figure 6.6 - Delivery of LiquiGel™ using a dual-lumen microcatheter.

The LiquiGel™ formulation is non-radiopaque in nature and hence must be delivered alongside contrast agent to enable temporary visualisation of the embolisation procedure. However, the radiopacity imparted by the contrast agent during the procedure is not retained due to the diffusion of contrast agent from the site. Therefore, an inherently radiopaque version of LiquiGel™ is proposed in which the PVA macromonomer system is modified using the radiopaque group TIBA in order to impart long-term radiopacity to the system (Figure 6.7). The system will be tested using a range of PVA macromonomer formulations, polymer concentrations and redox initiator concentrations to evaluate the suitability of the materials to behave as a radiopaque liquid embolic.

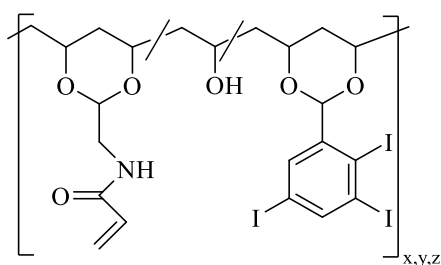
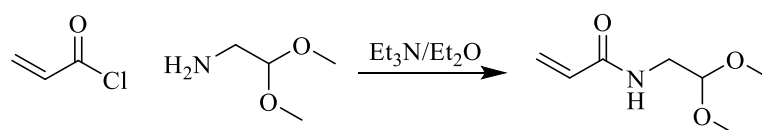


Figure 6.7 - I-PVA macromonomer.

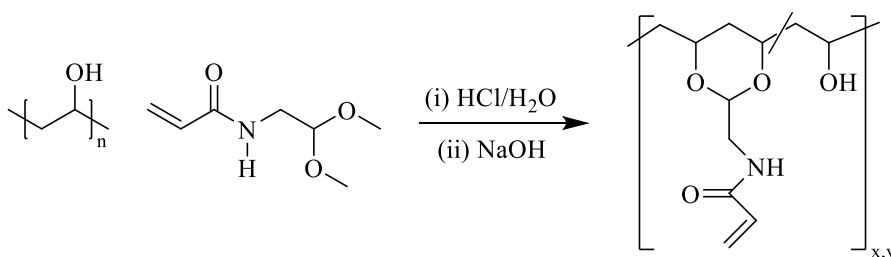
### 6.3.1.1. Preparation of PVA macromonomer

The crosslinker NAAADA, required for the preparation of the PVA macromonomer, was prepared by reaction of 2,2-dimethoxyethylamine with acryloyl chloride under anhydrous conditions (Scheme 6.3). The reaction was carried out using 20 w/w% solutions of the reactants in diethyl ether to maintain a solution of appropriate viscosity to allow for magnetic stirring. The product was isolated in a high yield of 94% providing sufficient sample for initial feasibility tests after which NAAADA was sourced from Biocompatibles UK Ltd.



Scheme 6.3 - Synthesis of *N*-acryloyl aminoacetaldehyde dimethyl acetal (NAAADA).

The NAAADA crosslinker group was used in the preparation of the PVA macromonomer at PVA molecular weights of 31 kDa and 67 kDa. The PVA macromonomer synthesis was carried out by an acid catalysed transacetalisation reaction in which the crosslinker group was covalently bound to the PVA backbone (Scheme 6.4). The reaction was carried out targeting 7, 21 or 63 double bond equivalents per PVA chain to provide varying degrees of crosslinking opportunities between the PVA chains. Upon completion, the reaction mixture was neutralised to pH 7 then purified and concentrated by tangential flow filtration.



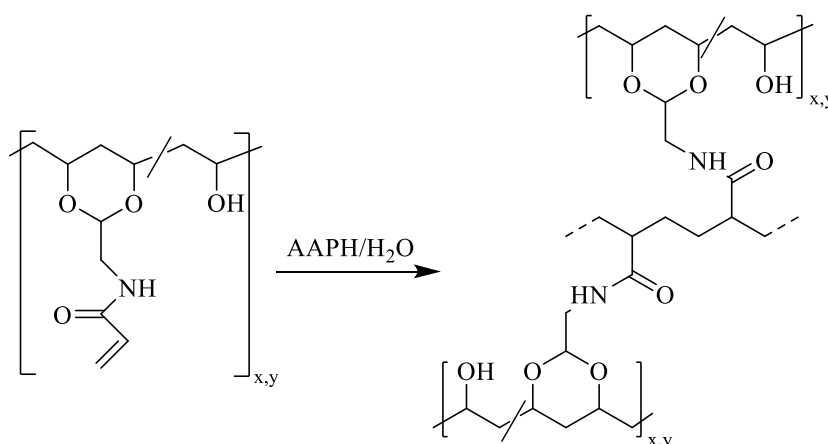
Scheme 6.4 - Synthesis of PVA macromonomer.

### 6.3.1.2. Gelation Tests

Gelation tests were performed using different initiator systems, PVA macromonomer formulations and polymer concentrations to optimise the non-iodinated PVA macromonomer system before the incorporation of the radiopaque group. The aim was to develop a suitable gelation system which could then be applied to the same polymerising system modified with TIBA.

#### 6.3.1.2.1. Azo Initiator

An initial experiment was carried out utilising an azo thermal initiator in order to ensure the ability of the PVA macromonomer prototype 3.4 (prepared using 67 kDa PVA and 7 double bond equivalents) to undergo gelation. A 70 w/w% solution of PVA macromonomer in water was reacted with the azo initiator 2,2'-azobis(2-methylpropionamide) dihydrochloride (AAPH) under a nitrogen flow (Scheme 6.5). Successful gelation of the reaction mixture was obtained within 1 hour. This demonstrates the capability of the PVA macromonomer to undergo gelation in the presence of radicals. However, the use of a thermal initiator limits the control of the reaction when delivered *via* a microcatheter. Additionally, AAPH is cytotoxic in nature deeming this an unviable approach to formulating an aqueous-based liquid embolic.<sup>145</sup>

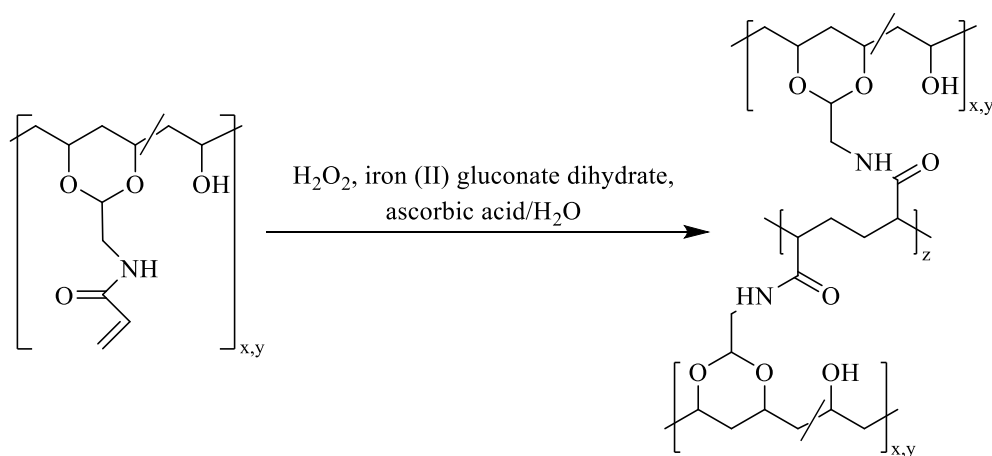


Scheme 6.5 - Synthesis of PVA gel using azo initiator.



### 6.3.1.2.2. REDOX System

Following successful gelation of the PVA macromonomer system using an azo initiator, gelation was trialled using redox initiators which would better mimic injectable materials suitable for use in therapeutic embolization. A redox system was chosen utilising hydrogen peroxide as an oxidant and iron (II) gluconate and ascorbic acid as reductants (Scheme 6.6).<sup>146,147</sup>



Scheme 6.6 - Synthesis of PVA gel using redox system.

Gelation tests were carried out at room temperature by mixing the contents of 2 syringes *via* a 3-way connector. Both syringes contained equal volumes of PVA macromonomer of the same concentration with 1 syringe containing the reductant component and the other syringe containing the oxidant component. The solutions were passed back and forth between the 2 syringes for 5 minutes or until the solutions could no longer be passed easily between the syringes and noted for any changes in viscosity which could be felt by changes in resistance when pushing the plungers. The gelation tests were carried out using various concentrations of PVA macromonomer solutions of prototype 3.4 (prepared using 67 kDa PVA and 7 double bond equivalents) and also varying amounts of oxidant and reductant components to determine the effects on gelation properties. The PVA macromonomer solution was not found to undergo gelation at room temperature under all the conditions tested and remained easily passable between the syringes following 5 minutes of mixing (Table 6.4).

Table 6.4 - Results of PVA macromonomer gelation test using REDOX initiator at room temperature ( $n=1$ ).

PVA Macromonomer Concentration (w/w%)	Volume of Stock Solution ( $\mu\text{L}$ )			Gelation Time (s)
	Iron Gluconate Dihydrate (20 mg mL <sup>-1</sup> )	Ascorbic Acid (73 mg mL <sup>-1</sup> )	Hydrogen Peroxide (4.15 M)	
10	40	32	32	No gel
	80	64	64	No gel
	120	72	96	No gel
15	40	32	32	No gel
	80	64	64	No gel
	120	72	96	No gel
20	40	32	32	No gel
	80	64	64	No gel
	120	72	96	No gel

Further gelation tests were performed using PVA macromonomer solutions pre-heated to 37 °C prior to gelation testing. Increased amounts of redox initiators were used with 160  $\mu\text{L}$  of iron gluconate dihydrate, 130  $\mu\text{L}$  of ascorbic acid and 130  $\mu\text{L}$  of hydrogen peroxide added to the polymer solutions. A range of polymer concentrations were tested from 10-50 w/w% in water to investigate the impact of concentration on the gelation properties. The PVA macromonomer solutions were found to undergo gelation at 37 °C for solutions of 30 w/w% or higher in water (

Table 6.5). This suggests there is a critical concentration and temperature after which gelation of the PVA macromonomer solution occurs. The number of double bond equivalents was also found to influence the onset of gelation with no gelation observed for the PVA macromonomer prototype 3.4 prepared using 7 double bond equivalents and formulated at 20 w/w% in water whereas gelation was observed for the same PVA macromonomer concentration when prepared using 63 double bond equivalents for prototype 3.6.

Table 6.5 - Results of PVA macromonomer gelation test using REDOX initiator at 37 °C (n=1).

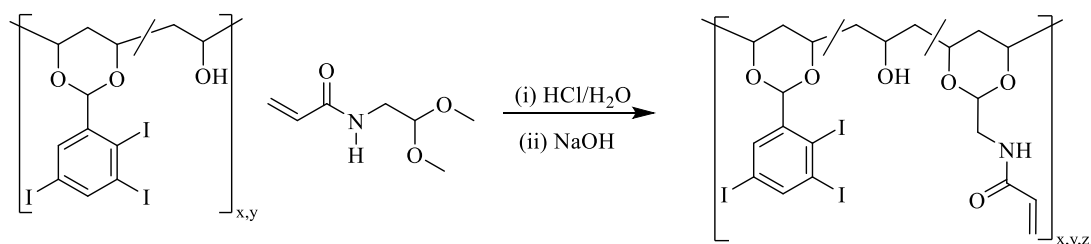
Prototype	Double Bonds (Eq per PVA Chain)	PVA	Gelation Time (s)
		Macromonomer Concentration (w/w%)	
3.4	7	10	No gel
		20	No gel
		30	7
		40	6
		50	4
3.6	63	10	No gel
		20	6
		30	3
		40	2
		50	1

The results of gelation testing using the non-iodinated PVA macromonomer system highlights the requirement of using PVA macromonomers of suitable double bond equivalents and concentration in water. For PVA macromonomer formulations prepared using 7 double bond equivalents of NAAADA, a minimum concentration of 30 w/w% should be used in order to ensure gel formation. Whereas, for PVA macromonomers prepared using 63 double bond equivalents of NAAADA, a lower concentration of 20 w/w% can be used whilst still ensuring gel formation. Hence, these parameters should be utilised for the PVA macromonomer system modified with the radiopaque group TIBA using the same redox system and concentrations.

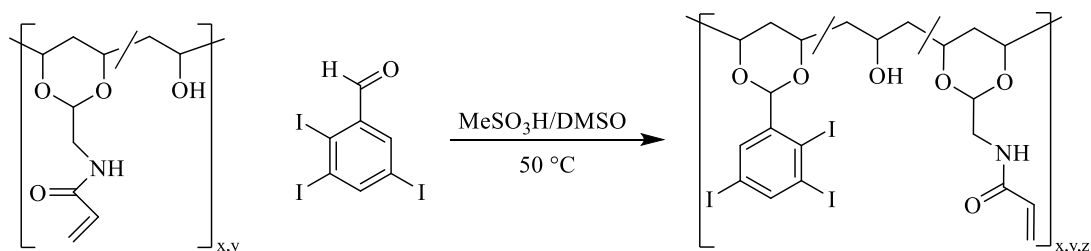
### 6.3.1.3. *Modification of PVA Macromonomer with Radiopaque Substituent*

The polymerising PVA macromonomer system discussed in the previous section was modified with TIBA in order to impart radiopacity. Synthesis of the iodinated PVA (I-PVA) macromonomer was initially trialled by an acid catalysed transacetalisation reaction between I-PVA prepared using 0.01 equivalents of TIBA to PVA diol groups (synthesis outlined in Chapter 4 Section 4.2.2) with the NAAADA crosslinking group (Scheme 6.7). The reaction was carried out using the same reaction conditions utilised for the preparation of PVA macromonomer. However, after allowing the reaction mixture to be stirred overnight it was

noted that a large proportion of polymer was seen to have precipitated out of solution. This was likely due to the poor solubility of I-PVA in the reaction solvent water (as demonstrated in the water solubility testing of I-PVA samples in Chapter 4, Section 4.3.3.1). Hence, the preparation of the I-PVA macromonomer was instead performed by reaction of PVA macromonomer with TIBA to avoid the reduced water solubility of the I-PVA macromonomer affecting the progress of the reaction by instead carrying out the reaction in DMSO (Scheme 6.8).



Scheme 6.7 - Initial synthetic route for the preparation of I-PVA macromonomer.



Scheme 6.8 - Preferred synthetic route for the preparation of PVA macromonomer.

The produced I-PVA macromonomer was purified by precipitation from the non-solvents THF or methanol depending on the level of iodination of I-PVA used. This synthetic route was used for the preparation of all subsequent synthesis of I-PVA macromonomer with different PVA molecular weights, numbers of double bonds and equivalents of TIBA to PVA diol groups (Table 6.6).

Table 6.6 - Formulation of PVA macromonomer prototypes.

Prototype	Molecular Weight (kDa)	Double Bonds (Eq per PVA Chain)	TIBA (Eq to PVA Diol Groups)
3.7	31	7	0.01
3.8		21	
3.9		63	
3.10		7	0.1
3.11		21	
3.12		63	
3.13	67	7	0.01
3.14		21	
3.15		63	
3.16		7	0.1
3.17		21	
3.18		63	

### 6.3.1.3.1. Gelation Testing of I-PVA Macromonomer

Gelation tests were performed for the prepared I-PVA macromonomers investigating the impact of PVA molecular weight, number of double bond equivalents and number of TIBA equivalents. The gelation system, previously optimised for the PVA macromonomer formulations, was modified for use with the I-PVA macromonomers. Reductant solutions of iron gluconate dihydrate (160  $\mu\text{L}$ , 20  $\text{mg mL}^{-1}$ ) and ascorbic acid (130  $\mu\text{L}$ , 73  $\text{mg mL}^{-1}$ ) were used alongside an oxidant solution of hydrogen peroxide (130  $\mu\text{L}$ , 4.15 M). Equal volumes of I-PVA macromonomer solutions (0.7 mL) were separately mixed with the oxidant and reductant components and pre-heated to 37 °C. Concentrations of 2 and 5 w/w% of the I-PVA macromonomer in water were used due to the poor water solubilities of the samples meaning the concentrations of 20-30 w/w% used for the non-iodinated PVA macromonomer solution could not be achieved. Each polymer solution was drawn into a syringe and mixed between the syringes using a 3-way connector. Whilst mixing, the solutions were observed for any signs of gelation and the time by which gelation occurred was noted (Table 6.7 and Table 6.8). It should be noted that insufficient sample was available for gelation testing of prototypes 3.13 and 3.16.

Table 6.7 - Gelation results of PVA macromonomers synthesised using 0.01 equivalents of TIBA at 37 °C.

Prototype	PVA Molecular Weight (kDa)	Double Bonds (Eq per PVA Chain)	I-PVA Macromonomer Concentration in Water (w/w%)	Gelation Time (s)
3.7		7	2	No gel
			5	No gel
3.8	31	21	2	No gel
			5	2 s – formed viscous lq
3.9		63	2	No gel
			5	1 s – formed viscous lq
3.13		7	2	-
			5	-
3.14	67	21	2	No gel
			5	1s – formed viscous lq
3.15		63	2	No gel
			5	1 s – formed viscous lq

Table 6.8 - Gelation results of PVA macromonomers synthesised using 0.1 equivalents of TIBA at 37 °C.

Sample	PVA Molecular Weight (kDa)	Double Bonds (Eq per PVA Chain)	I-PVA Macromonomer Concentration in Water (w/w%)	Gelation Time (s)
3.10		7	2	No gel
			5	No gel
3.11	31	21	2	No gel
			5	No gel
3.12		63	2	No gel
			5	1 s – formed viscous lq
3.16		7	2	-
			5	-
3.17	67	21	2	No gel
			5	No gel
3.18		63	2	1 s – formed viscous lq
			5	1 s – formed viscous lq

The results of the gelation study did not show any of the I-PVA macromonomers to form a gel at either 0.01 or 0.1 equivalents of TIBA when tested as 2 or 5 w/w% solutions in water. Several samples, particularly those of high double bond equivalents formulated as more

concentrated solutions of 5 w/w% in water, were observed to rapidly become more viscous in nature on mixing the oxidant and reductant macromonomer solutions. This suggests gelation of these samples did occur but due to the dilute nature of the macromonomer solutions used, the excess of liquid present resulted in gels of poor mechanical properties.

#### **6.3.1.3.2. Water Solubility Study of I-PVA Macromonomer**

The introduction of the highly hydrophobic radiopaque group TIBA to the polymerising PVA macromonomer system resulted in the inability to form aqueous polymer solutions of more than 5 w/w%. As demonstrated with the PVA macromonomer system, the formation of gels was found to be dependent on the concentration of PVA macromonomer in solution with 30 w/w% concentrations required for PVA macromonomer of 7 double bond equivalents and 20 w/w% concentrations required for PVA macromonomer of 63 double bond equivalents. Hence, in order to achieve radiopaque gels using this system, the water solubility of I-PVA macromonomer in water must be improved to attain aqueous solutions of higher concentrations.

In order to understand the factors influencing the water solubility of the I-PVA macromonomers, water solubility tests were performed. The solubility testing was performed by investigating a range of factors including the molecular weight of PVA, number of double bond equivalents and TIBA equivalents. In the preparation of the samples over different molecular weights of PVA, Mowiol® 4-88 and Mowiol® 8-88 were used which are 31 kDa and 67 kDa respectively. The use of these commercially sourced polymers meant that the initial degree of hydrolysis of the acetyl groups was kept the same across all samples at 88%. Maintaining identical levels of hydrolysis over all samples synthesised meant that comparisons could be made without the additional factor of the degree of hydrolysis effecting the water solubility.



Water solubility tests were carried out for all formulations of PVA, PVA macromonomer (strength and lab temperature.

Table 6.9) and I-PVA macromonomer (Table 6.10 and Table 6.11) samples to determine the change in water solubility of the polymer throughout the processing to form I-PVA macromonomers. The water solubility was determined by weighing out a known amount of each sample (between 0.2 and 0.3 g) into a vial. Deionised water (5.00 mL) was then added to the samples and the solutions heated at 50 °C for 2 hours. The solution was then allowed to cool and the liquid removed. Any remaining sample was dried in a vacuum desiccator for 48 hours to obtain a measurement of the dry mass. This was repeated for 3 replicates of each sample along with a PVA control for each time the test was carried out to account for any variation in water purity, vacuum strength and lab temperature.

Table 6.9 - Water solubility results of PVA macromonomers (n=3).

Prototype	PVA Molecular Weight (kDa)	Double Bonds (eq to PVA chain)	Water Solubility (mg mL <sup>-1</sup> )	Standard deviation (mg mL <sup>-1</sup> )
<b>Mowiol® 4-88</b>		0	47.1	12.7
<b>3.1</b>	31	7	44.0	0.2
<b>3.2</b>		21	51.5	3.7
<b>3.3</b>		63	11.5	0.6
<b>Mowiol® 8-88</b>		0	29.8	5.0
<b>3.4</b>	67	7	22.2	0.7
<b>3.5</b>		21	28.9	N/A
<b>3.6</b>		63	24.1	1.7

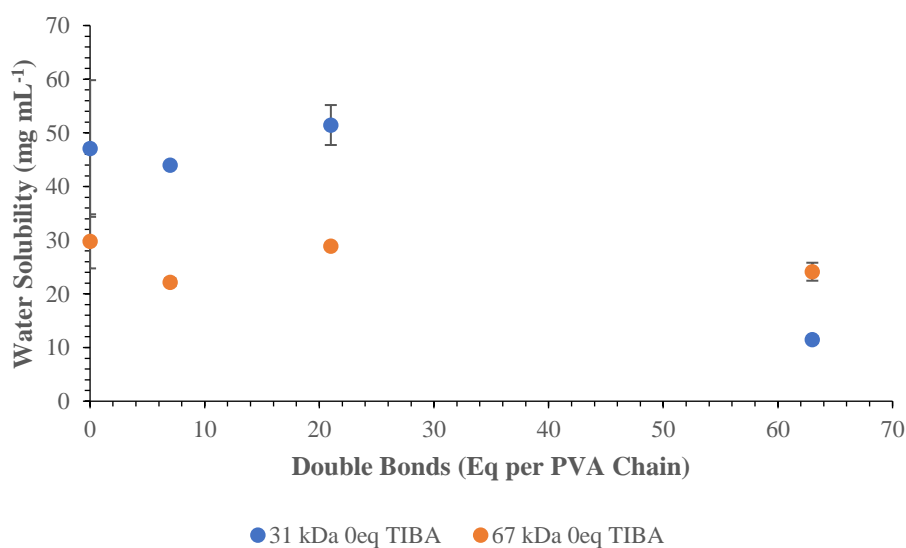
Table 6.10 - Water solubility results of I-PVA macromonomers synthesised using 0.01 equivalents of TIBA (n=3).

Sample	PVA Molecular Weight (kDa)	Double Bonds (kDa)	Water Solubility (mg mL <sup>-1</sup> )	Standard deviation (mg mL <sup>-1</sup> )
<b>I-PVA</b>		0	53.9	0.6
<b>3.7</b>	31	7	38.6	0.7
<b>3.8</b>		21	19.3	0.7
<b>3.9</b>		63	22.6	0.6
<b>I-PVA</b>		0	35.5	0.9
<b>3.13</b>	67	7	11.9	0.0
<b>3.14</b>		21	24.6	1.9
<b>3.15</b>		63	23.4	2.0

Table 6.11 - Water solubility results of I-PVA macromonomers synthesised using 0.1 equivalents of TIBA ( $n=3$ ).

Sample	PVA Molecular weight (kDa)	Double Bonds (eq to PVA Chain)	Water Solubility ( $\text{mg mL}^{-1}$ )	Standard deviation ( $\text{mg mL}^{-1}$ )
<b>I-PVA</b>	31	0	18.3	0.5
<b>3.10</b>		7	3.6	0.7
<b>3.11</b>		21	11.0	0.2
<b>3.12</b>		63	28.5	2.9
<b>I-PVA</b>	67	0	2.6	0.1
<b>3.16</b>		7	11.0	0.1
<b>3.17</b>		21	12.4	0.1
<b>3.18</b>		63	20.2	0.4

Comparison of the results for the PVA macromonomers synthesised using PVA of molecular weight 67 kDa, indicates similar water solubilities are not directly related to the number of double bond equivalents (Figure 6.8). The PVA macromonomer synthesised using PVA of molecular weight 31 kDa with 63 double bond equivalents was noted to have a low water solubility in comparison to the other PVA macromonomers of the same molecular weight. This could possibly be explained by interactions between the chains becoming more favourable due to the high number of equivalents of NAAADA groups and an increasing hydrophobicity with higher portions of cross-linker.

Figure 6.8 - Comparison of water solubility results for PVA macromonomer samples prepared using 31 & 67 kDa PVA ( $n=3$ ).

Comparison of the results for the I-PVA macromonomers synthesised at different iodination levels of 0, 0.01 and 0.1 equivalents of TIBA indicates a general trend of decreasing water solubility with iodination at 0.01 equivalents of TIBA and further reductions with iodination at 0.1 equivalents of TIBA in comparison to the non-iodinated PVA macromonomer when double bond equivalents of 21 or fewer were used. This trend was consistent for the I-PVA macromonomer samples synthesised using Mowiol 4-88 (Figure 6.9) and Mowiol 8-88 (Figure 6.10). The water solubility results of I-PVA macromonomers synthesised using 63 double bond equivalents were found to be similar across all levels of iodination. This suggests the iodination level of the I-PVA macromonomer to have little impact on the aqueous solubility as the number of double bond equivalents is more influential in these samples.

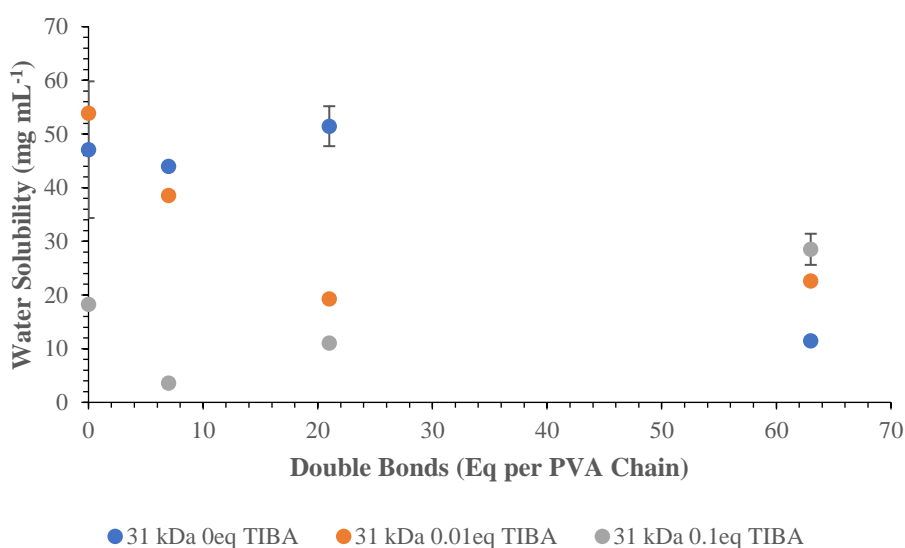


Figure 6.9 - Comparison of water solubility results for I-PVA macromonomer samples synthesised at 0, 0.01 & 0.1 eq of TIBA for 31 kDa PVA ( $n=3$ ).

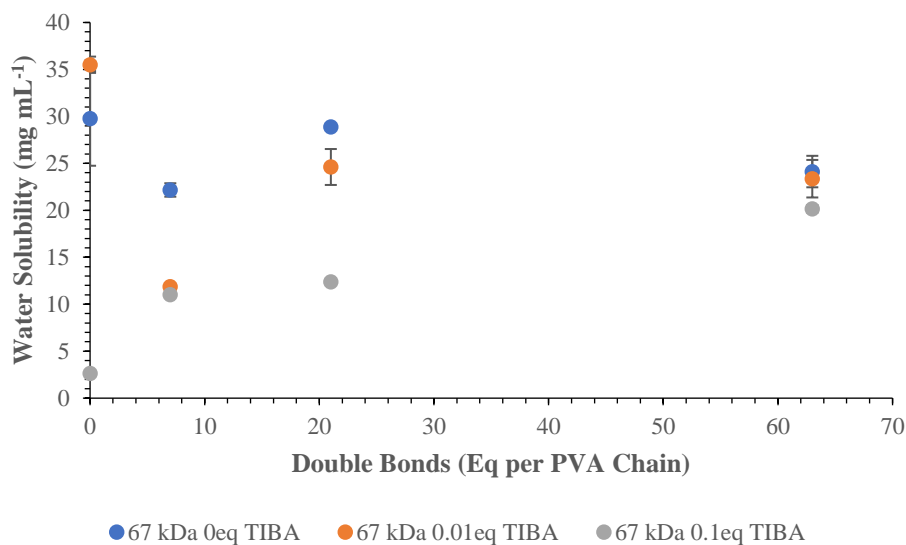


Figure 6.10 - Comparison of water solubility results for I-PVA macromonomer samples synthesised at 0, 0.01 & 0.1 eq of TIBA for 67 kDa PVA ( $n=3$ ).

Comparison of the results for the Mowiol 4-88 samples, shows a trend throughout the processing from PVA macromonomer to I-PVA macromonomer with decreasing water solubilities observed for increasing levels of iodination when using PVA macromonomers of 7 and 21 double bond equivalents (Figure 6.11). The I-PVA macromonomer prepared using 63 double bond equivalents was found to exhibit an increasing water solubility with higher levels of iodination. This is perhaps due to the high number of double bonds per PVA chain interrupting the hydrogen bonding between PVA chains, thereby increasing the water solubility as iodination increases which interrupts the hydrogen bonding further.

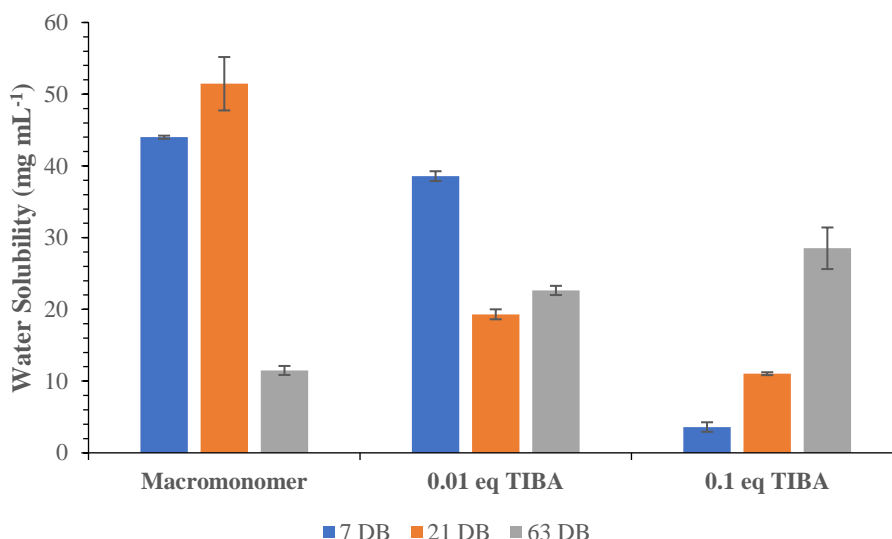


Figure 6.11 - Comparison of water solubility results during the preparation of I-PVA macromonomer synthesised using 31 kDa PVA over 7-63 double bond equivalents ( $n=3$ ).

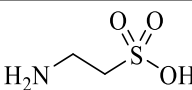
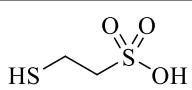
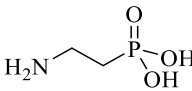
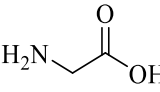
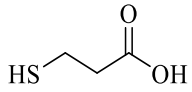
In general, water solubility testing of the PVA macromonomer and I-PVA macromonomer samples has indicated that the molecular weight of PVA used in the formulation has a large influence with higher water solubilities exhibited for lower polymer molecular weights. The use of higher equivalents of TIBA was found to reduce the aqueous solubility due to the increasing amounts of the hydrophobic radiopaque group. Investigation of the number of double bond equivalents used was observed to have a variable effect on the water solubility of the samples with higher solubilities for samples prepared using 63 double bond equivalents at the highest iodination level of 0.1 equivalent. These insights into the water solubility of the I-PVA macromonomer with lower molecular weights, reduced iodination levels and high numbers of double bond equivalents suggests the water solubility of the samples can be optimised. However, small improvements in water solubility would still not achieve the concentrations required to achieve suitable concentrations for gelation.

#### 6.3.1.4. *Modification of PVA Macromonomer with Hydrophilic Groups*

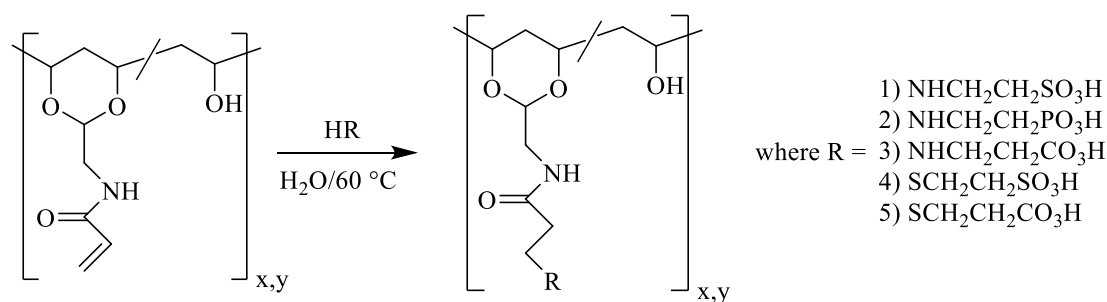
To overcome the difficulties experienced with formulating higher concentrations of I-PVA macromonomer solutions in water, a series of experiments were carried out in which the PVA

macromonomer was modified with various hydrophilic groups. The tests were performed using PVA macromonomer as a model for the I-PVA macromonomer system due to the lower cost of materials to prepare the non-iodinated macromonomer in comparison to the I-PVA macromonomer. Hydrophilic groups were chosen with either sulfonic acid, carboxylic acid or phosphonic acid end-groups and either amine or thiol linker groups (Table 6.12). The use of amine and thiol linkers allowed the hydrophilic groups to be covalently bound to the PVA macromonomer *via* a portion of NAAADA crosslinker groups.

Table 6.12 - Hydrophilic groups used in the modification of PVA macromonomers.

	<b>Amine linker</b>	<b>Thiol linker</b>
<b>Sulfonic acid</b>	 Taurine	 2-Mercaptoethanesulfonic acid
<b>Phosphonic acid</b>	 2-Aminoethylphosphonic acid	-
<b>Carboxylic acid</b>	 Glycine	 3-Mercaptopropionic acid

All modifications using hydrophilic groups were performed using PVA macromonomer synthesised using Mowiol® 8-88 and 63 double bond equivalents of NAAADA. The high number of NAAADA equivalents per PVA chain used in the PVA macromonomer preparation allowed a portion of these NAAADA groups to be targeted whilst preserving the crosslinking ability of the PVA macromonomer during gelation. Modification of the PVA macromonomer with the hydrophilic groups was performed by a self-catalysed Michael addition reaction for the amine linker groups and a base catalysed Michael addition reaction using triethylamine for the thiol linker groups (Scheme 6.9).<sup>148</sup> The reaction mixtures were allowed to stir for 24 hours and then neutralised to pH 7 before purification and concentration by tangential flow filtration from water.



Scheme 6.9 - Incorporation of hydrophilic groups onto PVA macromonomer.

#### 6.3.1.4.1. Water Solubility Testing of Modified PVA Macromonomers

Solubility testing of the modified PVA macromonomers was carried out to determine the impact on the resulting macromonomers solubility in water (Table 6.13). The water solubility tests were carried out following the same procedure as outlined for PVA macromonomers (Section 6.2.5). The only variation was the lower masses used, between 0.08 and 0.12 g of each sample, due to the small scale on which the modification reactions were performed.

Table 6.13 - Water solubility results of modified PVA macromonomers ( $n=3$ ).

Prototype	Incorporated Hydrophilic Group		Water Solubility ( $\text{mg mL}^{-1}$ )	Standard Error of Mean ( $\text{mg mL}^{-1}$ )
	Linker Group	Anionic Group		
3.6	None	None	29.8	5.0
3.19	Amine	Sulfonic acid	4.4	0.1
3.20		Phosphonic acid	0.3	0.1
3.21		Carboxylic acid	1.2	1.5
3.22	Thiol	Sulfonic acid	-0.1	0.5
3.23		Carboxylic acid	1.1	0.1

The results of the testing shows the water solubility of the macromonomer samples to be reduced following modification with the hydrophilic groups (Figure 6.12). Hence, further solubility testing was carried out instead using PBS to determine whether ionic interaction of the hydrophilic end-groups was preventing the polymer from dispersing in solution (Table 6.14).

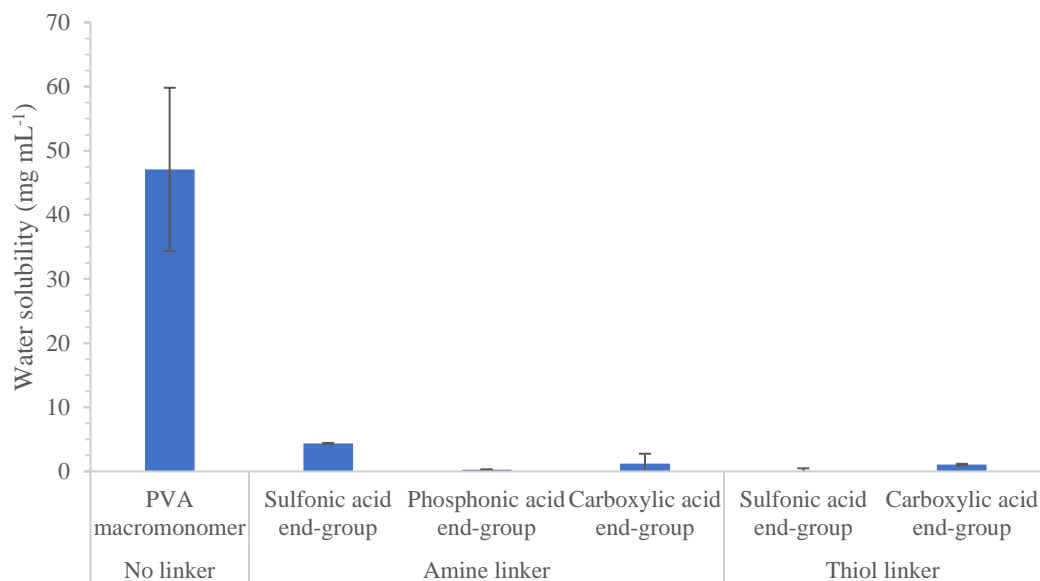


Figure 6.12 - Comparison of water solubility results for PVA macromonomer and PVA macromonomers modified with hydrophilic groups ( $n=3$ ).

Table 6.14 - Solubility results of modified PVA macromonomers in PBS ( $n=3$  where sufficient sample).

Prototype	Incorporated hydrophilic group		PBS solubility (mg mL <sup>-1</sup> )	Standard Error of Mean (mg mL <sup>-1</sup> )
	Linker group	Anionic group		
3.6	None	None	24.7	0.7
3.19	Amine	Sulfonic acid	-0.3	N/A
3.2		Phosphonic acid	1.4	1.1
3.21		Carboxylic acid	-5.6	0.6
3.22	Thiol	Sulfonic acid	-7.3	N/A
3.23		Carboxylic acid	2.9	1.1

Similar results were obtained for solubility testing in PBS as those found when testing in deionised water (Figure 6.13). A number of samples were found to have negative values



suggesting incomplete drying of the samples following solubility testing giving rise to an increase in mass.

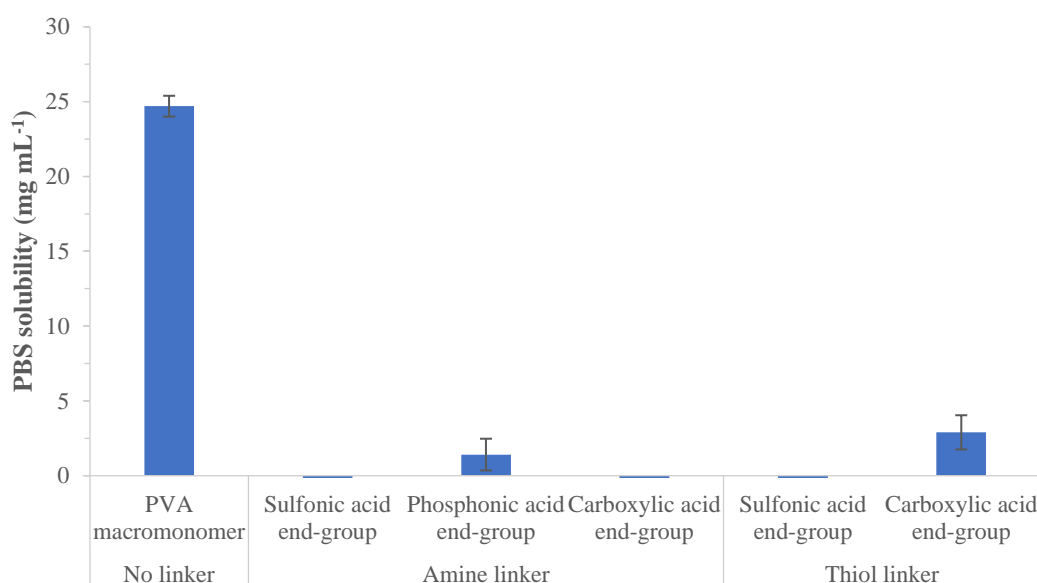


Figure 6.13 - Comparison of PBS solubility results for PVA macromonomer and PVA macromonomers modified with hydrophilic groups.

The results of PBS solubility testing indicates that ionic factors were not limiting the dispersion of the modified PVA macromonomers in solution. Instead, the modified PVA macromonomers were likely to have undergone crosslinking during the reaction with the hydrophilic groups. This was confirmed by testing in DMSO in which all samples were seen to swell indicating the formation of physically crosslinked structures (Table 6.15).

Table 6.15 - Solubility results of modified PVA macromonomers in DMSO ( $n=1$ ).

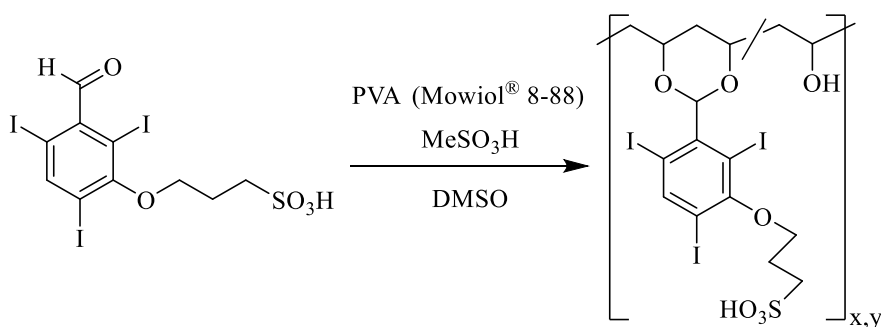
Sample	Incorporated Hydrophilic Group		Solubility in DMSO
	Linker Group	Anionic Group	
3.6	None	None	Soluble
3.19	Amine	Sulfonic acid	Swelled
3.20		Phosphonic acid	Swelled
3.21		Carboxylic acid	Swelled
3.22	Thiol	Sulfonic acid	Swelled
3.23		Carboxylic acid	Swelled

### 6.3.2. Approach 2: Precipitating Embolic

An alternative approach to producing a water-based radiopaque liquid embolic is by a precipitating mechanism. In a precipitating system, the radiopaque polymer must be water soluble and precipitate on contact with an external stimulus. The system proposed here is based on PVA modified with the radiopaque group S-TIBA to form polyanions (previously used in Chapter 5). The presence of a sulfonic acid pendent group on the radiopaque group imparts dual functionality to the S-TIBA group in that it provides radiopacity and a precipitation stimuli-responsive group. The sulfonic acid end-group is theorised to chelate with cations present in the blood including  $\text{Ca}^{2+}$  which will be used in the testing of this system. It is predicted that contact of the solubilised radiopaque polymer with  $\text{Ca}^{2+}$  ions will result in precipitation of the polymer due to chelation with the  $\text{Ca}^{2+}$  ions causing charge shielding between sulfonic acid end-groups and ionic cross-linking.

### 6.3.3. Modification of PVA with a Water Soluble Radiopaque Substituent

PVA (Mowiol 8-88) was modified using the radiopaque group S-TIBA (synthesised in Chapter 5) targeting modification of 0.1 of the PVA diol groups. This was carried out by an acid catalysed acetalisation reaction to bind the S-TIBA moieties to the PVA backbone by cyclic acetal bonds (Scheme 6.10). Following purification, the radiopaque polymer was formulated as a 20 w/w% solution in deionised water.



Scheme 6.10 - Modification of PVA with S-TIBA.

#### **6.3.4. Precipitation Test with Calcium Chloride**

Precipitation testing of the aqueous S-TIBA/PVA system (0.5 mL) was initially performed using Ringer's solution (60 mL) due to the comparable calcium concentrations of the isotonic salt solution to blood.<sup>149</sup> However, precipitation of the polymer was not observed on addition to Ringer's solution. Hence, further precipitation tests were trialled using Ringer's solutions with additional CaCl<sub>2</sub> of 25, 50 and 100 w/w% with respect to the original CaCl<sub>2</sub> concentration of Ringer's solution. Addition of the aqueous polymer solution to these calcium enriched solutions did not yield precipitates for any of the solutions tested. Precipitation of the system was instead induced by addition of CaCl<sub>2</sub> to the aqueous polymer solution (0.5 mL) in Ringer's solution (60 mL) with continuous stirring (Figure 6.14). A total of 1.19 g of CaCl<sub>2</sub> was required to induce precipitation which equates to a greater than a thousand-fold increase in the mass of Ca<sup>2+</sup> ions in comparison to Ringer's solution. It would be possible to deliver this aqueous system into the vasculature using a dual lumen-microcatheter injecting the solubilised radiopaque polymer and high concentration CaCl<sub>2</sub> solution separately. However, the mass of CaCl<sub>2</sub> required to induce polymer precipitation would likely be toxic if injected into the body.<sup>150</sup> Hence, this system would not be safe to use as a liquid embolic system.



*Figure 6.14 - Image of precipitate formed after excess addition of CaCl<sub>2</sub> to Ringer's solution.*

## 6.4. Conclusions

Two approaches for producing an aqueous-based radiopaque liquid embolic system have been discussed in this chapter, both of which have been deemed unsuitable for use as liquid embolics. The first system outlined was based on a polymerising system of PVA macromonomer. However, it was found that addition of the radiopaque group TIBA resulted in poor water solubility of the resulting I-PVA macromonomer. Addition of hydrophilic groups to the formulation in an attempt to offset the hydrophobicity imparted by the radiopaque group was trialled using a variety of hydrophilic groups with sulfonic acid, carboxylic acid or phosphonic acid end-groups and either amine or thiol linker groups. However, the incorporation of these groups resulted in gelation of the macromonomer system. Hence, this system was not seen as suitable for further development as a liquid embolic system due to the inability to form aqueous solutions of high enough concentration to yield suitable gel properties.

A precipitating system was utilised in the second approach to produce an aqueous-based radiopaque liquid embolic. In this approach PVA was modified with the charged radiopaque S-TIBA which functioned as the stimuli-responsive group to facilitate precipitation on contact with  $\text{Ca}^{2+}$  ions. The polyanion was found to precipitate on addition of a large excess of  $\text{Ca}^{2+}$  ions, however the amount of additional  $\text{CaCl}_2$  required to induce precipitation would likely be toxic if injected into the body. Therefore, this formulation would not be safe for use in an embolisation procedure.

## **Chapter Seven**

### **7. Conclusions & Outlook**

## 7.1. Conclusions & Outlook

The toolkit of embolic products used in therapeutic embolisation is vast and varied, ranging from mechanical devices to sclerosing agents.<sup>59</sup> Therapeutic embolisation using liquid agents is well established with the common use of Onyx<sup>®</sup> and cyanoacrylate glues. The field of liquid embolic materials has gained much interest in recent years with the development of numerous liquid embolics including Squid<sup>™</sup>,<sup>151</sup> PHIL<sup>®</sup>,<sup>89</sup> Easyx<sup>™90</sup> and GPX<sup>91,92</sup> reported since the start of this PhD project with many more undergoing development.<sup>96-98</sup>

This thesis has detailed the development process of inherently radiopaque *in situ* gelling materials. The development of materials with permanent radiopacity addresses the clinical need for intra-procedural and post-procedural feedback of the embolic material location which has been identified for embolic microspheres in recent years with the development of DC Bead LUMI<sup>™</sup> by Biocompatibles UK Ltd.<sup>152</sup> The inherent radiopacity of the developed liquid embolic prototypes alleviates the need to pre-mix the materials with radiopacifying agents prior to delivery which is a limitation in the use of Onyx<sup>®71</sup> and ensures long-term visualisation of the implanted embolic post-procedure which is not observed with the use of cyanoacrylate glues due to the loss of radiopaque contrast agent over time.<sup>153</sup>

Different approaches have been discussed towards the preparation of a potential radiopaque liquid embolic. The developed prototypes have been evaluated using the characterisation methods outlined in Chapter 2 and an X-ray imaging method outlined in Chapter 3. The development of tailored characterisation test methods enabled the evaluation of the potential systems for the properties required to function as a liquid embolic agent by replicating the varying aspects of an embolisation procedure from injection to solidification within the vasculature. These test methods provided an initial indication of liquid embolic performance to screen prototypes before any prospective testing in animal models. The development of an X-ray imaging method by microCT allowed the radiopacity of the materials to be quantified at higher resolutions than the X-ray imaging methods used clinically for embolisation

procedures. This provided insight into the expected imaging properties of the radiopaque materials if they were to be used in therapeutic embolisation.

An *in situ* gelling system which functioned by a precipitation mechanism was first investigated as a method for producing a radiopaque liquid embolic. The system was based on PVA modified with the radiopacifying group TIBA and formulated in the carrier solvent DMSO. A range of variables were investigated in Chapter 4 including the number of TIBA equivalents to PVA diol groups, PVA molecular weight and radiopaque polymer concentration in DMSO. It was found that the liquid embolic properties could be tailored depending on the number of TIBA equivalents, molecular weight of PVA and concentration in DMSO. The demonstration of the fulfilment of a number of key attributes required for the material to successfully function as a radiopaque liquid embolic permitted a patent application to be filed based on the system developed (filed by Biocompatibles UK Ltd., 29/06/2018, GB201810784).

The properties of the radiopaque liquid embolic prototypes developed in Chapter 4 were further modified in Chapter 5 by the incorporation of alternative radiopaque groups in combination with TIBA. The radiopaque group S-TIBA was used in the formulation as a more hydrophilic radiopaque group and IBA was used as a less hydrophobic group in comparison to TIBA. It was found that incorporation of these alternative radiopaque groups in small amounts (up to 25%) in combination with TIBA could regulate a number of the delivery and precipitate properties of the formulations allowing the liquid embolic properties to be tuned. The use of the alternative radiopaque groups at portions of 50% or higher resulted in properties that were no longer suitable as potential liquid embolic materials. This highlights the influence of the hydrophobicity and hydrophilicity of the radiopaque groups used on the performance of the liquid embolic prototypes.

In order to formulate this system as a viable product, further product development and animal testing would be required. All delivery tests discussed in this thesis were performed using 2.4 Fr microcatheters (0.67 mm internal diameter), hence further testing would be required using DMSO-compatible microcatheters of different sizes, types and brands to assess the

performance of the liquid embolic system under different delivery conditions. It is also important to evaluate the delivery properties of the system when delivered by different operators and using various injection techniques as this is likely to impact the type of embolic plug formed and embolisation efficiency. The delivery data discussed in this thesis has been attained using bench-top tests which were developed to replicate the conditions of therapeutic embolisation, hence evaluation of the system in animal models is required to assess the performance of the system *in vivo*. The samples used for *in vivo* testing would need to be appropriately sterilised before injection into an animal model. Sterilisation of liquid embolic samples based on the precipitating system was performed by Biocompatibles UK Ltd. under autoclave conditions. Following the autoclaving process, the liquid embolic samples were found to be less viscous (internal data on file). Therefore, characterisation of the liquid embolic samples before and after sterilisation would be needed to determine the changes in the materials and evaluate whether suitable liquid embolic properties are maintained following sterilisation.

The precipitating radiopaque system developed has been demonstrated to possess promising properties for use as an inherently radiopaque liquid embolic material with tuneable properties depending on the formulation used. However, the radiopaque polymer must be delivered using DMSO as the carrier solvent which presents the issue of vasospasm if the solvent is injected too quickly into the vasculature.<sup>76</sup> DMSO is also used as a carrier solvent in the liquid embolic formulations of Onyx<sup>®</sup>, Squid<sup>™</sup>, PHIL<sup>®</sup> and Easyx<sup>™</sup>. However, there is a clinical desire to move towards solvent-free formulations as identified by feedback gathered from *The Global Embolization Symposium and Technologies, May 2018*. Aqueous based liquid embolic formulations alleviate the need to inject solvent into the vasculature. Examples of aqueous based systems undergoing development include GPX, Instylla's Hydrogel Embolic System, silk elastin protein polymers and shear thinning biomaterials. However, there is the limitation of these systems in that they do not possess inherent radiopacity and must be pre-mixed with radiopacifying agents. If the aqueous system is pre-mixed with contrast agent, the gradual



diffusion of contrast agent from the injection site means the implanted embolic is not visible post-procedure.<sup>153</sup> In the case of aqueous systems which are delivered as a suspension with micronised tantalum powder, this raises the issues of streak artefact on imaging<sup>154</sup> and appearance of a tattooing effect if the implantation site is located close to the surface of the skin as is often observed with the use of Onyx<sup>®</sup>.<sup>125</sup>

Two distinct approaches were trialled into formulating aqueous based radiopaque *in situ* gelling materials. The first approach utilised a polymerising system consisting of a PVA macromonomer modified with TIBA to impart radiopacity to the system. It was found that the addition of the radiopacifying group to the polymer system resulted in a large reduction in water solubility. This led to the inability to produce aqueous radiopaque macromonomer solutions of sufficient concentration to form gels using redox initiation at 37 °C. Water solubility testing of various radiopaque PVA macromonomer formulations was performed. However, the water solubility could not be improved sufficiently to produce solutions of the concentrations required to form distinct gels. Modifications to the PVA macromonomer system were made using hydrophilic groups, either with sulfonic acid, carboxylic acid or phosphonic acid end-groups and either amine or thiol linker groups. These were bound by Micheal addition reactions to a portion of the macromonomer crosslinker groups in an attempt to improve the water solubility of the polymers. However, following modification with these hydrophilic groups it was found that all macromonomer samples had crosslinked under the reaction conditions used. Hence, this approach to producing an aqueous based radiopaque liquid embolic using a PVA macromonomer system was not deemed suitable for further development. Success with this system would require a water soluble radiopaque group, such as S-TIBA, to ensure sufficient concentrations can be achieved to produce distinct radiopaque gels.

The second approach investigated involved the modification of PVA with the radiopaque group S-TIBA. This group provided dual-functionality as a radiopacifying group and also a precipitation stimuli in the presence of Ca<sup>2+</sup> ions due to chelation with the pendent sulfonic

acid end-group. Successful precipitation of the radiopaque polyanion from an aqueous solution was noted after the addition of a large excess of  $\text{CaCl}_2$ . However, the amount of  $\text{Ca}^{2+}$  ions required to induce precipitation of the radiopaque polymer would likely be toxic if injected into the vasculature.<sup>150</sup> Hence, this approach was deemed unsafe for further development as a radiopaque liquid embolic.

There are numerous other potential polymer systems that could be used in the formulation of an aqueous based radiopaque *in situ* gelling material which are beyond the scope of this PhD project. These systems include *in situ* gelling materials which function by a phase transitioning mechanism such as poly(*N*-isopropylacrylamide)(PNIPAm) based microgels. PNIPAm microgels undergo a phase transition in response to changes in temperature and pH.<sup>155</sup> This is unlike linear chain PNIPAm which is solely temperature responsive<sup>156</sup> and therefore not suitable for pursuing as a liquid embolic agent due to the likelihood of gelation during delivery through a microcatheter. PNIPAm microgels have been shown to exhibit a volume phase transition temperature (VPTT) below which the hydrophilic polymer particles are swollen with water molecules due to the favourable hydrogen bonding between the amide groups of PNIPAm and water molecules. Above the VPTT, polymer-polymer interactions become more favourable resulting in the expulsion of water and deswelling of the microgels. If tuned to physiologically temperatures, this would result in reduced particle sizes as the material is delivered through a microcatheter allowing facile injection into the vasculature. Contact of the PNIPAm microgels with salt, such as the ionic conditions present in blood, causes flocculation of the particles due to the screening of the charged chain end group imparted by the polymerisation initiator groups which previously provided electrostatic stabilisation.<sup>157</sup> The propensity of PNIPAm microgels to undergo these changes at temperatures and pHs similar to those of physiological values makes them ideal candidates for pursuing in the development of an aqueous based liquid embolic as aggregation only occurs above the VPTT in the presence of salts. Hence, this avoids premature gelation within the microcatheter in which temperatures are likely to be above the VPTT.

Initial investigation into using a PNIPAm based system was carried out by Fiona Revell, a final year MChem student in 2017. The work involved the copolymerisation of NIPAm monomer with the radiopaque monomer 2,3,5-triodobenzoyloxyethyl propenamide to form a radiopaque PNIPAm based microgel based on the dual-responsive microgels reported by Town et al.<sup>158</sup> The radiopaque microgels produced exhibited a more gradual reduction in particle diameter on increasing temperatures to physiological value in comparison to the sharp change observed for the bland PNIPAm microgel above its VPTT. Flocculation of the particles was observed in the presence of salts above 34 °C suggesting dual-responsive behaviour. Radiopacity of the system was confirmed with a measured value of 712 HU which is unlikely to be of sufficient contrast to be identified if injected into the body. The system requires further work to increase the radiopacity of the microgel and further study the temperature and pH response at physiological values. Once optimised the system would require testing using methods replicating the conditions of an embolisation procedure to evaluate any embolic properties.

Another potential approach to formulating a solvent-free radiopaque liquid embolic is to utilise polyelectrolyte complexes as is the case for the GPX formulation.<sup>91</sup> The previously synthesised PVA modified with the radiopaque group S-TIBA could be used alongside a cationic polymer such as poly(3-(methacryloylamino)propyl-trimethylammonium chloride). This creates the possibility of the complexation of the oppositely charged polymer complexes on destabilisation of the electrostatic charges under decreasing salt concentrations. The resulting aggregated gel formed would have inherent radiopacity due to the S-TIBA radiopaque group thereby offering an advantage over the non-radiopaque GPX.

## 7.2. References

- 1 W. Brinjikji, D. F. Kallmes and R. Kadirvel, *Am. J. Neuroradiol.*, 2015, **36**, 1216–1222.
- 2 J. van Beijnum, H. B. van der Worp, D. R. Buis, R. Shahi Salman, L. J. Kappelle, G. J. E. Rinkel, J. W. B. van der Sprenkel, W. P. Vandertop, A. Algra and C. J. M. Klijn, *JAMA*, 2011, **306**, 2011–9.
- 3 P. Soyer, A. Dohan, R. Dautry, Y. Guerrache, A. Ricbourg, E. Gayat, M. Boudiaf, M. Sirol and O. Ledref, *Cardiovasc. Intervent. Radiol.*, 2015, **38**, 1068–81.
- 4 X. Cheng, P. Sun, Q.-G. Hu, Z.-F. Song, J. Xiong and Q.-C. Zheng, *J. Cancer Res. Clin. Oncol.*, 2014, **140**, 1159–70.
- 5 T. K. Helmberger, T. F. Jakobs and M. F. Reiser, *Abdom. Imaging*, **29**, 267–77.
- 6 B. Seibert, R. P. Tummala, R. Chow, A. Faridar, S. A. Mousavi and A. A. Divani, *Front. Neurol.*, 2011, **2**, 45.
- 7 C. Witt, B. Schmidt, A. Geisler, A. . Borges, M. John, I. Fietze and P. Romaniuk, *Eur. J. Cancer*, 2000, **36**, 1949–1954.
- 8 D. Wei, C. Wei, S. Huang, Q. Lin and Y. Wang, *Pakistan J. Med. Sci.*, 2013, **29**, 1334–7.
- 9 R. T. Higashida, V. V Halbach, C. F. Dowd, S. L. Barnwell and G. B. Hieshima, *Radiology*, 1991, **178**, 663–70.
- 10 T. H. Lee, C. H. Choi, K.-P. Park, S. M. Sung, S. W. Lee, B.-H. Lee, D. H. Kim, H. J. Kim, C. W. Kim and S. Kim, *Am. J. Neuroradiol.*, 2005, **26**, 1375–80.
- 11 R. I. White, K. H. Barth, S. L. Kaufman, V. DeCaprio and J. D. Strandberg, *Cardiovasc. Intervent. Radiol.*, 1980, **3**, 229–241.
- 12 N. M. deSouza and J. F. Reidy, *Clin. Radiol.*, 1992, **46**, 170–175.

- 13 P. Yu-Tang Goh, M. Lin, N. Teo and D. En Shen Wong, *Cardiovasc. Intervent. Radiol.*, **25**, 17–25.
- 14 R. López-Benítez, G. M. Richter, H.-U. Kauczor, S. Stampfl, J. Kladeck, B. A. Radeleff, M. Neukamm and P. J. Hallscheidt, *Cardiovasc. Intervent. Radiol.*, 2009, **32**, 615–622.
- 15 T. W. I. Clark, *Semin. Intervent. Radiol.*, 2006, **23**, 119–25.
- 16 T. Sorimachi, T. Koike, S. Takeuchi, T. Minakawa, H. Abe, K. Nishimaki, Y. Ito and R. Tanaka, *Am J Neuroradiol*, 1999, **20**, 1323–1328.
- 17 J. R. Bauer and C. E. Ray, *Semin. Intervent. Radiol.*, 2004, **21**, 11–22.
- 18 H. T. Abada, *Tech. Vasc. Interv. Radiol.*, 2007, **10**, 257–260.
- 19 W. O. Bank and C. W. Kerber, *AJR. Am. J. Roentgenol.*, 1979, **132**, 299–301.
- 20 J. D. Barr, T. J. Lemley and C. N. Petrochko, *J. Vasc. Interv. Radiol.*, **9**, 113–8.
- 21 C. Derdeyn, V. Graves, M. Salamat and A. Rappe, *Am. J. Neuroradiol.*, 1997, **18**, 647–653.
- 22 T. Katsumori and T. Kasahara, *Cardiovasc. Intervent. Radiol.*, **29**, 1077–83.
- 23 J.-P. Pelage, A. Laurent, M. Wassef, M. Bonneau, D. Germain, R. Rymer, P. Flaud, J. Martal and J.-J. Merland, *Radiology*, 2002, **224**, 436–45.
- 24 R. T. Andrews and C. A. Binkert, *J. Vasc. Interv. Radiol.*, 2003, **14**, 1311–1316.
- 25 A. Chatziioannou, D. Gargas, K. Malagari, I. Kornezos, I. Ioannidis, E. Primetis, H. Moschouris, A. Gouliamos and D. Mourikis, *Eur. J. Radiol.*, 2012, **81**, 2308–2312.
- 26 F. Xie, J. Zang, X. Guo, F. Xu, R. Shen, L. Yan, J. Yang and J. He, *J. Cancer Res. Clin. Oncol.*, 2012, **138**, 455–462.
- 27 A. Forner, M. Reig and J. Bruix, *Lancet*, 2018, **391**, 1301–1314.

- 28 J. B. Spies, *Semin. Intervent. Radiol.*, 2013, **30**, 340–6.
- 29 S. Lin, K. Hoffmann and P. Schemmer, *Liver Cancer*, 2012, **1**, 144–158.
- 30 D. Nicolini, G. Svegliati-Baroni, R. Candelari, C. Mincarelli, A. Mandolesi, I. Bearzi, F. Mocchegiani, A. Vecchi, R. Montalti, A. Benedetti, A. Risaliti and M. Vivarelli, *World J. Gastroenterol.*, 2013, **19**, 5622–32.
- 31 I. W. Graziadei, H. Sandmueller, P. Waldenberger, A. Koenigsrainer, K. Nachbaur, W. Jaschke, R. Margreiter and W. Vogel, *Liver Transpl.*, 2003, **9**, 557–63.
- 32 J. Doucet, L. Kiri, K. O’Connell, S. Kehoe, R. J. Lewandowski, D. M. Liu, R. J. Abraham and D. Boyd, *J. Funct. Biomater.*, 2018, **9**, 14–38.
- 33 R. Dhanasekaran, D. A. Kooby, C. A. Staley, J. S. Kauh, V. Khanna and H. S. Kim, *J. Surg. Oncol.*, 2010, **101**, 476–480.
- 34 K. V. Sharma, Z. Bascal, H. Kilpatrick, K. Ashrafi, S. L. Willis, M. R. Dreher and A. L. Lewis, *Biomaterials*, 2016, **103**, 293–304.
- 35 R. Duran, K. Sharma, M. R. Dreher, K. Ashrafi, S. Mirpour, M. Lin, R. E. Scherthaner, T. R. Schlachter, V. Tacher, A. L. Lewis, S. Willis, M. den Hartog, A. Radaelli, A. H. Negussie, B. J. Wood and J.-F. H. Geschwind, *Theranostics*, 2016, **6**, 28–39.
- 36 J. Alòs Villacrosa, P. Carreño, J. A. López, B. Estadella, M. Serra-Prat and J. Marinello, *Eur. J. Vasc. Endovasc. Surg.*, 2006, **31**, 101–107.
- 37 N. P. Munro, S. Woodhams, J. D. Nawrocki, M. S. Fletcher and P. J. Thomas, *BJU Int.*, 2003, **92**, 240–244.
- 38 R. F. Latshaw, R. L. Pearlman, B. M. Schaitkin, J. W. Griffith and W. A. Weidner, *Cardiovasc. Intervent. Radiol.*, 1985, **8**, 24–30.
- 39 J. Y. Sim, J. C. Alejos and J. W. Moore, *J. Interv. Cardiol.*, 2003, **16**, 425–448.

- 40 Y. J. Cho and J. H. Shin, *Springerplus*, 2016, **5**, 299–306.
- 41 K. H. Yoo, S.-J. Lee and S. H. Jeon, *J. Endourol.*, 2008, **22**, 2559–2563.
- 42 T.-S. Seo, J. H. Oh, Y. Yoon, J. W. Lim, S. J. Park, S.-G. Chang and Y. H. Jeon, *Cardiovasc. Intervent. Radiol.*, 2000, **23**, 177–181.
- 43 S.-H. Chung, M. Lee, K. S. Kim, S. I. Kim, J. Y. Won, D. Y. Lee and K.-H. Lee, *Cardiovasc. Intervent. Radiol.*, 2011, **34**, 1236–1243.
- 44 J. Croffie, L. Somogyi, R. Chuttani, J. DiSario, J. Liu, D. Mishkin, R. J. Shah, W. Tierney, L. M. Wong Kee Song and B. T. Petersen, *Gastrointest. Endosc.*, 2007, **66**, 1–6.
- 45 S. E. R. Horbach, M. M. Lokhorst, P. Saeed, C. M. F. de Gouyon Matignon de Pontouraude, A. Rothová and C. M. A. M. van der Horst, *J. Plast. Reconstr. Aesthetic Surg.*, 2016, **69**, 295–304.
- 46 T.-S. Seo, J. H. Oh, Y. Yoon, J. W. Lim, S. J. Park, S.-G. Chang and Y. H. Jeon, *Cardiovasc. Intervent. Radiol.*, 2000, **23**, 177–181.
- 47 T. Yonemitsu, N. Kawai, M. Sato, T. Sonomura, I. Takasaka, M. Nakai, H. Minamiguchi, S. Sahara, Y. Iwasaki, T. Naka and M. Shinozaki, *Cardiovasc. Intervent. Radiol.*, 2010, **33**, 1192–1197.
- 48 T. Yonemitsu, N. Kawai, M. Sato, H. Tanihata, I. Takasaka, M. Nakai, H. Minamiguchi, S. Sahara, Y. Iwasaki, Y. Shima, M. Shinozaki, T. Naka and M. Shinozaki, *J. Vasc. Interv. Radiol.*, 2009, **20**, 1176–1187.
- 49 R. Lencioni, *Hepatology*, 2010, **52**, 762–773.
- 50 L. Pierot, C. Cognard, D. Herbreteau, H. Fransen, W. J. van Rooij, E. Boccardi, A. Beltramello, N. Sourour, K. Kupcs, A. Biondi, A. Bonafé, W. Reith and A. Casasco, *Eur. Radiol.*, 2013, **23**, 2838–2845.

- 51 E. J. Speir, R. M. Ermentrout and J. G. Martin, *Tech. Vasc. Interv. Radiol.*, 2017, **20**, 258–262.
- 52 A. J. Ringer and R. Rahme, in *Cerebrovascular and Endovascular Neurosurgery*, Springer International Publishing, Cham, 2018, pp. 321–333.
- 53 J. C. Gentric, J. Raymond, A. Batista, I. Salazkin, G. Gevry and T. E. Darsaut, *Am. J. Neuroradiol.*, 2015, **36**.
- 54 R. J. Rosen and S. Contractor, *Semin. Intervent. Radiol.*, 2004, **21**, 59–66.
- 55 M. F. Brothers, J. C. Kaufmann, A. J. Fox and J. P. Deveikis, *Am. J. Neuroradiol.*, 1989, **10**, 777–86.
- 56 R. I. White, J. V. Strandberg, G. S. Gross, K. H. Barth, T. F. Groves and F. Starr, *Radiology*, 1977, **125**, 677–687.
- 57 H. V. Vinters, K. A. Galil, M. J. Lundie and J. C. E. Kaufmann, *Neuroradiology*, 1985, **27**, 279–291.
- 58 G. Wikholm, *Am. J. Neuroradiol.*, 1995, **16**, 479–82.
- 59 S. Vaidya, K. R. Tozer and J. Chen, *Semin. Intervent. Radiol.*, 2008, **25**, 204–215.
- 60 M. J. Gounis, B. B. Lieber, A. K. Wakhloo, R. Siekmann and L. N. Hopkins, *Am. J. Neuroradiol.*, 2002, **23**, 938–44.
- 61 H. Hill, J. F. B. Chick, A. Hage and R. N. Srinivasa, *Diagn. Interv. Radiol.*, 2018, **24**, 98–103.
- 62 Y. Takeuchi, H. Morishita, Y. Sato, S. Hamaguchi, N. Sakamoto, H. Tokue, T. Yonemitsu, K. Murakami, H. Fujiwara, K. Sofue, T. Abe, H. Higashihara, Y. Nakajima and M. Sato, *Jpn. J. Radiol.*, 2014, **32**, 500–517.
- 63 J. S. Pollak and R. I. White, *J. Vasc. Interv. Radiol.*, 2001, **12**, 907–913.



- 64 The n-BCA Trial Investigators, *Am. J. Neuroradiol.*, 2002, **23**, 748–755.
- 65 H. Oowaki, S. Matsuda, N. Sakai, T. Ohta, H. Iwata, A. Sadato, W. Taki and N. Hashimoto, *Biomaterials*, 2000, **21**, 1039–1046.
- 66 J. D. Barr, E. J. Hoffman, B. R. Davis, K. A. Edgar and C. R. Jacobs, *J. Vasc. Interv. Radiol.*, 1999, **10**, 165–168.
- 67 R. J. Komotar, E. R. Ransom, D. A. Wilson, E. S. Connolly, S. D. Lavine and P. M. Meyers, *Neurosurgery*, 2006, **59**, 464–469.
- 68 J. Mathis, A. Evans, A. DeNardo, K. Kennett, J. Crandall, M. Jensen and J. Dion, *Am. J. Neuroradiol.*, 1997, **18**, 1087–1091.
- 69 B. C. Flores, A. P. See, G. M. Weiner, B. T. Jankowitz, A. F. Ducruet and F. C. Albuquerque, *J. Neurosurg.*, 2019, **130**, 675–1038.
- 70 S. Paramasivam, D. Altschul, S. Ortega-Gutierrez, J. Fifi and A. Berenstein, *J. Neurointerv. Surg.*, 2015, **7**, 458–461.
- 71 Micro Therapeutics, *Onyx Liquid Embolic System - Instructions for Use*, 2003.
- 72 S. Luzzi, M. Del Maestro, D. Bongetta, C. Zoia, A. V. Giordano, D. Trovarelli, S. Raysi Dehcordi and R. J. Galzio, *World Neurosurg.*, 2018, **116**, 340–353.
- 73 W. J. van Rooij, M. Sluzewski and G. N. Beute, *Am. J. Neuroradiol.*, 2007, **28**, 172–177.
- 74 R. Siekmann, *Interv. Neuroradiol.*, 2005, **11**, 131–40.
- 75 R. Ashour and M. Ali Aziz-Sultan, *Neurol. Res.*, 2014, **36**, 363–367.
- 76 J. C. Chaloupka, F. Vinuela, H. V. Vinters and J. Robert, *Am. J. Neuroradiol.*, 1994, **15**, 1107–1115.
- 77 J. C. Chaloupka, D. C. Huddle, J. Alderman, S. Fink, R. Hammond and H. V. Vinters,

- Am. J. Neuroradiol.*, 1999, **20**, 401–410.
- 78 W. Taki, Y. Yonekawa, H. Iwata, A. Uno, K. Yamashita and H. Amemiya, *Am. J. Neuroradiol.*, 1990, **11**, 163–168.
- 79 T. Terada, Y. Nakamura, K. Nakai, M. Tsuura, T. Nishiguchi, S. Hayashi, T. Kido, W. Taki, H. Iwata and N. Komai, *J. Neurosurg.*, 1991, **75**, 655–60.
- 80 Center for Devices and Radiological Health, *Safety Communications - Catheter Entrapment with the ev3 Onyx Liquid Embolic System: FDA Safety Communication*, Center for Devices and Radiological Health, 2015.
- 81 J. B. Jia, C. S. Green, A. J. Cohen and M. Helmy, *Clin. Radiol.*, 2015, **70**, 326–332.
- 82 J. M. Llovet, M. I. Real, X. Montaña, R. Planas, S. Coll, J. Aponte, C. Ayuso, M. Sala, J. Muchart, R. Solà, J. Rodés and J. Bruix, *Lancet*, 2002, **359**, 1734–1739.
- 83 T. de Baère, A. Denys, R. Briquet, P. Chevallier, J. Dufaux and A. Roche, *J. Vasc. Interv. Radiol.*, 1998, **9**, 305–310.
- 84 T. de Baere, X. Zhang, B. Aubert, G. Harry, C. Lagrange, J. Ropers, J. Dufaux, J. Lumbroso, P. Rougier, M. Ducreux and A. Roche, *Radiology*, 1996, **201**, 731–735.
- 85 C. Georgiades, J. F. Geschwind, N. Harrison, A. Hines-Peralta, E. Liapi, K. Hong, Z. Wu, I. Kamel and C. Frangakis, *Radiology*, 2012, **265**, 115–123.
- 86 K. Takayasu, Y. Shima, Y. Muramatsu, N. Moriyama, T. Yamada, M. Makuuchi, H. Hasegawa and S. Hirohashi, *Radiology*, 1987, **163**, 345–351.
- 87 J. Mason, C. Dodge and G. Benndorf, *Interv. Neuroradiol.*, 2018, **24**, 574–579.
- 88 R. Pop, L. Mertz, A. Ilyes, D. Mihoc, J. S. Richter, M. Manisor, S. Kremer and R. Beaujeux, *J. Neurointerv. Surg.*, 2019, **11**, 706–709.
- 89 D. F. Vollherbst, C. M. Sommer, C. Ulfert, J. Pfaff, M. Bendszus and M. A. Möhlenbruch, *Am. J. Neuroradiol.*, 2017, **38**, 1377–1382.

- 90 Z. Kulcsár, A. Karol, P. W. Kronen, P. Svende, K. Klein, O. Jordan and I. Wanke, *Eur. Radiol.*, 2017, **27**, 1248–1256.
- 91 R. J. Stewart, C. S. Wang, I. T. Song and J. P. Jones, *Adv. Colloid Interface Sci.*, 2017, **239**, 88–96.
- 92 J. P. Jones, M. Sima, R. G. O’Hara and R. J. Stewart, *Adv. Healthc. Mater.*, 2016, **5**, 795–801.
- 93 M. Johnson, in *Global Embolization Symposium and Technologies*, 2018.
- 94 S. Ganguli, in *Global Embolization Symposium and Technologies*, 2018.
- 95 S. Ganguli, in *Global Embolization Symposium and Technologies*, 2018.
- 96 J. Cappello, J. . Crissman, M. Crissman, F. . Ferrari, G. Textor, O. Wallis, J. . Whitledge, X. Zhou, D. Burman, L. Aukerman and E. . Stedronsky, *J. Control. Release*, 1998, **53**, 105–117.
- 97 Z. Megeed, M. Haider, D. Li, B. W. O’Malley, J. Cappello and H. Ghandehari, *J. Control. Release*, 2004, **94**, 433–445.
- 98 A. Poursaid, R. Price, A. Tiede, E. Olson, E. Huo, L. McGill, H. Ghandehari and J. Cappello, *Biomaterials*, 2015, **57**, 142–152.
- 99 R. K. Avery, H. Albadawi, M. Akbari, Y. S. Zhang, M. J. Duggan, D. V Sahani, B. D. Olsen, A. Khademhosseini and R. Oklu, *Sci. Transl. Med.*, 2016, **8**, 156–168.
- 100 K. Ashrafi, Y. Tang, H. Britton, O. Domenge, D. Blino, A. J. Bushby, K. Shuturminska, M. den Hartog, A. Radaelli, A. H. Negussie, A. S. Mikhail, D. L. Woods, V. Krishnasamy, E. B. Levy, B. J. Wood, S. L. Willis, M. R. Dreher and A. L. Lewis, *J. Control. Release*, 2017, **250**, 36–47.
- 101 B. Biocompatibles UK Ltd, *DC Bead LUMI Radiopaque Embolic Drug-Eluting Bead - Instructions For Use*, 2018.

- 102 A. Fakhari and J. Anand Subramony, *J. Control. Release*, 2015, **220**, 465–475.
- 103 L. I. Karsh, E. T. Gross, C. M. Pieczonka, P. J. Aliotta, C. J. Skomra, L. E. Ponsky, P. T. Nieh, M. Han, D. A. Hamstra and N. D. Shore, *Urology*, 2018, **115**, 39–44.
- 104 K. van Gysen, A. Kneebone, F. Alfieri, L. Guo and T. Eade, *J. Med. Imaging Radiat. Oncol.*, 2014, **58**, 511–516.
- 105 A. Komemushi, N. Tanigawa, Y. Okuda, H. Kojima, H. Fujii, Y. Shomura, M. Sougawa and S. Sawada, *Acta radiol.*, 2002, **43**, 186–191.
- 106 K. Sugiu, K. Kinugasa, S. Mandai, K. Tokunaga and T. Ohmoto, *J. Neurosurg.*, 1995, **83**, 531–8.
- 107 F. Duffner, R. Ritz, A. Bornemann, D. Freudenstein, H. Wiendl and R. Siekmann, *Clin. Neuropathol.*, 2002, **21**, 13–17.
- 108 M. Caine, D. Carugo, X. Zhang, M. Hill, M. R. Dreher and A. L. Lewis, *Adv. Healthc. Mater.*, 2017, **6**, 1601291.
- 109 A. J. Audet-Griffin, S. Pakbaz and F. G. Shellock, *J. Neurointerv. Surg.*, 2014, **6**, 624–629.
- 110 J. E. Lopera, *Semin. Intervent. Radiol.*, 2010, **27**, 14–28.
- 111 A. Poursaid, M. M. Jensen, E. Huo and H. Ghandehari, *J. Control. Release*, 2016, **240**, 414–433.
- 112 L. Vikingsson, B. Claessens, J. A. Go, G. G. Ferrer and J. L. Go, *J. Mech. Behav. Biomed. Mater.*, 2015, **48**, 60–69.
- 113 N. Imai, M. Ishigami, Y. Ishizu, T. Kuzuya, T. Honda and K. Hayashi, *World J. Hepatol.*, 2014, **6**, 844–850.
- 114 G. R. Guillen, G. Z. Ramon, H. P. Kavehpour, R. B. Kaner and E. M. V. Hoek, *J. Memb. Sci.*, 2013, **431**, 212–220.

- 115 J. Fu and D. Hsia, *Chest*, 2015, **148**, 997A.
- 116 P. J. Emans, K. Saralidze, M. L. W. Knetsch, M. J. J. Gijbels, R. Kuijer and L. H. Koole, *J. Biomed. Mater. Res. - Part A*, 2005, **73**, 430–436.
- 117 K. Nicholson, *Skyscan 1172 MicroCT Scanning SOP*, Sheffield, 2015.
- 118 K. Nicholson, *NRecon SOP*, Sheffield, 2015.
- 119 J. F. Barrett and N. Keat, *RadioGraphics*, 2004, **24**, 1679–1691.
- 120 N. Otsu, *IEEE Trans. Syst. Man. Cybern.*, 1979, **9**, 62–66.
- 121 M. Saeed Kilani, J. Izaaryene, F. Cohen, A. Varoquaux, J. Y. Gaubert, G. Louis, A. Jacquier, J. M. Bartoli, G. Moulin and V. Vidal, *Diagn. Interv. Imaging*, 2015, **96**, 319–326.
- 122 R. Saraf, M. Shrivastava, N. Kumar and U. Limaye, *Indian J. Radiol. Imaging*, 2010, **20**, 26–33.
- 123 L. Rangel-Castilla, A. H. Shah, R. P. Klucznik and O. M. Diaz, *J. Neurointerv. Surg.*, 2014, **6**, 51–56.
- 124 C. M. Schirmer, V. Zerris and A. M. Malek, *Oper. Neurosurg.*, 2006, **59**, 413–419.
- 125 D. Raissi, Q. Yu and S. H. Mardini, *J. Clin. Imaging Sci.*, 2018, **8**, 46–56.
- 126 Antia Therapeutics AG and Assistance Publique - Hôpitaux de Paris, *EASYX-1 : A Multicenter Study on Safety and Efficacy of Easyx Liquid Embolization Agent Used in Five Separate Indications*, 2018.
- 127 Microvention-Terumo and ClinSearch, *PHIL Evaluation in the Endovascular Treatment of Intracranial Dural AVF*, 2017.
- 128 MicroVention, *Urgent Field Safety Notice FCA*, 2016.
- 129 K. V. Sharma, Z. Bascal, H. Kilpatrick, K. Ashrafi, S. L. Willis, M. R. Dreher and A.

- L. Lewis, *Biomaterials*, 2016, **103**, 293–304.
- 130 World Intellectual Property Organization, WO2015033093A1, 2015, 1–58.
- 131 D. A. Dias and M. A. Kerr, *Org. Lett.*, 2009, **11**, 3694–3697.
- 132 Y.-H. Zhao, Y.-L. Qian, B.-K. Zhu and Y.-Y. Xu, *J. Memb. Sci.*, 2008, **310**, 567–576.
- 133 Y. Y. Jiang, Y.-E. Jo, J. M. Woo, O. K. Lim, C. Hwang, J. Y. Maeng, J. Kim, N. Kim and D. H. Lee, *Neurointervention*, 2017, **12**, 3–10.
- 134 A. I. Qureshi, N. Mian, H. Siddiqi, M. H. Qureshi, A. M. Malik, M. Rauf Afzal, A. A. Khan and M. F. K. Suri, *J. Vasc. Interv. Neurol.*, 2015, **8**, 37–41.
- 135 A. K. Hořda and I. F. J. Vankelecom, *J. Appl. Polym. Sci.*, 2015, **132**, n/a-n/a.
- 136 F. Mottu, P. Gailloud, D. Massuelle, D. . Rüfenacht and E. Doelker, *Biomaterials*, 2000, **21**, 803–811.
- 137 Z.-M. Huang, Y.-Z. Zhang, M. Kotaki and S. Ramakrishna, *Compos. Sci. Technol.*, 2003, **63**, 2223–2253.
- 138 GE Healthcare, *OMNIPAQUE<sup>TM</sup> (iohexol) Injection - Instructions For Use*, 2017.
- 139 GE Healthcare, *Omnipaque (iohexol) injection - full prescribing information*, Princeton, 2010.
- 140 S. D. Simon, A. S. Reig, K. J. Archer and R. A. Mericle, *J. Neurointerv. Surg.*, 2012, **4**, 211–214.
- 141 F. G. Bordwell and D. Algrim, *J. Org. Chem.*, 1976, **41**, 2507–2508.
- 142 K. V. Sharma, Z. Bascal, H. Kilpatrick, K. Ashrafi, S. L. Willis, M. R. Dreher and A. L. Lewis, *Biomaterials*, 2016, **103**, 293–304.
- 143 Ling Xu, Xin Li, \* Maolin Zhai, Ling Huang, Jing Peng, and Jiuqiang Li and G. Wei, 2007.

- 144 United States Patent, 8221735B2, 2012, 1–14.
- 145 R. Scarpato, C. Gambacciani, B. Svezia, D. Chimenti and G. Turchi, *Mutat. Res. Toxicol. Environ. Mutagen.*, 2011, **722**, 69–77.
- 146 D. Mawad, P. J. Martens, R. A. Odell and L. A. Poole-Warren, *Biomaterials*, 2007, **28**, 947–55.
- 147 D. Mawad, L. A. Poole-Warren, P. Martens, L. H. Koole, T. L. B. Slots and C. S. J. van Hooy-Corstjens, *Biomacromolecules*, 2008, **9**, 263–268.
- 148 N. Naidu, M. Sorenson, T. Connolly and U. Yasutsugu, *J. Org. Chem.*, 2003, **68**, 10098–10102.
- 149 W. H. King, E. D. Patten and D. E. Bee, *Anesthesiology*, 1988, **68**, 115–121.
- 150 P. S. Douglas, K. A. Carmichael and P. M. Palevsky, *Am. J. Cardiol.*, 1984, **54**, 674–675.
- 151 I. Akmangit, E. Daglioglu, T. Kaya, F. Alagoz, M. Sahinoglu, A. Peker, S. Derakshani, D. Dede, D. Belen and A. Arat, *Turk. Neurosurg.*, 2014, **24**, 565–570.
- 152 A. L. Lewis, S. L. Willis, M. R. Dreher, Y. Tang, K. Ashrafi, B. J. Wood, E. B. Levy, K. V Sharma, A. H. Negussie and A. S. Mikhail, *Futur. Oncol.*, 2018, **14**, 2741–2760.
- 153 H. Tokue, A. Tokue and Y. Tsushima, *Indian J. Radiol. Imaging*, 2018, **28**, 81–84.
- 154 J. B. Jia, C. S. Green, A. J. Cohen and M. Helmy, *Clin. Radiol.*, 2015, **70**, 326–332.
- 155 R. Pelton, *Adv. Colloid Interface Sci.*, 2000, **85**, 1–33.
- 156 H. G. Schild, *Prog. Polym. Sci.*, 1992, **17**, 163–249.
- 157 M. Rasmusson, A. Routh and B. Vincent, *Langmuir*, 2004, **20**, 3536–3542.
- 158 A. R. Town, M. Giardiello, R. Gurjar, M. Siccardi, M. E. Briggs, R. Akhtar and T. O. McDonald, *Nanoscale*, 2017, **9**, 6302–6314.

# Chapter Eight

## 8. Appendix



## 8.1. Cross-Sectional Videos of Reconstructed MicroCT Scans

1. MicroCT cross-sectional video of syringe pump injection of liquid embolic sample delivered at  $0.01 \text{ mL min}^{-1}$  under PBS flow:

<https://drive.google.com/open?id=12wgWrzlgFxmmOXHrevqUQK1NH8y8BEao>

2. MicroCT cross-sectional video of syringe pump injection of liquid embolic sample delivered at  $0.5 \text{ mL min}^{-1}$  under PBS flow:

[https://drive.google.com/open?id=1S0J2RD5Q\\_QDTtVi3VpwHIBojNNY\\_voFr](https://drive.google.com/open?id=1S0J2RD5Q_QDTtVi3VpwHIBojNNY_voFr)

3. MicroCT cross-sectional video of syringe pump injection of liquid embolic sample delivered at  $0.01 \text{ mL min}^{-1}$  under no flow of PBS:

[https://drive.google.com/open?id=1P4dfvZMJwMPj9O\\_DentyAbNTLtDLAcU](https://drive.google.com/open?id=1P4dfvZMJwMPj9O_DentyAbNTLtDLAcU)

4. MicroCT cross-sectional video of syringe pump injection of liquid embolic sample delivered at  $0.5 \text{ mL min}^{-1}$  under no flow of PBS:

<https://drive.google.com/open?id=1qA6sEDxvqUJh2LSwAiSjNT0sRvtdaDUf>

5. MicroCT cross-sectional video of pulsed syringe pump injection of liquid embolic sample delivered at  $0.1 \text{ mL min}^{-1}$  with 10 s pulse intervals under PBS flow:

[https://drive.google.com/open?id=1sskSG2N7U9Alc4Xg\\_2mlQYi84oigyuw-](https://drive.google.com/open?id=1sskSG2N7U9Alc4Xg_2mlQYi84oigyuw-)

6. MicroCT cross-sectional video of pulsed syringe pump injection of liquid embolic sample delivered at  $0.1 \text{ mL min}^{-1}$  with 180 s pulse intervals under PBS flow:

<https://drive.google.com/open?id=1zvC6WAQN9AEdn2ScVI7fOt4q4h5e8g4R>

7. MicroCT cross-sectional video of pulsed syringe pump injection of liquid embolic sample delivered at  $0.1 \text{ mL min}^{-1}$  with 10 s pulse intervals under no flow of PBS:

[https://drive.google.com/open?id=1zLpCNQOw3jPONlhQIsDrT5YLPXtJy\\_sN](https://drive.google.com/open?id=1zLpCNQOw3jPONlhQIsDrT5YLPXtJy_sN)

8. MicroCT cross-sectional video of pulsed syringe pump injection of liquid embolic sample delivered at  $0.1 \text{ mL min}^{-1}$  with 180 s pulse intervals under no flow of PBS:

<https://drive.google.com/open?id=19JArVI4Zx9TEYUPpKF2Hg3bSKm6651PO>